University of Glasgow

Tropism of Bluetongue Virus in *Culicoides* Midges

Alice Adair Muntzer

BSc (hons) MSc (R)

Submitted in fulfilment for the requirements for the degree of

Doctor of Philosophy in Virology

The Institute of Infection, Immunity and Inflammation

College of Medical Veterinary and Life Sciences

University of Glasgow

March 2017

Abstract

Arthropod-borne viruses (arboviruses) cause diseases of significant consequence to human and animal health. The aspect of the lifecycle that distinguishes an arbovirus from another viral group, is the requirement for replication in an arthropod vector and vertebrate host. *Culicoides* midges (order: Diptera; family: *Ceratopogonidae*) transmit several arboviral diseases of economic importance including bluetongue virus (BTV), a double-stranded RNA virus within the genus *Orbivirus* (family: *Reoviridae*).

The ability of an arbovirus, such as BTV, to replicate, disseminate and be transmitted to a susceptible host is determined by the interaction between extrinsic factors, such as the titre of ingested virus, and intrinsic factors such as the particular viral and vector genotype. This process is poorly understood. Here, data are presented to address this, describing BTV infection and replication in a model species, *Culicoides sonorensis*.

The percentages of infected cells were objectively determined in insect tissues using automated image classification. BTV infected cells of the posterior midgut and the number of cells infected were viral strain and dose-dependent and correlated with infection rate. Virus replicated to high levels in the compound eyes, fat body and epithelial cells. The brain and other neural tissues were infected at later times tested, coinciding with the expected time of BTV transmission. Viral RNA and antigen were undetectable in the salivary glands and oocytes, but were detected at high prevalence in the mouthparts.

These data show, for the first time, that *Culicoides*-borne arboviruses may exploit an alternative mechanism for transmission to a host than that used by mosquito-borne arboviruses. BTV may be transmitted directly from the mouthparts, without requiring the ability to replicate in the salivary glands.

Contents

Tables

Figures

Acknowledgements

I would like to thank all of my supervisors for their support, advice and hard work throughout the project. I would like to thank Anthony Wilson for supporting me throughout the project and encouraging me to plan and organise my time more carefully. I would like to thank my University supervisor, Massimo Palmarini, for hosting me in his lab during my first year, and for the excellent advice he has offered me throughout the project. I am especially grateful to Andrew Shaw and Gill Pullinger for training me in the lab, teaching me valuable molecular laboratory techniques and sharing their in-depth knowledge of BTV with me. Without their support, I wouldn't have been able to submit this thesis. I'm also particularly to Peter Mertens, who offered me funding, a space to work and has contributed a great deal to the direction of the project.

Many people at both Pirbright and Glasgow have offered me invaluable support and help when needed and I would not have made it to submission stage without them. Particularly, Marc Guimera, who has helped me out in the lab an uncountable number of times, taught me the ropes in RA and Epidem, arranged many dinners at the pub and provided support during many stressful occasions during my project. I'm very grateful to Julian Seago for his lunchtime chats and for the taken time away from his experiments to teach me western blotting. I'm also grateful to Chris Sanders who painstakingly sorted some midges for me. I'm not sure I could have survived the loneliness and isolation of West wing without him or Marc. I'd also like to thank Manju Belaganahalli, Lizzie Morecroft, Jana Baron and Kiki Nomikou for putting up with me in the lab and for their good lunchtime discussions in the sun outside the old canteen. Also, Honorata Ropiak for arranging drinks out after work and the members of the NVRL for being such amazing company throughout my time at the institute. I'd lastly like to thank members of the Palmarini lab for being really helpful and such good company, including Eleanora Melzi, Ania Janowitz, Catrina Mullen, Maxime Ratinier, Gerald Barry and Filipe Nunes.

Declaration

I declare that, except where explicit reference is made to the contribution of others, this thesis is the result of my own work and has not been submitted for any other degree at the University of Glasgow or any other institution.

Signature: 

Full name: Alice Adair Muntzer.

Date: 20/03/2017

Abbreviations

+RNA	Sense single-stranded ribonucleic acid
µg	Microgram
µl	Microliter
aa	Amino acids
AHSV	African horse sickness virus
AICC	Automated infected cell counter
Arbovirus	Arthropod-borne virus
bp	Base pairs
BSR	Baby hamster kidney adenocarcinoma cell line
BT	Bluetongue
BTV	Bluetongue virus
BUNV	Bunyamwera virus
CHIKV	Chikungunya virus
CI	Confidence interval
CPE	Cytopathic effect
CPT	Ovine cell line
d	Days
DAPI	4'-6-Diamidino-2-phenylindole
DENV	Dengue virus
dsRNA	Double-stranded ribonucleic acid
EEEV	Eastern equine encephalitis virus
EHDV	Epizootic haemorrhagic disease virus
FACS	Fluorescence-activated cell sorting
FISH	Fluorescence *in situ* hybridisation
FMDV	Foot and mouth disease virus
GFP	Green fluorescent protein
GLMM	Generalised linear mixed effects model
h	Hours
IF	Immunofluorescence
IFN	Interferon
IHC	Immunohistochemistry
Imd	Immune deficiency pathway
IT	Intrathoracic

JAK	Janus kinase
JEV	Japanese encephalitis virus
kb	Kilo base
KC	Culicoides sonorensis cell line
LACV	La Crosse encephalitis virus
LB	Luria-Bertani media
mg	Milligram
MicroCT	X-Ray Micro-Computed Tomography
ml	Millilitre
MOI	Multiplicity of infection
mRNA	Messanger ribonucleic acid
n	number
ng	Nanogram
NS	Non-structural
nt	Nucleotide
OIE	World Organisation for Animal Health
ORF	Open reading frame
p.i.	Post infection
PBS	Phosphate buffered saline
PCR	Polymerase chain reaction
PFU	Plaque forming units
PV	Polio virus
qPCR	Quantitative polymerase chain reaction
RdRp	RNA depended RNA polymerase
RG	Reverse genetics
RIG-I	Retinoic acid-inducible gene 1
RNA	Ribonucleic acid
-RNA	Antisense single-stranded ribonucleic acid
RNAi	RNA interference
RT	Reverse transcription
RVFV	Rift valley fever virus
SA	South Africa
SBV	Schmallenberg virus
SE	Standard error
Seg	Segment

SLEV	St. Louis encephalitis virus
ssRNA	Single-stranded ribonucleic acid
STAT	Signal transducer and activator of transcription
TCID	Tissue culture infectious dose
TEM	Tranmission electron microscopy
TLR	Toll-like receptor
Tsg101	Tumour susceptibility gene 101 protein
UTR	Untranslated region
VEEV	Venezuelan equine encephalitis virus
VIB	Viral inclusion body
VP	Viral protein
VSV	Vesicular stomatitis virus
WEEV	Western equine encephalitis virus
WNV	West Nile virus
YFV	Yellow fever virus

Chapter 1

Introduction

1.1. Introduction to Bluetongue virus

Bluetongue virus (BTV) (genus: *Orbivirus*; family: *Reoviridae*) is a globally distributed arbovirus capable of infecting ruminants (taxa: Ruminantia; sub-order: Tylopoda) as well as carnivorous species, specifically canines and felines (Alexander et al., 1994). The resulting bluetongue disease in cattle and sheep is of major economic and veterinary importance. Since BTV was first described by Hutcheon (Hutcheon, 1881, Hutcheon, 1902) and Spreull (Spreull, 1905) in South Africa, 27 serotypes of BTV (BTV-1 to BTV-27) have been identified and formally recognised (Jenckel et al., 2015, Maan et al., 2011). Several other strains that represent additional serotypes are currently under analysis. Most BTV serotypes are endemic to regions between latitudes approximately 40°N and 35°S (Wilson and Mellor, 2009), correlating with the presence of species of *Culicoides* biting midges (order: Diptera; family: *Ceratopogonidae*) competent to transmit BTV (Foster et al., 1963, Du Toit, 1944). Possible exceptions to this rule include strains of BTV-25, 26 and 27, which may be spread by direct contact transmission (Maan et al., 2011, Batten et al., 2013, Pullinger et al., 2016, Schulz et al., 2016).

BTV is the causative agent of Bluetongue (BT) disease (Theiler, 1904), a highly pathogenic disease of sheep and, less frequently, cattle (which serve as a reservoir host) (Bekker et al., 1934, Luedke et al., 1967). The duration of viraemia infectious to *C. sonorensis* can last up to 21 days post-infection (dpi) in sheep and cattle (Bonneau et al., 2002). However, viral RNA in blood can be isolated as early as 3 days dpi in sheep (Darpel et al., 2007). Clinical manifestations of BT correspond with high levels of viral RNA (Worwa et al., 2010) and include: cyanosis of the tongue, pyrexia, hyperaemia, oedema and eventual death (Erasmus, 1975, Darpel et al., 2007, Worwa et al., 2010). The frequency and severity of such clinical signs depends on the breed, age and immune status of the affected animal, as well as on the serotype/strain.

Although severe outbreaks of BT can occur in endemic regions, recently seen in southern India (Rao et al., 2016). BT is predominantly sub-clinical in endemic regions, including the Americas, northern Australia, Africa, the Iberian Peninsula of Europe and southern Asia (MacLachlan, 2004, Kahn and Anon, 2005), largely due to high levels of acquired immunity, protection from infection by vaccination with live-attenuated BTV strains, inactivated tissue culture derived vaccines and the use of BT-resistant livestock breeds. BT causes substantial economic losses, with global costs resulting from high mortality and morbidity levels,

reduced reproductive performance, growth rates and milk yields, as well as costs associated with control of animal movements, trade, vaccination programmes and enhanced surveillance (MacLachlan and Osburn, 2006). The global costs due to incidence of BT is estimated to amount to $3 billion per annum (Tabachnick, 1996).

In areas outside of endemic regions, such as northern Europe, substantial losses can result from direct mortality and morbidity in European sheep breeds (Bekker et al., 1934). Since 1998, outbreaks of BT caused by seven serotypes (BTV-1, 2, 4, 8, 9, 16 and 27) have occurred in over 12 European countries (Purse et al., 2005), resulting in the death of over 1.5 million sheep (Carpenter et al., 2006). Infections associated with mild or unapparent clinical signs have also been detected, caused by vaccine derived strains of BTV-6, 11 and 14 (Batten et al., 2008), or a 'novel' serotype, BTV-25 (Hofmann et al., 2008). BTV poses an increasing risk to the economies in northern temperate climes due to recent changes in climate, specifically temperatures exceeding 12.5°C for 7 months per annum (Sellers and Mellor, 1993). Such climate changes have enabled, or facilitated, the overwintering of BTV as well as transmission of the virus during warmer winter months (Purse et al., 2005).

In 2006, BTV serotype 8 (BTV-8) was detected in several countries in northern Europe and reached the UK in 2007 (Wilson and Mellor, 2009). The outbreak provided the first report of BTV beyond latitude 52°N (OIE, 2006) and was likely caused by a strain originating from sub-Saharan Africa (Maan et al., 2008). The recrudescence of BTV-8 in France during 2015, shows that the threat of BTV to the UK is still present. A qualitative risk assessment predicted a 60 to 80% risk of incursion of BTV-8 into the UK in late summer 2016 (Carpenter et al., 2016). Although this did not happen, the restriction zones spread to the north coastal regions of France in 2016 (OIE, 2016). It is therefore of topical and socioeconomic importance to understand the mechanisms of transmission and the biology of BTV.

1.1.1. Structure of the BTV particle

Although there are twenty-two arboviruses within the non-enveloped genus *Orbivirus* (Casals, 1973), BTV is the type species (Mertens et al., 2005) and is the best characterised structurally. The 10 segments of linear dsRNA which form the ~19.2 kbp genome of BTV (Grimes et al., 1998, Gouet et al., 1999, Roy, 1989) encode 7 structural proteins (VP1 to VP7) and 4 non-structural proteins. The non-structural proteins encoded by BTV are NS1,

NS2, NS3 (Fukusho et al., 1989, Van Dijk and Huismans, 1988, Mertens et al., 1984) and NS4 (Ratinier et al., 2011, Belhouchet et al., 2011). Recently, a possible fifth non-structural protein (S10-ORF2) was identified (Stewart et al., 2015) (table 1.1).

Table 1.1: Bluetongue virus genomic segments, the proteins encoded and protein functions (Boyce et al., 2012a, Chauveau et al., 2013, Mertens et al., 2004, Mertens and Diprose, 2004, Ratinier et al., 2011, Roy, 2005, Roy, 2008a, Roy, 2008b, Stewart et al., 2015)

Genomic segment	Length (bp)*	Protein (size KDa**)	Protein function
1	3944	VP1 (1302)	RNA-dependent RNA-polymerase
2	2940	VP2 (961)	Outer-capsid protein. Receptor binding; cell entry
3	2772	VP3 (901)	Sub-core shell protein. Cell exit
4	1981	VP4 (644)	RNA-capping enzyme
5	1772	NS1 (552)	Molecular chaperone in assembly; regulation of BTV protein expression
6	1635	VP5 (526)	Outer-capsid protein. Cell entry; endosome membrane penetration
7	1156	VP7 (349)	Binding of core particles to insect cells
8	1125	NS2 (354)	VIB formation; ssRNA binding and packaging
9	1049	NS4 (77) VP6 (329)	IFN antagonist Helicase
10	822	NS3/NS3a (229) *S10ORF2* (NS5) *(50)*	Viral egress; IFN antagonist *Vector or host infection*

* Correspond to BTV-1 RSArrrr/01 (GenBank accession numbers: JX680457 to 66).

** Correspond to BTV-1 (GenBank accession numbers: AFV68261 to 71).

Every 86 nm BTV virion (Figure 1.1) contains one copy of each genome segment (Gouet et al., 1999, Grimes et al., 1998, Prasad et al., 1992), enclosed within the three-concentric protein layers of the capsid. Each genome segment usually encodes a separate protein, with the exception of segment 9, which encodes both NS4 and VP6 (Belhouchet et al., 2011, Ratinier et al., 2011, Stauber et al., 1997) and segment 10, which encodes both S10-ORF2 (NS5) and NS3 (Bansal et al., 1998, Stewart et al., 2015). The protein layers forming the virion includes an inner most 'sub-core', composed of 120 copies of VP3, containing the genome segments associated with the transcription complexes, comprising VP6, VP1 and VP4, which are located at the inner surface of VP3 (T2) shell (Gouet et al., 1999). The outer layer of the 700 angstrom (Å) diameter core is composed of 780 copies of VP7 arranged in trimers (T13) (Grimes et al., 1998) and provides the basis for attachment of the outer capsid layer, comprised of 360 copies of VP5 and 180 copies of VP2 (Grimes et al., 1995). VP2 is arranged in 60 trimeric sub-units that are responsible for haemaglutination (Cowley and Gorman, 1987), serotype specificity (as assessed by serum neutralisation assay, (Mertens et al., 1989) or PCR, (Mertens et al., 2007)), cell attachment and receptor binding (Zhang et al., 2010b).

Figure 1.1

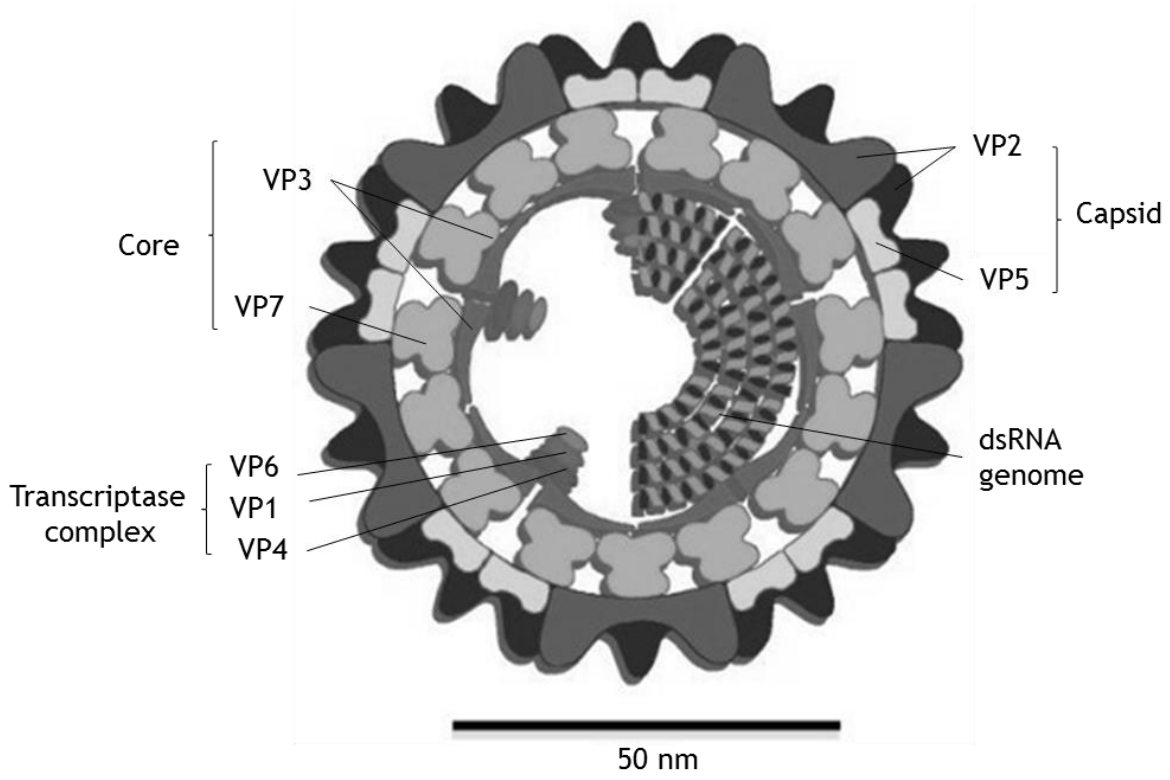

Figure 1.1: Structure of a Bluetongue virus particle (adapted from (Mertens et al., 2005)).

1.1.2. The BTV replication cycle

The lifecycle of BTV is relatively well characterised in mammalian cell culture (Figure 1.2). BTV particles can attach to a host cell as intact particles, or as core particles (CPs) lacking the outer VP2-VP5 capsid layer. CPs bind to an insect cell membrane via the arginine-glycine-aspartate (RGD) tripeptide on VP7 (Tan et al., 2001). CPs are much less infectious for BHK cells than intact particles, but have a 1000-fold higher infectivity for *Culicoides sonorensis* (KC) cells as compared to BHK-21 cells (Mertens et al., 1996b). In view of the high sequence diversity detected in VP2 of BTV, it is possible that different serotypes use different entry pathways. Indeed, entry of intact BTV particles may arise either via clathrin-mediated endocytosis (CME), shown for BTV-10 (Forzan et al., 2007), or a macropinocytosis-like pathway, demonstrated for BTV-1 (Gold et al., 2010, Stevens, 2016). VP5 of intact BTV particles penetrates the cellular membrane (Hassan et al., 2001) and may penetrate the lysosome of late endosomes by interacting with host lipid factor, 2,2-dioleoyl lysobisphosphatidic acid (LBPA) (Patel et al., 2016). Particles are uncoated by the low pH of early endosomes upon CME (Forzan et al., 2007). Uncoating involves initial cleavage of VP2 and release of the 69 nm core particle into the cytosol (Prasad et al., 1992, Forzan et al., 2004, Zhang et al., 2010b).

Within the transcriptionally active core, VP6 acts as a helicase to separate the negative and positive strands of the genomic dsRNA (Stauber et al., 1997). The non-proofreading RNA-dependent RNA-polymerase, VP1, transcribes viral mRNA copies (vmRNA) from the negative strand of each genomic dsRNA (Urakawa et al., 1989, Boyce et al., 2004). Newly synthesised transcripts are capped at their 5' termini by VP4 (Martinez-Costas et al., 1998, Ramadevi and Roy, 1998, Ramadevi et al., 1998, Fukusho et al., 1989), prior to release into the cytosol through Mg^{2+}-dependent pores at the 5-fold axis of the VP3 (Diprose et al., 2001).

Cytosolic vmRNAs are recruited to viral inclusion bodies (VIBs). VIBs are primarily formed by phosphorylated NS2, which binds ssRNAs (Modrof et al., 2005, Thomas et al., 1990). VIBs are rich in viral RNA, but also contain the viral structural proteins, with the exception of VP2 (Brookes et al., 1993). Within the VIBs, vmRNAs are used as the template for negative strand synthesis (Boyce et al., 2004). Specific RNA-RNA base pairing between motifs on interacting segments forms a packaging complex which is packaged into assembling core particles (Boyce et al., 2016).

In mammalian cells, newly assembled BTV particles are trafficked to the plasma membrane which involves interaction of NS3 with cellular p11 (calpaxin light chain) and VP2 (Beaton et al., 2002). Highly abundant cytosolic NS1 may also act to facilitate virus release from infected cells (Owens et al., 2004).

A minor fraction of virus particles may transmit cell-to-cell (Bhattacharya and Roy, 2008) without inducing lysis. Non-lytic budding is a common form of BTV release from insect cells, although can occur in mammalian cells (Fu, 1995). Budding and direct membrane penetration involve the interaction of NS3, whose expression is upregulated in insect cells (Guirakhoo et al., 1995), with endosomal sorting complexes required for transport-I (ESCRT-I) complex, Tsg101 (Wirblich et al., 2006, Celma and Roy, 2009, Beaton et al., 2002). Budding enables BTV infection to persist in cells without inducing CPE for the remainder of the life span of the vector (Mellor, 1990). The mechanisms responsible for arbovirus persistence in insect cells remain poorly characterised. Studies in *Drosophila melanogaster* revealed that infection with positive strand RNA viruses persists through synthesis of endogenous dsRNA by the host cell, homologous to viral RNA, which is then targeted by RNA interference (RNAi) reducing virus replication efficiency (reviewed in section 1.3.2) in preference to viral replication intermediates (Goic et al., 2013).

Figure 1.2

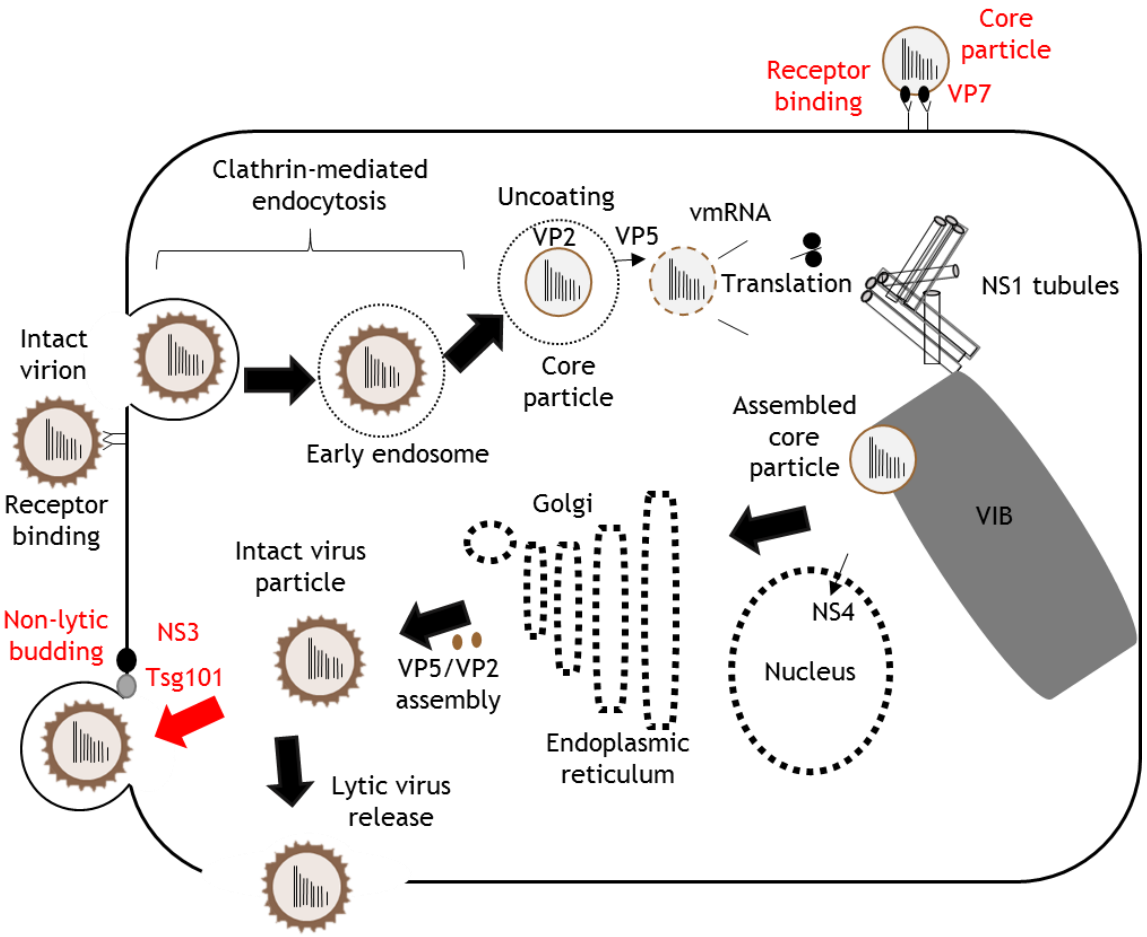

Figure 1.2: Replication cycle of bluetongue virus. Core particles enter insect cells via interaction of the RGD motif of VP7 with the cell membrane (shown in red), whereas intact BTV particles likely enter by clathrin-mediated endocytosis (CME) or macropinocytosis. During CME, VP2 is degraded in early endosomes. VP5 triggers the release of transcriptionally active core particles into the cytosol. VP1 synthesises vmRNAs, which are recruited to viral inclusion bodies (VIBs) where genomic segments are packaged into assembling core particles, via interactions with NS2. BTV protein synthesis is upregulated by NS1, which forms cytosolic tubules (Huismans, 1979, Huismans and Els, 1979b, Urakawa and Roy, 1988b). NS4 accumulates in the nucleus and suppresses host cell interferon induction (Ratinier et al., 2011). VP2 and VP5 are added and intact virus particles are trafficked to the cell membrane. Egress arises either by cell lysis, budding, or by direct membrane penetration and involves association of NS3 with VP2 and interaction with Tsg101 (shown in red).

1.2. *Culicoides* species as insect vectors

Culicoides (Diptera: *Ceratopogonidae*) is a genus of small, biting flies, measuring 1 to 4 mm in body length (Mullens, 1987, Mellor et al., 2000). *Culicoides* belong to the family *Ceratopogonidae*, which contains 6267 extant and 283 extinct species (Borkent, 2016), grouped into 125 genera (Downes and Wirth, 1981, Remm, 1988). There are 1357 species of *Culicoides* (Borkent, 2014), distinguished from other genera by their characteristic wing pigmentation (Munoz-Munoz et al., 2011). *Culicoides* date back in the fossil record 120 to 122 million years (Borkent, 2000) and today, are highly abundant, colonising all large land masses except New Zealand, Patagonia, the Hawaiian Islands, extreme polar regions and altitudes 4000 m or more above sea level (Mellor et al., 2000).

Females of approximately 96% of *Culicoides* species are hematophagous (Meiswinkel et al., 2004) and blood-feed on a vertebrate host to sequester protein for egg development (Campbell and Kettle, 1975, Lavoipierre, 1965). *Culicoides* females feed by retracting their mandibles to lacerate the superficial tissue of the host then ingest the resulting dermal pool of blood. Blood feeding and the resulting immune responses to Culicoides salivary proteins (Darpel et al., 2011), can cause dermatitis (O'Toole et al., 2003, Yeruham et al., 2004, Correa et al., 2007). Adult *Culicoides* are capable of transmitting a variety of blood-borne pathogens, including, filarial nematodes such as *Onchocerca cervicalis*, (Mellor, 1971), bacteria including Enterobacteriaceae spp. (Parker et al., 1978), viruses, and protozoa, such as *Haemoproteus* spp. (Atkinson, 1988, Bukauskaite et al., 2015, Ziegyte et al., 2016), including the protozoan *Leishmania* spp. (Seblova et al., 2015).

Over 50 viruses have been isolated from *Culicoides*, including representatives of the family *Bunyaviridae* (20 species), *Reoviridae* (19 species) and *Rhabdoviridae* (11 species). Despite the ability of *Culicoides* to transmit viruses and other pathogens of international significance, including African Horse Sickness virus (AHSV), BTV and human febrile illness-inducing Oropouche virus (OROV), *Culicoides* have attracted little research interest compared with other dipteran vector groups. Consequently, many of the factors which determine their competence as arboviral vectors remain unknown. This is partly due to lack of methods for the study of viral infection within individual insects, which provides the focus for studies described in Chapters 3 and 4 of this thesis.

1.2.1. Life cycle

Partly due to their small size, the diversity of breeding sites (Kettle, 1977) and the vulnerability of life stages to physical damage during collection (Veronesi et al., 2009), the life cycle of *Culicoides* has been poorly studied in the field. The *Culicoides* life cycle is summarised in figure 1.3 and consists of four distinct life stages: egg, larva, pupa and adult.

Adult *Culicoides* are crepuscular and most active at dawn and dusk (Nelson and Bellamy, 1971, Mullens et al., 1995), during times when solar intensities and wind velocities are under 200 Wm^{-2} and 3 ms^{-1}, respectively (Blackwell, 1997, Carpenter et al., 2008). Males form mating swarms close to a swarm marker, such as a vertebrate host or larval development site (Downes, 1955, Gerry and Mullens, 1998). Upon mating and completion of the gonadotrophic cycle, which ranges from 10 days after blood meal acquisition at 13°C to 2 days at 30°C in *C. sonorensis* (Mullens and Holbrook, 1991), gravid female *Culicoides* oviposit batches of 30 to 450 (Russell et al., 2013) mature elongate convex eggs (Cribb and Chitra, 1998) onto substrate, such as mosses. Females seek oviposition sites in moisture-rich habitats, including irrigation pipe leaks, marshes, streams, tree holes, animal dung and rotting vegetation (Wirth, 1989, Dyce and Marshall, 1989, Harrup et al., 2013, Foxi and Delrio, 2010). The site of oviposition provides the location of development of the motile larval life stages (Kettle, 1977).

Larvae reside in the surface of mud (Vaughan and Turner, 1987, Barnard and Jones, 1980) and predominantly feed on particulate vegetable matter, nematodes, small invertebrates, rotifers and protists (Vaughan and Turner, 1987, Barnard and Jones, 1980, Meiswinkel et al., 1994). At the third or fourth instar, larvae in cooler regions burrow into substrate submerged by up to 50 cm of water, where they overwinter in diapause (Mullens and Rutz, 1983, Jones, 1967). The timing of onset and cessation of diapause is determined by environmental thermal and photoperiodic cues (Isaev, 1974).

Each life stage is susceptible to desiccation and is influenced by local meteorological conditions (McDermott and Mullens, 2014). *Culicoides* are poikilothermic ectotherms, and their body temperature is therefore determined by ambient temperature, which also affects their rate of development and mortality levels (Wittmann et al., 2002). Temperature increases can result in an extreme reduction in development time, for instance, the development rate of the North American vector, *C. sonorensis*, can range from 7 weeks at 17°C to 2 weeks at 30°C (Russell et al., 2013). Longevity of the adult life stage is dependent

on ambient temperature and in *C. sonorensis* ranges from 19 days at 10ºC to 9 days at 30ºC (Lysyk and Danyk, 2007).

In cooler temperate climes, most *Culicoides* species are univoltine, developing through a single generation per year (Foxi and Delrio, 2010) and activity is seasonal with low or absent populations during winter. In the UK, there is a peak of emergence in April to May (Mellor et al., 2000) that is triggered by rising temperatures (Luhken et al., 2015). The thermal tolerance of life stages to low ambient temperatures over winter determines the population abundance, distribution and geographic limits of a given species of *Culicoides*, which in turn can restrict the global incidence of *Culicoides*-borne pathogens including BTV (Wilson and Mellor, 2009).

Figure 1.3

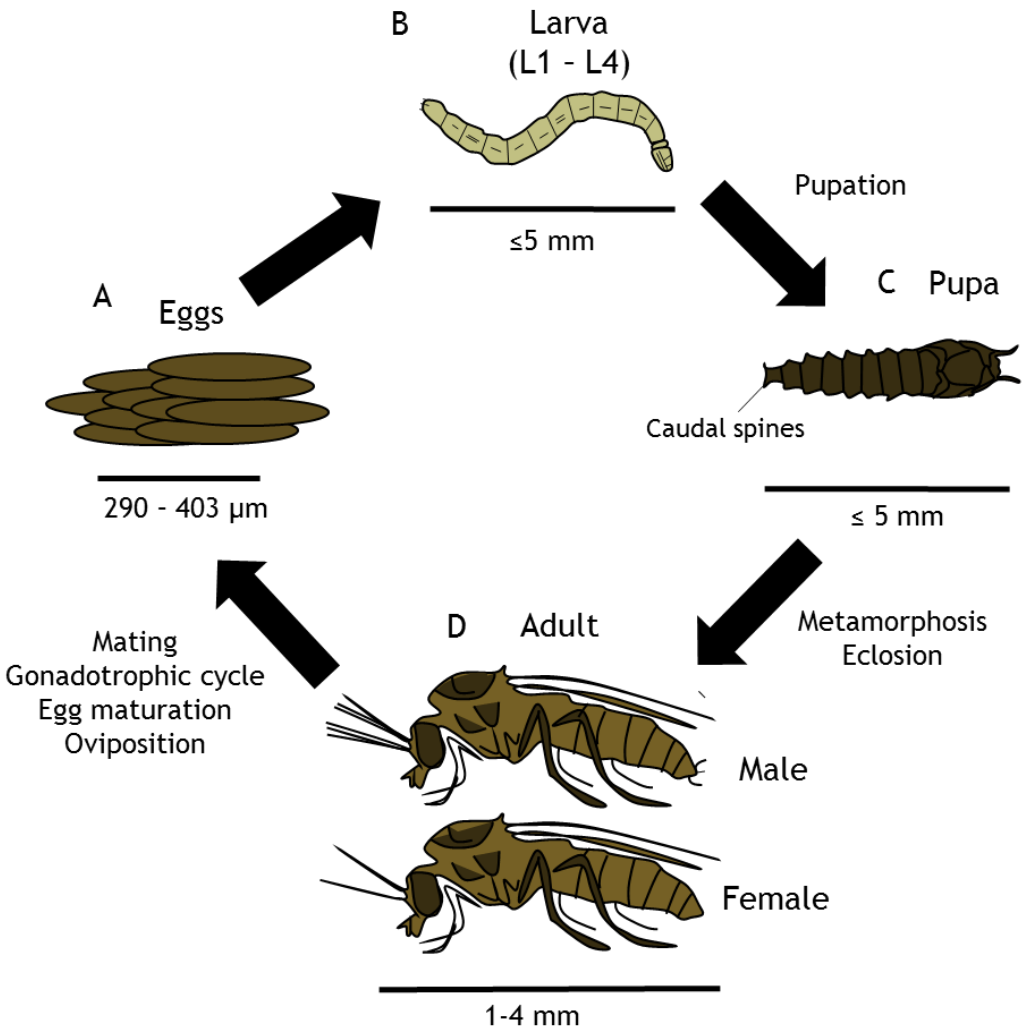

Figure 1.3: Lifecycle of a *Culicoides* midge. (**A**) Upon mating and completion of the gonadotrophic cycle, gravid female *Culicoides* oviposit batches of 30 to 450 eggs (Russell et al., 2013) (**B**) Semi-aquatic, vermiform shaped larvae usually hatch within a few days of oviposition and moult through four instars (L1 to L4). (**C**) Once larval development is complete, upon final ecdysis, larvae pupate into a short-lived, motile, non-feeding pupa. (**D**) Pupae are usually buried in substrate, upon completion of metamorphosis (usually within three days of pupation), caudal spines enable pupae to move to the surface of the substrate (Russell et al., 2013) prior to eclosion into a sexually mature adult *Culicoides*. Scale bars show the approximate body size of each life stage.

1.2.2. Morphology

Few accounts exist describing the morphology of *Culicoides* which is characterised in Chapter 4 of this thesis. The structure of the alimentary tract was described in studies of dissected *C. nubeculosus* (Megahed, 1956), which is comprised of an anterior oesophageal diverticulum (the crop), the oesophagus, foregut, midgut, Malpighian tubules and hindgut.

Despite the availability of limited information on the anatomy of *Culicoides*, several investigators have described the structure of the mouthparts of female *Culicoides* in detail (Blackwell, 2004, Sutcliffe and Deepan, 1988, Mckeever et al., 1994). Interest in characterising the mouthparts is fuelled partly due to the relevance of features, such as the size and number of mandibular teeth, in species identification (Mckeever et al., 1988). The mouthparts of *Culicoides* are summarised in figure 1.4 and are composed of the maxillary palps, labium, toothed labrum and the cuticular, toothed mandibles, which are located between the cuticular hypopharynx and, additionally to the labrum, function in tissue incision (Sutcliffe and Deepan, 1988). The hypopharynx contains the cuticular salivary duct and, additionally to the labrum, is inserted into the bite site during blood feeding (Blackwell, 2004, Sutcliffe and Deepan, 1988).

Figure 1.4

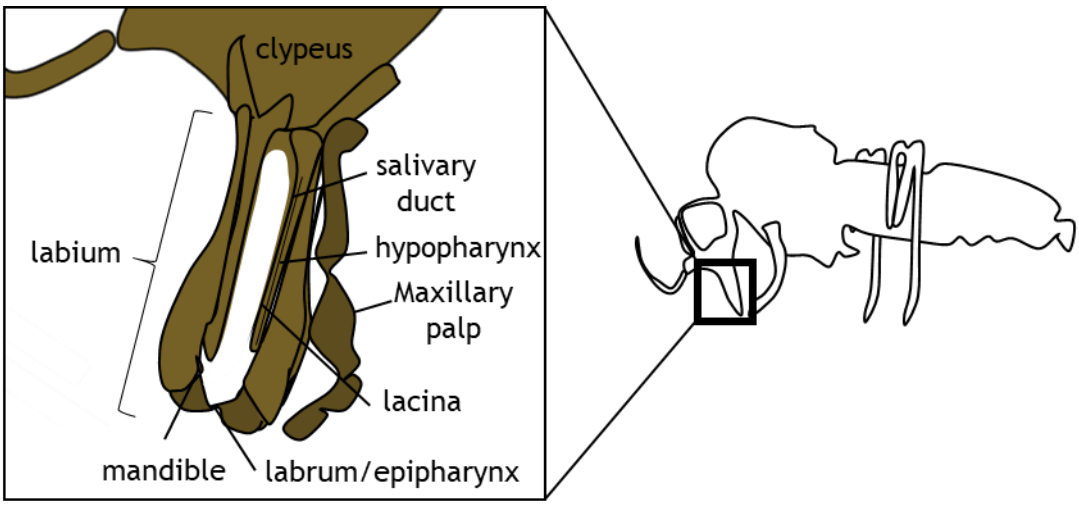

Figure 1.4: Morphology of the mouthparts of female *Culicoides* (adapted from (Jobling, 1928)).

1.2.3. Epidemiology

Two geographically distinct clades of BTV exist based on a phylogenetic analysis of genome segments which group strains into eastern and western 'topotypes'. Western topotypes circulate in the Americas and Africa, whereas eastern topotypes are located in the Middle East, Asia and Australia, respectively (Bonneau and MacLachlan, 2004, Balasuriya et al., 2008). Topotypes are identified by geographic region-specific multiple point mutations (Maan et al., 2012) and are evident for all BTV genome segments.

The considerable genetic diversity of BTVs has been generated through high rates of mutation, typical of RNA viruses, in addition to high progeny yield, short generation times (reviewed by (Domingo and Holland, 1997)) and low or high frequency reassortment during mixed infection of a ruminant host or *Culicoides* vector (Samal et al., 1987a, Samal et al., 1987b, el Hussein et al., 1989, Nomikou et al., 2015).

The global distribution of BTV strains and serotypes is constantly changing and incursions into non-endemic regions often occur. After the first reports of BT disease in Africa and Cyprus in the early 1900s (Hutcheon, 1881, Hutcheon, 1902, Spreull, 1905), BT outbreaks were reported across several countries between 1951 and 1979 including, Israel, the USA, India, Spain and Portugal (BTV-10), Australia (St George et al., 1978) and Greece (BTV-4) (Wilson and Mellor, 2009). Since 1998, multiple BTV serotypes have been detected and in many cases have spread within Europe (BTV-1, 2, 4, 6, 8, 9, 11, 14, 16, 25 and 27) (Carpenter et al., 2009, Purse et al., 2005, Schulz et al., 2016), the south-eastern states of America (BTV-1, 3, 5, 6, 9, 12, 14, 19, 22 and 24) and novel serotypes have emerged in Australia and the Middle East (Maclachlan, 2011, Maan et al., 2011).

Thirty species of *Culicoides* have been associated with BTV transmission (Meiswinkel et al., 2004). However, *C. imicola, C. brevitarsis, C. bolitinos, C. obsoletus, C. scoticus, C. pulicaris, C. sonorensis* and *C. insignis* are widely accepted as the main vector species. In Afro-asiatic regions *C. imicola* is thought to be responsible for over 90% of BT transmission and has recently expanded its range into southern Europe (Wittman et al., 2001). Range expansion, in addition to the involvement of indigenous *Culicoides* species such as the *C. pulicaris* and *C. obsoletus* groups (Wilson and Mellor, 2009, Purse et al., 2005), has facilitated a northward expansion in the range of BT epidemics. Figure 1.5 shows the current distribution of BTV serotypes and primary vector species.

Figure 1.5

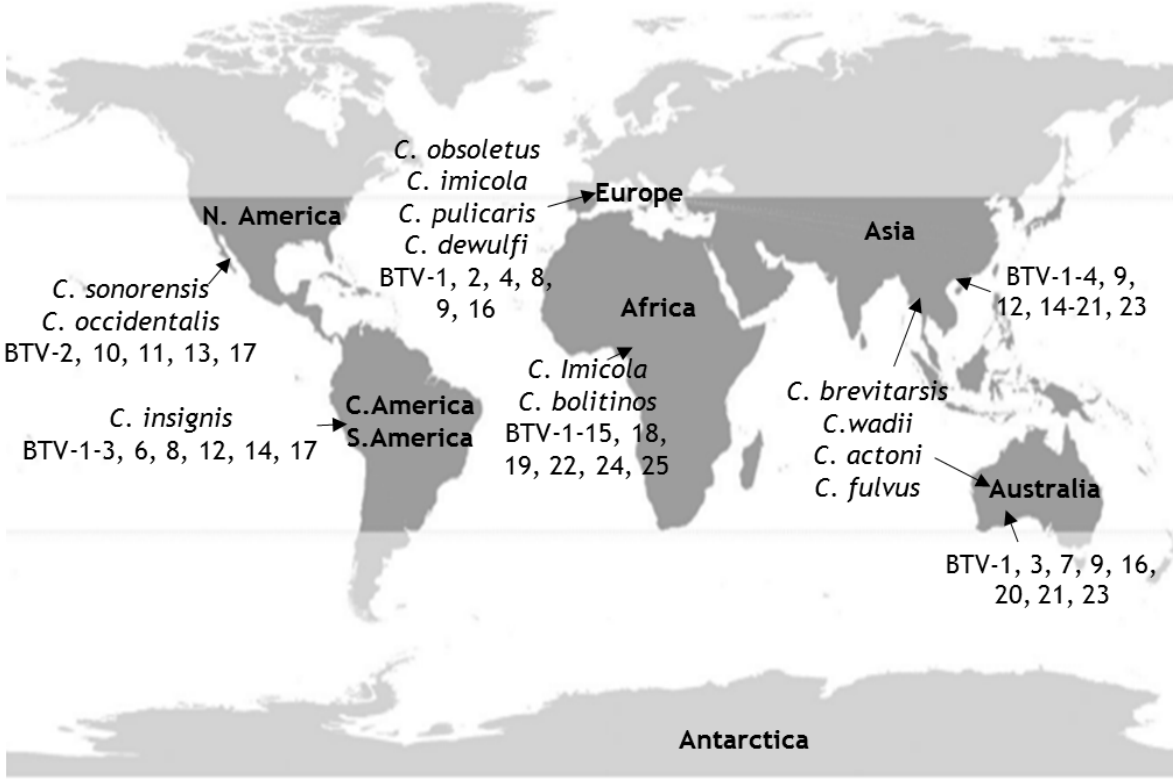

Figure 1.5: Projected global distribution of BTV serotypes and primary vector species of *Culicoides*. Endemic regions prior to 1998 are shown in dark grey (Wilson and Mellor, 2009, Tabachnick, 2004, Walton, 2004) and areas outside of endemic regions in light grey. Arrows indicate the main *Culicoides* vector species and serotypes circulating in the endemic region of each continent.

1.3. Arbovirus infection and factors affecting vector competence

Arboviruses must be capable of replicating in both invertebrate vector and vertebrate host cells for propagation and transmission. The transmission potential of an arbovirus is determined by the number of infected vectors generated from a single host (which in turn is influenced by the number of vectors feeding on the host), the efficiency of arbovirus infection within individual vectors, the duration and level of host viraemia and the efficiency of transmission from an infected vector to a susceptible host.

An understanding of the events that occur when an arbovirus infects and successfully replicates in multiple tissues within an arthropod vector, is lacking in sufficient detail to predict which tissues are likely to become infected and when. This is particularly true for *Culicoides*, as current knowledge of the infection process is based only on a single study (Fu et al., 1999) and early observational studies of excised salivary glands, or detection of infectious virus or viral RNA in body compartments, such as the head. An understanding of viral dissemination between tissues is needed to model and predict the series and sequence of events that need to occur for a vector to successfully transmit virus. The current model to explain how BTV infects *Culicoides* is summarised in figure 1.6.

Figure 1.6

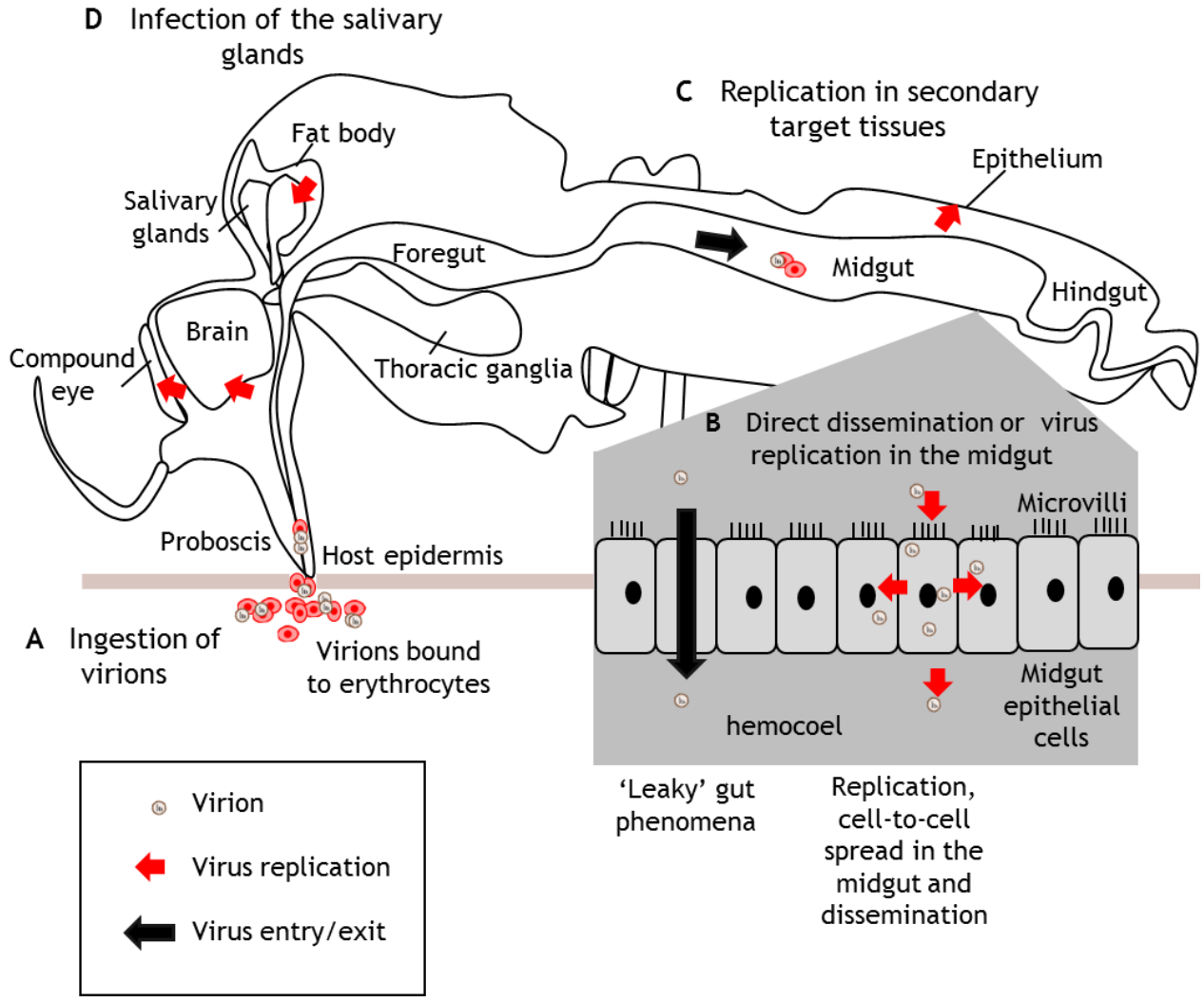

Figure 1.6: Model of bluetongue virus infection of *Culicoides*. (**A**) Virions are ingested with an infectious blood meal and enter midgut cells through the posterior midgut epithelium (Weaver et al., 1991, Fu et al., 1999). (**B**) Virus particles undergo initial replication and cell-to-cell spread in the midgut epithelial cells (red arrows) or disseminate without replicating in midgut cells ('leaky gut phenomena') (black arrow). (**C**) Virus disseminates from the midgut cells to infect and replicate in multiple tissues, most commonly the fat body, ommatidia of the compound eyes, the brain and epithelium (indicated by red arrows) (Fu et al., 1999, Fu, 1995). (**D**) Infection and replication in the salivary gland occurs (Bowne and Jones, 1966). Infectious viral particles, secreted in the saliva (Fu et al., 1999), are capable of infecting a susceptible host upon blood feeding (black arrows).

1.3.1. Pattern of arbovirus infection in arthropods

The general process of arbovirus infection within an arthropod vector is discussed in the following section and a summary is provided in table 1.2

Table 1.2: Summary of the stages involved during arbovirus infection of an arthropod vector. Processes that have not been shown during BTV infection of *Culicoides* are underlined and stages that may be bypassed by direct dissemination of virus into the haemocoel (Mellor et al., 2000) are shown in grey.

Infection stage	Time post-feeding	Description
1 Blood meal ingestion	0 h	Erythrocytes are lysed and VP2 is cleaved by gut proteases.
2 Infection of midgut epithelial cells	1 h	Virions (or core particles) bind to cell-surface receptors and enter midgut cells *by* CME, macropinocytosis or another mechanism. The location and timing and mechanism of entry may vary.
3 Replication in midgut cells	3 d	Virus particles spread cell-to-cell and replicate to a threshold titre prior to disseminating.
4 Dissemination into the haemocoel	Variable	Virus particles disseminate through *the* cardia, tracheal system, neural system or a combination of routes and are transported by haemocytes.
5 Infection of secondary target tissues	Variable	Virus infects and replicates in neural tissues, the foregut, malphigian tubules, ommatidia of the compound eyes, the fat body, antennae, oocytes and epithelial cells.
6 Infection and replication in salivary glands	>2 d	Virus particles enter the distal lateral lobes, replicate and bud from acinar cells entering the saliva. 0.32 to 7.79 $TCID_{50}$ of BTV is transmitted to a successive host during blood feeding.

During blood feeding, viruses and other pathogens circulating in the peripheral blood supply of the infected host are ingested concurrently with a blood meal (figure 1.6A). BTV particles aggregate in invaginations on erythrocytes (Sieburth et al., 1991, Brewer and Maclachlan, 1992, Brewer and Maclachlan, 1994) via NANA- and NGNA alpha 2-6GalNAc residues of glycophorins (Eaton and Crameri, 1989). The blood meal is directed to the posterior midgut by contraction of the diverticulum sphincter (Chamberlain and Sudia, 1961), where cell lysis and digestion are mediated by secreted hydrolytic proteases (table 1.2, infection stage 1), chiefly late (LT and 5GI) and early (ET) trypsins (Felix et al., 1991, Briegel and Lea, 1975), aminopeptidases (α-glucosidase) (Billingsley and Hecker, 1991, Billingsley, 1990, Graf and Briegel, 1989) and possibly by bacteria present in the posterior midgut, as shown for *Ae. aegypti* (Gaio et al., 2011). Gut proteases (e.g. trypsin or chymotrypsin) cleave VP2 of BTV into short polypeptides (Mertens et al., 1989), resulting in infectious sub-viral particles (ISVP) with approximately 10 to 100-fold higher infectivity for *C. sonorensis* (KC) cells, compared to intact BTV particles (Mertens et al., 1996b, Darpel et al., 2011).

The midgut lacks the cuticular lining, which is present in the foregut and hindgut (Richards and Richards, 1971, Maddrell and Gardiner, 1980, Billingsley and Lehane, 1996a). In the majority of cases, virus particles must infect midgut cells (table 1.2, infection stage 2), prior to inactivation in the lumen, formation of the peritrophic membrane (discussed in section 1.3.2) or excretion 3 to 4 days after feeding (Filimonova, 2005).

The mechanism of BTV entry is unknown and could depend on the viral strain and target cell type (mammalian or insect) (Stevens, 2016), which has made identification of receptors and entry mechanisms more complex. Other arboviruses bind to and enter microvilli via cell-surface receptors in a mechanism previously shown for *Cx. tarsalis* during western equine encephalitis virus (WEEV) entry and *Ae. aegypti* (Houk et al., 1990) during entry of chikungunya virus (CHIKV) (Mourya et al., 1998) and dengue virus (DENV) particles (Munoz et al., 1998, Mercado-Curiel et al., 2006, Mercado-Curiel et al., 2008). Entry of CHIKV arises by CME in *Ae. albopictus* C6/36 cells (Lee et al., 2013), prior to replication in midgut epithelial cells (figure 1.6B). The receptors targeted by most arboviruses for entry are not definitively known, however proteins, including prohibitin (Kuadkitkan et al., 2010), tubulin (Chee and AbuBakar, 2004), heat shock proteins (Salas-Benito et al., 2007), heparan sulphates (Chen et al., 1997) and LPS/CD14-associated binding proteins (Chen et al., 1999) have been implicated as putative cellular receptors for DENV and CHIKV.

Cell types in the midgut are heterologous (Filimonova, 2005) and covered with surface carbohydrate, which in *Ae. aegypti* may have an undefined role in pathogen entry (Zieler et al., 2000). Infrequently, dissemination may arise without replication in midgut cells, termed the 'leaky gut phenomenon', which was shown by limited studies during dissemination of Semliki forest virus (SFV) in *Ae. aegypti* (Boorman, 1960), Whataroa virus in *Ae. australis* (Miles et al., 1973), AHSV in *C. imicola* (Mellor et al., 1998) and eastern equine encephalitis virus (EEEV) in *Culiseta melanura* (Weaver et al., 1991) (figure 1.6B), but is not known to arise during BTV infection of *Culicoides*.

Ingested eastern equine encephalitis virus (EEEV) (Weaver et al., 1991) and BTV virions (Fu et al., 1999) can enter midgut cells present in the posterior midgut epithelium of *C. sonorensis*. The events during infection and replication of BTV in the midgut of *Culicoides* are not known. In other arboviruses, entry usually arises within an hour of ingestion (Smith et al., 2008, Weaver, 1986) (figure 1.6B). In some cases, infection can also occur through the proventriculus (the junction between the foregut and midgut), as shown for Rift valley fever virus (RVFV) (Romoser et al., 1987) and WEEV (Oviedo et al., 2011), and may depend on the site of contact between ingested viral particles and gut cells (Nuckols et al., 2013). Infection can initiate from as few as 1 to 5 (Smith et al., 2008) or 15 midgut cells (Scholle et al., 2004) in studies utilising VEEV and WNV VLPs, respectively. Isolated replication foci of O'nyong'nyong virus (ONNV) expressing GFP in the posterior midgut of *Anopheles gambiae* (Brault et al., 2004a) and DENV-2 in *Ae. aegypti* (Salazar et al., 2007) indicate that virus enters cells in a series of separate infection events. Replicating virus spreads cell-to-cell within the midgut (table 1.2, infection stage 3), usually by 3 days after feeding for DENV-2 in *Ae. aegypti* (Salazar et al., 2007). This period may be sufficient to reach a threshold titre required for dissemination (Hardy et al., 1983, Kramer et al., 1981).

At varying times post-infection, depending on the individual vector (Faran et al., 1988), virus particles can disseminate rapidly from the midgut epithelia into the haemocoel (Romoser et al., 1992) (table 1.2, infection stage 4). Dissemination may arise through the cardia (anterior end of the midgut at the proventriculus), shown for RVFV in *Cx. pipiens* (Lerdthusnee et al., 1995, Romoser et al., 1992), the tracheal system, demonstrated for SINV (Bowers et al., 1995), LACV (Chandler et al., 1998), DENV-2 (Salazar et al., 2007) and VEEV (Romoser et al., 2004), neural system (Hardy et al., 1983), via the haemolymph, or by a combination of these routes, shown for WEEV in *Cx. tarsalis* (Oviedo et al., 2011). These mechanisms enable virus particles to bypass the basal lamina, which may perhaps be facilitated by

structural alterations (Derksen and Granados, 1988, Weaver et al., 1988). The route by which BTV disseminates from infected midgut cells is unknown.

Within 6 hours of entering the haemocoel by IT inoculation, studies of a SINV clone expressing GFP (TE/592J/GFP) indicate that virions may be transported to non-midgut tissues by over 90% of haemocytes, predominantly by abundant granulocytes (Parikh et al., 2009, Castillo et al., 2006). Virions circulating in the haemolymph can infect multiple tissues within the insect (figure 1.6C).

The tissues infected and the timing of infection differ between studies e.g. DENV-2 in *Ae. albopictus* (Sriurairatna and Bhamarapravati, 1977) and *Ae.aegytpi* (Salazar et al., 2007), SLEV (Whitfield et al., 1973), WNV (Girard et al., 2004) and WEEV in *Cx. pipiens* (Wang et al., 2010). Infection of *C. sonorensis* with BTV and VSV involves: the neural tissues, (including the thoracic and oesophageal ganglia), ommatidia of the compound eyes, salivary glands, foregut, the fat body (Fu et al., 1999, Drolet et al., 2005) and the cardial epithelial cells (Fu et al., 1999). In other arboviruses, instances of infection of the Malpighian tubules (Salazar et al., 2007) and antennae (olfactory organs) were recorded , in which DENV is expressed at high levels (Sim et al., 2012).

Some arboviruses, including BTV-1 (Fu et al., 1999), are unable to infect oocytes, nurse cells, mature eggs (Romoser et al., 1992, Kuberski, 1979) or skeletal and smooth muscle (Salazar et al., 2007, Linthicum et al., 1996). In contrast, WEEV (Wang et al., 2010), VSV (Drolet et al., 2005) and La Crosse virus (LACV) (Chandler et al., 1998) were detected in chorionated eggs and ovaries of *Cx.tarsalis*, *C. sonorensis* and *Ae. triseriatus*, respectively, indicating that some arboviruses have the potential for vertical, transovarian transmission. If BTV is transovarially transmitted to progeny, the virus could remain dormant in overwintering larvae in temperate regions (Nevill, 1971) and might potentially cause an outbreak the subsequent year. Although VP7 was detected at 10% (3/319) and 30% (15/56) prevalence by RT-PCR in field collected *C. sonorensis* pupae and larvae (White et al., 2005), studies of laboratory reared *C. sonorensis* failed to isolate infectious BTV by plaque assay, or detect viral RNA by real-time PCR in first generation progeny (Nunamaker et al., 1990, Osborne et al., 2015). Hence, vertical transmission of BTV by *Culicoides* sp. is regarded as being improbable.

BTV infection of the salivary glands has been recorded in *C. sonorensis* by studies employing Transmisssion electron microscopy (TEM) (Bowne and Jones, 1966) and

immunohistochemistry (IHC) (Fu et al., 1999). Incidences of salivary gland infection (Janzen et al., 1970, Bergold et al., 1968) and replication are well documented in other arboviruses by studies using TEM, confocal imaging e.g. of EEEV in *Ae. triseriatus* (Whitfield et al., 1971), VEEV, SINV (Gaidamovich et al., 1973) and DENV-2 (Salazar et al., 2007) in *Ae. aegypti* and *in situ* hybridisation e.g. VSV in *C. sonorensis* (Drolet et al., 2005). Infection of the salivary glands has been considered a prerequisite for virus transmission upon blood feeding (figure 1.6D) and can arise as early as 2 days after virus ingestion for CHIKV in *Ae. aegypti* (Dubrulle et al., 2009).

Despite the suggested importance of the salivary gland for virus transmission, the means by which a virus can infect the salivary glands and enters the saliva are unknown for BTV and poorly characterised in other arboviruses (table 1.2, infection stage 6). The distal lateral lobes of the salivary gland are proposed as the site of entry for a number of mosquito-borne viruses, including DENV (Salazar et al., 2007), CHIKV (Janzen et al., 1970, Bowers et al., 1995) and VEEV (Gaidamovich et al., 1973).

Following replication, EEEV virions bud from the apical plasma membrane of acinar cells (Whitfield et al., 1971), entering luminal saliva and pass into a host upon blood feeding in conjunction with other salivary components. Salivary anti-hemostatic apyrase and purine nucleosidase (deLeon and Tabachnick, 1996) and immunomodulatory agents (Schneider and Higgs, 2008, Bishop et al., 2006) are secreted by *C. sonorensis* and may be capable of suppressing type II interferon (IFN-γ) production, which has been shown during SINV infection of *Ae. aegypti* (Schneider et al., 2004). During feeding, a small number of virions are transmitted to the host, averaging 0.5 to 3.2 potato virus Y particles (Moury et al., 2007). A titre of 0.32 to 7.79 $TCID_{50}$ (Foster et al., 1968) or 1.79 $TCID_{50}$ (Fu et al., 1999) of BTV is transmitted by *C. sonorensis* during blood feeding on a ruminant host.

Although no behavioural alterations during BTV infection of *Culicoides* have been proven. Mosquito-borne arboviruses can promote transmission-favourable activities, such as increased probing rate on a host (Grimstad et al., 1980, Platt et al., 1997b), enhanced locomotor activity (Lima-Camara et al., 2011a, Maciel-de-Freitas et al., 2013) and host-seeking behaviour (Sim et al., 2012). In some mosquito species, infection may increase overwinter survival, indicated by the overexpression of a salivary antifreeze protein during CHIKV infection of *Ae. aegypti* (Tchankouo-Nguetcheu et al., 2012).

1.3.2. Intrinsic within-vector 'barriers' inhibiting virus infection

The events during virus infection and dissemination within an insect vector are described in the previous section (1.3.1.). Key components of an insect's role in pathogen transmission can be described by equation 1.1, including vectorial capacity (*V*) (Garrett-Jones, 1964).

Equation 1.1

$$V = \frac{ma^2 2p^n b}{-ln(p)}$$

Where: *m* is the vector density per host, *a* is the daily probability of a vector biting a host, *p* is the daily probability of vector survival, *n* is the number of days of pathogen extrinsic incubation period (EIP) in the vector and *b* is vector competence.

Vector competence describes the ability of an arthropod vector to become infected and biologically transmit an arbovirus to a susceptible host (Gerry et al., 2001, Carpenter et al., 2015). Competence varies between different virus and vector combinations and vector species belonging to the same family can transmit pathogens with vastly different lifecycles, for instance *An. gambiae* are refractory to all arboviral infections, except ONNV. In contrast, *Ae. aegypti* can transmit a number of arboviruses, including DENV and CHIKV (Lambrechts, 2011). Even within a single vector species, such as *C. sonorensis*, only a proportion of individuals are susceptible to oral infection by a given virus, including BTV (Foster and Jones, 1973, Jennings and Mellor, 1987). The determinants of vector competence are poorly understood, despite their importance in enabling predictions of the likelihood of arbovirus transmission, its epidemic potential and 'risk'.

Intrinsic 'barriers', which include heritable, genetically determined immunological and physiological factors (Tabachnick, 1991), are one of the factors that underlie variation in vector competence. These barriers can be subdivided, depending on the stage of viral infection where they act, and are summarised in figure 1.7. The first organ that virions contact following ingestion is the midgut, which is arguably the most important organ in determining vector competence and may provide the sole determinant of infection of *Culicoides* spp. by BTV (Fu et al., 1999). Inhibition of virus entry or replication, during the early stages of midgut infection (e.g. receptor binding, viral genome transcription or translation), is considered to represent a 'midgut infection barrier' (MIB) and may be present in individuals that remain uninfected. If virions are unable to disseminate into the haemocoel

or establish infection in secondary target tissues, replicating virus remains non-disseminated in midgut cells, this is regarded as a 'dissemination barrier' (DB) or 'midgut escape barrier' (MEB). The existence of midgut barriers is confirmed by the failure of whole body titres less than $10^{2.5}$ to $10^{3.0}$ $TCID_{50}$ of infectious BTV or AHSV to infect orally dosed, non-transmissible *C. sonorensis* (Fu et al., 1999, Jennings and Mellor, 1987, Mellor et al., 2000). Non-transmissible individuals with a disseminated infection may possess a 'salivary gland infection or escape barrier' (SGIB or SGEB) which is absent in *C. sonorensis* (BTV-1) (Fu et al., 1999). Transmissible individuals, unable to vertically transmit virus to progeny possess a 'transovarial transmission barrier' (TOTB), as indicated by the absence of BTV-1 antigen in the oocytes or nurse cells of *C. sonorensis* (Fu et al., 1999).

Figure 1.7: Depiction of the theoretical 'barriers' known to inhibit infection of an arbovirus within an arthropod vector (adapted from (Mellor et al., 2000, Hardy et al., 1983)). Uninfected individuals (No infection, white) may possess a midgut infection barrier (MIB). Virus is restricted to the midgut of individuals with a midgut escape barrier (MEB) (Non-disseminated infection, grey) (Fu et al., 1999, Paulson et al., 1989). If virus disseminates but fails to infect secondary target tissues, salivary glands or ovaries (Disseminated non-transmissible infection, brown), a dissemination barrier (DB), transovarial transmission barrier (TOTB) (Fu et al., 1999), salivary gland infection (SGIB) or, salivary gland escape barrier (SGEB) (Paulson et al., 1989, Grimstad et al., 1985) operate, respectively. Transmissible vectors (orange) possess no barriers or either a salivary gland barrier or TOTB, depending on the route of transmission. Where: black font shows events during BTV infection of *Culicoides*, brown font shows events during arbovirus infection of mosquitos, arrow thickness indicates the likelihood of the infection route arising, with a thick arrow indicating a more likely outcome and infected regions are indicated in red.

Figure 1.7

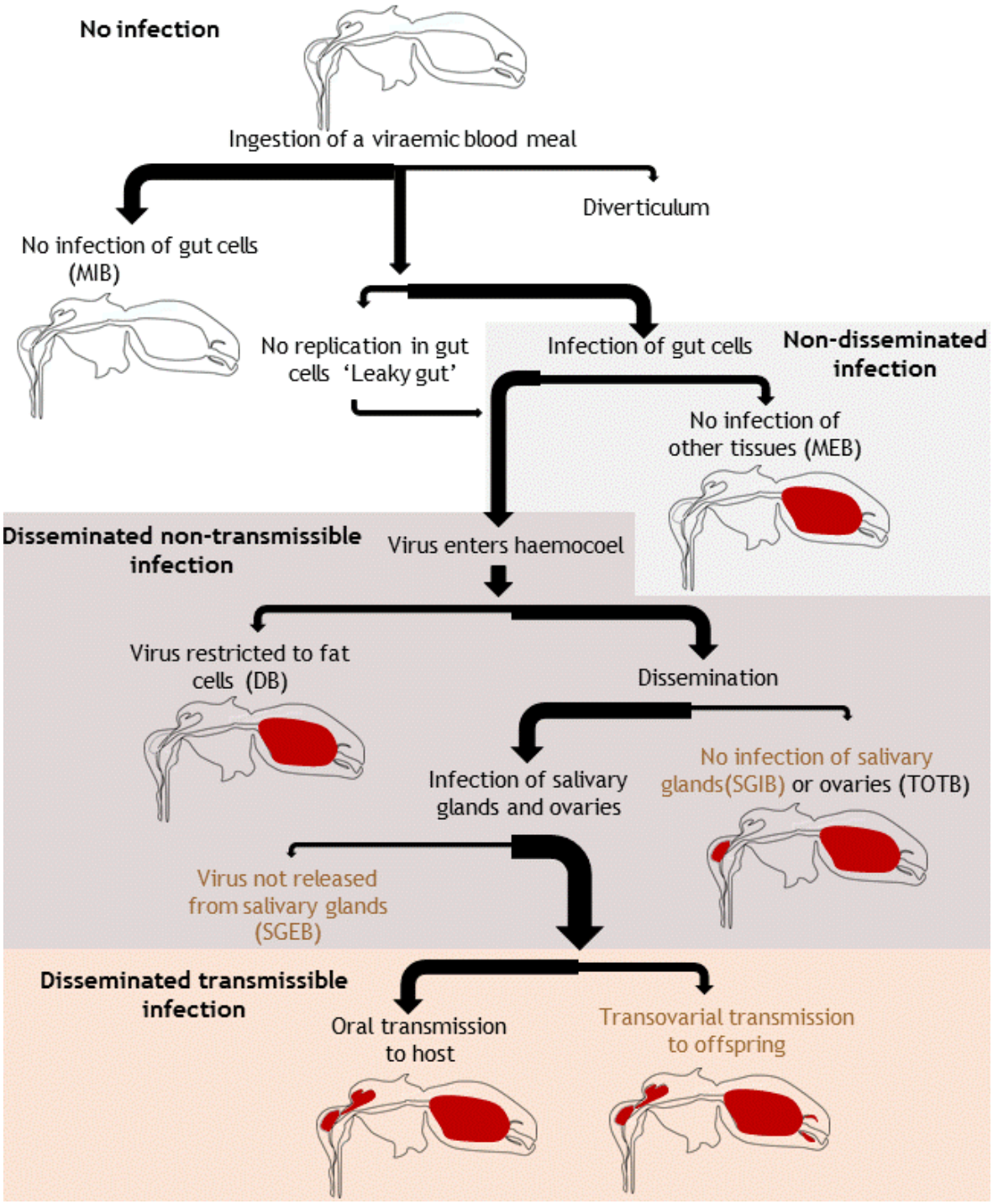
No infection
Ingestion of a viraemic blood meal
Diverticulum
No infection of gut cells (MIB)
No replication in gut cells 'Leaky gut'
Infection of gut cells
Non-disseminated infection
No infection of other tissues (MEB)
Disseminated non-transmissible infection
Virus enters haemocoel
Virus restricted to fat cells (DB)
Dissemination
Infection of salivary glands and ovaries
No infection of salivary glands(SGIB) or ovaries (TOTB)
Virus not released from salivary glands (SGEB)
Disseminated transmissible infection
Oral transmission to host
Transovarial transmission to offspring

Infection barriers

Infection barriers operate within a vector to inhibit virus entry into target cells. Mechanisms include: inactivation of virions by gut proteases, as demonstrated in *Ae. aegypti* by silencing of 5G1 (late trypsin), which resulted in a 25% increase in DENV-2 infection rate (Brackney et al., 2008). Additionally, physical infection barriers have been proposed as MIBs, including redirection of viraemic blood into the cuticular ventral diverticulum (Hardy et al., 1983) and, in non-*Culicoides* species (Filimonova, 2005), immobilisation of virions by thrombosis formation (Hardy et al., 1983), although there is poor evidentiary support for these mechanisms.

Basal laminae and the peritrophic membrane

Almost every tissue within an insect, with the exception of haemocytes, is separated from the haemolymph by a non-cellular basal lamina (BL) (Filimonova, 2004, Richards and Richards, 1971) which varies in thickness (Reddy and Locke, 1990). The BL is the primary barrier limiting movement of macromolecules between tissues and the haemolymph, depending on their size (Reddy and Locke, 1990, Houk et al., 1981) and molecular charge (Brac, 1983).

The BL forms during metamorphosis of *Cx. pipiens* (Romoser et al., 2005) and surrounds the midgut and salivary gland, posing a potential barrier to viral midgut escape (MEB) and salivary gland infection (SGIB). The mechanism enabling *Culicoides* and mosquito-borne arboviruses to bypass the BL is unknown. However, structural disruption of the BL (Houk et al., 1981, Weaver et al., 1988), formation of proteinaceous (P1-7) tubules containing virus particles (Jia et al., 2014) and infection of structures such as trachea, which intercept the BL of the midgut (Romoser et al., 2004), are proposed as mechanisms of evading the BL.

Most dipterans possess a proteinaceous type I peritrophic membrane (PM) (Richards and Richards, 1971) composed of chitin and heterologous layers of lamellae (Megahed, 1956) that is secreted on the basolateral surface of posterior midgut epithelial cells (Yurchenco and Orear, 1994) between 12 and 60 h after feeding (Megahed, 1956, Filimonova, 2005) in response to distension of the midgut epithelium (Freyvogel and Staeubli, 1965). The PM may function in haem detoxification in mosquitoes (Pascoa et al., 2002, Magalhaes, 2014) and provides a physical barrier against abrasive particles (Richards and Richards, 1977), separating blood from epithelial cells for up to 72 h after feeding in *Culicoides* spp. (Megahed, 1956, Sieburth et al., 1991). This spatial separation is presumed to prevent

contact of pathogens with epithelial cells and inhibit infection, which has been shown for *Cx.tarsalis* (Houk et al., 1979), *An. stephensi* (Orihel, 1975) and *Ae.aegytpi* (Villalon et al., 2003). However, the role of the PM as a MIB is not reinforced by experimental evidence in the case of *Glossina morsitans* infection by *Trypanosoma* sp. and *Enterobacter* sp. (Weiss et al., 2014). Indeed, the DENV infection rate was unaffected by silencing of chitin synthase and inhibition in PM formation in *Ae.aegypti* (Kato et al., 2008) and the presence of the PM did not prevent BTV infection of *C. sonorensis* midgut cells (Sieburth et al., 1991). Virus infection may arise prior to or after formation of the PM, as shown for DENV in *Ae.aegypti* (Suwanmanee et al., 2009) or, less likely, virus particles may structurally modify the PM to associate with epithelial cell receptors (Derksen and Granados, 1988).

Virus-specific cell receptors

Insect cells, namely C6/36 cells, possess multiple virus-specific receptors on their cell surface, which are utilised by arboviruses, such as WNV (Lee et al., 2006, Chu et al., 2006) and CHIKV (Lee et al., 2013), for entry in receptor-mediated endocytosis. A higher density of viral receptors on microvilli may increase the chance of virus infection, as midguts of susceptible mosquitoes, *Cx. tarsalis* and *Ae. aegypti*, bound more VEEV particles (Houk et al., 1990) and possessed a greater number of DENV binding proteins (R67/R64) than refractory strains, respectively (Mercado-Curiel et al., 2008). The absence of compatible receptors may prevent viral infection. Indeed, prohibitin, a 35 KDa DENV-2 receptor protein in *Ae. aegypti* C6/36 cells, is undetectable in the membrane proteins of non-DENV vector species (Kuadkitkan et al., 2010), or *C. quinquefasciatus* (Huang et al., 1992), implicating viral receptors as a determinant of competence. A 45 KDa protein which forms part of the DENV-4 receptor complex (Salas-Benito et al., 2007) was detected by western blot in excised midguts, ovaries and salivary glands of *Ae. aegypti* (Yazi Mendoza et al., 2002), indicating the role of virus-receptor interactions in infection of the salivary glands and ovaries(Cao-Lormeau, 2009).

The affinity with which virions bind to specific receptors may be dependent on virus genotype. Since the serotype of BTV and cell attachment by virions are both mediated by the highly variable outer-capsid protein, VP2, binding affinity may also vary with BTV serotype, or VP2 nucleotype. These variations could partially underlie vector compatibility for a specific viral strain. Indeed, midgut infection rate was 57% lower in *O. taeniorhynchus* orally infected with VEEV possessing a Ser → Asn substitution in the putative cell-binding domain of the E2 envelope protein (Brault et al., 2004b). Similarly, deletion of a 90 bp region

of the 3' terminus of SINV E2 conferred a 69% reduction in detection rate of E1 antigen in excised *Ae. aegypti* midguts (Myles et al., 2003), indicating that mutations in putative cell-binding domains impaired the ability of virions to bind to and/or enter midgut cells to initiate infection. However, strain-specific variation in viral-receptor binding affinity may not operate in the field as eight American and southeast Asian DENV-2 strains bound to midguts excised from two *Ae. aegypti* populations (Mexico and Texas) at the same rate when tested by real-time PCR, despite different competence rates (Cox et al., 2011). Differences in vector infection rate between viral strains may be due to variability in replication efficiency, perhaps associated with the antiviral immune response.

The antiviral immune response

Arthropods possess only an innate immune system, summarised in figure 1.8, which has been well characterised in *Drosophila* and mosquitoes. Conversely, little is known about the immune response of *Culicoides*, partly due to the lack of an openly available annotated genome. The publication of the *C. sonorensis* genome, which is currently under analysis at The Pirbright Institute, will facilitate these studies. Information presented here mostly derives from studies of mosquitos.

Figure 1.8: Summary of pathways implicated in the anti-viral immune response in arthropods (adapted from (Kingsolver et al., 2013, Barnard et al., 2012)).

(A) The Toll pathway (shown for *Drosophila*) is activated by pattern recognition receptors (PRRs), which recognise fungi or gram-positive bacteria, leading to activation of Toll ligand, Spätzle (Arnot et al., 2010). 'Spätzle' binds to the Toll receptor and induces the Toll-induced-signalling complex, consisting of MyD88, Tube and Pelle. Cactus is phosphorylated and cleaved from Dif. Dif translocates into the nucleus to upregulate antimicrobial peptide (AMP) production (Meng et al., 1999). The point at which viruses are recognised by the Toll pathway is unknown (Sanders et al., 2005, Xi et al., 2008).

(**B**) The immune deficiency (IMD) pathway (shown for *Drosophila*) is activated in response to detection of gram-negative bacteria (Lemaitre et al., 1995) and can inhibit viral infection by an unknown mechanism (Avadhanula et al., 2009). Death protein, dFADD, associates with the IMD protein (Naitza et al., 2002). A mitogen-activated protein (MAP) kinase, homologous to TGF-β-activated kinase 1 (dTAK1) (Vidal et al., 2001), triggers phosphorylation of Relish, which following proteolytic cleavage, translocates to the nucleus and upregulates antiviral gene expression.

(**C**) The Jak-STAT pathway is activated in response to viral infection (Souza-Neto et al., 2009, Dostert et al., 2005) by binding of Vago to an uncharacterised specific receptor (Paradkar et al., 2012). Ligand binding induces receptor dimerization, which allows for the trans-phosphorylation of the Janus kinase Hopscotch (hop), and recruitment of trans-phosphorylated 'signal transducer and activator of transcription' (STAT). Phosphorylated STATs dimerise and are transported to the nucleus, where they regulate the expression of anti-viral genes.

(D) The RNA interference (RNAi) response is elicited in response to dsRNA detection (Sanchez-Vargas et al., 2009, Kemp and Imler, 2009, Hoffmann, 2003). Viral-derived dsRNA is recognised by Dicer proteins and processed into 21 bp siRNAs, which are loaded onto pre-RNA induced silencing complexes (RISC). During recognition by Dicer2, Vago expression is induced, providing crosstalk with the Jak-STAT pathway (Paradkar et al., 2012). Double-stranded siRNAs are cleaved to generate a guide strand, which base pairs to complementary mRNA. Hybridised mRNA is degraded thus specifically downregulating viral protein synthesis.

Figure 1.8

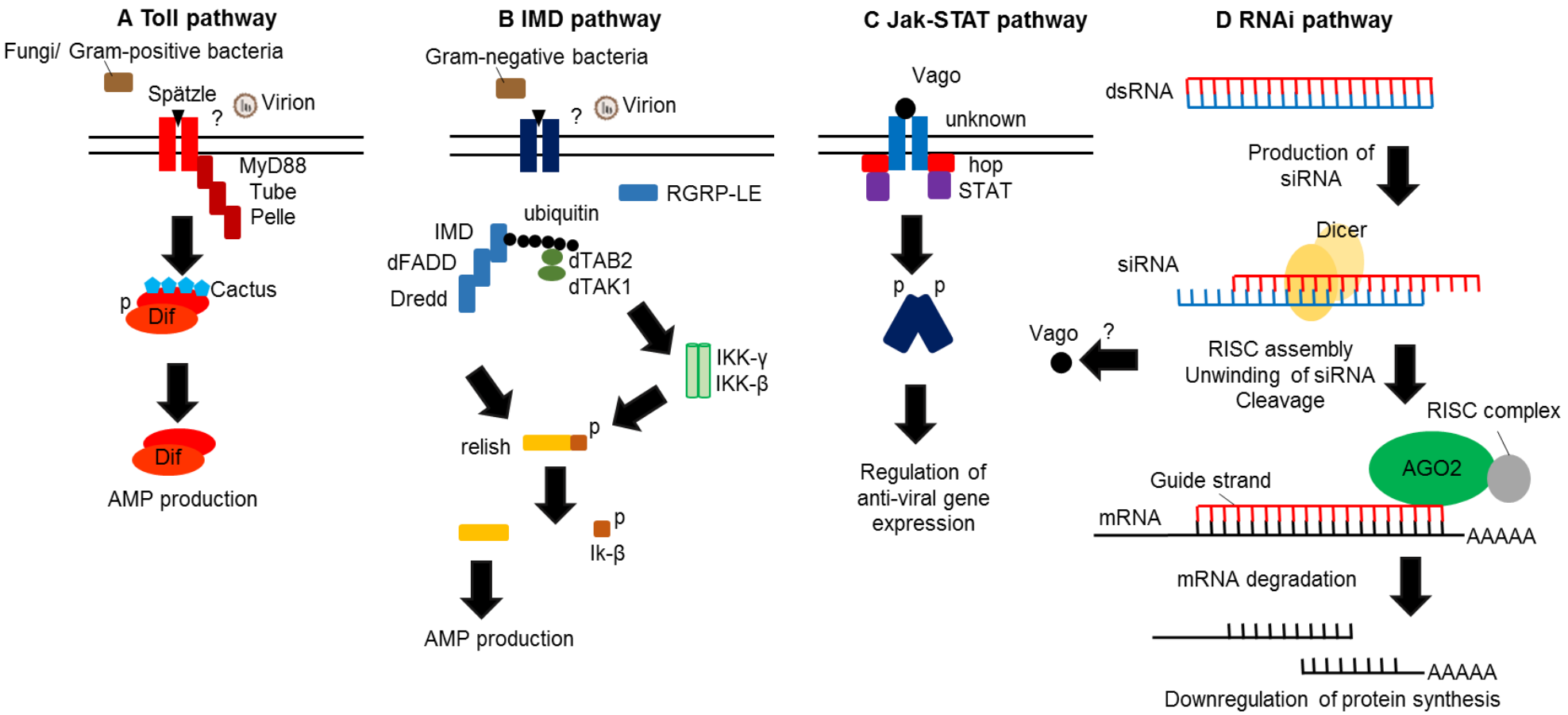
A Toll pathway
Fungi/ Gram-positive bacteria
Spätzle
?
Virion
MyD88
Tube
Pelle
p
Cactus
Dif
Dif
AMP production
B IMD pathway
Gram-negative bacteria
?
Virion
RGRP-LE
ubiquitin
IMD
dFADD
Dredd
dTAB2
dTAK1
IKK-γ
IKK-β
relish
p
p
Ik-β
AMP production
C Jak-STAT pathway
Vago
unknown
hop
STAT
p
p
Regulation of
anti-viral gene
expression
D RNAi pathway
dsRNA
Production of
siRNA
Dicer
siRNA
Vago
?
RISC assembly
Unwinding of siRNA
Cleavage
RISC complex
AGO2
Guide strand
mRNA
AAAAA
mRNA degradation
AAAAA
Downregulation of protein synthesis

Arthropod immunity against fungal and bacterial pathogens is mediated by the Toll (figure 1.8A) and immune deficiency (IMD) pathways (figure 1.8B) (reviewed by (Hoffmann, 2003)). Activation by reactive oxygen species (ROS) (Beutler, 2004, Iwanaga and Lee, 2005) triggers nuclear translocation of NF-kB transcription factors, resulting in the production of structurally diverse antimicrobial peptides (AMPs), including defensins and cecropins, which are upregulated during blood feeding in *C. sonorensis* (Nayduch et al., 2015). Bacterial infection can also activate the Janus Kinase, Signal Transducer and Activator of Transcription (JAK-STAT) pathway (figure 1.8C). The IMD, JAK-STAT and Toll pathways may also function in part as an anti-viral response e.g. in *Drosophila* and *Ae.aegypti* (Dostert et al., 2005, Xi et al., 2008, Avadhanula et al., 2009), as upregulation of Toll pathway genes, Rel-1 and putative Pattern Recognition Receptors (PPRs), corresponds with a reduction in infectious DENV titre in *Ae. aegypti* (Xi et al., 2008). Similarly, defensins and cecropins which normally act against gram positive and gram negative bacteria (Hoffmann, 2003), respectively, also inhibit DENV proliferation in *Ae. aegypti* (Pan et al., 2012).

ROS expression is upregulated during CHIKV infection, and in *Ae. aegypti* experimentally infected with certain species of symbiotic bacteria, *Wolbachia* (Pan et al., 2012, Tchankouo-Nguetcheu et al., 2010). Upregulation of ROS is proposed to indicate that a pre-existing infection could activate Toll-mediated antiviral immunity and suppress subsequent viral replication (Luplertlop et al., 2011). Although the mechanisms responsible for reduced viral replication in pre-infected individuals are unknown, many incidences have been demonstrated. Indeed, *Cx. pipiens* with a pre-existing SLEV infection had a lower WNV infection and dissemination rate than uninfected *Cx. pipiens* (Pesko and Mores, 2009). Similarly, DENV replication may be suppressed in *Wolbachia*-infected *Ae. aegypti* (Bian et al., 2010). The inhibitory effect on DENV replication only occurred when *Wolbachia* reached a density above that occurring in *Ae. albopictus* tissues in the field (Bian et al., 2010, Lu et al., 2012), indicating that *Wolbachia*-mediated inhibition in viral replication may only hold relevance for DENV control strategies, rather than as a naturally occurring MIB. Removal of endogenous bacteria increased DENV titre in the midgut of *Ae. aegypti*, suggesting that commensal bacteria of some arthropods may also upregulate antiviral responses and act as a MIB (Xi et al., 2008, Ramirez et al., 2012). However, the effect of commensal midgut bacteria on arboviral infection may vary between arthropod species as ONNV load was reduced in antibiotic treated *An. gambiae* (Carissimo et al., 2015). The influence of midgut bacteria on BTV infection rate of *C. sonorensis* is examined in detail in Chapter 5.

Evolutionary-conserved RNAi-mediated gene silencing is considered the major anti-viral response in arthropods (figure 1.8D) (Sanchez-Vargas et al., 2009, Kemp and Imler, 2009, Hoffmann, 2003) and has been demonstrated to act in *Culicoides* (KC) cells during BTV infection (Schnettler et al., 2013). RNAi-related genes were not upregulated during DENV infection of *Ae. aegypti*, suggesting that components of the RNAi pathway may be constitutively expressed in arthropod cells (Xi et al., 2008, Campbell et al., 2008). RNAi is triggered in the presence of intracellular dsRNA and encompasses the micro RNA (miRNA), Piwi-interacting RNA (piRNA) and small-interfering RNA (siRNA) pathways. The exogenous siRNA pathway (figure 1.7D) is activated in response to long intracellular dsRNA, formed by the virus genome or viral replication intermediates such as RNA stem-loop structures (Flynt et al., 2009, Sabin et al., 2013), and results in degradation of mRNA complimentary to the dsRNA target sequence, thereby downregulating viral protein synthesis. The siRNA pathway limits initial infection of midgut epithelial cells of the small brown plant hopper by Southern rice black-streaked dwarf virus (SRBSDV) infection (Lan et al., 2016). The systemic spread of the target sequence specific RNAi signal, shown in mosquitoes (Attarzadeh-Yazdi et al., 2009), likely restricts virus dissemination to contacting secondary target tissues, providing a barrier inhibiting viral dissemination, predominantly in the midgut and fat body (DB and MEB) (Deddouche et al., 2008). The role of the siRNA pathway during arboviral infection of *Culicoides* requires further investigation.

In contrast to vertebrates, where type I IFN-β synthesis upregulates proapoptotic genes (Chawla-Sarkar et al., 2003, Chen et al., 2001); arboviral infections are generally considered as non-pathogenic and persistent in arthropods. Apoptotic changes in midgut (Vaidyanathan and Scott, 2006) and salivary gland cells (e.g. *Cx. pipiens* (Girard et al., 2007) and *Ae. albopictus* (Kelly et al., 2012)) and downregulation of inhibitor of apoptosis gene (*IAP*-1) during SINV and WNV infection, indicate that arboviral infections can also induce apoptosis and elevated vector mortality (Lambrechts and Scott, 2009). Apoptosis of insect cells could act as a potent anti-viral response e.g. during SINV and WNV infection (O'Neill et al., 2015, Wang et al., 2012, Vaidyanathan and Scott, 2006). Indeed, replication and salivary viral titre were lowered and infection of the midgut was delayed in a SINV clone expressing the proapoptotic gene, reaper (MRE/Rpr), compared to parental SINV in *Ae. aegypti* (O'Neill et al., 2015), indicating that apoptosis can act as midgut and salivary gland escape barriers.

1.3.3. Factors affecting intrinsic 'barriers'

Barrier efficiency, and hence vector competence rates, are altered by a number of genetic and extrinsic environmental conditions (Richards et al., 2009, Oviedo et al., 2011). These factors include: viral strain, which was shown to alter competence of *C. sonorensis*, *C. imicola* and *C. bolitinos* to infection with BTV (Wittmann et al., 2002, Venter et al., 1998) and CHIKV in *Ae. albopictus* (Vazeille et al., 2007); ambient temperature, (shown for BTV-1 in *C.imicola* (Paweska et al., 2002b)); viral dose ingested; vector species; body size and nutritional status (Pesko et al., 2009, Grimstad and Haramis, 1984, Grimstad and Walker, 1991). Interplay between these factors determines the length of the extrinsic incubation period (EIP) of a virus, the earliest time at which a virus is released into the saliva and is transmissible, which ranges from 4 days for BTV-9 (Carpenter et al., 2011) to 15 days after ingestion for BTV-10 in *C. sonorensis* maintained at 25ºC (Wittmann et al., 2002).

Vector physiology and genetics

Most of the barriers underlying differences in competence discussed in the previous section are genetically controlled (Bosio et al., 2000, Bennett et al., 2005). Susceptibility to arboviral infection is encoded by multiple, heritable genes in *Ae. aegypti* (Miller and Mitchell, 1991, Bosio et al., 1998) which vary between different field populations within a vector species (Pongsiri et al., 2014a) and are transcriptionally upregulated in response to blood feeding (Shin et al., 2014). Many studies have employed mating strategies to select for increased vector competence, identifying a maternally inherited recessive allele, *blu*(s), responsible for susceptibility to BTV infection in cross-bred *C. sonorensis* (Tabachnick, 1991). Genetic mapping of refractory and susceptible vector stains has revealed multiple 'quantitative trait loci' (QTL) involved in susceptibility (Bosio et al., 2000, Gomez-Machorro et al., 2004), including two QTL for a MIB on chromosomes II and III, accounting for about 30% of phenotypic variance and 44 to 56% of overall genetic variance between DENV-2 susceptible and refractory *Ae. aegypti* (Bosio et al., 2000).

Many of the genes underlying vector competence are still uncharacterised (Bosio et al., 1998). The availability of a growing number of arthropod vector genomes and increasing affordability of high throughput sequencing technologies, will help to identify novel genes associated with susceptibility to arboviral infection. A transcriptomics study of two *Cx. pipiens* populations with different WNV competence rates, revealed differential expression of 118 gene transcripts, involved in catalysis (including trypsins) and vitellogenesis, in response to blood feeding on WNV (Shin et al., 2014). This indicates that these genes may

play a role in determining refractory or susceptible phenotypes. Similarly, the basal level of immune gene expression was higher, but vascular ATPase subunit G (vATPase) expression was downregulated in midgut and carcass transcriptomes of DENV refractory *Ae. aegypti*, compared to susceptible strains. This indicates the involvement of immune genes (including components of Toll, IMD, RNAi and JAK-STAT pathways) and vATPase during DENV entry and egress, respectively (Sim et al., 2013).

Non-genetically determined physiological traits, including adult age, condition and body size, act additively to alter competence (Richards et al., 2009, Richards et al., 2007). Younger vectors are more likely to survive to completion of the EIP and obtain a second blood meal and are more susceptible to infection than older vectors (e.g. WNV in *Cx. tritaeniorhynchus* (Richards et al., 2009) and SLEV in *Cx. pipiens* (Baqar et al., 1980)). The influence of age on vector competence is less likely to hold much relevance for arbovirus transmission in field populations (Richards et al., 2009) due to a mixed, temporally and environmentally variable age demographic (Walker, 2001).

A smaller adult body size can be caused by high ambient temperatures during larval development and a high level of larval competition for resources (Grimstad and Walker, 1991, Bara et al., 2015). Body size has long been suspected as an important factor contributing to vectorial capacity (Grimstad and Haramis, 1984), but this is not definitively proven. The 'leaky gut phenomenon' may be more prevalent in smaller individuals, as BL thickness is body size-dependent and shown to be 10 µm thinner in smaller, nutritionally deprived female *Ae. triseriatus* (Grimstad and Walker, 1991), enabling virions to bypass the BL. Indeed, some studies indicated that *Ae. agypti* and *Ae. albopictus* with a smaller body size, fed on DENV, were more likely to become infected than larger mosquitoes, independent of vector species (Alto et al., 2008). However, other studies have found no association between dissemination rate and body size (Bosio et al., 1998, Schneider et al., 2007, Dodson et al., 2011), or even a reduced dissemination rate in smaller individuals (Bara et al., 2015, Sumanochitrapon et al., 1998).

Age and determinants of body size, including larval rearing temperature and nutrition, are standardised in experiments presented in Chapters 4 and 5.

Ambient temperature

Incidence, seasonal variation and global distribution of vector-borne viruses, such as BTV (briefly discussed in Section 1.2.2.) are influenced by climate and are likely to alter with climate warming (Wittmann and Baylis, 2000). Ambient temperature is a major element of vectorial capacity and has been the subject of numerous reviews (Mullens et al., 2004, Hardy et al., 1983). Host biting rate, adult survival, development time and duration of the EIP of many vector-borne pathogens, are temperature dependent. High ambient temperatures, within the range above the minimum threshold for *Orbivirus* replication of 11 to 13ºC (Carpenter et al., 2011), can reduce vector survival rates (Hunt et al., 1989), EIP (Wittmann et al., 2002, Mullens et al., 1995) and, in most instances increase vector competence (Turell and Lundstrom, 1990), depending on viral strain (Wittmann et al., 2002), as shown for BTV-1 in *C. sonorensis* (Paweska et al., 2002b).

Indeed, susceptibility of adult female *C. sonorensis* to AHSV increased from 15% when maintained at 15ºC throughout development, to between 70 and 80% at 25ºC (Mellor et al., 1998). Exposure of immature life stages to elevated temperatures is a contentious determinant of vector competence and is considered likely to depend on vector species, with studies concluding no effect (e.g. WNV in *Cx. tarsalis* (Dodson et al., 2012)), an increase (e.g. AHSV-9 in *C. nubeculosus* (Mellor et al., 1998)) or a reduction in viral dissemination and infection rate (e.g. CHIKV in *Ae. albopictus* (Westbrook et al., 2010)).

In nature, vectors are subjected to temperature variations throughout the day. Large temperature fluctuations (Carrington et al., 2013) and variation in daily temperature range of 16 and 20ºC, have been shown to reduce infection rate at temperatures above 21ºC for *Plasmodium* sp. and 18ºC for DENV, respectively, but at temperatures below 18ºC and 21ºC EIP is reduced and predicted transmission rates increase (Paaijmans et al., 2010, Paaijmans et al., 2009, Lambrechts et al., 2011). Clearly the influence of temperature on vectorial capacity of field vector populations is complex. Seasonal and annual stability in BTV-1 infection rate (17 to 23%) of field populations of *C. sonorensis* (Gerry et al., 2001) could result from an averaging effect of stochastic environmental conditions.

Ingested viral dose

It is assumed with some empirical evidence (Lord et al., 2006) that threshold host viremias are needed to infect different insect vector species in nature (Reisen et al., 2005, Turell et al., 2005, Mertens et al., 1996b) and that the infectious titre varies between vector

populations (Bennett et al., 2002, Pesko et al., 2009), depending on vector genotype. If this is the case, low host viremias could reduce vector-borne transmission rate in the field (Lord et al., 2006).

Correlation between the number of vectors infected and viral dose ingested is well established and has been demonstrated for DENV-2 in *Ae. aegypti* (Pongsiri et al., 2014b, Bennett et al., 2002); WEEV in *Cx. tarsalis* (Mahmood et al., 2006); *C. sonorensis* and *C. nubeculosus* (Mertens et al., 1996b). Vectors ingesting a higher dose are more likely to become infected, reflecting the independent action hypothesis (IAH). In the IAH each virion acts independently and has a probability of infection (Furumoto and Mickey, 1967, Zwart et al., 2009, Druett, 1952). The effective population size (Zwart et al., 2011), and therefore probability of viable virions entering to midgut epithelial cells, increases with dose (Houk et al., 1990, Cox et al., 2011) and at low doses the mean number of virions causing infection approaches 1 (Zwart et al., 2011) and many blood meals may contain no infectious virus particles.

Generally, EIP is shortened and more vectors develop a disseminated infection after ingesting a higher viral titre (Anderson et al., 2010, Richards et al., 2009, Mahmood et al., 2006). It may be that entry of a greater number of virus particles, i.e. a higher initial MOI, may enable the minimum threshold titre for dissemination from the midgut to be reached more rapidly (Mahmood et al., 2006). However, the influence of ingested viral dose on disseminated infection rate varies between studies (Bennett et al., 2002, Richards et al., 2007, Kramer et al., 1981), as MOI does not always reflect initial dose and changes at different stages of infection (Gutierrez et al., 2015) or in different organs and varies between virus genotypes e.g. VEEV (Weaver et al., 1984, Smith et al., 2007).

Although infection rate and potentially dissemination rate are lower at low doses, baculovirus infectivity (White et al., 2012) and genetic diversity are higher during infections initiating from low doses e.g. *Helicoverpa armigera* nucleopolyhedrovirus (Baillie and Bouwer, 2013). Taken together, this may mean that fewer, but more highly infectious vectors could result from a blood meal containing a lower viral dose. Dose-dependent changes in virus infectiousness warrant further investigation in arbovirus-vector systems. The influence of viral dose ingested during blood feeding on within-vector infection dynamics provides the focus of studies in Chapter 5.

1.3.4. Approaches to modelling virus infection within insects

A multicellular organism is a complex, spatially organised environment, offering challenges and opportunities for viral evolution and proliferation. Barriers that inhibit arbovirus transmission (discussed in Section 1.3.2) are vector or virus specific and may be modified by complex interactions between factors such as ambient temperature, viral dose, other bacterial or viral infections and, controversially, vector physiology including age (reviewed in Section 1.3.3). Modelling is an important tool in assessing how processes within an organism can affect pathogen transmission dynamics and behaviour under stochastic interacting factors.

Although, pathogen spread at population and at cellular levels has been documented empirically (Power et al., 1992, Lord and Day, 2001), the dynamics of within-host pathogen infection remain poorly understood (White et al., 2012). During the last decade, several studies have examined changes in viral genetic diversity to estimate the size of within-host population bottlenecks, by quantifying the number of viral genotypes, or cells that become infected by a given genotype in mammalian or invertebrate host tissues (Kuss et al., 2008, Miyashita and Kishino, 2010, Moury et al., 2007). Only a few, recent studies have empirically determined the rate of cellular, within-host, viral spread and localisation (Gutierrez et al., 2015, Tromas et al., 2014). A study of TEV replication in *Nicotiana tabacum* fitted a 'susceptible-infectious' (SI) meta-population dynamics model to flow cytometry TEV-fluorescent cell counts, showing that TEV growth ranged from 1.342 cells/cell/d at 3 dpi, to 0.196 cells/cell/d, 7 dpi and depended on the leaf type (Tromas et al., 2014). Current models of within-arthropod host growth have concerned fitness of pathogenic baculoviruses (Ebert and Weisser, 1997, White et al., 2012) and hold little relevance to non-pathogenic arboviruses.

Viral quantity and localisation have not been directly compared at cellular resolution within tissues of individual insects, partly due to the lack of suitable techniques to generate quantitative and qualitative data. Techniques including imaging of labelled virions e.g. [3H]uridine-labelled EEEV (Weaver et al., 1991), real-time PCR e.g. DENV-2 (Zhang et al., 2003), virus isolation, immunofluorescence and *in situ* hybridisation e.g. VSV (Drolet et al., 2005), YFV (McElroy et al., 2008) and DENV-3 (Linthicum et al., 1996), have been applied separately to determine temporal changes in arboviral growth within whole insects, or viral

presence in excised organs e.g. for RVFV (Faran et al., 1988) and EEEV (Scott et al., 1984, Weaver et al., 1991). Studies that have indirectly related virus quantity to localisation e.g. DENV-2 (Salazar et al., 2007), LACV (Chandler et al., 1998) and EEEV (Scott et al., 1984), applied techniques at different resolution, for instance comparing whole-insect viral titre with viral antigen localisation in sectioned organs, shown for BTV-1 (Fu et al., 1999).

The recent development of fluorescent reporter viruses (Pierson et al., 2005), have included a replication-competent BTV (Shaw et al., 2012) (reviewed in Chapter 3), and hold promise for future efforts to quantitatively and map dissemination of arboviruses within the tissues of hosts (Palha et al., 2013) and insect vectors (McGee et al., 2010) at accurate, cellular resolution. Such data could provide a foundation for the first empirically-based, quantitative model of pathogen growth within an arthropod vector.

1.4. Summary and project objectives

Infection of an insect with an arbovirus, the dissemination of the infecting viral particles and virus replication through susceptible tissues is complex and, presently, very poorly understood. In nature, environmentally determined factors, such as ingested dose and ambient temperature, operate with varying magnitude at each stage of the infection process to either promote or inhibit viral infection and replication. These factors act additively with polygenic traits, determined by virus stain, to control the overall competence of the vector for a specific arbovirus. Predicting the probability of a vector developing a transmissible infection within an individual arthropod vector, is central to forecasting shifts in arboviral epidemiology with projected climate change, or changes in the distribution of the virus, or of known vector species, and involves first understanding the events that occur within the arthropod vector prior to transmission. This is particularly important for targeting control strategies for non-endemic or emerging arboviruses, such as BTV and Zika virus, respectively.

The importance of a quantitative description of pathogen infection within an individual arthropod vector, for control of socioeconomically significant pathogens has fuelled interests in modelling 'within-vector' pathogen replication. Currently, the infection process within an arthropod vector has only been described qualitatively, the timing and approximate order of tissue infection is crudely known and factors influencing vector competence have mostly been examined in terms of their effect on whole-insect infection rate. There are no quantitative empirically-based studies of pathogen growth within an arthropod vector under fixed, or varying conditions that would enable investigators to model the infection process. Quantitative studies have been constrained by lack of high-throughput, accurate means of localising virus with cellular resolution in individual insects, which would enable viral quantity to be compared between and within tissues.

The overarching purpose of studies presented in this thesis is to describe the replication of an arbovirus within an arthropod vector. Specifically, studies aim to determine temporal changes in viral quantity within individual insect tissues and examine the influence of viral strain and initial viral dose on within and between tissue virus localisation and quantity. These studies use the BTV-*C. sonorensis* interaction as a model arbovirus-vector system.

The individual objectives of studies presented in this thesis are as follows:

I. Develop a precise and reproducible means of localising BTV within tissues of *C. sonorensis*, which is robust to changes in intrinsic conditions including BTV strain and ingested viral dose.

II. Develop an accurate and reproducible method of quantifying BTV infection, including the quantity of viral particles and/or viral gene expression, at cellular resolution in tissues of interest.

III. Analyse the infection process, including viral quantity and temporal changes in the tissues of *C. sonorensis* that have been infected with BTV under standard laboratory conditions.

IV. Examine the influence of altering BTV strain on a standardised infection process, including any characterising temporal changes and viral quantity within the infected tissues.

V. Determine the effect of removing endogenous midgut bacteria on the infection rate of *C. sonorensis* with BTV.

VI. Determine the outcome of ingestion of a blood meal containing a high or low dose of BTV, on the infection rate and disseminated infection rate of *C. sonorensis*. Then compare differences in BTV localisation and quantity within and between tissues.

Chapter 2

Materials and methods

2.1 Cell lines

BSR cells, a clone of BHK-21 cells known to exhibit severe cytopathic effect (CPE) during BTV infection (Shaw et al., 2012), were cultured in Dulbecco's Modified Eagle's Medium (DMEM) supplemented with 10% heat inactivated Fetal Bovine Serum (FBS), 100 U/ ml penicillin and 100 mg/ml streptomycin (P/S) (Gibco®). CPT-*Tert* cells (Arnaud et al., 2010), sheep choroid plexus cells immortalised with the simian virus 40 T antigen and human telomerase reverse transcriptase (hTERT), were grown in Iscove's modified Dulbecco's medium (IMDM) (Gibco®), supplemented with 10% FBS and P/S as above. Both cell lines were incubated at 37°C and 5% CO_2.

KC cells were originally derived from *Culicoides sonorensis* pupae (Wechsler et al., 1989) and were grown in Schneider's Drosophila medium (Gibco®), supplemented with 15% FBS and P/S as previously described in this section. KC cells were maintained at 28°C and 5% CO_2 for the duration of the study.

2.2 Virus isolates

An isolate of the South African reference strain of BTV-1 (P2 CE, P9 BHK) (ICTVdb isolate accession number [RSArrrr/01]), termed BTV-1 SA, and BTV-11 (EC 1, P3 BHK, P2 KC) (ICTVdb isolate accession number [USA2005/01]), which was originally isolated from an outbreak in deer in South Dakota and referred to here as BTV-11 USA, were kindly provided by Dr Gillian Pullinger and Dr Kyriaki Nombiou (The Pirbright Institute, UK) from the *Orbivirus* Reference Collection at the Pirbright Institute (available at www.iah.bbsrc.ac.uk/dsRNA virus proteins/ReoID/orbiviruses.htm) for use in studies presented in Chapters 4 and 5 of this thesis.

Virus stocks were generated by infecting BSR cells at an MOI of 0.05 and harvesting cell-free supernatant at 72 h post-infection. Stocks for infecting *C. sonorensis* were generated by harvesting the cell layer at ~80% CPE and lysing cells by freeze-thawing twice on dry ice, to maximise titre. Viruses were passaged twice in BSR cells (P2 BSR) prior to storage at 4°C. Mammalian cells were selected to avoid prior adaption to KC cells (Stevens, 2016), and more closely mimic transmission from mammal to arthropod. The titre of virus stocks was assessed by end-point dilution assay described in section 2.5.

2.3 Experimental oral infection of *Culicoides*

Adults of the North American BTV vector species, *C. sonorensis* (PIRB-s-3 strain), which was selected for susceptibility to BTV infection (Tabachnick, 1991), were kindly provided by Mr Eric Denisen (The Pirbright Institute, UK) and maintained with *ad lib* access to 10% sucrose (Sigma-Aldrich) at 25±2°C and 70 to 80% relative humidity in card pill boxes. *C. sonorensis* were starved overnight prior to feeding on defibrinated horse blood (TCS Biosciences), as previously described (Mellor, 1971) with substitution of chick skin for Parafilm® M (Sigma-Aldrich). Blood was supplemented with a specified dose of BTV-1 or BTV-11, generated as above. A mock infected control was included, fed on blood containing DMEM with 5% FBS Immediately after feeding, *C. sonorensis* were anaesthetised with CO_2 and engorged females were identified by their swollen red abdomen, counted, transferred to a fresh card box and maintained as previously. Blood inoculum was retained at 4°C and engorged *C. sonorensis* (n = 8) were stored individually in nuclease free H_2O at -80°C, then processed for quantitative reverse transcription PCR to determine the number of copies of BTV ingested, in accordance with methods described in section 2.15.

At stated times after feeding, *C. sonorensis* were anaesthetised under CO_2 on a 'Fly Pad' (Fisher Scientific) overlain with AeraSeal™ film (Excel Scientific). Live *C. sonorensis* were identified by movement in response to a physical stimulus, counted and processed for imaging as described in 2.18.2, or stored individually in nuclease free H_2O at -80ºC for quantitative reverse transcription PCR, as described in section 2.14. Prior to sorting *C. sonorensis* for quantitative reverse transcription PCR, equipment was treated with DNAZap™ PCR DNA Degradation Solutions, followed by RNaseZap® RNase Decontamination Solution (Ambion™). To assess disseminated and non-disseminated infection rates by quantitative reverse transcription PCR under various BTV-1 SA blood meal doses (see section 5.2.3, Chapter 5), *C. sonorensis* were decapitated on a Superfrost™ slide (SLS Scientific) using separate BD PrecisionGlide™ Needles (BD Biosciences). Excised heads and bodies were stored individually in nuclease free H_2O at -80ºC.

The survival rate was calculated by expressing the number of surviving *C. sonorensis* as a percentage of the number of *C. sonorensis* sorted immediately after blood feeding and plotted using Microsoft Excel software (Microsoft Office 2013).

2.3.1 Antibiotic treatment

Recently emerged *C. sonorensis* were maintained as described above (section 2.3) with *ad lib* access to 10% sucrose (Sigma-Aldrich) supplemented with 15 mg/ml of Gentamicin (Gibco™), 100 mg/ml of streptomycin and 100 U/ml of penicillin (Sigma-Aldrich), respectively. An untreated control group were supplied *ad lib* with 10% sucrose (Sigma-Aldrich). At stated times after treatment, *C. sonorensis* (n ≈ 60) were euthanised at -20ºC, females were identified and sterilised by submerging in 70% ethanol, followed by sterile PBS. Midguts (n = 40) were removed on a Superfrost™ slide (SLS Scientific) using 25 gauge BD PrecisionGlide™ Needles (BD Biosciences).

Midguts were homogenised in groups of ten in Super Optimal Broth with Catabolite repression (S.O.C) medium (Invitrogen™) using a sterile 5 mm steel bead (QIAGEN) at 25 Hz for 1 min with a TissueLyser II disruption system (QIAGEN) (Veronesi et al., 2008). A control of S.O.C medium was included to test for contamination. Homogenates were incubated with shaking at 25±1ºC for 1h, diluted in a 10-fold series and plated onto LB agar plates. Plates were incubated overnight at 25±1ºC; colonies were counted and expressed as Colony Forming Units (CFU/ml) using equation 2.1.

Equation 2.1

$$\mathrm{CFU/ml} = \frac{n \text{ x } \mathrm{d}}{v}$$

Where: d = $\log_{10}$ of the dilution factor, n = the number of colonies, v = volume of culture plate.

Molecular methods

2.4 Reverse genetics

2.4.1 Plasmids for virus rescue

Plasmids containing cDNA copies, one of each of the 10 segments of BTV-1 (ICTVdb isolate accession number [RSArrrr/01]) were as described previously (Ratinier et al., 2011, Boyce et al., 2008). Copies of each BTV genome segment were cloned into a pUC57 backbone (Fermentas) immediately downstream of a T7 promoter and upstream of a *BsaI* restriction site, permitting linearisation. Plasmids were kindly provided by Dr Andrew Shaw (University of Glasgow, UK).

The coding sequence of eGFP, possessing P64L and S65T polymorphisms shown to enhance fluorescence intensity (Cinelli et al., 2000), was amplified from 50 ng of plasmid DNA using primers listed in Table 2.1 and PfuUltra™ II Fusion HotStart DNA polymerase (Agilent Technologies), according to the manufacturer's instructions. The PCR product was purified following agarose gel electrophoresis using the QIAquick gel extraction and PCR purification kits (QIAGEN).

The eGFP gene was introduced at either of two sites on the cDNA copy of segment 5: immediately upstream of the 3' UTR, generating a *C*-terminal NS1 polyprotein (NS1-eGFP). Alternatively, eGFP, possessing the segment 5 UTR, was fused to the 3' terminus of segment 5 (NS1/eGFP), creating a dimeric segment with separate ORFs encoding NS1 and eGFP (figure 2.1).

Figure 2.1

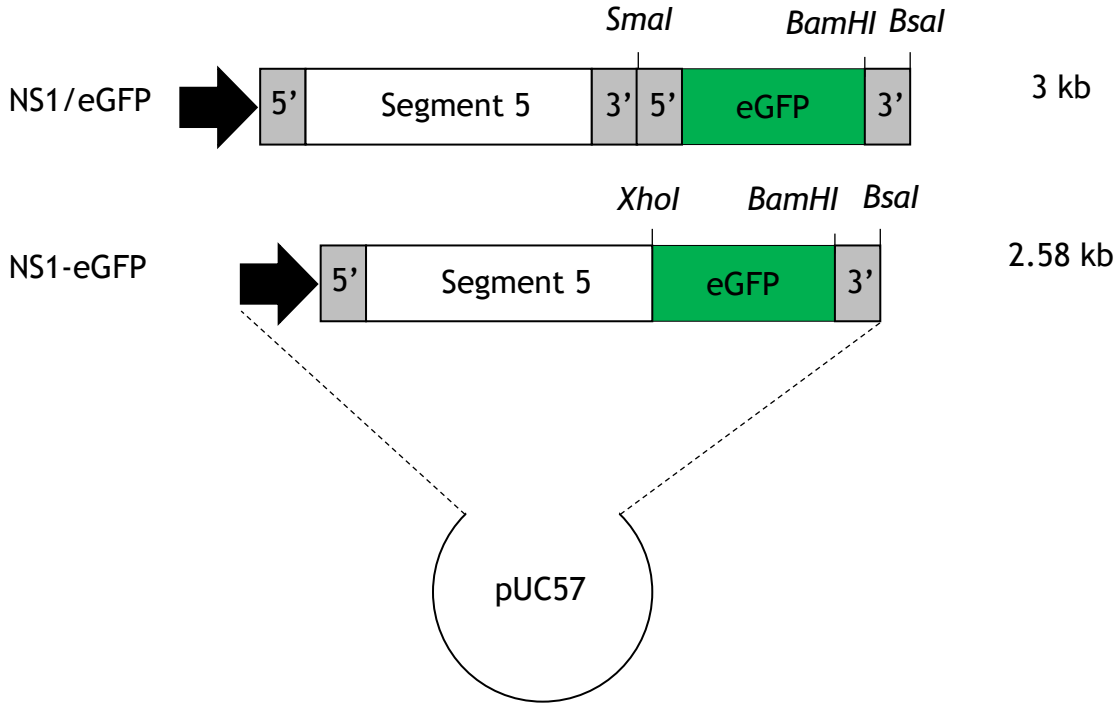

Figure 2.1: Plasmids for rescue of BTV-1 viruses expressing eGFP.
Schematic representation of plasmids (pUC57) possessing segment 5 of BTV-1 incorporating eGFP as a separate ORF to NS1 (NS1/eGFP) in the top panel, or eGFP fused to the C-terminus of NS1 (NS1-eGFP), shown in the bottom panel. Grey shaded regions represent the 5' and 3' UTRs of segment-5, arrows denote the T7 promoter and the size of each genomic segment is shown to the right of the figure. Restriction sites are shown in italics.

Prior to the commencement of this study, *XhoI* and *BamHI* restriction sites were introduced after nt 1689 of segment 5 of BTV-1 by Dr Andrew Shaw (University of Glasgow, UK). Digestion of the introduced restriction sites enabled insertion of the eGFP gene into the pUC57 expression cassette using the Rapid DNA Ligation Kit (Roche Diagnostics GmbH) in accordance with manufacturer's recommendations (Table 2.1).

To introduce eGFP at the second site, the segment 5 ORF was removed from pUC57 by digestion with *XhoI* and *BamHI* (New England Biolabs), according to the manufacturer's protocol and gel purified as described above. The eGFP open reading frame was amplified from 50 ng of the pUC57 DNA (possessing segment 5 and eGFP) using primers possessing

the *XhoI* and *BamHI* restriction sites (Table 2.1) and purified using the QIAquick PCR purification kit (QIAGEN). The purified PCR product was ligated as before, next to the segment 5 UTRs on the linearised plasmid, then amplified using primers with *SmaI* and *BsaI* restriction sites (Table 2.1) and gel purified as detailed above in the current section. To enable insertion of the modified eGFP, a *SmaI* site was introduced by mutagenesis after ntp 2040 of the 3' terminus of segment 5, using the QuickChange Lightening Site-Directed Mutagenesis Kit (Stratagene) (Table 2.1). The mutagenesis reaction was subsequently used to transform XL-10 Gold ultracompetent *E. coli* cells (Agilent Technologies) according to manufacturer's instructions, with substitution of NZY$^+$ broth for S.O.C medium. The resulting colonies were screened for the *SmaI* site.

Following ligation of eGFP possessing the Seg-5 UTRs, the *SmaI* site was removed by mutagenesis, as described previously using 3'TermMutF2 primer pair (table 2.1). Colonies were then screened for the absence of the *SmaI* site. Each ligation reaction was used to transform One Shot® TOP10 chemically competent *E. coli* (Invitrogen™) according to the manufacturer's protocol. Minipreps of plasmid DNA were performed using the QIAprep spin kit (QIAGEN) protocol, with an additional wash step with PE buffer. Insert size was assessed by XhoI and BsaI restriction enzyme digestion followed by agarose gel electrophoresis, and sequences were confirmed (Source Biosciences, Dundee, UK) using primers shown in Table 2.2. Raw reads were assembled using CLC Genomics Workbench 7.5 (QIAGEN).

Mutagenesis to introduce the A207K (GCC → AAA) mutation at nt 619 to 621 of eGFP in both constructs, was performed as already described using the GFPa207k_F2 and GFPa207k_R2 primer pair listed in Table 2.1, ensuring its monomeric state (von Stetten et al., 2012). Colonies were sequenced as described above. Plasmids possessing the confirmed sequences were used to transform Sub-cloning Efficiency™ DH5α *E. coli* (Invitrogen™). A miniprep (QIAGEN) was performed on a sample of a starter culture for sequencing. The remaining culture was added to 200 ml LB supplemented with ampicillin and incubated overnight at 37°C with shaking. Plasmids were purified using the HiSpeed Plasmid Maxiprep purification kit (QIAGEN).

Table 2.1: Primers used to insert eGFP at two sites in segment 5.

Primer name	Nucleotide sequence (5' → 3')
Mutagenesis of eGFP:	
GFPa207k_F2	ACTACCTGAGCACCCAGTCC*AAA*CTGAGCAAAGACCCCAACGA
GFPa207k_R2	TCGTTGGGGTCTTTGCTCAG*TTT*GGACTGGGTGCTCAGGTAGT
Amplification of eGFP:	
eGFP_R	ACTAAGGATCCCTTATACAGCTCGTCCATGC
eGFP_F	TATCTCGAGATGGTGAGCAAGGGCGAGGAG
*SmaI*S5_F	TATACCCGGGTTAAAAAAGTTCTCAGTTGCAAC
*SalIBsaI*S5_R	TATAGTCGACGGTCTCTGTAAGTTGAAAAGTTCTAGTAGAGTGCT
Addition of *SmaI* in segment 5:	
3'TermMutF1	CTAGAACTTTTCAACTTACCCGGGCCCGTCGACTGCAGAGGCC
3'TermMutF1	GGCCTCGCAGTCGACGGGCCCGGGGTAAGTTGAAAAGTTCTAG
Deletion of *SmaI* in segment 5 after eGFP ligation:	
3'TermMutF2	CTAGAACTTTTCAACTTACTTACGTTAAAAAAGTTCTCTAGTTGGC
3'TermMutF2	GCCAACTAGAGAACTTTTTTAACGTAAGTAAGTTGAAAAGTTCTAG

a Restriction sites are underlined and mutated nucleotides are italicised.

Table 2.2: Primers used to sequence segment 5 and eGFP.

Primer name	Nucleotide sequence (5' → 3')
M13F	GTAAAACGACGGCCAGTG
M13R	GGAAACAGCTATGACCATG
PucF	TGTGCTGCAAGGCGATTAAG
NS1TMUNIF	GGATTGGAATAACCTTGGAAG
F_BTV1_NS1_MEGFP	AGATCCCGACCTGTGGTGT
R_BTV1_NS1_MEGFP	ATCTCCGATCCTGCCAATTTG
F_BTV8_S5_560	GCTGATGATTGGATCGATCCAAACT
F_BTV8_S5_1120	GGGGTGCTCGCCATTCAAG
NS1EGFP_R2454	CTGGGTGCTCAGGTAGTGGT

2.4.2 Virus rescue

Rescue of unmodified BTV-1 and recombinant BTVs was performed using reverse genetics as previously described (Boyce et al., 2008). Briefly, 20 µg of each plasmid was fully digested with *BsaI* and non-cut plasmid was checked by confirmation of a single band of expected size by electrophoresis. The digested product was purified twice by phenol/isoamylalcohol then chlorophorm/isoamylalcohol extraction. DNA was precipitated with isopropanol and 3M sodium acetate overnight at -20ºC. Precipitated DNA was washed twice with 70% ethanol and resuspended in nuclease free water. 2 µg of purified, linearised plasmid provided the template for *in vitro* synthesis of BTV-like 5' capped single stranded RNA transcripts using the mMESSAGE mMACHINE® T7 Ultra Kit (Ambion®), according to the manufacturer's protocol, with addition of 20U of T7 polymerase (Ambion®). Following a RNA synthesis during a 2h incubation at 37ºC, plasmid DNA was digested with 2 U of TURBO DNase (Ambion®) and transcripts extracted with acidic phenol/isoamylalcohol, then purified with chlorophorm/isoamylalcohol and Illustra™ Microspin™ G-25 Columns, according to advised protocol (GE Healthcare). The integrity of the single stranded BTV RNA transcripts was assessed by agarose gel electrophoresis.

BSR cells were grown to ~80% confluency in 12 well microtitre plates in DMEM supplemented with 5% FBS. Purified ssRNA transcripts encoding BTV-1 segments 1, 3, 4, 5, 8 and 9 were diluted to $2x10^{11}$ copies/µl in Opti-MEM® I Reduced Serum

Medium (Gibco®) supplemented with 0.5 U/µL RNAsin plus (Promega). The transcripts were mixed with Lipofectamine 2000 reagent (Invitrogen™), diluted in Opti-MEM®/RNAsin mixture for approximately 30 minutes prior to dropwise addition to BSR cells and overnight incubation. The medium was replaced with fresh DMEM and purified single stranded RNA transcripts encoding all ten of the BTV-1 segments were transfected as previously described. A negative control mix lacking Seg-9 was included. The medium was replaced 4 h after transfection. The transfected BSR cells were incubated at 35°C and 5% CO_2 and monitored for CPE and eGFP fluorescence every 24 h for up to 4 days post transfection using an AMG EVOS fl Digital Inverted Fluorescence Microscope (Fisher® Scientific). Supernatant was harvested upon completion of CPE and used to infect BSR cells to generate virus stocks. Stocks (P1 BSR) were titrated by plaque assay in CPT-*Tert* cells as described in section 2.6.

2.5 End-point dilution assay

Virus inoculum was diluted in quadruplicate in a 10-fold series in 100 µl of DMEM supplemented with 5% FBS and P/S in a 96 well assay plate. 1.5 x 10^4 BSR cells, diluted in DMEM, were added to each well and incubated at 37°C and 5% CO_2 for 4 days. CPE in each well was assessed and the end-point dilution was calculated using the Spearman-Kärber formula (equation 2.2) (Spearman, 1908) and expressed as ($TCID_{50}$/ml).

Equation 2.2

$$\log_{10} 50\% \text{ end point dilution} = \left\{x0 - \frac{d}{2} + d\sum\frac{ri}{ni}\right\}$$

Where: x0 = $\log_{10}$ of the reciprocal of the highest dilution at which all wells are infected, d = $\log_{10}$ of the dilution factor, ni = number of wells used in each individual dilution, ri = number of infected wells.

2.6 Plaque assay

CPT-*Tert* cells were seeded at 1.5 x 10^5/ml into a 12 well microtitre plate to give ~80% confluency at time of infection. Virus inoculum was diluted in triplicate in a 10-fold series in IMDM supplemented with 10% FBS and P/S. Each dilution was added to a separate well of CPT-*Tert* cells and incubated for 1 h at 37°C. Cells were washed twice with Mg^{2+} and Ca^{2+} free DPBS, then overlain with 2 ml of semi-solid 1.4% Avicel® PH-101 (Sigma-Aldrich) overlay and incubated for 3 d at 37°C. Cells were washed twice with DPBS, fixed for 1 h in 4% PFA, then stained with 0.5% crystal violet solution (Sigma-Aldrich) and washed as before. Individual plaques were counted and the mean number of plaques was used to calculate virus titre, expressed as PFU/ml.

2.7 Plaque purification

BSR cells were seeded at 2 x 10^5/ml in 1 ml into a 12 well microtitre plate. At ~90% confluency (24 h after seeding), cells were infected at an MOI of 0.01 with BTV-1 NS1-eGFP (P1 BSR) and incubated for 1 h at 35°C. Inoculum was removed and cells were washed

twice with Mg^{2+} and Ca^{2+} free DPBS, then a solid 1% agarose/1x DMEM overlay was added and cells were incubated at 35°C for 3 d. eGFP fluorescent plaques were identified using JuLI™ Smart Cell Analyser (Ruskinn Technology) and selected through the overlay. Plaques were stored at 4°C in DMEM. Stocks of plaque purified NS1-eGFP-BTV-1 were generated in BSR cells.

2.8 Growth curves

Growth curves were performed in KC cells and CPT-*Tert* cells in a 12 well assay plate. Cells were infected at ~80% confluency as described in Chapter 3 (section 3.2.2), then incubated at the required temperature (see section 2.1). Inoculum was discarded after 2 h and a sample was retained for titration as described in section 2.5. Cells were washed twice with Mg^{2+} and Ca^{2+} free DPBS and 1ml of fresh culture media was added to each well, then cells were incubated for 96 h at the appropriate temperature. At 0, 8, 24, 48, 72 and 96 h pi, supernatants were harvested and centrifuged at 500xg to remove cell debris. Virus titre in cell free supernatants was determined by titration and expressed as $TCID_{50}$/ml, as described in section 2.5.

2.9 Isolation of dsRNA

Cell pellets were harvested and stored in RNAlater (Sigma-Aldrich). Total RNA was extracted from cell pellets using TRIzol (Ambion), according to manufacturer's protocol. Total RNA was precipitated in isopropanol, washed twice with 70% ethanol. ssRNA was precipitated in 3M lithium chloride and discarded. dsRNA was harvested from the supernatant by precipitation in isopropanol supplemented with 7.5M ammonium acetate, then resuspended in nuclease free H_2O.

2.10 Polyacrylamide gel electrophoresis (PAGE) of dsRNA

Monolayers of KC cells were grown to ~80% confluency in a 6 well assay plate and were infected as described in Chapter 3 (section 3.2.4). Supernatant was retained for end point dilution (as described in section 2.5). dsRNA, extracted as described before (section 2.9), was diluted to 100 ng/µl in nuclease free H_2O, then 10 µl was loaded on an 11% polyacrylamide gel (final composition 11% acrylamide, 1.5M Tris [pH 8.8], 1% SDS, 1%

APS, TEMED, dH_2O). A separate gel was loaded for each independent replicate. dsRNA species were separated by electrophoresis at 150 V for 5.5 h in running buffer (1% SDS, 25mM Tris base and 142 mM glycine), then stained using 1 x SYBR® Gold Nucleic Acid Gel Stain (Molecular Probes). Images were captured using a Gel Doc™ XR+ system (Bio-Rad).

2.11 Sequencing of passaged viruses

PCR products were generated using SuperScript® III One-Step RT-PCR System with Platinum® Taq DNA Polymerase (Invitrogen™) from a heat denatured dsRNA template, according to advised protocol using F_TF (1-21) and R_TR (2479-2502) primers listed in Table 2.3. A control lacking RNA was included. PCR products were purified and product sizes confirmed by electrophoresis as already described (section 2.4.1) (QIAGEN). The PCR products (50 ng) provided a template for Sanger sequencing using BigDye Terminator v3.1 Cycle Sequencing Kit, with an ABI Prism 377 DNA sequencer (Applied Biosystems), according to recommended protocols, with primers listed in tables 2.2 and 2.3, with the exception of M13F, M13R and PucF. Reads were aligned to the nucleotide sequence of Seg-5 of the BTV-1 reference strain and eGFP (GenBank accession numbers: JX680461 and JQ394986) in SeqMan Pro software (DNASTAR® Inc.). A BLASTn search was performed on unknown sequences (available at https://blast.ncbi.nlm.nih.gov/Blast). Sequencing was repeated twice for each independent replicate.

2.12 TA cloning of passaged viruses

Viral dsRNA was heat denatured and PCR products were generated as described in section 2.10, with P3KC_F (1820-1850) and R_TR (2479-2502) primers listed in Table 2.3, then gel purified as previously described (QIAGEN). Purified cDNA products were incubated with 0.2 mM dATP (Invitrogen™) and 5U Taq polymerase (New England Biolabs) at 70°C for 30 min, then ligated into a pGEM-T vector using the Rapid ligation kit (Promega), according to the recommended protocol. Each ligation reaction was used to transform XL-10 Gold ultracompetent *E. coli* cells (Agilent Technologies) as outlined in section 2.4.1. 20 to 40 colonies from each replicate were selected for sequencing. Following miniprep (QIAGEN), 150 to 300 ng of plasmid were used as the template for Sanger sequencing, as described in section 2.10, using P3KC_F (1820-1850) and R_TR (2479-2502) primers listed

in Table 2.3. The sequence reads were assembled in BioEdit V7.0.5.3 (available at http://www.mbio.ncsu.edu/bioedit/page2.html). Reads with mixed traces, were presumed to originate from multiple or mixed colonies and were eliminated. The selected reads were aligned to the known sequence of segment 5 of the BTV-1 reference strain and eGFP using ClustalW multiple sequence alignment (Higgins and Sharp, 1988). Intramolecular base pairing of single stranded segment 5 RNA species of all sequenced clones were predicted by minimum free energy in Mfold (available at http://unafold.rna.albany.edu/?q=mfold) (Zuker, 2003).

Table 2.3: Primers used to amplify and sequence segment 5 of passaged viruses.

Primer name	Nucleotide sequence (5' → 3')
TA cloning of partial segment 5:	
P3KC_F (1820-1850)	GTTCACTTCGCTGGGTTCGCGGCACCTGCGT
R_TR (2479-2502)	GTAAGTTGWAAAGTTCTAGTAGAG
Amplification of Segment 5:	
F_TF (1-21)	GTTAAAAAGTTCTCTAGTTGG
R_TR (2479-2502)	GTAAGTTGWAAAGTTCTAGTAGAG

2.13 Western blotting and SDS-polyacrylamide gel electrophoresis (SDS-PAGE) of proteins

Monolayers of BSR cells at ~80% confluency in 25cm^2 flasks, were infected in triplicate as described in Chapter 3 (section 3.2.5). Supernatant and cell pellets were treated with 1x Halt™ Protease Inhibitor (Thermo Scientific) and resuspended in dissociation buffer (200mM Tris-HCl [pH6.8], 8% β ME, 20% sucrose, 10% SDS, 0.01% bromophenol blue) then denatured at 95°C for 5 minutes.

Proteins were separated by SDS-PAGE in a 10% polyacrylamide gel (resolving gel: 10% Bis-acrylamide, 1.5M Tris-HCl [pH 8.8], 1% SDS, 1% APS, TEMED, dH_2O, with a stacking gel: 10% Bis-acrylamide, 0.5M Tris-HCl [pH 6.8], 1% SDS, 1% APS, TEMED, dH_2O). PAGE analyses were repeated in duplicate on separate gels and a Novex® Sharp Pre-stained Protein Standard (Novex™) was included as a size reference. Separated proteins were

transferred to Hybond P membranes (Amersham) and blocked for 1 h in 5% Oxoid™ dried skimmed milk (Thermo Scientific™) in PBS with 0.1% TWEEN®-20 (Sigma-Aldrich). BTV proteins were probed in blocking buffer with a 1:1000 dilution of a guinea pig antibody against purified BTV-1 (ORAB279) at 4°C overnight, after which the membrane was washed three times with blocking buffer and incubated with a 1:5000 dilution of HRP conjugated goat anti-guinea pig antibody (Thermo Scientific™), diluted in blocking buffer as before. Blots were washed three times with PBS, supplemented with 0.1% TWEEN®-20 (Sigma-Aldrich) and visualised using Pierce™ ECL Western Blotting Substrate (Thermo Scientific™), according to manufacturer's protocol, on G BOX Chemi XR5 (Syngene) gel detection system.

The protein blots were blocked as above and probed with a 1:40 dilution of a rabbit antibody against β-actin (Abcam), then a 1:5000 dilution of HRP conjugated goat anti-rabbit antibody (Sigma-Aldrich) as previously described. Proteins were visualised, identified by size and densitometry analysis was conducted. Each protein was quantified by measuring pixel intensity of corresponding bands in each lane using the 'selection' and 'measure' tools in Fiji software (available at http://imagej.net/Fiji) (Image J, (Rasband, 2002)). Pixel intensity was subtracted from background and normalised against β-actin intensity. Normalised intensity was averaged across replicates to give the mean ± standard error (SE). The intensity of each BTV protein in the supernatant and cell fraction was expressed as a percentage of total BTV protein intensity. Two-way analysis of variance (ANOVA) was applied to identify differences in the percentage of each protein at $p = 0.05$ level of significance, and a post-hoc Tukey's test was conducted in Minitab 17 statistical software (Minitab Inc.).

2.14 Quantitative (real-time) reverse transcription PCR (RT-qPCR)

2.14.1 Amplification of *Culicoides* homogenate

The quantity of BTV RNA was assessed in *C. sonorensis* by real-time RT-qPCR as described previously (Veronesi et al., 2013), with some modifications. Briefly, *C. sonorensis* were homogenised in nuclease free H_2O by shaking with 5 mm steel beads (QIAGEN) treated with RNase ZAP® decontamination solution (Ambion™) at 25 Hz for 1 min using a TissueLyser II disruption system (QIAGEN) (Veronesi et al., 2008). Nucleic acid was extracted from homogenate and blood meals using the KingFisher™ Purification System

Flex with 96 deep well head and LSI MagVet Express Isolation kit (Thermo Scientific) according to the advised protocol.

For each sample, 6 µl of nucleic acid was denatured by heating to 99ºC for 5 min, then amplified by RT-qPCR using BTVuni 291-311F and BTVuni 381-357R primers and BTV 348-323 probe for BTV Seg-1 (Table 2.5) with the Superscript® III Platinum® Taq one-step qRT-PCR kit (Invitrogen™) and Mx3005P qPCR machine (Agilent), according to conditions described previously (Shaw et al., 2007b) and listed in Appendix 1, with 40 amplification cycles. The EF1bCson265_F and EF1bCson467_R primer pair and EF1b-Cson354 probe for amplifying Elongation factor 1β (eF1β), used as a normalising gene (Mills et al., 2015), were designed according to TaqMan® specifications using Primer3 (available at http://simgene.com/Primer3) to amplify a 202 bp region of eF1β (Table 2.5). RT-qPCR was conducted using the same conditions as for Seg-1 (see Appendix 1).

Standard curves presented in Appendix 2 were generated by amplifying known RNA concentrations diluted as described below. Segment 1 and eF1β copy numbers in cell lysate or homogenate were expressed as $\log_{10}$ copies per ml or normalised per *C. sonorensis*, respectively. Average copies of Seg-1 ($\mu + 1\sigma$) in engorged *C. sonorensis* within 4 h following the initial blood meal, provided a baseline for calculating infection rate. Infection rate was expressed as a percentage of total *C. sonorensis* analysed. Differences in infection rates were examined using Pearson's chi-square test. A Mann-Whitney *U* test was applied to compare differences in normalised BTV copy numbers. Tests were performed using Minitab 17.0 statistical software (Minitab Inc.) at $p = 0.05$ significance.

2.14.2 Generation of qPCR standards

Batches of ten *C. sonorensis* were homogenised in quadruplicate (as described above) and RNA was isolated using TRIzol (Ambion), according to the manufacturer's protocol, with modifications. Total RNA was precipitated in isopropanol with 3 M sodium acetate, washed twice with 70% ethanol, then resuspended in nuclease free H_2O and quantified using the Qubit® RNA BR Assay Kit with the Qubit® 2.0 Fluorometer (Invitrogen™). PCR products were generated from RNA templates using the SuperScript® III One-Step RT-PCR System with Platinum® Taq DNA Polymerase (Invitrogen™) and further amplified with KOD Hot Start Master Mix (Novagen), according to the advised protocol, using EF1β 211-232 F and EF1β 532-554 R primers in Table 2.4. Amplification was assessed by electrophoresis,

sequencing was performed as described in section 2.11 and sequence identity was compared to eF1β transcript (GenBank accession number GAWM01010754) (Nayduch et al., 2014) as described previously (see section 2.11).

A T7 promoter and *XbaI* restriction site were introduced at the 5' terminus, and a *BamHI* restriction site at the 3' terminus using EF1b+T7XbaI211-232F and EF1b-BamHI532-554R primers, listed in Table 2.4. PCR was conducted with a KOD Hot Start Master Mix (Novagen), according to the advised protocol. The PCR products were gel purified and ligated into a pUC57 backbone (Fermentas), as described in section 2.4.1. Miniprep (QIAGEN – see section 2.4.1) and sequencing were performed as described before (section 2.10). The purified plasmid was linearised by *SmaI* digestion and single stranded eF1β and Seg-1 RNA transcripts were generated from purified plasmids as described in section 2.4.2. RNA transcripts representing eF1β and Seg-1 were quantified and diluted to a starting concentration of 11 $\log_{10}$ copies/µl, then diluted in triplicate as a 10-fold dilution series, down to 1 copy/ µl in nuclease free H_2O, to provide standard curves.

To determine the specificity of primers for *C. sonorensis*, RNA was extracted from homogenised *C. sonorensis*, treated twice with 2 U of TURBO DNase (Ambion®) and provided a template for cDNA synthesis and amplification, performed as before (see current section) with EF1bCson265_F and EF1bCson467_R primers listed in Table 2.5. Self-priming and amplification controls were included whereby reactions lacked RNA or reverse transcriptase respectively. Template RNA was removed by treating with 5U of Ribonuclease H (New England Biolabs). cDNA was precipitated in isopropanol, washed twice with 70% ethanol and amplification was assessed after electrophoresis (as described in section.2.4.1).

Table 2.4: Primers for amplifying and cloning eF1β.

Primer name	Nucleotide sequence (5' → 3')
Amplification of eF1ß:	
EF1b 211-232 F	CGTATCACGGTGCCAAGAATTC
EF1b 532-554 R	GGTGCATCAAAAACTGCAGTTTC
Addition of the T7 promoter, *XhoI* and *BamHI* restriction sites:	
EF1b+T7XbaI211-232F	GTAAAACGACGGCCAGTGTCTAGATAATACGACTCACTATAGGGCGTA TCACGGTGCCAAGAATTC
EF1b-BamHI532-554R	GGAAACAGCTATGACCATGGGATCCGGTGCATCAAAAACTGCAGTTTC

a Restriction sites are underlined.

Table 2.5: Primers and probes for segment 1 and elongation factor 1β real-time PCR assays.

Primer name	Nucleotide sequence (5' → 3')
Segment 1 assay[+]:	
BTV 348-323	[6FAM]TCCTCCGGATCAAAGTTCACTCCAC[TAM]
BTVuni 291-311F	GCTTTTGAGGTGTACGTGAAC
BTVuni 381-357R	TCTCCCTTGAAACTCTATCCTTACG
Elongation factor 1ß assay:	
EF1b-Cson354	[HEX]TCGAGGARATTATGGGACTTGGMGC[TAM]
EF1bCson265_F	AAACGCGATTCATTTTCACC
EF1bCson467_R	GGCAATGGCAAATCTTTTGT

a probe labels are shown in brackets.

[+](Shaw et al., 2007b)

Imaging methods

2.15 Immunofluorescence (IF) labelling of cells

BSR, CPT-*Tert* or KC cells were seeded onto 15 mm coverslips (SLS Scientific) in a 24 well assay plate. Cells were infected (or mock infected) at ~80% confluency, then washed twice with Mg^{2+} and Ca^{2+} free DPBS 2 h after infection. Fresh media was added and cells were incubated for various times after infection, as indicated in relevant chapters.

Following incubation, samples of cells were washed twice with Mg^{2+} and Ca^{2+} free DPBS. Cells were fixed with 4% PFA, washed three times with PBS and permeabilised with 0.1% Triton X100 (Sigma-Aldrich). Permeabilised cells were washed as described before, then labelled with a 1:2000 dilution of a polyclonal rabbit antibody against NS2 (ORAB1) or NS1. Cells were washed three times with PBS, then labelled with Alexa Fluor 594 or Alexa Fluor 568 Goat anti-Rabbit IgG Secondary Antibody (Invitrogen™), diluted to 1:200 in PBS supplemented with 0.5% BSA (Sigma-Aldrich). Nuclei were stained with a 1:10 000 dilution of 4',6-diamidino-2-phenylindole (DAPI) (Invitrogen™) and cells were mounted onto Superfrost™ slides (SLS Scientific) using Vectashield mounting medium (Vector Laboratories Ltd.). A Leica SP2 Confocal Microscope or SP8 TCS confocal microscope (Leica Microsystems Ltd.) was used to image cells and images were analysed using Fiji software (ImageJ).

2.16 Fluorescence activated cell sorting (FACS)

KC cells were plated in $25cm^2$ flasks at 1.5 x 10^6/ml and infected at ~80% confluency as specified in Chapter 3 (section 3.2.3). Cell pellets were harvested and resuspended in fresh culture media at uniform suspensions containing single cells. Cells were fixed with 4% PFA, washed with PBS and permeabilised with PBS supplemented with 0.2% Saponin and 1% BSA (Sigma-Aldrich). NS1 was then labelled using rabbit polyclonal NS1 antibodies diluted 1:2000 in permeabilisation buffer, followed by three washes with permeabilisation buffer, then Alexafluor 647 goat anti-rabbit (Invitrogen™) secondary antibodies, which were diluted to 1:200 in permeabilisation buffer. The cells were then washed three times with permeabilisation buffer and FACS analysis was performed using BD LSRFortessa™ cell

analyser (Becton Dickinson). Unlabelled and no primary antibody controls were included. The numbers of eGFP and NS1 positive cells were analysed by Dr Katie Lloyd-Jones (The Pirbright Institute, UK) using FlowJo single cell analysis software (FlowJo). Single cells were gated and BTV-1 infected cells were used as a threshold for NS1 and eGFP detection (figure 2.2). The percentage of unlabelled cells and cells expressing eGFP and NS1 were determined and plotted in Microsoft Excel software (Microsoft 2013).

Figure 2.2

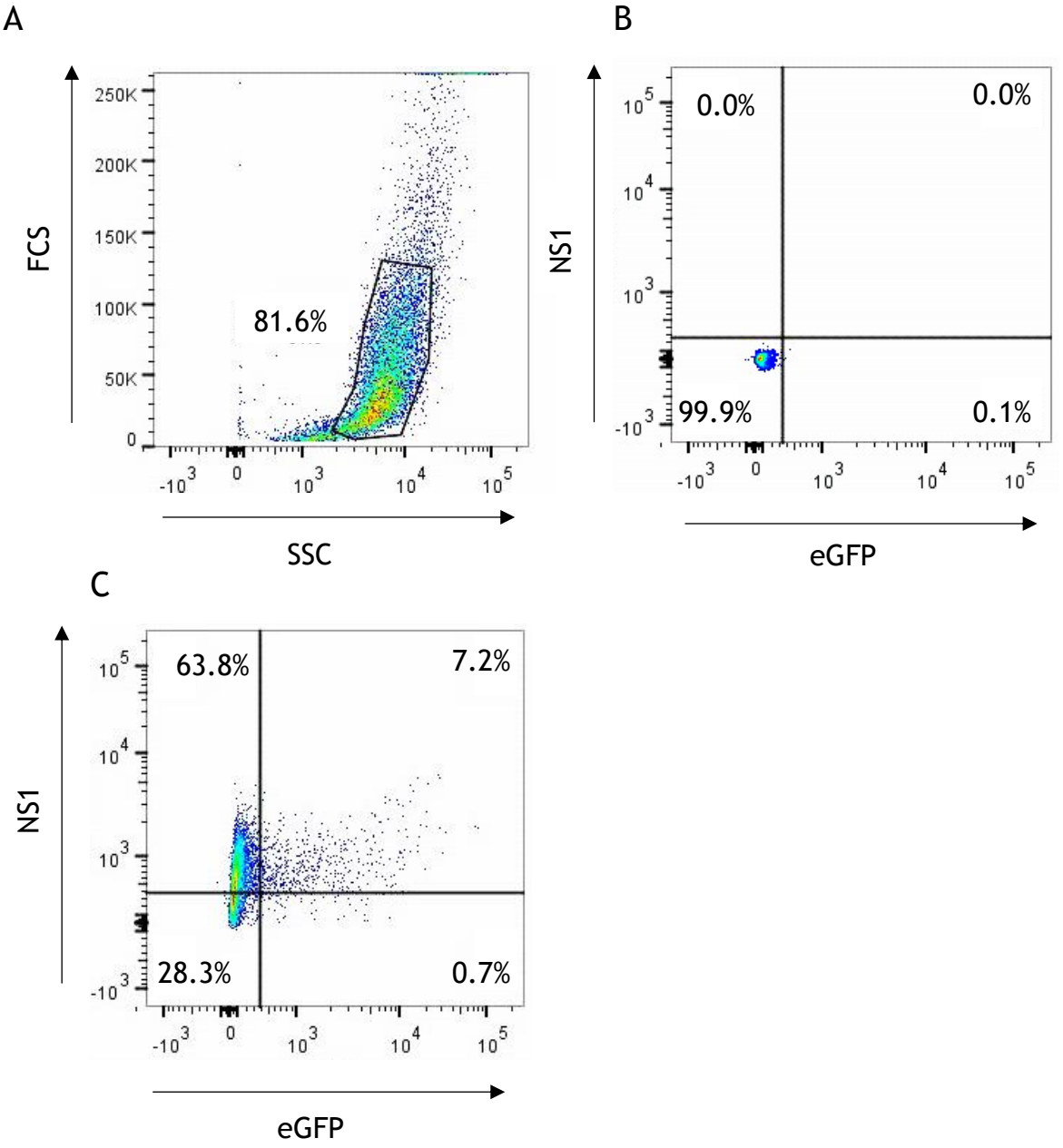

Figure 2.2: Gating for detection of NS1 and GFP.

(**A**) Single KC cells infected with BTV-1-NS1-eGFP and labelled for NS1 were gated (black line) using cell density plots and (**B**) unlabelled BTV-1 infected KC cells were used as a background control to set thresholds for detection of NS1 and eGFP. Where: forward scatter = FSC and side scatter = SSC. (**C**) eGFP and NS1 were detected in BTV-1-NS1-eGFP infected KC cells.

2.17 Transmission electron microscopic imaging (TEM)

'Tubules' composed of the BTV NS1 protein are characteristically generated within the cytoplasm of BTV infected cells (Huismans and Els, 1979b). To visualise tubules during NS1-eGFP BTV-1 infection, KC cells were plated at $2x10^6$/ml in 0.5 ml onto Nunc™ Thermanox™ Coverslips (Thermo Scientific™) in 24 well plates, to give ~80% confluency at time of infection. These cells were infected as described in Chapter 3 (section 3.2.2). At 2 h pi, cells were washed twice with Mg^{2+} and Ca^{2+} free DPBS, and fresh culture media was added. After incubation for 4 d, EM fix (kindly supplied by the Bioimaging Department - The Pirbright Institute, UK), was added and the fixed cells were processed for TEM imaging by Miss Jennifer Simpson (The Pirbright Institute, UK).

2.18 Fluorescence *in situ* hybridisation (FISH)

2.18.1 Probe design and detection of segment 5 RNA

Custom Stellaris® FISH Probes, abbreviated to TAM_S5, incorporating 5' 5-Carboxytetramethylrhodamine (TAMRA) (Table 1) were designed targeting the positive strand of Seg-5 of the South African reference strain of BTV-1 (GenBank accession number JX680461) using the Stellaris® FISH Probe Designer (LGC Biosearch Technologies) (available at www.biosearchtech.com/stellarisdesigner) (Table 2.6).

The cDNA template for transcription of negative ssRNA was generated previously (see section 2.4.1) by PCR using the KOD Hot Start Master Mix (Novagen) from 50 ng of purified plasmid containing a cDNA copy of Seg-5 of BTV-1. The T7 promoter sequence was incorporated downstream of Seg-5 using Seg5_1 F and Seg5+T7_1773 R primers listed in Table 2.7. The PCR products were gel purified (QIAGEN) as before (see section 2.4.1). Positive and negative Seg-5 ssRNA transcripts were generated as described in section 2.4.2 from 200 ng of purified PCR product. RNA was precipitated in isopropanol with the addition of 3M sodium acetate, washed twice with 70% ethanol, then resuspended in nuclease free H_2O. Synthetic Seg-5 dsRNA was generated by denaturing and annealing the negative and positive ssRNA transcripts by heating to 95°C for 2 min, then reducing the temperature every 5 min in 10°C decrements over 1 h. Double stranded RNA was gel purified (QIAquick,

QIAGEN). The amount of RNA generated was quantified as previously described (section 2.14) and the quality assessed by agarose gel electrophoresis (section 2.4.1) after denaturation in formaldehyde loading buffer (Ambion®).

To determine the specificity of the TAM_S5 probes for positive strand Seg-5 RNA, BSR cell monolayers were grown to ~90% confluency on coverslips (SLS Scientific) in a 12 well assay plate. Cells were mock transfected (without RNA) or were transfected with 1 µg of positive strand, negative strand or 0.5 µg of double-stranded segment 5 RNA in triplicate, as described in section 2.3.2. 2 h after transfection, the cells were washed twice with Mg^{2+} and Ca^{2+} free DPBS, fixed with 4% PFA, permeabilised in nuclease free 70% ethanol overnight at 4°C, then labelled with 12.5 nM TAM_S5, according to the manufacturer's protocol (LGC Biosearch Technologies). Nuclei were stained with DAPI and cells were mounted as before. Labelled cells were imaged as previously described (section 2.15).

To determine whether probes were able to detect segment 5 RNA during infection, KC and BSR cells were grown to ~90% confluency on coverslips (SLS Scientific) in a 24 well plate. Cells were mock infected by the addition of fresh media or were infected at an MOI of 0.01 with BTV-1 or BTV-11, washed twice with Mg^{2+} and Ca^{2+} free DPBS 2 h pi and replenished with fresh media. At 24 h pi, BSR and KC cells were washed twice with Mg^{2+} and Ca^{2+} free DPBS and fixed with 4% PFA. Cells were labelled with 12.5 nM TAM_S5 and a 1:500 dilution of a polyclonal guinea pig antibody against purified BTV-1 (ORAB279), then a 1:200 dilution of Alexa Fluor 488 Goat anti-Guinea Pig IgG Secondary Antibody (Invitrogen™), according to manufacturer's protocol (LGC Biosearch Technologies). A background control, lacking the secondary antibody, was included. Nuclei were stained with DAPI and cells were mounted and imaged as described in section 2.15.

The intensity of TEM_S5 and ORAB279 labelling was measured in individual BSR cells mock infected or infected with BTV-1 or BTV-11 using Fiji software (Image J). Cells were analysed in quadruplicate in three separate images of a single coverslip. A student's t-test and Mann-Whitney *U* test were performed in Minitab 17.0 Statistical software (Minitab Inc.) to compare differences between BTV-1 and BTV-11 in +Seg-5 and VP5 labelling intensity, respectively.

Table 2.6: Probes specific to the sense (+ve) strand of segment-5 RNAs of BTV-1 (pS5-BTV1_TAM).

Nucleotide sequence (5' → 3')	
CCCACTGATGTTGTATTTTC	GCCAAAAAAGTTCTCGTGGC
GCAAGTCCATTGTGGTGAAA	TTTGTTTAACACACATCCCA
CGCAATCATTGCTCTCTCAA	AATTTATATGCTTTCGCCGG
TTTTGAAGCATTGGAGCCAG	CTCTTCGTATGGTTGGGAAA
CGGTAATCTTCGAGCAGTTG	TAACCAATGCGGATTGCTTC
TCCAATCTAACTCTTTCCGA	TGGCACATAGATGTAAGGCA
GTTGGATTCACGATTTGACC	GCATCCGGGTTGTAGAAATA
GCATCCGGGTTGTAGAAATA	GCATCCGGGTTGTAGAAATA
AGTTTGGATCGATCCAATCA	TCTCAACCTCACGTTTGATT
CAGTGTAGGGACATGTGTTA	TCACTTGAAATACTCTGCCT
GATCAGCTGAATCGGCAAGA	TCGCAAAATCATCCATCCTT
AATATTGCTGTATCGCCATC	ATCTGACCTCTTCAGCATAA
CCTTCCAAAAAGTTGTTGCA	TAATGGAAATTCGCCCGTTG
GTTGGGAAATCGCGTCTTAT	TAATCATAGGTAGCAGCCAG
TGATCCAATCCTTCACGAAC	AATCAATAAGCCATTCCCAC
GCTGACATGTATGCTTTCTA	GATCTGCTTTGAGTGTTTCA
CGTACATCAATCACACCACA	AACACCCAGTTAGTTCTGAT
ATCTTCACCGTCTTGAATGG	GAATCATTTCCCACATGTTC
CCAATTTGTTCATCGCGAAC	CCCCAGTGTAACAATTTGTA
ATCGCAGTTGTAATCAAGGC	CTCTAATCCAGCGGTGAATG
CGCGTCCGAGCATGAAAATA	AGAATAACCTGAGCAGAGCG
AGAATAACCTGAGCAGAGCG	GCATATCCGTAGCACACAAA
AAGGTTATTCCAATCCGGTA	TCCGGTCCTTTCAAAATGAT
AAACATCGTAGCATAAGCCC	GGGTGATAATGCATCGAACC
CAGCGAAGTGAACCTTTTCT	CATACGAGCAGCGAGATTGA
AATACTCCATCCACATCTGA	

Table 2.7 Primers used to add a T7 promoter to segment-5

Primer name	Nucleotide sequence (5' → 3')
Seg5_1 F	GTTAAAAAAGTTCTCTAGTTGGCAAC
Seg5+T7_1773 R	GGATTC*TAATACGACTCACTATA*GTAAGTTG

a the T7 promoter sequence is italicised

2.18.2 Labelling of *Culicoides* sections

Insects were anaesthetised with CO_2 and transferred to nuclease free H_2O supplemented with 0.1% TWEEN®-20 (Sigma-Aldrich), washed twice with nuclease free H_2O, then fixed in 4% PFA. The fixed insects were washed twice with nuclease free H_2O and incubated overnight at 4°C in 12% sucrose supplemented with 40 U per ml of RNAsin RNase inhibitor (Invitrogen™) and treated with DEPC (Sigma-Aldrich) according to manufacturer's recommended protocol. Groups of fifteen to fifty *C. sonorensis* were laterally mounted at uniform depth in Peel-A-Way® Embedding Moulds (Sigma-Aldrich) with Tissue-Tek® O.C.T compound (Sakura® Finetek USA Inc.), frozen on dry ice and stored at -80°C.

Mounted *C. sonorensis* were warmed to -15±2°C and serial sections were taken, with 15 µm intervals between sections, using a Leica CM3050 S Research Cryostat (Leica Microsystems Ltd.) with Feather S22 Microtome Blades (CellPath Ltd.). Each section was dried onto a Superfrost™ plus slide (SLS Scientific), fixed in 4% PFA, washed twice in nuclease free PBS, and dehydrated for 1 h in nuclease free 70% ethanol. Slides were rehydrated in 50% and 30% nuclease free ethanol. An ImmEdge™ hydrophobic barrier pen (Vector Laboratories) was used to draw around the boarder of each slide. Slides were submerged in wash buffer A (Biosearch technologies Ltd.), then were incubated at 37ºC for ~4 h with 12.5 nM TAM_S5 probes and a polyclonal guinea pig antibody against BTV-1 (ORAB279), diluted 1:500 in hybridisation buffer (100mg/ml Dextran sulphate (MP Biomedicals), 10% deionised formamide, 2x saline-sodium citrate (SSC) (Ambion™), nuclease free H_2O). Labelled slides were submerged in wash buffer A, then incubated with Alexa Fluor 488 Goat anti-Guinea Pig IgG Secondary Antibody (Invitrogen™), diluted 1:200 in wash buffer A. Background controls lacking secondary antibody or primary antibody and probe were included. Nuclei were stained with DAPI (Sigma-Aldrich), diluted 1:10 000 in wash buffer A. Slides were washed twice in wash buffer B (Biosearch technologies Ltd.) Coverslips (SLS Scientific) were mounted and slides were imaged as before (section 2.15). Images of 1023 x

1023 pixels were captured at 20 x objective. To reduce autofluorescence, the gain for red and green channels was adjusted above levels detected in mock infected *C. sonorensis*.

2.19 Imaging of *Culicoides* tissues

Tissues were identified in labelled *C. sonorensis* sections (see section 2.18.2) using the following methods. Newly emerged *C. sonorensis* were sectioned as described in section 2.17.2. Nuclei were stained with a 1:10 000 dilution of DAPI, or cytoplasm was stained with 0.1% Fast Green FCF (Sigma-Aldrich), shown to stain salivary glands and fat body tissues (Hershberger, 1946). DAPI stained sections were captured by confocal microscopy as described previously (section 2.15). A Leica DM IL LED microscope (Leica Biosystems Ltd) with sCCD Camera (OLYMPUS) was used to capture images of Fast Green stained sections at 40x objective. Images were analysed using Fiji software (ImageJ).

2.19.1 X-ray microtomography (microCT) of adult *Culicoides*

Newly emerged adult *C. sonorensis* were killed by freezing at -20ºC then fixed in 70% ethanol. Whole-volume microCT imaging was performed on fixed *C. sonorensis* and three-dimensional reconstructions were provided by Dr Orestis Katsamenis at the µ-VIS X-Ray Imaging Centre (University of Southampton, UK).

2.20 Sample size calculations

Sample sizes for experiments described in Chapter 5 assumed a medium effect size and were calculated by $N \geq 50+8m$ (Green, 1991), where N is the number of subjects and m is the number of predictors. A large effect size with $N \geq 35$ was assumed for experiments in Chapter 4.

2.21 Statistical analyses

Descriptive analyses were performed in Microsoft Excel software (Microsoft Office 2013). Heatmap plots were obtained using the 'imagesc' function of MATLAB® software (Mathworks Ltd.). Minitab 17.0 statistical software (Minitab Inc.) was used to implement statistical analyses outlined in Chapter 5, with $p = 0.05$ level of significance.

The 'binofit' function of the Statistics and Machine Learning Toolbox of MATLAB® (Mathworks Ltd.) was used to calculate confidence intervals (CI) of estimates of the 'true' population mean, with a 95% level of confidence, and assumed a binomial distribution.

Chapter 3

Construction, detection and characterisation of recombinant bluetongue viruses

3.1. Introduction

Recent advances in microscopic imaging and the development and expression of genetically encoded fluorescent tagged 'reporter' proteins, and use of antibodies or fluorescent tagged nucleic acid probes have helped to reveal details of the complex interactions between host and pathogen. Studies have included observing the host's immune response at a new level of spatial and temporal resolution by direct visualisation of these molecules in infected cells and tissues (Peters et al., 2008, Palha et al., 2013, Coombes and Robey, 2010, Melzi et al., 2016). The data generated provide the foundation for a systems-level understanding and multiscale models of within-host pathogen infection, replication and dissemination mechanisms (Kumberger et al., 2016), explored in Chapter 5. The purpose of the studies described in the current chapter is to develop a means of visualising BTV *in vivo,* during infection.

Genetically encoded fluorescent proteins, such as green fluorescent protein (GFP), its spectral variants and GFP-related proteins (Matz et al., 2002), are perhaps the most widely used reporters as they can be imaged non-invasively in living cells without requiring a co-factor (other than oxygen) to synthesise the chromophore (Tsien, 1998). The suitability of a fluorescent reporter protein for studies of protein localisation depends on its photostability, signal level above autofluorescence, potential for oligomerisation, if expressed as a fusion protein, and its emission spectrum when used in multiplexing (Shaner et al., 2005).

The genome of some viruses can be extended to incorporate additional 'reporter' genes, enabling viral replication and dissemination to be precisely monitored, not only in cell cultures, but also in host plants, animals, or arthropod vectors (Manicassamy et al., 2010, Palha et al., 2013, Fukuyama et al., 2015, Shaw et al., 2012, Ziegler et al., 2011). Whether extension of the viral genome is possible, depends on: the requirements for assembly and packaging of the progeny viruses; the existence of a reverse genetics system to 'rescue' wild-type or modified viral/reporter nucleic acids as part of a functional virion; the targeted insertion site within the viral genome segment (Wertz et al., 2002); the insert size and specific nucleotide or amino acid sequence of the insert (Teterina et al., 2010).

Several studies have reported the 'rescue' of non-segmented viruses that express a fluorescent 'reporter' as part of a viral 'fusion' protein, including: poliovirus (PV) (Teterina et al., 2010, Mueller and Wimmer, 1998); Sindbis virus (SINV) (Frolova et al., 2006,

Atasheva et al., 2007); Chikungunya virus (CHIKV) (Kummerer et al., 2012) and Semliki Forest virus (SFV) (Tamberg et al., 2007). Influenza A viruses, which have a segmented ssRNA genome, have also been successfully rescued, expressing variants of GFP (Perez et al., 2013, Manicassamy et al., 2010, Li et al., 2010).

Rescuing a recombinant BTV that expresses a viral-reporter fusion protein and is also replication competent, is complicated by the nature of its ten segmented dsRNA genome, which requires cells to uptake at least one copy of each genome segment, usually in the form of functional ssRNAs (Boyce and Roy, 2007, Boyce et al., 2008).

Recombinant strains of BTV-1 and 10 were successfully generated, expressing the red fluorescent mCherry reporter protein as a fusion with the transmembrane domain of NS3/NS3A (Shaw et al., 2012). These viruses exhibit reduced growth in BFAE and KC cells. A recombinant strain of BTV-1 was also engineered expressing a short, 6 amino acid, tetracysteine tag incorporated into VP2 (Du et al., 2014), that is suitable for live cell labelling. Additionally, reverse genetics systems were recently been published for rotavirus (Desselberger, 2017). These studies prove that the rescue of segmented dsRNA viruses is achievable.

The studies presented in this Chapter expand previous work by the Shaw group (Shaw *et al*. 2012) and were intended to rescue a BTV strain that stably expresses a fluorescent reporter protein over multiple replication cycles in KC cells, with a similar growth profile to the parental virus. To achieve this, the open reading frame (ORF) of enhanced GFP (eGFP) was inserted into segment 5 (Seg-5) of BTV-1, upstream of the 3' non-coding sequence, enabling expression of either an eGFP-NS1 fusion polypeptide, or independent expression of unmodified NS1 and eGFP proteins, from 'concatemeric' but distinct open reading frames (Eaton and Gould, 1987, Gould and Hyatt, 1994).

The 64 kDa NS1 protein provides a suitable candidate for integration of a reporter protein as it is dispensable in primary BTV replication (Matsuo and Roy, 2013) and maintains normal function and targeting upon incorporation of a 16 or 116 foreign amino acid sequence at its *C*-terminus (Monastyrskaya et al., 1994, Mikhailov et al., 1996), indicating that eGFP addition is unlikely to impair NS1 functionality. Additionally, NS1 is expressed at high levels in both insect and mammalian cells (Urakawa and Roy, 1988a), prior to the formation of progeny virus. The tubular NS1 polyprotein assemblies are closely associated with mature

virus particles (Huismans and Els, 1979a). Hence NS1 is a relatively precise, early and abundant indicator of BTV infection and intracellular particle localisation.

3.2. Results

3.2.1. Rescue of recombinant BTV-1 viruses

Seg-5 of BTV encodes a single 552 aa protein, NS1, which forms abundant and characteristic cytoplasmic tubules in infected cells (Urakawa and Roy, 1988a, Huismans and Els, 1979a). The NS1 coding sequence was modified by insertion of the coding sequence for green fluorescent protein, eGFP, which had been selected in order to express a detectable fluorescence signal in *C. sonorensis* tissues, which naturally exhibit strong red-violet autofluorescence, notably around the oocytes and cuticle (data not shown).

Initially, three different plasmids were developed containing either the unmodified Seg-5 sequence from BTV-1 as a control, which was developed by Dr Andrew Shaw (University of Glasgow, UK) prior to the start of the project. The remaining plasmids possessed the eGFP coding sequence integrated at the C-terminus of the NS1 ORF (NS1-eGFP), or Seg-5 incorporating the eGFP coding sequence as a separate ORF downstream of the 3' terminal sequence (NS1/eGFP) were developed during the project. Recombination occurred at nt 687 to 1624 during initial attempts to clone eGFP into the ORF of NS1, inserted sequences corresponded to *E. coli* DNA. Reduced colony size indicated that the inserted eGFP and Seg-5 sequences were toxic to *E. coli*.

An unmodified BTV-1, genetically identical to the BTV-1 reference strain (ICTVdb isolate accession number [RSArrrr/01]) was rescued from synthetic RNA transcripts using standard procedures (Boyce et al., 2008) as described previously (Chapter 2, section 2.4). Two additional modified BTV-1 strains, expressing NS1 and eGFP either as separate proteins (NS1/eGFP), or as a single 793 aa fusion-protein that includes eGFP (NS1-eGFP) at the *C*-terminal of NS1, were also both rescued successfully (figures 3.1A and C). Fluorescent plaques of >50 BSR cells, that were expressing eGFP, were visible at 48 h post-transfection (pt) with the ten *in vitro* RNA transcripts that included either NS1-eGFP (figure 3.1B) or NS1/eGFP transcripts. However, by 96 h pt eGFP fluorescence was undetectable in the cells transfected with ssRNAs that included NS1/eGFP, (data not shown), indicating that eGFP was not retained over multiple rounds of replication of BTV-1 NS1/eGFP. The BTV-1 NS1/eGFP strain was therefore eliminated from further analyses. Fluorescence due to transient expression of eGFP was detected in single cells in wells transfected as a mock control with the NS1-eGFP (figure 3.1B – Mock) or NS1/eGFP transcript (data not shown),

in the absence of Seg-9. eGFP expression in control wells was distinguishable from wells transfected with all ten BTV segments including modified Seg-5, indicating that NS1-eGFP and NS1/eGFP were incorporated into progeny virus, rather than transiently expressed.

Stocks of the rescued BTV-1 NS1-eGFP were generated in BSR cells and titrated as described before (Chapter 2, sections 2.4.2 and 2.5). At 24 h pi with the rescued BTV-1 NS1-eGFP strain, eGFP fluorescence was localised as large aggregates in the cytoplasm of BSR cells and co-localised with NS1 expression (figure 3.1E), indicating that eGFP was expressed as an NS1 fusion protein. BTV-1 NS1-eGFP produced smaller plaques and grew to a lower titre of 2.53×10^{-5} PFU/mL, compared to unmodified BTV-1 which replicated to a titre of 4.27×10^{-6} PFU/mL in CPT-*Tert* cells (figure 3.1C), indicating that extension of the NS1 ORF to incorporate eGFP resulted in growth deficiency relative to the parental/wild-type BTV-1.

Figure 3.1: Rescue and initial characterisation of a BTV-1 expressing eGFP.

(**A**) Schematic representation of 'constructs' used for the rescue of BTV-1 viruses expressing eGFP. Segment 5 (Seg-5) of unmodified parental BTV-1 (WT) and modified BTV-1 viruses incorporating eGFP fused to the C-terminus of NS1 (NS1-eGFP), or as a separate ORF are shown. Arrows represent the start of the ORF and the size of each genome segment is shown to the right of the figure. (**B**) Fluorescence of BSR cells 48 h after transfection with RNA transcripts of the BTV-1 reference strain genome segments, synthesised *in vitro,* but including a modified Seg-5 incorporating eGFP (NS1-eGFP); by replacing the modified Seg-5 with the parental / wild type version (WT), or lacking the Seg-9 transcript (Mock). (**C**) Crystal violet staining of the CPT-*Tert* cell monolayer showing plaque formation 96 h pi with a 10^{-4} dilution of unmodified BTV-1 (WT), BTV-1 NS1/eGFP or BTV-1 NS1-eGFP. (**D**) Profile of segments 1 to 10 of unmodified BTV-1 (WT) and BTV-1 NS1-eGFP. The location of Seg-5 incorporating eGFP is denoted by a black arrow. The orange arrow denotes the location of parental Seg-5 at position 6. dsRNA was isolated from KC cells 48 h pi at an MOI of 0.01 and segments were separated by polyacrylamide gel electrophoresis. (**E**) NS1 expression and eGFP fluorescence (shown in green) in BSR cells 24 h pi with BTV-1 NS1-eGFP at an MOI of 0.1. The same cells were also fixed and NS1 was labelled with a polyclonal rabbit anti-NS1 antibody, shown in red (scale = 20 μm).

Figure 3.1

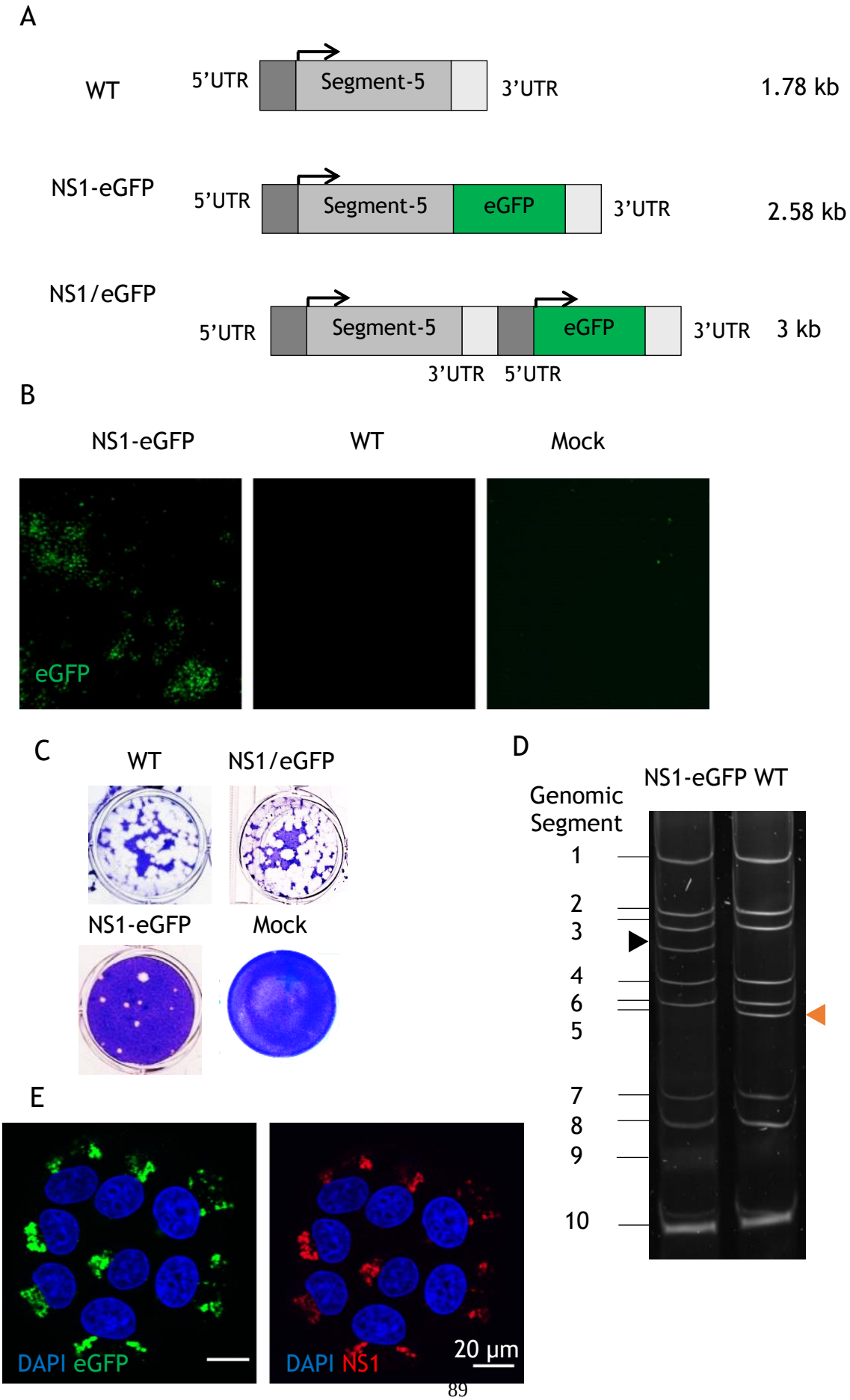
A
WT
5'UTR
Segment-5
3'UTR
1.78 kb
NS1-eGFP
5'UTR
Segment-5
eGFP
3'UTR
2.58 kb
NS1/eGFP
5'UTR
Segment-5
eGFP
3'UTR
3 kb
3'UTR
5'UTR
B
NS1-eGFP
WT
Mock
eGFP
C
WT
NS1/eGFP
NS1-eGFP
Mock
D
NS1-eGFP WT
Genomic Segment
1
2
3
4
6
5
7
8
9
10
E
DAPI eGFP
DAPI NS1
20 µm

3.2.2. Growth of BTV-1 NS1-eGFP is reduced and tubule aggregation is increased *in vitro*

The growth rate of BTV-1 NS1-eGFP was compared with the unmodified BTV-1 over multiple replication cycles in ovine and *Culicoides* cells. CPT-*Tert* and KC cells were infected in triplicate in two independent experiments at an MOI of 0.01 with NS1-eGFP, parental BTV-1, or were mock infected. Viral titres in supernatant were quantified at various time points after infection by end-point dilution (see sections 2.5 and 2.8 of Chapter 2). The modified BTV-1 NS1-eGFP strain, replicated only slowly for the first 24 h pi in mammalian cells, while the wild type BTV-1 showed little initial delay. As a result, the growth curve of BTV-1 NS1-eGFP, although showing a similar slope, was delayed relative to the unmodified BTV-1 in CPT-*Tert* cells, to the extent that it produced approximately 2.5 $\log_{10}$ lower $TCID_{50}$/ml between 24 to 48 h pi. Although both viruses generated a titre of approximately 6.00 log $TCID_{50}$/ml (6.09 $\log_{10}$ ± 0.18(SE)) by 72 to 96 h pi, wild type BTV-1 reached this plateau by 48 h pi, 24 h earlier than BTV-1 NS1-eGFP (figure 3.2A).

In contrast replication of the wild type virus showed a small initial delay for 8h pi in the KC cells, while the modified BTV-1 NS1-eGFP showed a rapid initial rise in replication in these cells and achieved higher titres than in the mammalian cells for the first 48 h pi (figure 3.2A). Despite this more rapid start in replication, the modified virus was slightly delayed in KC cells compared to the unmodified BTV-1, generating ~10 fold lower virus titres between 8 h and 96 h pi, and reaching a similar final titre (~6.50 $\log_{10}$ $TCID_{50}$/ml) 24 hours later at 96 h pi (figure 3.2B). There was no virus growth in the mock infected control over the time course (figure 3.2A, B).

To determine whether delayed replication could result from impaired ability of NS1-eGFP to form tubules, KC cells were mock infected, or infected at an MOI of 0.1 with the unmodified BTV-1 or BTV-1 NS1-eGFP and tubules were observed by TEM 4 dpi. As expected, no tubules were detected in the cytoplasm of mock infected cells (figure 3.3). Although NS1 tubules were formed during both BTV-1 NS1-eGFP and parental BTV-1 infections and were morphologically similar. The tubules generated by BTV-1 NS1-eGFP appeared to be more densely packed in large cytosolic aggregates in close proximity to VIBs (figure 3.3). Increased aggregation of NS1 tubules during BTV-1 NS1-eGFP infection was consistent with confocal microscopic observations of NS1 in BSR cells (figure 3.1D) which showed aggregation of NS1.

Figure 3.2

A

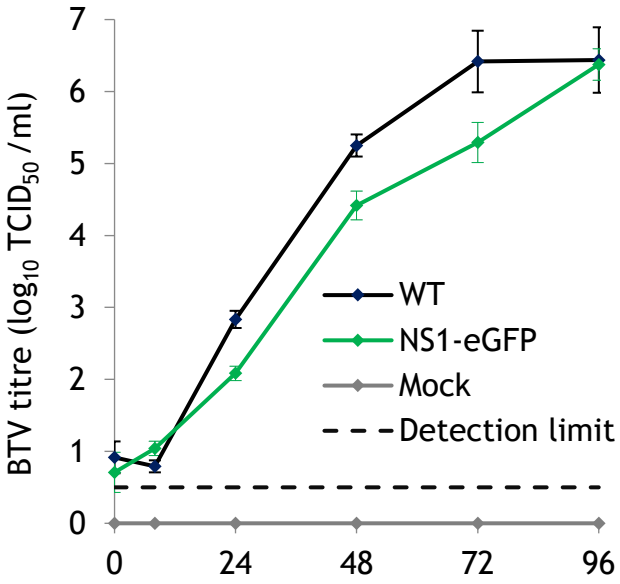

B

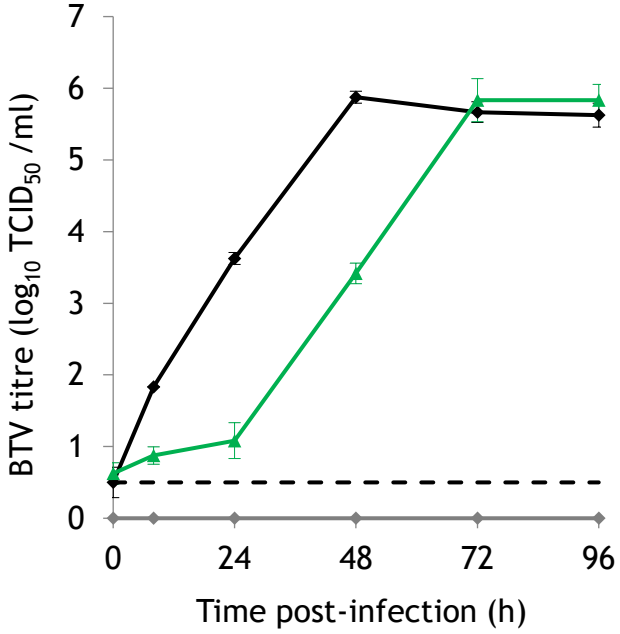

Figure 3.2: Growth of BTV-1 NS1-eGFP is delayed *in vitro*. (**A**) Mean titre (log_{10} $TCID_{50}$/ml) of unmodified BTV-1 (WT), uninfected control (Mock) and BTV-1 NS1-eGFP (N1-eGFP) in *C. sonorensis* (KC) cells and (**B**) sheep (CPT-*Tert*) cells and at 0, 8, 24, 48, 72 and 96 h pi with an MOI of 0.01. Inoculum was titrated to ensure initial titre did not differ between viruses or cell lines (data not shown). Bars represent the standard error of the mean and the dashed line represents the assay detection limit.

Figure 3.3

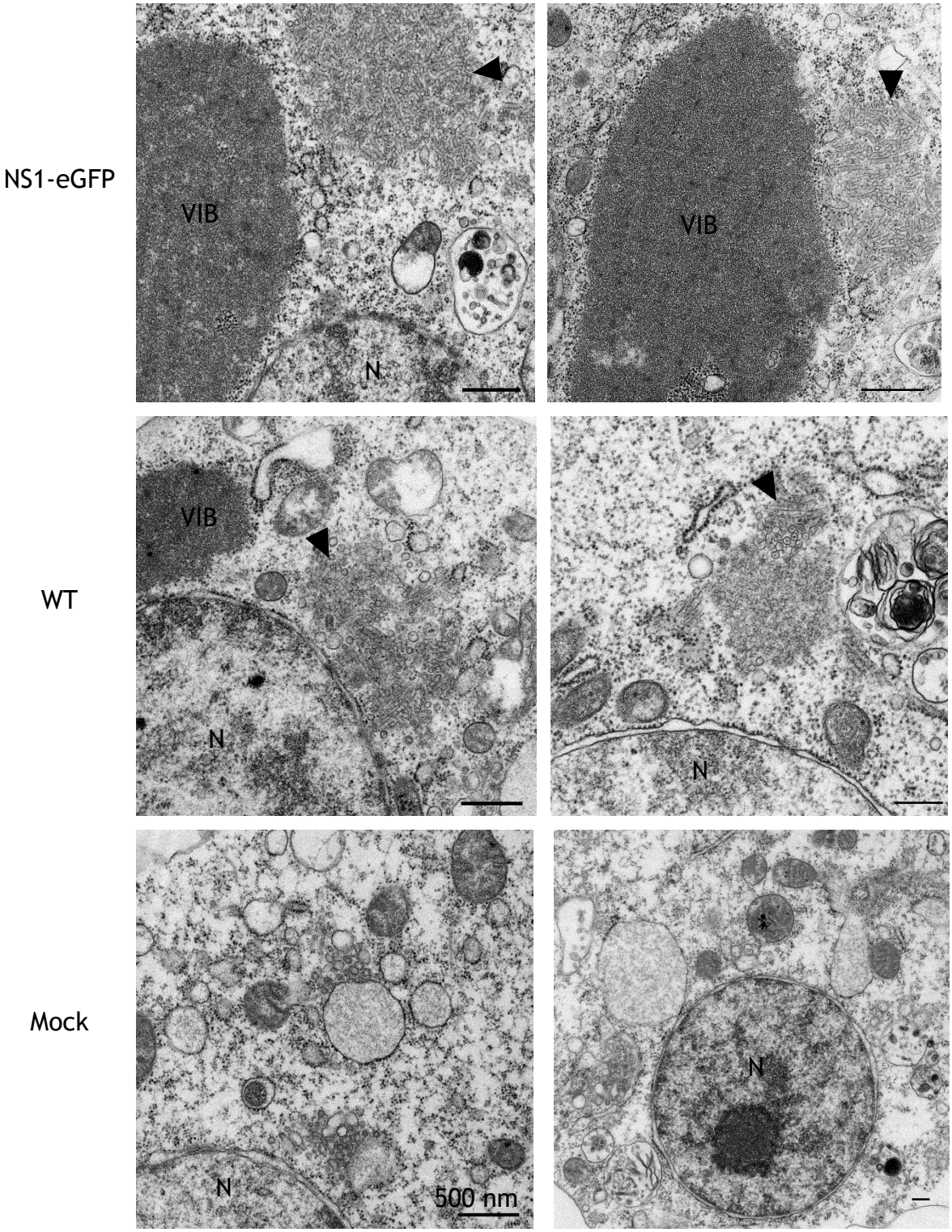

Figure 3.3 BTV-1 NS1-eGFP forms dense aggregates of NS1 tubules during infection. KC cells were infected at an MOI of 0.1 with BTV-1 NS1-eGFP (NS1-eGFP), unmodified BTV-1 (WT), or were mock infected (Mock). At 96 h pi, cells were fixed and tubules were observed by TEM. Cell nuclei (N) and cytoplasmic viral inclusion bodies (VIB) are labelled (scale = 500 nm). Arrows indicate the NS1 tubules.

3.2.3. Loss of eGFP fluorescence during multiple passages of BTV-1 NS1-eGFP

The level of eGFP fluorescence was assayed over multiple replication cycles to assess the potential of BTV-1 NS1-eGFP as a reporter for *in vivo* studies of BTV replication and localisation. Unmodified BTV-1 and BTV-1 NS1-eGFP in supernatant were independently passaged in triplicate at an initial MOI of 0.01, for 48 h, over 7 passages in KC or CPT-*Tert* cells. Passaging was repeated in two independent experiments. At each passage, NS2 was detected by labelling with polyclonal rabbit anti-NS2 antibodies (Orab1) (see Chapter 2, section 2.15 for methods), to identify infected cells. The percentage of cells singly or co-expressing eGFP and/or NS2 were calculated from confocal images. To ensure that titre did not vary between passages, endpoint dilution assays of supernatant from each passage were performed on BSR cells (not shown).

At passages 1, 3 and 6, eGFP fluorescence was undetectable in between 63 to 91% of infected (NS2 positive) KC cells (figure 3.4A, B). Partial co-localisation of eGFP with NS2 at KC cell passage 3 (figure 3.4A) was consistent with aggregation of NS1 tubules in close proximity to VIBs. FACS analysis confirmed that eGFP fluorescence was lost early after infection with only 7% of KC cells expressing both NS1 and eGFP fluorescence at 24 h pi, despite detection of NS1 in 64% of cells. The percentage of infected cells detected by FACs 24 h after BTV-1 NS1-eGFP infection at an MOI of 0.01 was lower than with the unmodified BTV-1 (figure 3.4C), consistent with a reduction or delay in growth. The longevity of eGFP fluorescence during serial passage in KC cells was not increased after three rounds of plaque purification, indicating that the eGFP-negative BTV population arose during serial infection and may have been absent in the initial rescue supernatant (data not shown).

eGFP fluorescence was undetectable following 6 passages in KC cells (data not shown in figure) or 4 passages in CPT-*Tert* cells (figure 3.4A). This difference may reflect the greater similarity in growth rates of the wild type and modified viruses in KC cells (figure 3.2A) and therefore less selective pressure for a ‘wild type strain’ during serial passages in these cells. The majority (81 to 95%) of infected CPT-*Tert* cells expressed eGFP at passage 1, while eGFP fluorescence was only detectable in 6 to 21% of infected cells at passage 3, and at passage 6 eGFP fluorescence was undetectable in all infected CPT-*Tert* cells (figure 3.4A, C).

In both KC and CPT-*Tert* cell lines, a minority of infected cells (0.4 to 6%) expressed eGFP in the absence of NS2 (figure 3.4B, C).

Figure 3.4: Loss of eGFP fluorescence during serial passage of BTV-1 NS1-eGFP.

(**A**) The stablity of eGFP (green) expression in KC cells or CPT-*Tert* cells infected with BTV-1 NS1-eGFP was examined. BTV-1 NS1-eGFP was serially passaged to produce passages 1, 3 and 6, shown. NS2 was labelled after each passage with polyclonal rabbit anti-NS2 antibody (red), and confocal images were captured (see Chapter 2, section 2.15). White arrows indicate eGFP negative infected cells and sites of NS2 and eGFP partial co-localisation are shown by the orange arrows (scale = 20 µm).

Figure 3.4

A

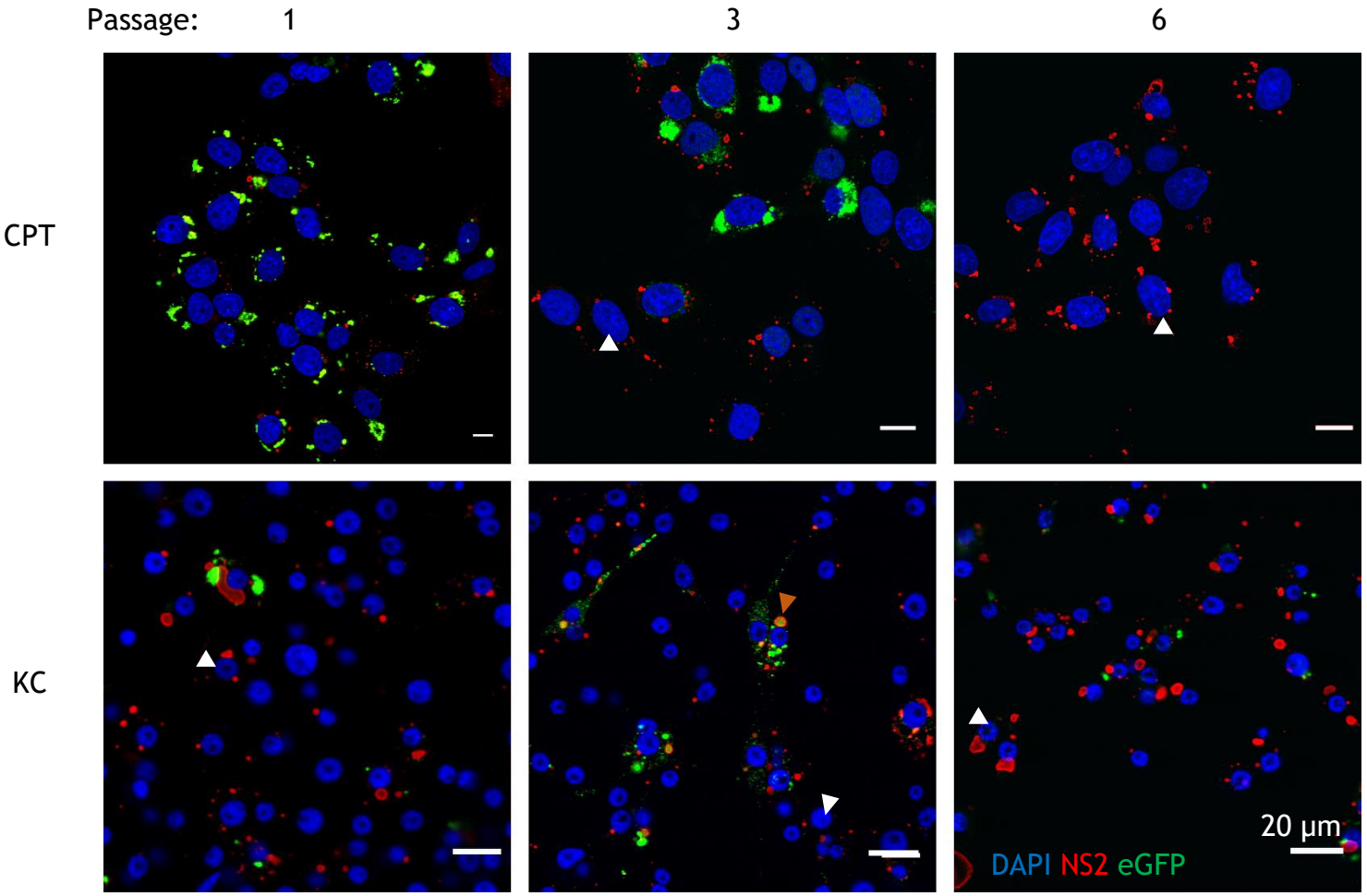

Figure 3.4

B

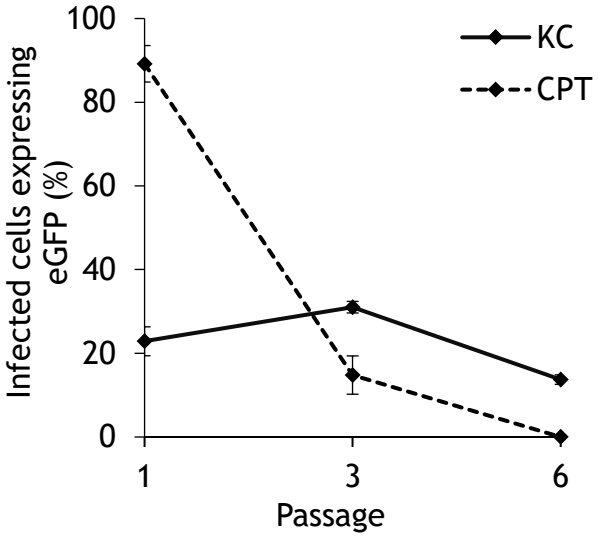

C

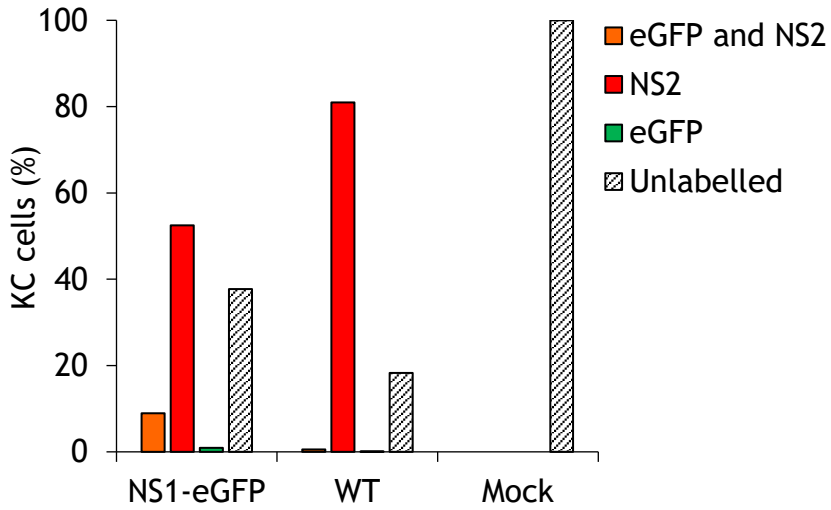

Figure 3.4: Loss of eGFP fluorescence during serial passage of BTV-1 NS1-eGFP. (**B**) The number of KC or CPT-*Tert* cells expressing NS2 and eGFP were counted in confocal images at passage level 1, 3 and 6. The average percentage of cells expressing both NS2 and eGFP was determined in confocal images of each independent replicate for every passage shown. Bars represent the standard error of the mean. (**C**) The percentage of KC cells expressing eGFP and NS1 during early infection was determined. KC cells were mock infected, or infected at an MOI of 0.01 with unmodified BTV-1 (WT) or BTV-1 NS1-eGFP. Cells were fixed at 24 h pi, eGFP was detected by direct fluorescence, NS1 was labelled using polyclonal rabbit NS1 antibodies and the uninfected cells remained unlabelled. Cells were sorted by FACs (for methods see section 2.16 of Chapter 2).

3.2.4. Genetic changes in Seg-5-eGFP that correspond to loss of eGFP fluorescence

The genetic mechanisms underlying loss of eGFP fluorescence early during BTV-1 NS1-eGFP infection and maintenance in a minority of infected KC cells (demonstrated above) are unknown, but may have significance in understanding the requirements for NS1 during BTV replication. To test whether deletions in the full length Seg-5 that also incorporated eGFP, could be responsible for loss of the eGFP fluorescence during serial passage of BTV-1 NS1-eGFP, KC cells from each replicate were harvested after every passage, until passage 6, and dsRNA was isolated and analysed.

Initially, the size of each genomic segment (kb) was assessed by polyacrylamide gel electrophoresis, to identify any gross rearrangments in the viral genome-segments during passaging. The size of unmodified segments 1 to 4 and 6 to 10 of BTV-1 NS1-eGFP were indistinguishable from the parental BTV-1, as expected. A band of 1.7 kb, corresponding to parental Seg-5, was present in the unmodified BTV-1 at all passages analysed (figure 3.5A, B).

BTV-1 NS1-eGFP possessed a 2.6 kb band, corresponding to the predicted size of Seg-5 incorporating eGFP at passage levels 1 to 5 in KC cells (figure 3.5A, B). However, the intensity of the 2.6 kb band reduced with increasing passage, indicating a reduction in the percentage of virus particles possessing Seg-5 with full length eGFP. A smaller segment of unknown sequence identity, at approximately 1.6 kb was visible in BTV-1 NS1-eGFP at passage levels 4 to 6 in KC cells. The intensity of the smaller segment increased with increasing passage (figure 3.5A, B), suggesting that it was replacing the larger full-length ‘fusion’ segment. Results were consistent between three independent replicates tested.

Figure 3.5: Deletion of the eGFP ORF sequence from the genome of BTV-1 NS1-eGFP during serial passage.

The profile of genomic segments 1 to 10 from unmodified BTV-1 (WT) and BTV-1 NS1-eGFP (NS1-eGFP) after (**A**) 1, 3 and 6 *C. sonorensis* (KC) cell passages, and (**B**) 4, 5 and 6 passages in KC cells. The profile of a mock infected control is included following 6 passages in KC cells (Mock) to demonstrate the absense of cross-infection between wells during serial passaging. KC cells were harvested after each passage, genomic dsRNA was isolated and BTV segments were separated by polyacrylamide gel electrophoresis. Data shown is representative of the three independent replicates of each passage. Arrows indicate the location of the novel small segment at approximately 1.6 kb. The location of the full length Seg-5 possessing eGFP is shown by the orange arrows.

Figure 3.5

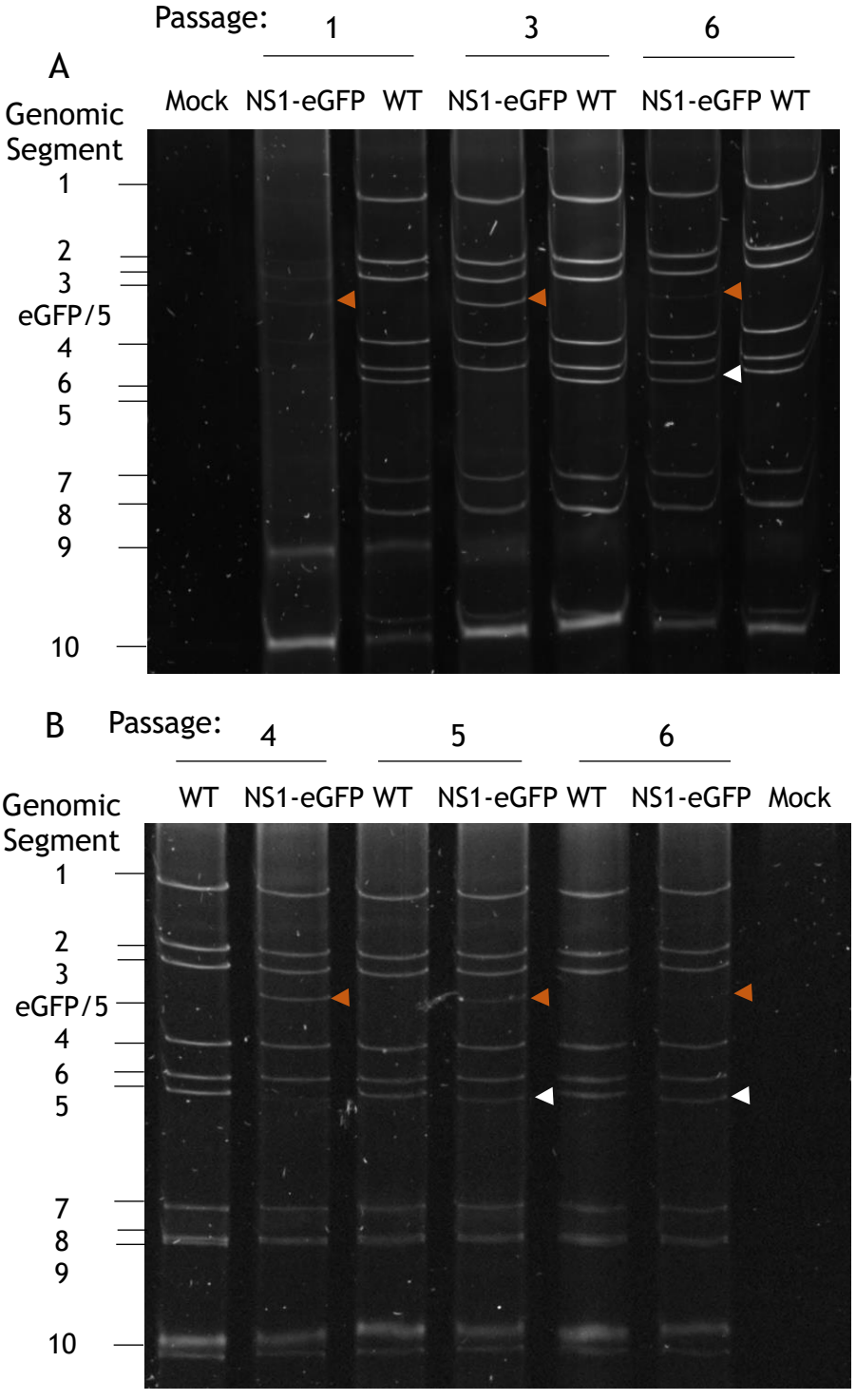
A
Passage:
1
3
6
Mock
NS1-eGFP
WT
NS1-eGFP
WT
NS1-eGFP
WT
Genomic Segment
1
2
3
eGFP/5
4
6
5
7
8
9
10
B
Passage:
4
5
6
WT
NS1-eGFP
WT
NS1-eGFP
WT
NS1-eGFP
Mock
Genomic Segment
1
2
3
eGFP/5
4
6
5
7
8
9
10

To genetically characterise the novel 1.6 kb segment, cDNA was reverse transcribed from dsRNA isolated as above, using primers targeting the 3' and 5' termini, to generate the full length Seg-5 of BTV-1 NS1-eGFP viruses in KC cell passages 1, 3 and 6. The size of amplified cDNA was assessed on an agarose gel, then Sanger sequenced, as described in Chapter 2 (section 2.11).

Although Seg-5 isolated at passage 1 of BTV-1 NS1-eGFP appeared to be the 'correct' size predicted for Seg-5 possessing the eGFP coding sequence, at approximately 2.6 kb (figure 3.6A), deletion of the existing stop codon at the 3' terminus of the eGFP ORF had resulted in a Glycine and Serine amino acid extension to the C-terminus of the eGFP ORF.

In all three replicates tested, Seg-5 isolated from BTV-1 NS1-eGFP at passage 3, ranged in size from approximately 1.6 to 2.6 kb (figure 3.6A). A 45 bp sequence of heterologous sequences was identified between the NS1 and eGFP ORFs, indicating a mixed BTV population. The consensus sequence of this region was found to be analogous to the 3'UTR sequence of Seg-5 (figure 3.6B), indicating that population of BTVs exist which are lacking the eGFP ORF. Seg-5 isolated from passage 6 was approximately 1.7 kb in size and lacked the GFP coding sequence, but possessed a full length 3'UTR analogous to the BTV-1 reference strain. Indicating that Seg-5 had reverted to 'wild-type' (figure 3.6A, B).

To characterise individual variants within the heterologous BTV-1 NS1-eGFP population at passage 3, the sequence of the variable intergenic region between Seg-5 and eGFP ORFs was determined. A total of 90 independent cDNA clones were produced by amplifying a region from the genomic dsRNA isolated from three independent replicate passages (figure 3.6 A, a to c), spanning Seg-5 nt 1820 (NS1 aa 523) through to nt 2502 of the 3'UTR of Seg-5 (figure 3.6C). Amplified sequences were cloned into a pGEM-T vector, as described previously (see Chapter 2, section 2.12), clones were sequenced and the resulting nucleotide and amino acid sequences covering the length of the intergenic region were compared with Seg-5 of the BTV-1 reference strain and full length eGFP. High quality variable sequence data were obtained from 84.4% (76/90) of cDNA clones. Only 1.3% of successfully sequenced clones (1/76 clones) possessed eGFP with no deletions, whereas the remaining clones possessed full length deletions in the eGFP ORF. Between 79.4 to 93.9% of clones analysed were homologous to Seg-5 of the BTV-1 reference strain (replicate: a = 26/28, b = 13/14, c = 27/34 clones).

A clone was identified possessing a 21 bp deletion at the terminus of the Seg-5 ORF, which extended into the initial 29 bp of the 3'UTR. This deleted sequence corresponded to a 4 amino acid *C*-terminal extension to NS1 (NS1_552-LPIF). A second clone was identified, with a 22 amino acid truncation to NS1 (NS1Δ530-FSSSIFS), resulting from a 42 bp deletion at the terminus of the Seg-5 ORF which extended into the initial 38 bp of the 3'UTR. The NS1_552-LPIF and NS1Δ530-FSSSIFS deletion mutants represented a small proportion of the virus population and were detected in 1.3% (1/76 clones) to 2.6% (2/76 clones) of cDNA clones analysed, respectively (figure 3.6D). These data indicate that the heterologous sequence between the NS1 and eGFP ORFs (described above) was likely to represent a mixed population of BTVs possessing the full length eGFP or deleted eGFP.

To effectively package their genome, NS1-eGFP variants are predicted to maintain the structure of the unpaired loop formed between 5' and 3' termini, required for intermolecular base pairing between Seg-10 (Boyce et al., 2016). Secondary structure predictions based on minimum free energy calculations of the variant sequences (Zuker, 2003) showed no differences in the 5' and 3' termini of Seg-5 of NS1-eGFP, NS1Δ530-FSSSIFS and NS1_552-LPIF with the BTV-1 reference strain (figure 3.6E), indicating that the sequence differences conferred no alteration in RNA folding between segment termini.

Figure 3.6: Sequence characterisation of Seg-5 of BTV-1 NS1-eGFP variants from different passages.

(A) Profile of full length Seg-5 from cDNA isolated from three independent replicates (a to c) of NS1-eGFP passaged 1, 3 and 6 times in KC cells. Mock infected (Mock) and unmodified BTV-1 (WT) controls were included and the expected size of unmodified Seg-5 (black arrow) and Seg-5 possessing eGFP (red arrow) are shown. (**B**) Full length Seg-5 was sequenced and consensus sequences from passages 3 and 6 are illustrated, showing a partial or full-length 'upstream' 3'UTR at the intergenic region of NS1 and eGFP. Numbers indicate the size of each genomic segment (kb). (**C**) cDNA clones of Seg-5 from passage 3 of BTV-1 NS1-eGFP were amplified using primers flanking the intergenic region. (**D**) Amino acid sequences at the C-terminus of NS1 (black shaded area) in cDNA clones possessing NS1, NS1Δ530-FSSSIFS or NS1_552-LPIF. Amino acids that are absent in unmodified NS1 are underlined and numbers indicate amino acid positions. (**E**) Representative free minimum energy secondary structure prediction of the 5' and 3' termini of Seg-5 from cDNA clones generated in Mfold (Zuker, 2003). Numbers indicate the base position within unmodified segment 5 and bases of an unpaired loop predicted to interact with Seg-10 are shown (red) (Boyce et al., 2016).

Figure 3.6

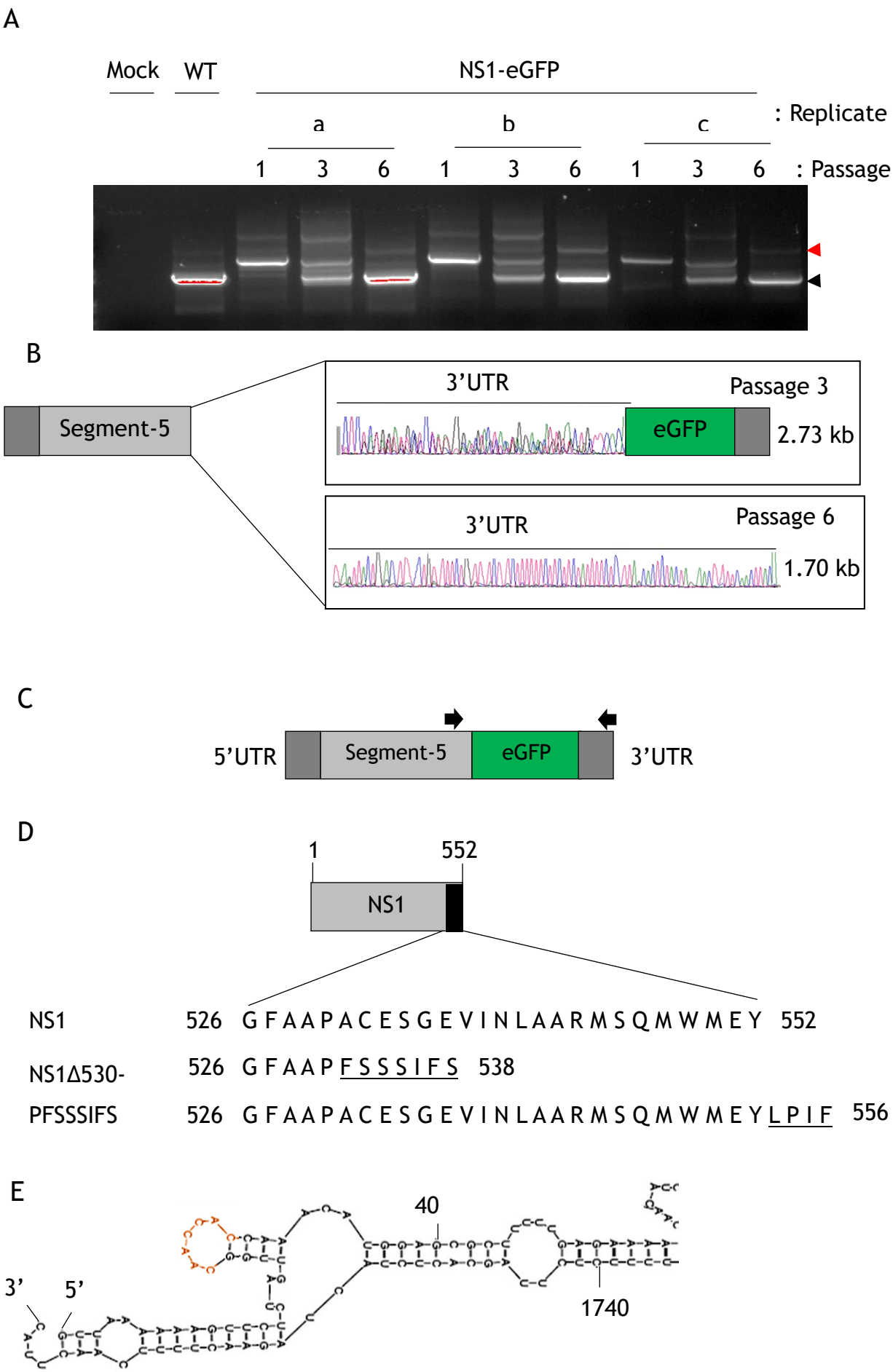
A
Mock
WT
NS1-eGFP
: Replicate
a
b
c
1 3 6 1 3 6 1 3 6
: Passage
B
Segment-5
3'UTR
Passage 3
eGFP
2.73 kb
3'UTR
Passage 6
1.70 kb
C
5'UTR
Segment-5
eGFP
3'UTR
D
1
552
NS1
NS1 526 G F A A P A C E S G E V I N L A A R M S Q M W M E Y 552
NS1Δ530- 526 G F A A P F S S S I F S 538
PFSSSIFS 526 G F A A P A C E S G E V I N L A A R M S Q M W M E Y L P I F 556
E
40
1740
3'
5'

3.2.5. Fluorescence labelling of BTV in infected KC cells

It was concluded that expression of eGFP is unlikely to provide an accurate indicator of BTV-1 NS1-eGFP localisation in whole *Culicoides* due to early loss of eGFP fluorescence. Simultaneous fluorescence labelling of BTV protein and non-genomic BTV RNA were therefore tested as alternative means of detecting BTV and BTV replication *in vivo*.

To determine which proteins were detected by antisera against purified BTV (Orab 279), BSR cells were infected in triplicate at an MOI of 0.1 with BTV-1 SA (P1 BSR), or were mock infected. Viral proteins were detected in cell lysate and supernatant by western blot analysis with polyclonal Guinea pig antiserum against purified BTV-1 virus particles (Orab 279), which was generated prior to the project by Professor Peter Mertens (The Pirbright Institute, UK). β–actin was used as a loading control. BTV proteins were only detected in infected cells (figure 3.7A).

VP5 was detected at high levels in cell lysate by western blotting compared to VP7 and VP2 or VP3 (ANOVA: $r^2 = 87\%$, $f_5 = 16$, $p<0.001$) and constituted a mean of 54±1.67(SE)% of BTV protein detected. Similarly, VP5 in supernatant accounted for 40±4.40% of the detected BTV protein, whereas VP2 and VP3 were less readily detected and constituted only a minor fraction of between 19±3.71(SE)% to 24±2.65(SE)% of the protein detected using this antiserum (figure 3.7B), indicating that Orab 279 antibodies primarily detect denatured VP5 protein.

To test the specificity of probes designed targeting Seg-5 of BTV-1, BSR cells were transfected without RNA (mock) or with transcripts of the positive strand (+Seg-5), negative strand (-Seg-5) (generated as described in Chapter 2, section 2.18.1) or duplexed strands of Seg-5 of the BTV-1 reference strain. At 2 h pt, cells were incubated with BTV-specific probes, each possessing a 5' TAMRA label. Fluorescence was detected in BSR cells transfected with +Seg-5 (figure 3.8) but was undetectable in cells transfected with –Seg-5, duplexed strands or without RNA, indicating that probes detect +Seg-5.

Figure 3.7: Staining and detection of VP5 at high levels in BTV-1 SA infected cells.
BSR cells were mock infected (uninfected) or infected in triplicate (replicates A to C) at an MOI of 0.1 with BTV-1 SA (P1 BSR). At 48 h pi, supernatant and cell pellets were harvested. **(A)** Cell and supernatant protein extracts were analysed by western blotting with polyclonal rabbit antisera against β-actin and Guinea pig antisera against purified BTV-1 (Orab 279). BTV VP5, VP7, VP2 and VP3 (VP2/VP3) were detected. (**B**) The intensity of each BTV protein was expressed as a percentage of total BTV protein intensity in cell lysate or supernatant, normalised against β-actin and background (** = $p<0.001$ by ANOVA with post-hoc Tukey's test). Bars represent the mean ± standard deviation of triplicate samples.

Figure 3.7

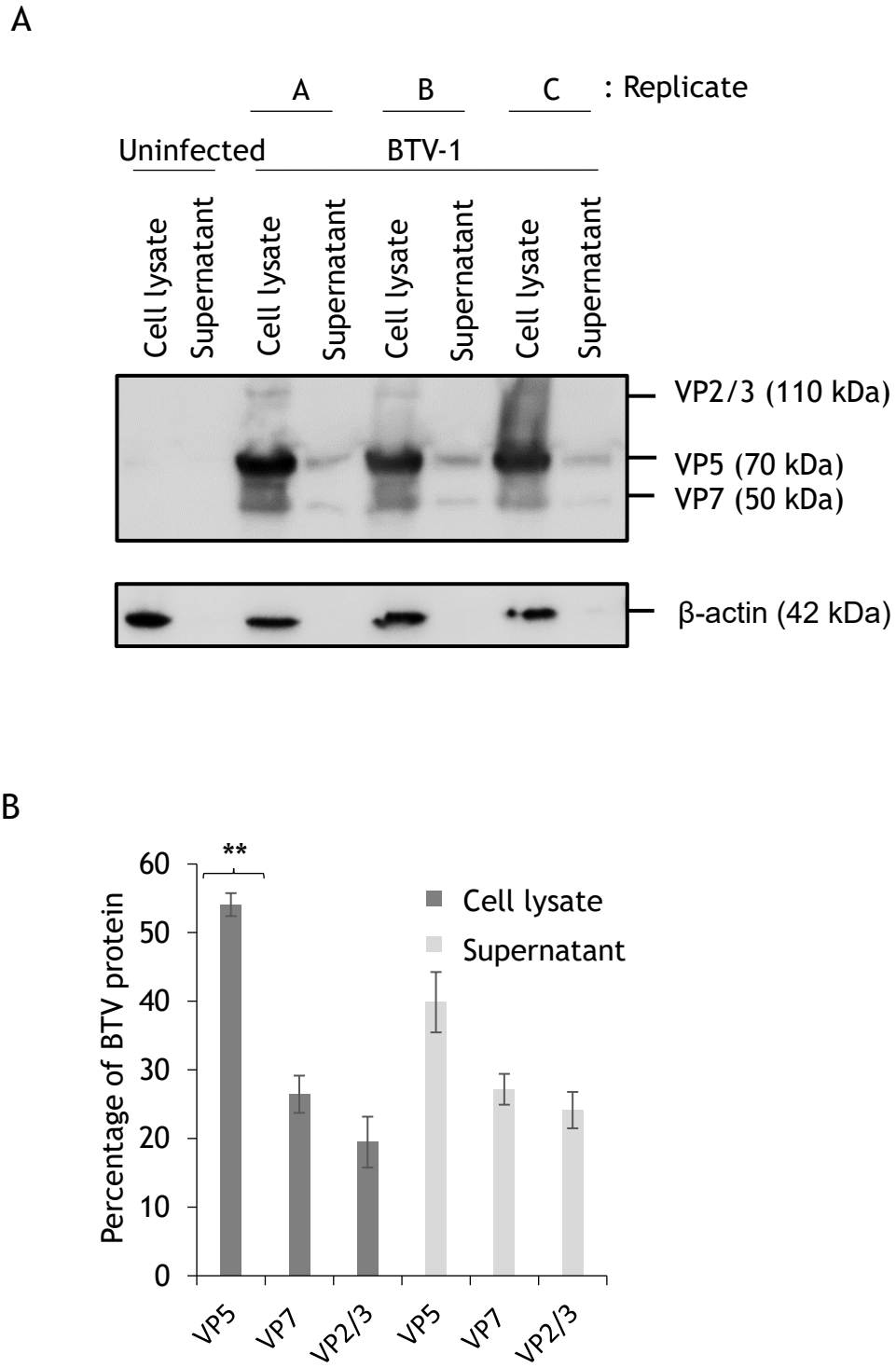
A
A
B
C
: Replicate
Uninfected
BTV-1
Cell lysate
Supernatant
Cell lysate
Supernatant
Cell lysate
Supernatant
Cell lysate
Supernatant
VP2/3 (110 kDa)
VP5 (70 kDa)
VP7 (50 kDa)
β-actin (42 kDa)
B
Percentage of BTV protein
60
50
40
30
20
10
0
**
Cell lysate
Supernatant
VP5
VP7
VP2/3
VP5
VP7
VP2/3

Figure 3.8

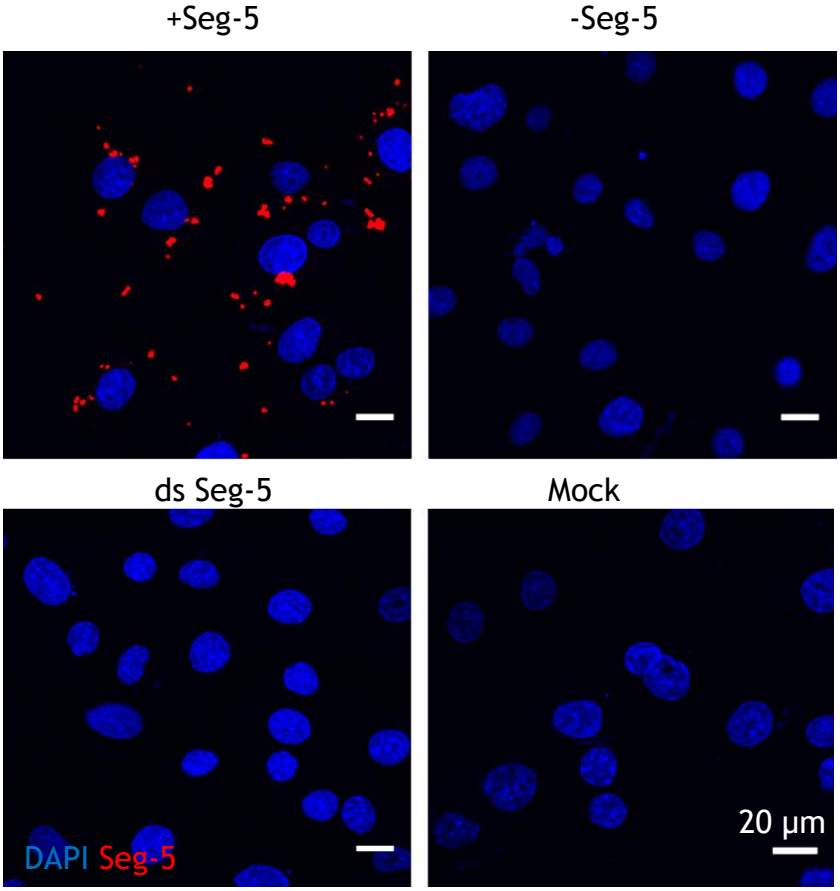

Figure 3.8: Detection of single-strand positive sense Seg-5 RNA of BTV-1 SA.

BSR cells were transfected with either single-stranded negative sense (-Seg-5), single-stranded positive-sense (+Seg-5) or double-stranded RNA (ds Seg-5) of BTV-1 Seg-5 generated from annealed transcripts. A negative control was included, transfected without RNA (Mock). Cells were hybridised with probes designed against the positive strand of Seg-5 of the BTV-1 reference strain (pS5_TAM). Each probe was tagged at the 5' by TAMRA, shown in red (scale = 20 µm).

Since +Seg-5 RNAs are only expressed in detectable, single-stranded form during BTV replication, expression indicates cells in which BTV mRNAs are expressed. Whereas, BTV protein (mostly, VP5) indicates presence of protein synthesis or viral particles. BTV proteins and +Seg-5 were both detected in the cytoplasm of KC cells (figure 3.9A) and BSR cells (figure 3.8B) at 48 h pi at an MOI of 0.01 with BTV-1 SA or BTV-11 USA (P2 BSR), but were undetectable in mock infected cells (figure 3.9A, B). Indicating that BTV strains used in the studies described in Chapter 5 are detectable with +Seg-5 probes and polyclonal antisera.

Intensity of +Seg-5 (t-test: $t_{21} = 0.77$, $p = 0.449$) and protein (Mann-Whitney *U*: $W_{12} = 125.0$, $p = 0.157$) labelling did not differ between BSR cells infected with BTV-1 or BTV-11, indicating that BTV-1 and BTV-11 are detectable with +Seg-5 probes and antivirus antisera. Intensity of +Seg-5 and protein was close to background levels in mock infected control BSR cells, which is as expected and indicates minimal non-specific binding (figure 3.8C).

3.2.6. Fluorescence labelling of BTV in infected adult *Culicoides*

C. sonorensis sections (see Chapter 2, Section 2.18.2) were co-incubated with Orab 279 antisera and +Seg-5 probes. BTV proteins and +Seg-5 were both expressed in cells of 35% (n = 12/34) of *C. sonorensis*, 5 days after feeding on blood supplemented with 6.3 $\log_{10}$ $TCID_{50}$/ml of unmodified BTV-1 (P2 KC). Cells expressing BTV proteins and +Seg-5 were detected in the midgut or multiple tissues, including epithelial cells. BTV proteins and +Seg-5 were undetectable in mock infected *C. sonorensis* (figure 3.10A, B), indicating that signal was below the intensity of autofluorescence in these 'negative' controls. These data indicate that cells expressing BTV proteins and +Seg-5 can be visualised in *Culicoides* tissues.

Figure 3.9: Detection of BTV-1 SA and BTV-11 USA in KC cells.

(**A**) KC cells and (**B**) BSR cells were mock infected (Mock), or infected at an MOI of 0.01 with BTV-1 SA or BTV-11 USA (P2 BSR). At 24 h pi, cells were co-labelled with polyclonal Guinea pig antisera against purified BTV-1 virus particles (Orab 279, VP), shown in green, and oligonucleotide probes against the positive strand of Seg-5 (+Seg-5), shown in red. Nuclei were counterstained with DAPI, shown in blue (scale = 20 µm). (**C**) The intensity of +Seg-5 and viral protein (VP) labelling in BSR cells mock infected (Mock) or infected with BTV-1 or BTV-11 was normalised against background. Bars show the standard error of the mean intensity of individual cells measured in quadruplicate in three images (ns = non-significant difference using a Student's t-test (+Seg-5) or a Mann-Whitney *U* test (VP)).

Figure 3.9 A

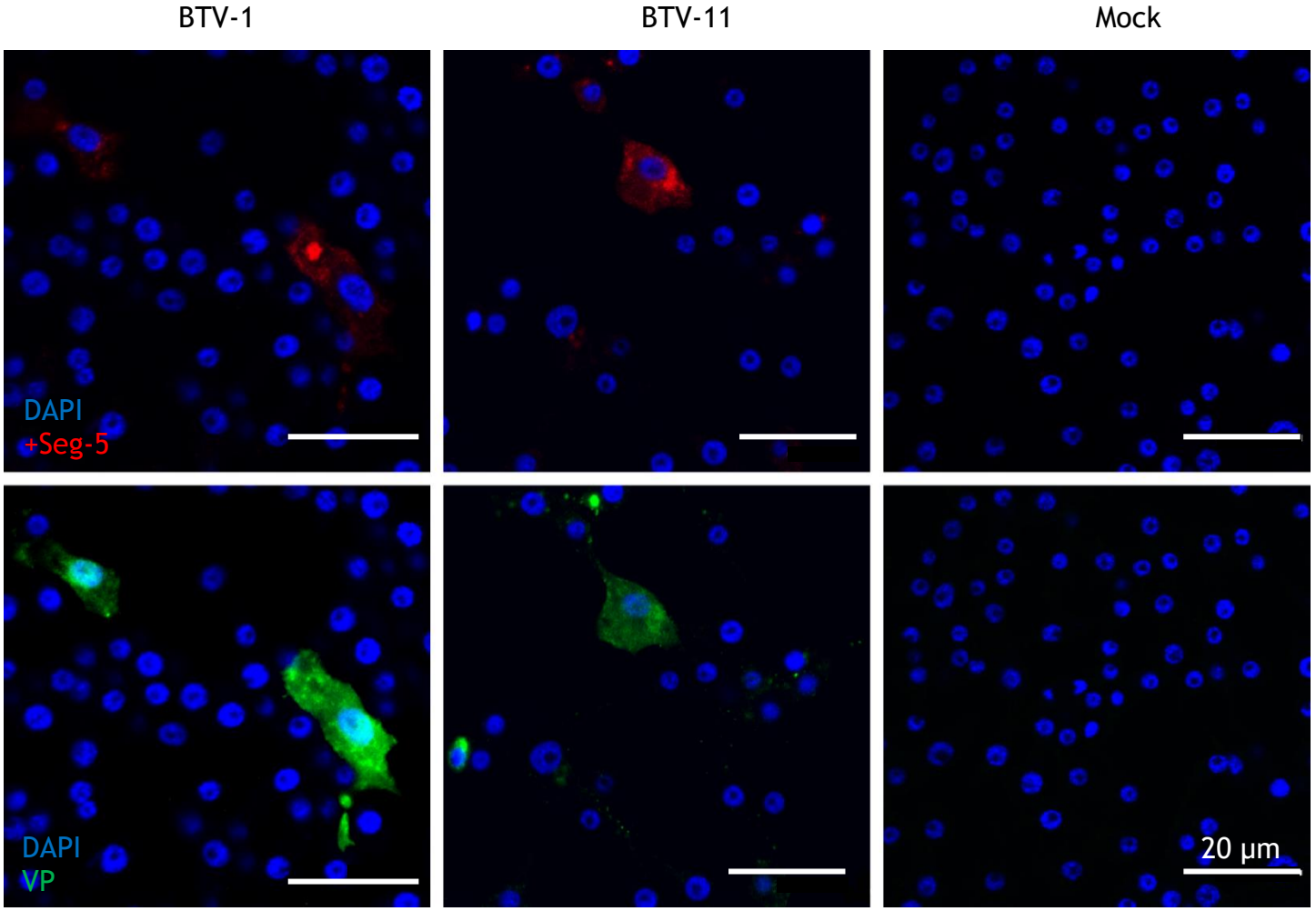

Figure 3.9 B

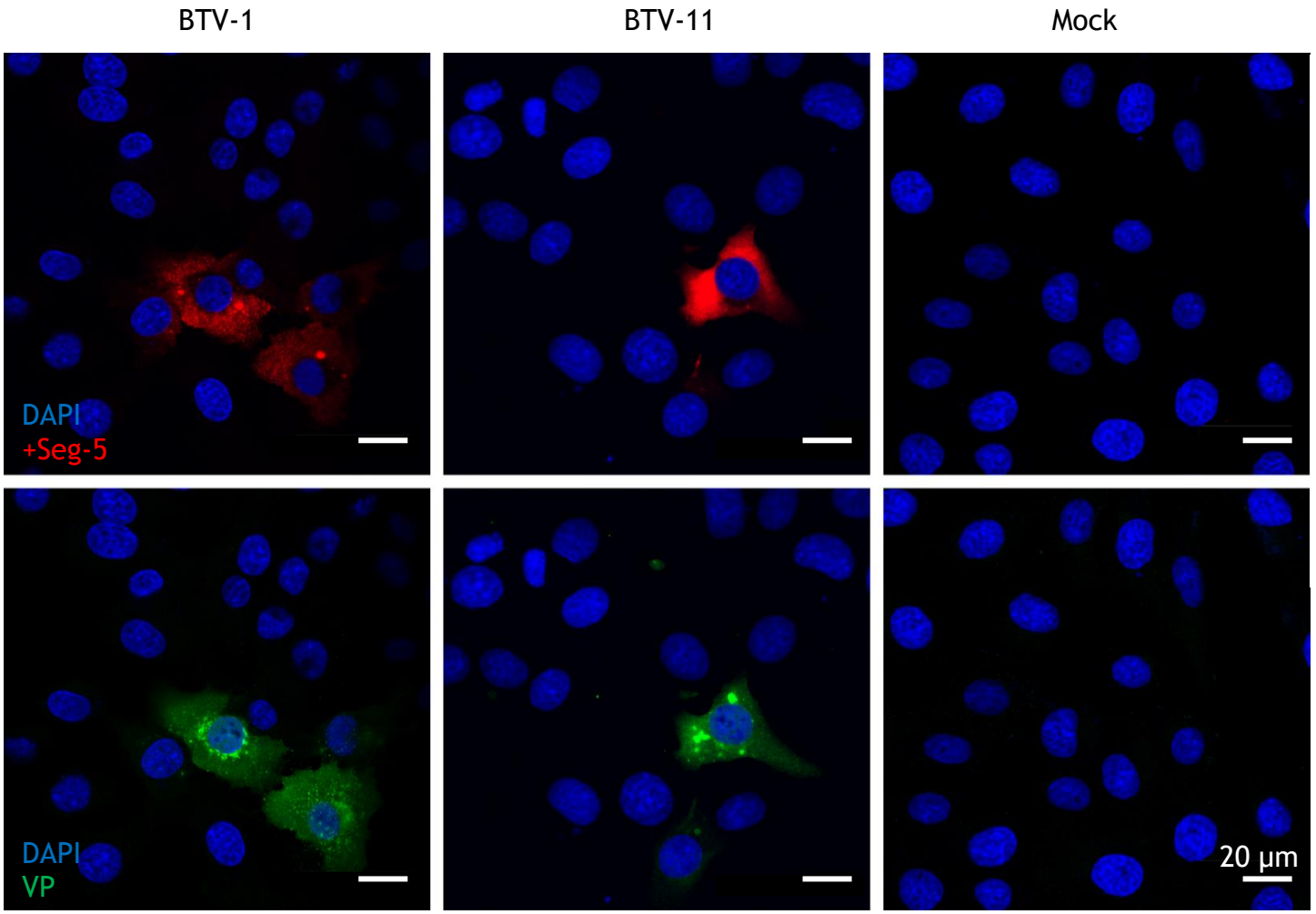
BTV-1
BTV-11
Mock
DAPI
+Seg-5
DAPI
VP
20 µm

C

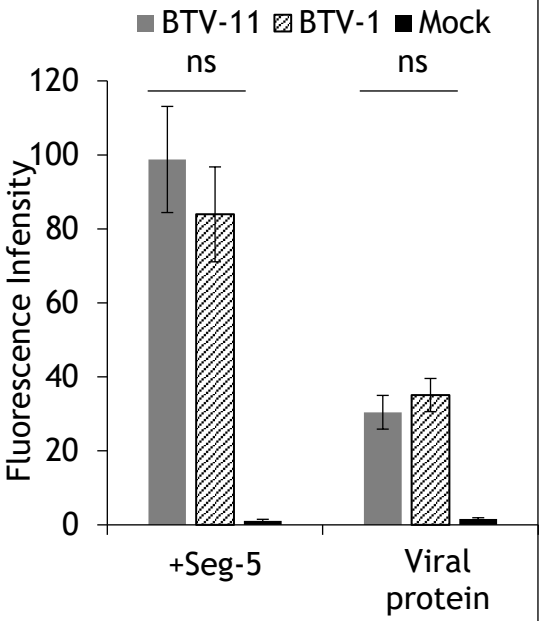
BTV-11
BTV-1
Mock
ns
ns
120
100
80
60
40
20
0
Fluorescence Infensity
+Seg-5
Viral protein

Figure 3.10: BTV-1 SA detection in *Culicoides*.

(A) Diagrammatic representation of the tissues of *C. sonorensis* as described in section 4.3.1 of Chapter 4. Showing the locations of the thorax and abdomen. The crop, ovaries and mouthparts are also illustrated (scale = 200 µm).

(**B**) *C. sonorensis* were fed on blood containing 6.3 $\log_{10}$ $TCID_{50}$/ml of unmodified BTV-1 (P2 KC). An uninfected control group was included that had been fed on blood supplemented with DMEM (Uninfected). At 5 days post-blood meal (PBM), *C. sonorensis* were sectioned (see Chapter 2, Section 2.18.2). Sections were incubated with polyclonal Guinea pig antisera against BTV protein (VP), shown in green, and oligonucleotide probes against positive sense Seg-5 (+Seg-5), shown in red. Cells expressing +Seg-5 and BTV protein were identified in the midgut (and were classified as a non-disseminated infection) or in multiple tissues (termed a disseminated infection). Selected infected areas (including the midgut) are outlined and shown enlarged right of the corresponding image (scale = 75 µm).

Figure 3.10

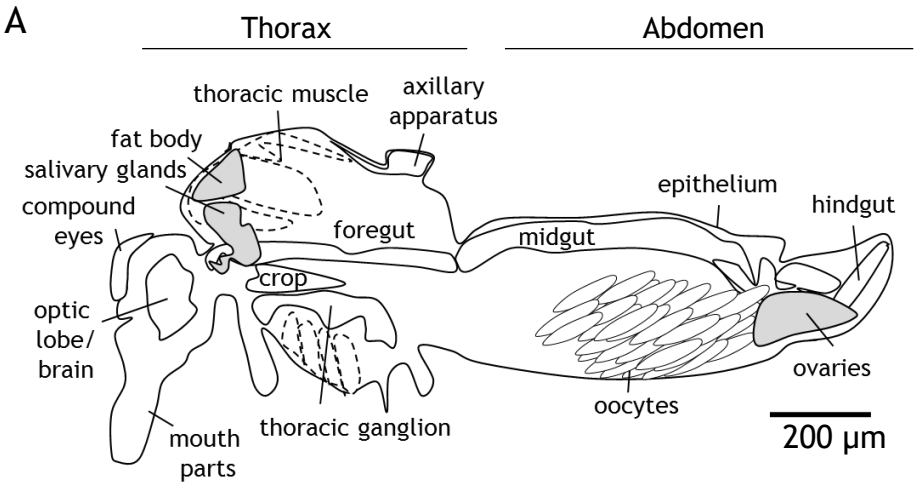
A
Thorax
Abdomen
thoracic muscle
axillary apparatus
fat body
salivary glands
compound eyes
foregut
crop
midgut
epithelium
hindgut
optic lobe/ brain
ovaries
oocytes
thoracic ganglion
mouth parts
200 µm

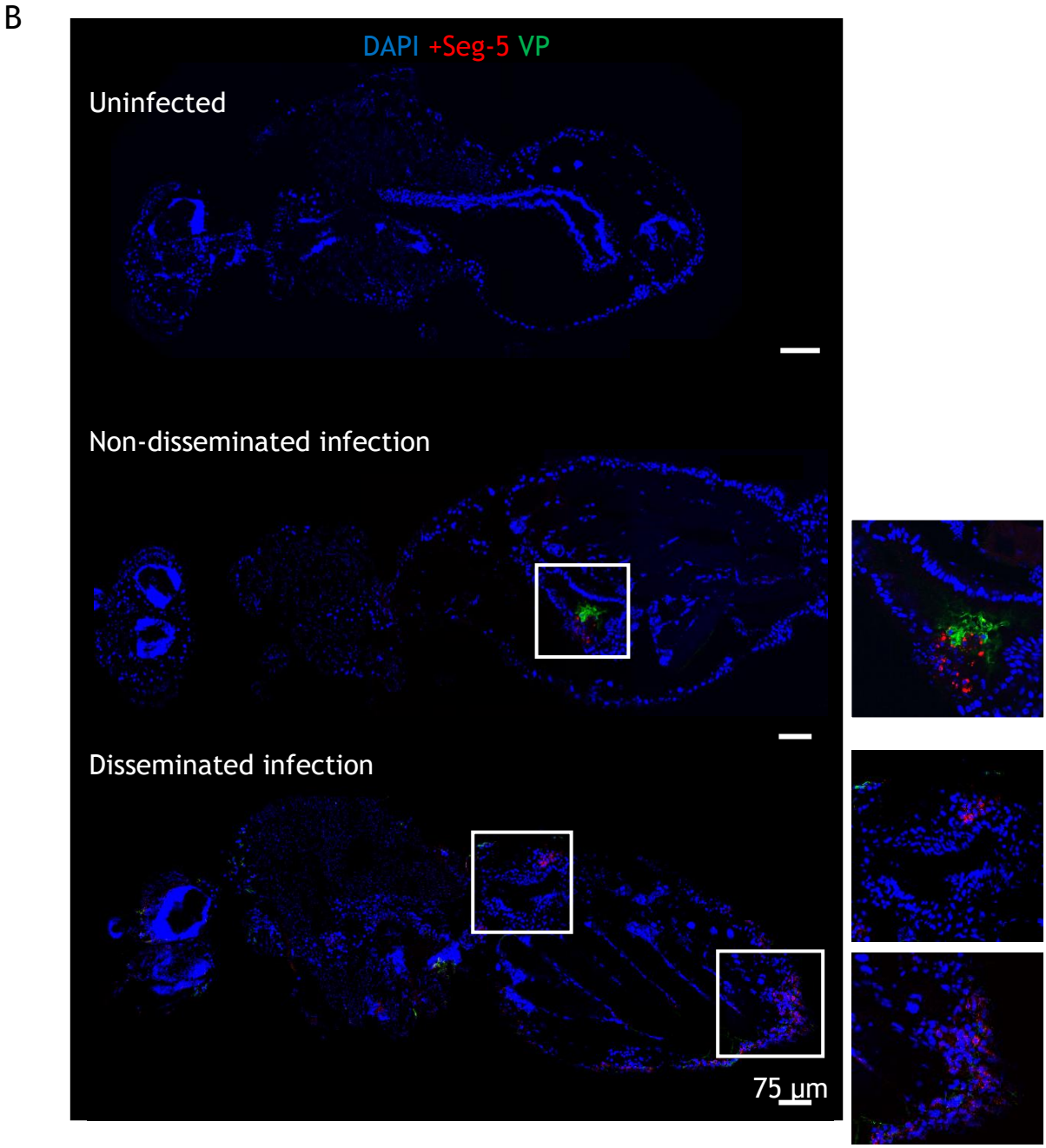
B
DAPI +Seg-5 VP
Uninfected
Non-disseminated infection
Disseminated infection
75 µm

3.3. Discussion

Integration of a reporter gene into the viral genome enables virus localisation to be determined at precise, cellular resolution, as a fluorescence signal will only be detectable in cells in which viral protein has been synthesised. The current chapter describes the rescue and characterisation of a replication competent BTV-1 expressing an eGFP reporter (NS1-eGFP), designed to enable visualisation of NS1 within infected cells. The eGFP reporter was expressed at high levels in mammalian cells during initial replication and may be exploited as an indicator of BTV entry or localisation during early infection. The application of BTV-1 NS1-eGFP as a model of BTV-1 localisation within whole *Culicoides,* was assessed by assaying growth and eGFP expression in KC cells. However, the results obtained demonstrate that genomic insertions are removed through deletions during successive BTV replication cycles, which result in loss of eGFP expression and fluorescence while maintaining the structure and function of NS1 in *Culicoides* cells. Given that loss of eGFP expression arose during early stages of BTV infection, quantitative fluorescence imaging studies of BTV-1 NS1-eGFP would not be an accurate model of parental viral quantity and precise localisation within tissues of whole *Culicoides*. These data generated highlight a need for an in depth understanding of BTV packaging and structural analyses of targeted proteins for future attempts to construct BTVs encoding reporter proteins. Studies should also consider the effects of incorporating foreign genes on the protein's ability to form essential contacts with molecular partners, which may be essential to protein function.

The eGFP reporter was introduced after the *C*-terminus of NS1, producing a BTV-1 expressing a viral NS1-eGFP fusion protein (NS1-eGFP). Many studies have developed viruses expressing reporter proteins fused to either terminus of a viral polypeptide (Kittel et al., 2004, Kummerer et al., 2012, Perez et al., 2013, Tran et al., 2013), including Influenza A viruses expressing GFP variants, eCFP, eGFP, mCherry and Venus fused to the *C*-terminus of NS1; and BTV-10 expressing mCherry in the predicted transmembrane domain of NS3/NS3A (Shaw et al., 2012, Fukuyama et al., 2015). Such reporter viruses frequently exhibit attenuated growth and reduced pathogenicity (Fukuyama et al., 2015, Kittel et al., 2004) compared to parental 'wild-type' viruses. Indeed, incorporation of a 26.9 KDa protein at the *C*-terminus of NS1 in studies presented here resulted in a delay in growth and increased tubule aggregation close to VIBs.

BTV NS1 promotes translation of viral mRNAs which lack a 3' poly(A) sequence (Boyce et al., 2012b). Therefore, aggregation of tubules could impair interactions of NS1 with the UTRs that is needed to upregulate protein synthesis (Boyce et al., 2012b), which may result in the delayed growth phenotype observed for BTV-1 NS1-eGFP in both cell lines tested. Additionally, NS1 is involved in BTV morphogenesis (Boyce and Roy, 2007, Roy, 2008b). Localisation of enlarged tubule clusters to VIBs, rather than in an ordered configuration across the cytoplasm (Huismans and Els, 1979a, Urakawa and Roy, 1988a), may inhibit cellular pathogenicity of BTV-1 NS1-eGFP and delay virus replication. This reduced growth profile of BTV-1 NS1-eGFP would therefore inhibit CPE in mammalian cells compared to unmodified BTV-1. A reduction in CPE would account for smaller plaque formation and a lower observable growth of BTV-1 NS1-eGFP, as infectious viral titre was assayed by observing CPE formation.

An increase in tubule agglomeration and inhibition in growth caused by polypeptide extension could be due, in part, to the presence of a sequence insert, as addition of a small insert of 19 amino acids to the *C*-terminus of NS1 of BTV-10 prevented tubule formation (Monastyrskaya et al., 1995), but may also be caused by the site of insertion (Wertz et al., 2002) and specific amino acid sequence of the insert (Teterina et al., 2010), shown to affect vesicular stomatitis virus (VSV) and poliovirus (PV) replication potential.

Sequences extending into the 5' and 3' termini of the NS2 ORF (Seg-8) were previously shown to be essential for replication (Burkhardt et al., 2014) and uncharacterised *cis*-acting elements are present in the coding sequence of at least one other BTV segment (Boyce et al., 2016). The insertion site and polypeptide sequence need to be carefully considered in future attempts to generate reporter BTVs possessing a functional parental-strain growth phenotype. Potential reporter gene insertion sites may be identified by generating a library of transposon-induced random insertions in NS1; previously employed to generate PV (Teterina et al., 2010), hepatitis C virus replicons (Moradpour et al., 2004) and Sindbis virus (Frolova et al., 2006, Atasheva et al., 2007) with GFP inserted into non-structural proteins.

We subsequently investigated whether expressing eGFP and NS1 as single proteins would overcome growth defects associated with expressing eGFP as an NS1 polyprotein. In an approach applicable to the dsRNA orbiviruses, which are capable of head-to-tail segment duplications (Eaton and Gould, 1987, Anthony et al., 2011, Navarro et al., 2013), eGFP was incorporated as an ORF downstream of NS1 (NS1/eGFP), but enabled only transient expression of unmodified eGFP. Loss of eGFP fluorescence during rescue of BTV-1

NS1/eGFP may be due in part to size constraints on the BTV genome caused by subcore formation (Grimes et al., 1998), which could restrict efficient packaging to dimeric concatemers formed by only the smallest genomic segments 9 and 10 (Eaton and Gould, 1987, Gould and Hyatt, 1994, Anthony et al., 2011). Concatemers form naturally from segment dimerisation, rather than insertion of foreign sequences and stability of an insert within the viral genome may also depend on specific sequence, as shown in rotaviruses (Navarro et al., 2013).

RNA viruses, such as BTV are thought to replicate rapidly with low fidelity and accumulate mutations at high frequency (Domingo and Holland, 1997, Smith et al., 2014), especially under population bottlenecks (Clarke et al., 1993), imposed on a mammalian host-adapted virus (Cooper and Scott, 2001) by replication in insect cells (Novella et al., 1999, Forrester et al., 2014). Despite this, several strains of BTV have shown very high levels of sequence conservation in the field over several decades. However, deletion events in the eGFP ORF did occur during low MOI passage in KC cells generating heterologous BTV-1 NS1-eGFP viruses that had lost the ability to express eGFP. The complete eGFP coding sequence was deleted in a single event at passage 3, at which time most sequences were comparable to parental Seg-5.

Recombination events between related molecules or distinct virus strains can occur with high frequency in Foot and Mouth Disease viruses (Seago et al., 2013) or PV (Mueller and Wimmer, 1998, Teterina et al., 2010) expressing a viral protein-GFP polyprotein. Further evidence is needed to conclude that events leading to the reconstruction of the 3'UTR, noted here, occur due to intragenic recombination, which may arise at low frequency in BTV genome segments (He et al., 2010). The 7 nt deletion in the 3' terminus of eGFP presumably accounted for loss of eGFP fluorescence in 78% of infected KC cells after initial passage and conferred a replication advantage to BTV-1 NS1-eGFP, when compared to reduced growth and increased eGFP expression in CPT-*Tert* cells. Further studies are needed to determine the prevalence of this sequence and confirm its origin from a deletion event, rather than an artefact of sequencing or cDNA synthesis. Loss of eGFP fluorescence in 64% of KC cells within 24 h after infection is consistent with emergence of deletion variants within the first round of replication, as demonstrated previously with human immunodeficiency virus (HIV) and picornaviruses (Lu et al., 1995a, Lu et al., 1995b). Hence, even during early KC cell infection, eGFP expression is likely to prove an inaccurate indictor of BTV-1 NS1-eGFP localisation.

Directly labelling BTV-1 using anti-virus antisera and +Seg-5-specific probes provided a means of visualising BTV proteins (predominantly, VP5) and non-genomic RNA in individual cells of *C. sonorensis* tissues. Anti-BTV-1-virion antisera and +Seg-5-specific probes could detect both BTV-1 SA and BTV-11 USA strains in BSR and KC cells. Since the intensity of BTV-1 SA labelling was comparable to BTV-11 USA in BSR cells, the affinity of antibodies and probes for target protein and RNA, respectively, is unlikely to differ between viral strains, despite variation in amino acid and nucleotide sequences. Application of fluorescence labelling for quantifying BTV in *C. sonorensis* tissues provides the focus of studies in Chapter 4.

Despite the presence of deletion variants, eGFP is expressed in approximately 9 to 37% of infected KC cells over multiple passages, indicating that BTV-1 NS1-eGFP replicates sufficiently well to remain in a population that contains variants possessing shorter inserts or the 'wild-type' segment. BTV-1 NS1-eGFP represented only 1.3% of sequenced BTV variants at passage 3, but eGFP fluorescence was detected in approximately 30% of infected cells at this time. The surprisingly low prevalence of BTV-1 NS1-eGFP in viral genotypes, likely reflects the high sensitivity of eGFP fluorescence detection or the frequent selection and sequencing of cDNA clones possessing shorter inserts, as the cloned insert possessing eGFP showed deficient growth in *E. coli* during cloning to generate a plasmid containing NS1-eGFP and reduced PCR amplification efficiency possibly due to its longer size.

Deletion events were generally conserved between replicates and favoured specific genotypes, as previously demonstrated for PVs (Lu et al., 1995a). Variant diversity could be limited by requirements for replication of the BTV genome, as genome segments retained stem-loop base pairing between the 5' and 3' ends of the molecule, required for packaging (Burkhardt et al., 2014, Boyce et al., 2016).

Characterisation of NS1-eGFP variants, NS1Δ530-FSSSIFS and NS1_552-LPIF, indicated that their Seg-5 ssRNAs possessed a deleted region in 3'UTR and 3' ORF of segment 5. Deletion of this region indicates that sequences within the terminus of the NS1 ORF and upstream 3'UTR are not essential for genome packaging, unlike Seg-9, (encoding VP6), where sequences extending into the 5' and 3' ORF were essential for packaging (Burkhardt et al., 2014). However *cis*-acting functional RNA elements and elements involved in upregulation and efficiency of protein translation that may exist within the deleted regions could be involved in optimising efficiency of genome sorting and packaging. The role of the

upstream 3’UTR and ORF of Seg-5 in packaging requires further investigation, beyond the scope of this thesis.

Chapter 4

Automated detection of bluetongue virus infection in *Culicoides sonorensis*

4.1 Introduction

In order to become transmissible, an arbovirus must successfully infect, replicate in and disseminate between tissues of its arthropod vector. The ability of an arthropod to become infected and biologically transmit an arbovirus is described as its 'vector competence' (Carpenter et al., 2015, Gerry et al., 2001). Vector competence is controlled by multiple genes (Bosio et al., 1998, Miller and Mitchell, 1991) and extrinsic factors (Richards et al., 2009, Oviedo et al., 2011), including the dose of ingested virus (Pongsiri et al., 2014a, Bennett et al., 2002, Mahmood et al., 2006) (see Chapter 5). The effects of these factors are conventionally measured by calculating the changes that they cause in the average infection rate of a vector population (Paweska et al., 2002b, Vazeille et al., 2007, Pesko et al., 2009). However, this approach can mask heterogeneity within a population, regarding an individual vector's response to viral infection. Events during infection of an individual arthropod vector are poorly characterised, in part due to insufficient knowledge concerning the anatomy for some groups of vector insects (such as *Culicoides*) where only early descriptions of the mouthparts (Jobling, 1928) and alimentary canal exist (Sutcliffe and Deepan, 1988, Megahed, 1956) (reviewed in section 1.2.2 of Chapter 1). The aim of the current chapter is to develop a method of automated image analysis to detect BTV in *Culicoides* midges.

A number of studies have identified temporal changes in the amount of virus present in whole insects, or in excised organs. The methods used include: imaging of radiolabelled virions (Weaver et al., 1991), real-time PCR (Dubrulle et al., 2009, Zhang et al., 2010a), virus isolation (Fu et al., 1999, McGee et al., 2010), immunofluorescence, *in situ* hybridisation (Drolet et al., 2005, McElroy et al., 2008, Linthicum et al., 1996) and imaging of fluorescently labelled virus particles (McGee et al., 2010). A combination of these methods was applied to compare the amount of virus and viral antigen in whole insects relative to levels in excised tissues: for dengue virus (DENV) (Salazar et al., 2007), la Crosse virus (LACV) (Chandler et al., 1998) and western equine encephalitis virus (WEEV) (Scott et al., 1984).

Recent advances in quantitative imaging have revealed the complexities of the pathogen lifecycle and the intricacies of pathogen spread through infected tissues with greater spatial resolution (Amino et al., 2006, Frischknecht et al., 2004, Palha et al., 2013). Evaluation of such image data, which is typically conducted manually, is time consuming, subjective, requires a high level of experience and is frequently error prone (Wahlby et al., 2004, Zhou and Wong, 2006). Numerous image analysis algorithms have been developed over the last

decade, which have increased the amount of data that can be obtained from digital images, allowing large image datasets to be analysed and manipulated (Carpenter et al., 2012). Despite this, many commercially available programs are expensive and are not specifically developed for the analysis of tissue datasets. A procedure was therefore developed to measure the amount of virus present in insect tissues by automated image analysis.

Previously, a recombinant BTV expressing eGFP as a *C*-terminal polypeptide of NS1 was rescued (see Chapter 3). However, it was concluded that the resulting virus strain was unlikely to provide an accurate indicator of NS1-eGFP-BTV-1 localisation *in vivo,* due to the rapid loss of eGFP signal after even a small number of replication cycles. Alternative methods were therefore developed to detect and visualise BTV Seg-5 positive sense ssRNA (+Seg-5) and proteins (predominantly VP5) (see Chapter 3, section 3.2.5) in *C. sonorensis* sections by confocal imaging. Algorithms (which we have called 'the Automated Infected Cell Counter' (AICC)) were developed in a meta-language (MATLAB®) to calculate the number of nuclei in imaged tissues and assign them to either infected or uninfected cells, based on viral protein (VP) and +Seg-5 detection. The AICC was used to analyse a set of confocal images of tissues from BTV infected *C. sonorensis,* in order to detect and quantify infected cells. The counts obtained were directly comparable to those acquired by manual counting and are therefore thought to be accurate, while allowing more rapid assessment of BTV loads in these tissues.

4.2 Methods

The AICC method, (shown in figure 4.1) was developed in MATLAB® 6.0 with the Image Processing Toolbox (Mathworks Ltd.). Scripts are available in the Appendix (section A.3). The AICC was tested using a dataset of confocal images of *C. sonorensis* (n = 54), captured at 7 and 12 days after blood feeding on 6.2 or 7.0 $\log_{10}$ $TCID_{50}$/ml of BTV-1 SA (P2 BSR) (see Chapter 2, section 2.3 for methods). The dataset was obtained by labelling serial sections of *Culicoides* with antisera against purified BTV-1 (Orab279) and the +Seg-5 probes, as described in Chapter 2 section 2.18.2. Confocal image tiles of each section were captured at 1024 x 1024 pixels in size and were saved using Tagged Image File Format (TIFF). The tiles were 'stitched' with the ImageJ 'Pairwise Stitching' tool (Preibisch et al., 2009). Stitched images, from the same *Culicoides*, were z-stacked, to combine multiple images at different focal depths, using Fiji software (Image J).

A user-defined 'region of interest' (ROI) was created for every tissue, in each image slice in a given z-stack, using the 'roipoly' function (figure 4.1A). The abdominal and thoracic epithelium, thoracic muscle, fat body, salivary glands, thoracic ganglia, optic lobe (including the central brain), compound eyes, midgut, foregut, hindgut and axillary apparatus were analysed. The analysis was divided into two main stages: stage 1 entailed the identification and summation of cell nuclei, while stage 2 classified nuclei as belonging to uninfected or infected cells, depending on the proximity to pixels with a green or red intensity above a certain specified threshold. Both stages are described in full detail below.

Figure 4.1: Illustration of the Automated Infected Cell Counter (AICC).

(**A**) Original RGB image showing a user-specified 'Region Of Interest' (ROI) of known area, outlined in red. (**B**) Binarization of the ROI and application of distance transform and watershed algorithms. (**C**) Close contacting nuclei were separated and the number of binarized clusters provides a count of nuclei. (**D**) A Voronoi diagram was applied to the ROI. The number of infected cells was defined as the number of Voronoi polygons containing pixels above the specified threshold value. The infected area was also counted. Shaded areas represent individual polygons; white lines show polygonal boundaries; red and green pixels above threshold are shown (red; green).

Figure 4.1

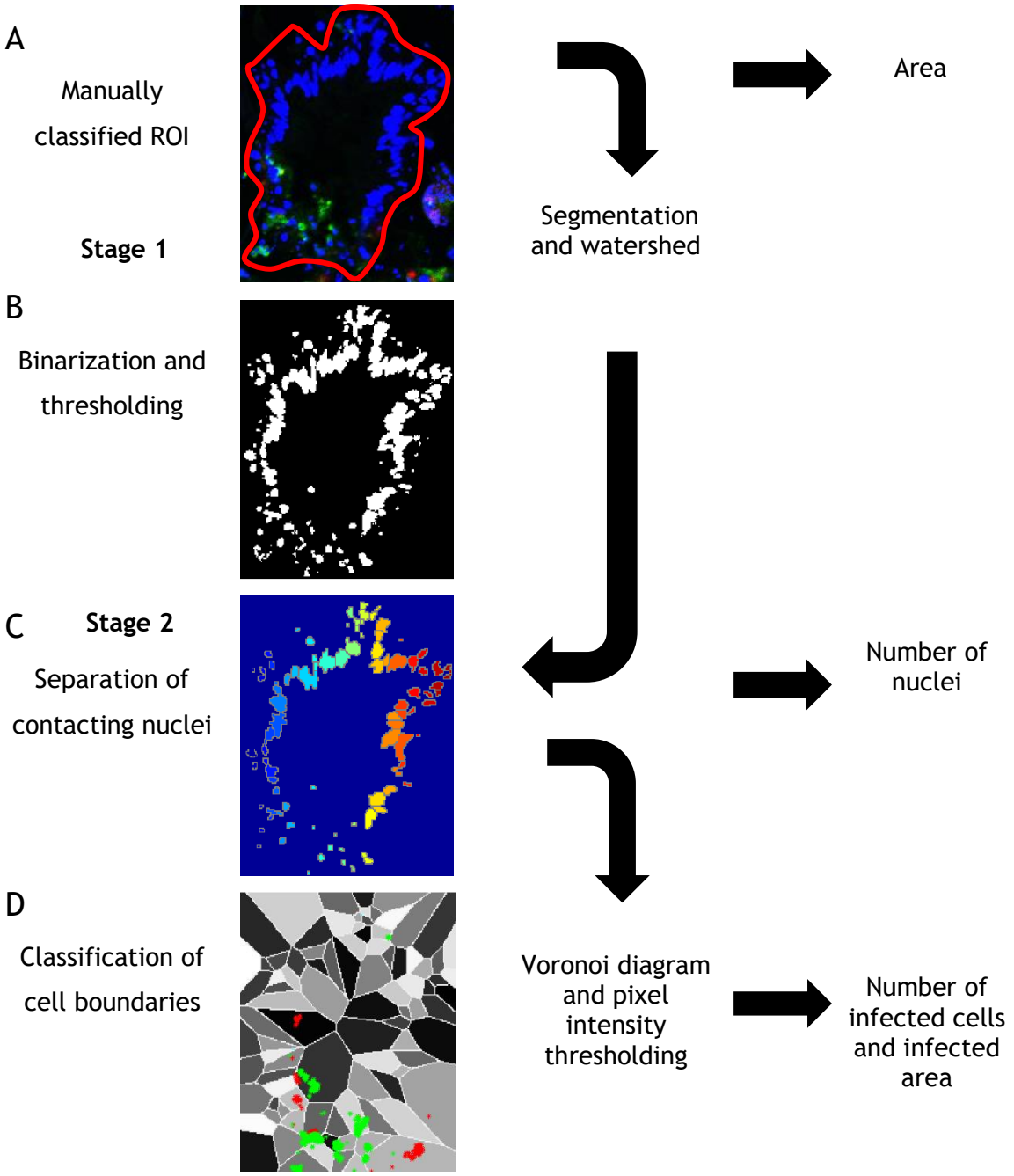
A
Manually classified ROI
Stage 1
Segmentation and watershed
Area
B
Binarization and thresholding
C
Stage 2
Separation of contacting nuclei
Number of nuclei
D
Classification of cell boundaries
Voronoi diagram and pixel intensity thresholding
Number of infected cells and infected area

4.2.1 Stage 1: Identification and summation of cell nuclei

In a TIFF-format image, the red, green and blue colour channels are each represented by an array of pixels, with 8-bit integer intensity values between 0 and 255. In confocal images fluorescence intensity was 'normalised' so that a value of 255 represents maximum intensity. Initially, the area of each ROI was measured by the number of pixels, *P*, with non-zero intensities in the blue colour channel (representing DAPI stained nuclei) of image *g*(*x, y*) (where, *x* is the image row, *y* is the column and g is the greyscale image). This value was converted to an area in μm^2 using equation 4.1, where 1 pixel = 1.76 μm at 20x objective. This provided a measure of the area of the syncytial salivary glands (Bowne and Jones, 1966) and neural tissues (thoracic ganglia and optic lobe), which exhibit dense cell clustering (shown in figure 4.7 of the results section).

Equation 4.1

$$\text{Area } (\mu m^2) = \sum P_{g(x,y)} \times \left(\frac{1}{1.76}\right)^2$$

Cell nuclei were detected as clusters of pixels above a defined intensity threshold, as described previously (Al-Khazraji et al., 2011). Nuclei were identified by converting the image *g*(*x, y*) to a binary image *b*(*x, y*) by 'thresholding' using the 'graythresh' function (figure 4.1B). Pixel intensities in the image *g*(*x, y*) were assumed to be bimodal; grouped into a 'background pixels' with low intensities, and of 'foreground pixels' with high intensities. A value for the threshold (*T*) was estimated using Otsu's method (Otsu, 1975), which minimises the weighted within-class variance ($\sigma^2 W_{g(x,\ y)}$) of background and foreground pixel intensities in the image *g*(*x, y*). The weight applied to filter the foreground ($fW_{g(x,\ y)}$) from the background pixels ($bW_{g(x,\ y)}$) in the image, was defined by the sum of pixel intensities (I_{pix}) divided by the number of pixels (N_{pix}) (equation 4.2). The aim was to remove low intensity background fluorescence and nuclei outside of the focal plane.

Equation 4.2

$$bW_{g(x,\ y)} = \sum \frac{bI_{pix}}{bN_{pix}}$$

$$fW_{g(x,\ y)} = \sum \frac{fI_{pix}}{fN_{pix}}$$

$$T \sim \sigma^2 Wg_{(x,\ y)} = bw_{g(x,y)}\, b\sigma^2{}_{g(x,y)} + fw_{g(x,y)}\, f\sigma^2{}_{g(x,y)}$$

If the intensity of a given pixel in image $g(x, y)$, is above the defined threshold (T), the value of the pixel in $b(x, y)$ is set as equal to one, otherwise the pixel value equals zero, enabling labelled regions to be separated from unlabelled regions.

Clustered pixels in some cases represented contacting cell nuclei. Nuclei were segmented by partitioning pixels into groups by applying a Euclidean distance transform and watershed segmentation to the binary image $b(x, y)$ using the 'bwdist' and 'watershed' functions, respectively (figure 4.1C). The watershed algorithm is commonly applied to segment nuclei (Malpica et al., 1997, Liempi et al., 2015, Gudla et al., 2008). The segmentation methods compared each pixel in the image with adjacent pixels in the 8-adjacent pixel positions (figure 4.2). Each pixel was labelled with the distance between that pixel and the nearest non-zero pixel (equation 4.3).

Equation 4.3

$$b(x, y) = \begin{cases} 0 & b(x, y) \ni bg \\ \min(\|x - x_0, y - y_0\|, \forall b(x_0, y_0) \ni fg) & b(x, y) \ni fg \end{cases}$$

$$\text{Where Euclidean distance, } \|x, y\|_{L_2} = \sqrt{x^2 + y^2}$$

A gradient image $b(x, y)$ was created where the numerical value of each pixel indicates the number of pixels from the nearest non-zero value pixel. This enabled the watershed algorithm (Roerdink and Meijster, 2001) to identify pixel clusters (connected components) in the image (figure 4.2B).

Figure 4.2

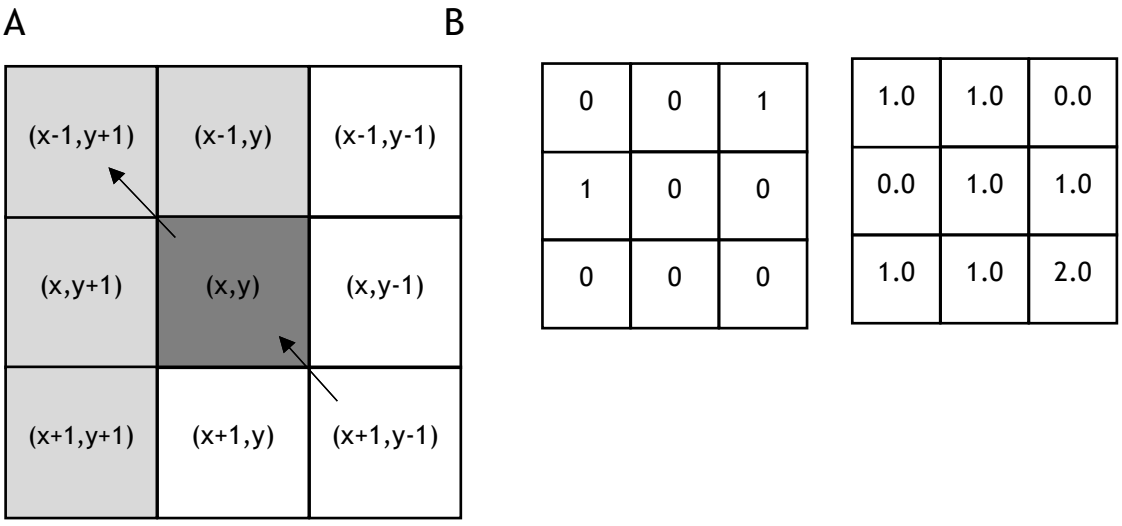

Figure 4.2: Segmentation of neighbouring pixels and clustering.

(**A**) Detection of 8-adjacent pixels. The central pixel at position (x,y) is compared with neighbouring pixels (grey) and is itself compared by neighbouring pixels (white). Arrows indicate the straight line Euclidian distance, which was applied as the distance metric.

(**B**) The binary image is shown in the left panel and corresponding distance transform, in the right panel.

The location of the centre mass of clustered pixels in image $c(x, y)$ was calculated using the 'regionprops' function. The number of 'centre points' provided a measure of the number of cells.

4.2.2 Stage 2: Assignment of cell nuclei to infected or uninfected cells

A threshold (*T*min) was applied to the greyscale image $g(x, y)$ of the red or green colour channel. If the intensity of a given pixel in image $g(x, y)$ was greater than the threshold, the value of the pixel in the binarised image $b(x, y)$ was set equal to one, else zero. Values of 40, 60, 100 and 150 for *T*min were tested. Red and green pixel numbers in five randomly selected images, after applying *T*min, were compared with pixel numbers after applying a visually defined threshold in Fiji software (ImageJ) (figure 4.3). This, manually defined, threshold removed background pixel intensities in the segmented image. The *T*min value which resulted in pixel counts closest to numbers generated after manual segmentation was applied to images. A *T*min of 100 was selected for the green colour channel, which removed the lowest 39.22% of pixels, and 60 for the red colour channel, which eliminated the lowest 23.53% of pixels.

The number of pixels with intensities > *T*min in image *b*(*x*, *y*) provided a measure of the infected area in the salivary glands, thoracic ganglia and optic lobe; this was converted to μm^2 as before (see equation 4.1).

A Voronoi diagram was plotted using the coordinates of the centre-mass of clustered pixels in the image *c*(*x*, *y*) (figure 4.1D). The location of pixels > *T*min in *c*(*x*, *y*) were defined separately for the red and green colour channels. Voronoi polygons (VP) overlapping with pixel locations were assigned a value of one (VP(*x*, *y*) =1), else zero (VP(*x*, *y*) = 0). The number of polygons VP(*x*, *y*) = 1 in an image was considered equivalent to the number of infected cells, as each cell was considered to have a single nucleus (Liempi et al., 2015).

Figure 4.3

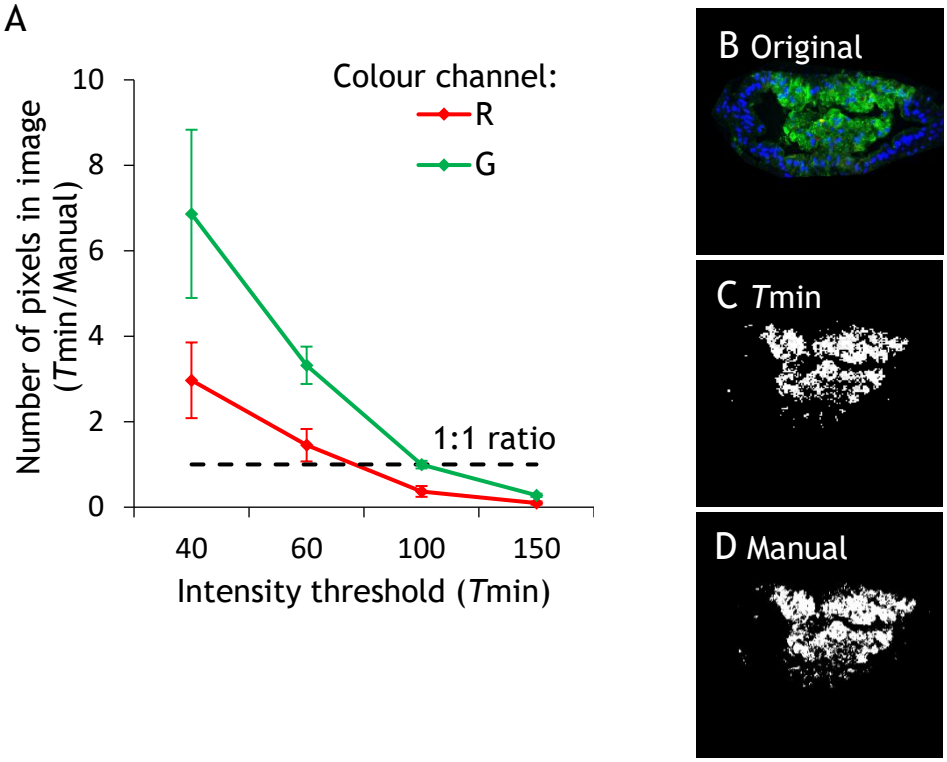

Figure 4.3: Selection of the minimum pixel intensity threshold (*T*min).

A threshold was applied visually using Fiji software (ImageJ) to segment labelled pixels in the red or green colour channel of five randomly selected images of the midgut, foregut, fat body, optic lobe and compound eyes. (**A**) The number of red (R) and green (G) pixels in manually segmented images were counted using Fiji software. These pixel numbers (Manual) were expressed as a ratio of the number of pixels counted after applying a *T*min of 40, 60, 100 or 150 using MATLAB® software (Mathworks Ltd.). Bars show the standard error of the mean of the five images. The dashed line indicates a ratio of 1:1 between pixel counts. (**B**) A representative RGB image of the midgut is shown after segmentation using (**C**) a T*min* of 100 or (**D**) a manual threshold to remove background pixel intensities in the green colour channel. Pixels remaining in the segmented image are shown in white.

4.2.3 Validation of automated image analysis for counting and classifying nuclei

Results obtained from the automated analysis were tested by separately comparing the number of counted and classified nuclei, with nuclei numbers obtained manually (figure 4.4). A single ROI of every tissue, excluding the salivary glands, thoracic ganglia and optic lobe, was selected for each of the fifty-four *Culicoides* analysed, as described in the previous sections 4.2.1 and 4.2.2. The multipoint' tool in Fiji (ImageJ) was used to count nuclei in each image. Cell nuclei in close proximity to red or green pixels were counted as positive for BTV +Seg-5 RNA or viral protein labelling, respectively.

The number of cells co-expressing red and green pixels were counted (see section A.5 of the Appendix) and differences in the number of co-infected and singly infected cells were compared using Friedman test (Friedman, 1937), for non-parametric, repeated measures, and post-hoc multiple comparisons test (Hochberg and Tamhane, 1987) with the Statistics and Machine Learning Toolbox of MATLAB® 6.0 software (Mathworks Ltd.).

Figure 4.4

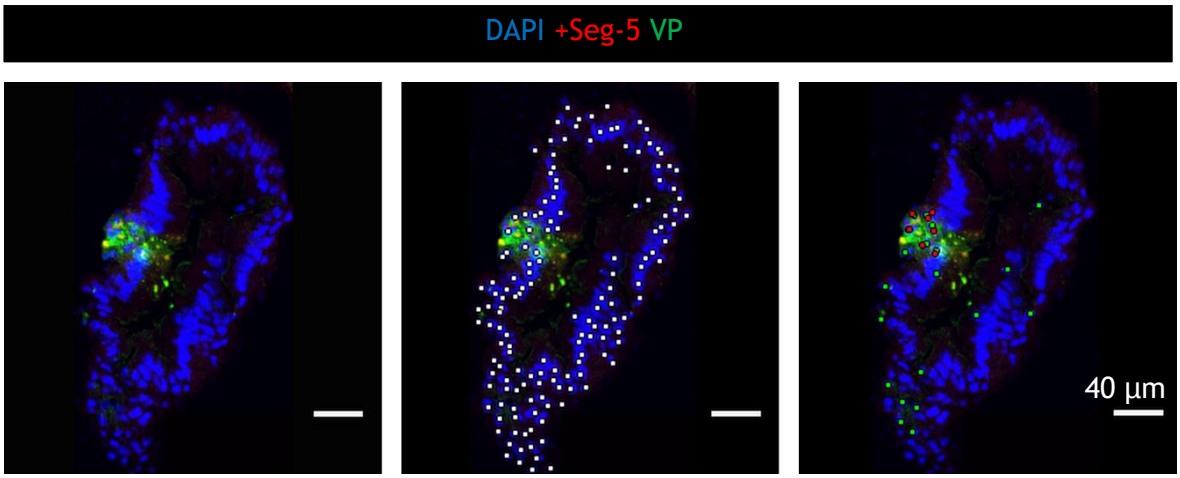

Figure 4.4: Manual cell count in tissues of *Culicoides*.

A representative image of a single region of the midgut of BTV-1 infected *Culicoides* at 4 days after feeding on a blood-virus mixture containing 6.2 or 7.0 $\log_{10}$ $TCID_{50}$/ml of BTV-1 SA (P2 BSR) is shown in the left image. Cell nuclei are shown (white) in the middle image, whereas nuclei in close proximity to BTV +Seg-5 (red) or structural protein (VP, green) are shown in the right image by the red and green points, respectively. Each point represents a single cell nucleus (scale = 40 µm).

Separate generalised linear mixed effects models (GLMM) were applied to compare the automated nuclei count to a manual count, using the Statistics and Machine Learning Toolbox of MATLAB® 6.0 software (Mathworks Ltd.). Scripts for GLMMs are available in the Appendix section A.4. The models consisted of a Poisson distribution and log link function. A Poisson distribution was selected, as the response (automated nuclei count) was a count variable. Tissue type was included as a fixed categorical factor. A unique identifier was assigned to each *C. sonorensis* and included as a 'random categorical effect'. Residuals were tested for normality and a White's test (White, 1980) was performed to test homoscedasticity. Outliers, with a Cook's Distance >4 /N, where N is the same size (Bollen, 1990), were identified. A deviance test was performed to compare the model fit to a constant model. The number of infected cells was correlated with total cell counts using Spearman's correlation coefficient. Correlation in the percentage of overestimated, or underestimated nuclei, and the number of nuclei counted, were determined as described before. Tests were performed using the Statistics and Machine Learning Toolbox of MATLAB® 6.0 software (Mathworks Ltd.).

4.2.4 Validation of red and green channel intensity thresholds

To ensure that the minimum pixel intensity threshold (*T*min) for the red and green colour channels was below the level of labelling and above autofluorescence, images of the salivary glands, thoracic ganglia and optic lobe were analysed. A value of one was assigned to a binarized image, $b(x, y)$, with pixel intensities > *T*min ($b(x, y) = 1$) and zero for images with pixels ≤ *T*min ($b(x, y) = 0$). Labelling intensity was visualised and images were categorised as unlabelled, weakly, intermediately or strongly labelled, as shown in figure 4.5 and as described previously (Harvey et al., 1999, Hatanaka et al., 2003). Intensity ranks were compared with binary values assigned for *T*min using a Chi-squared test with $p = 0.05$ statistical significance in the Minitab 17 statistical software (Minitab Inc.).

Figure 4.5: Representation of methods for calculating intensity scores.

Labelling intensity was visually observed in an image and images were categorised as unlabelled, weakly, intermediately and strongly labelled. Labelled cells are represented by red shaded areas and unlabelled cells by white shading in the upper panel. Brighter shading indicates an increased labelling intensity. The lower panel shows representative images corresponding to the labelling intensity shown above, in a region of the thoracic ganglia. Arrows indicate regions of BTV protein (VP, green) and +Seg-5 RNA (red) expression. Nuclei are shown in blue (scale = 20 μm).

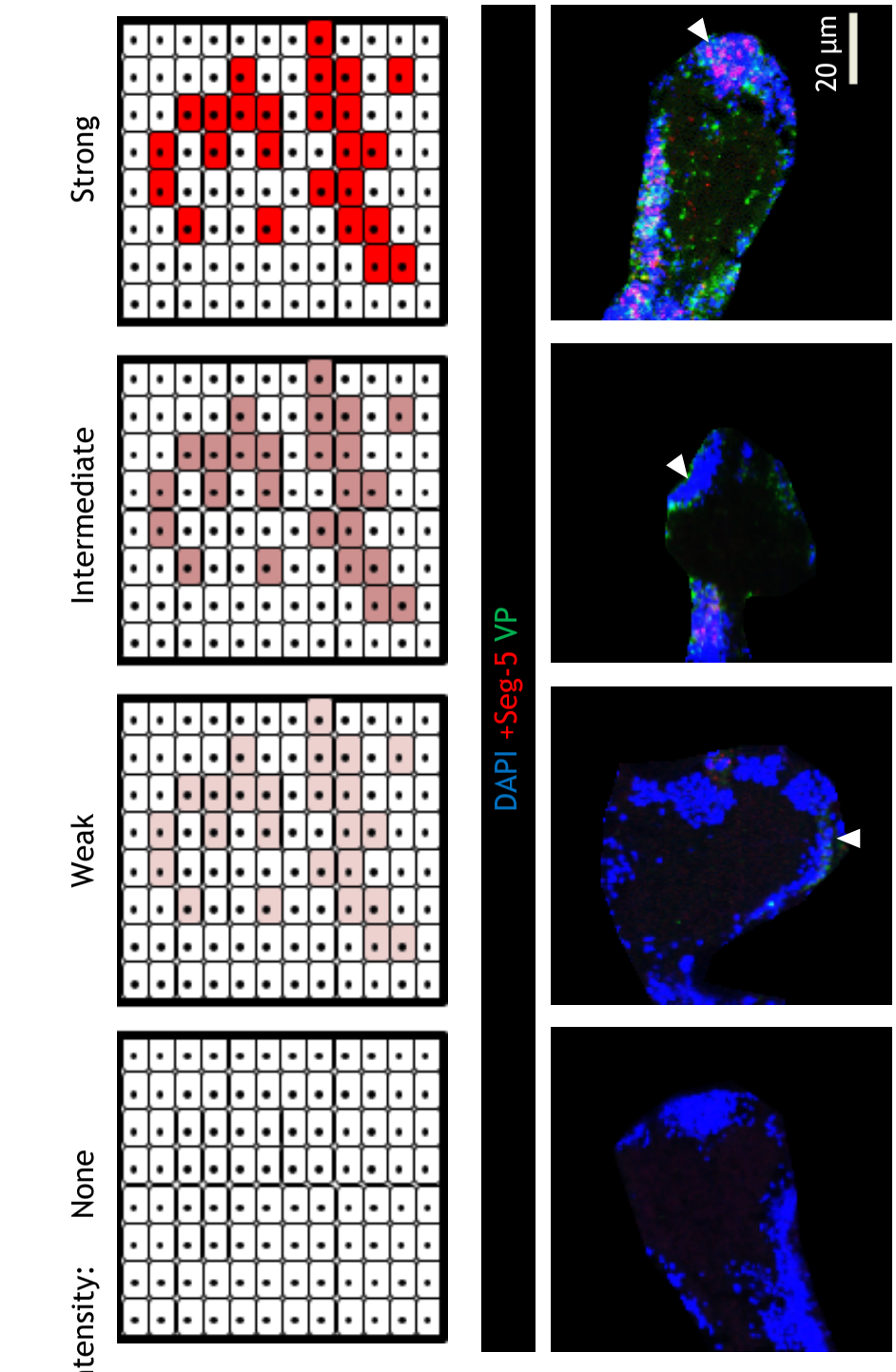
Labelling intensity:
None
Weak
Intermediate
Strong
DAPI +Seg-5 VP
20 µm

Figure 4.5

4.3 Results

4.3.1 Morphology of *Culicoides*

The different tissues visible in sectioned *Culicoides* were first identified. The spatial arrangement and morphology of the different tissues were examined visually by comparing sections to three-dimensional reconstructions of *C. sonorensis*, generated by whole-volume microCT (see Chapter 2, sections 2.19 and 2.19.1). The tissues identified include: the compound eye, the midgut, foregut and hindgut, the axillary apparatus (which forms the connective tissues of the wings), the optic lobe (including the central brain) and thoracic ganglia (which form the central nervous system), salivary glands, fat body and thoracic muscle (which comprised a large portion of the thorax). Additionally the outer epithelial layer, including the hardened cuticle, of the thorax and abdomen was identified (figure 4.6). The salivary glands are situated in the anterior thorax, dorsal of the foregut, and are surrounded by the fat body. The morphology of the cell nuclei varied between and within the tissues analysed. Variation in nucleus size was especially notable in the hindgut (figure 4.6). The fat body, axillary apparatus, abdominal epithelium and the inner region of the compound eye consisted of spherical lipid droplets, which were distinguishable by dark cytoplasmic staining (figure 4.7A to D). The elongate thoracic ganglion was situated ventral of the foregut. Nuclei of the thoracic ganglia and optic lobes were notably small and highly clustered (figure 4.8A, B).

Figure 4.6: Identification of tissues within *Culicoides*.

Uninfected *Culicoides* were cryosectioned (see Chapter 2, section 2.19) and nuclei were counterstained (blue), cytoplasm was stained using Fast Green (grey). Images were captured and tissues, including the midgut (mg), foregut (fg), hindgut (hg), salivary and accessory glands (sg, ag), fat body (fb), compound eye (ce), axillary apparatus (ax), thoracic ganglia (tg), thoracic muscle (tm), epithelium (ep) and optical lobe and brain (ol) were identified. Blue lines indicate the locations of tissues within a three-dimensional reconstruction of the body of *C. sonorensis*, shown in black and white. The viewing angle is laterally positioned and locations of the abdomen and thorax are indicated (scale = 200 µm).

Figure 4.6

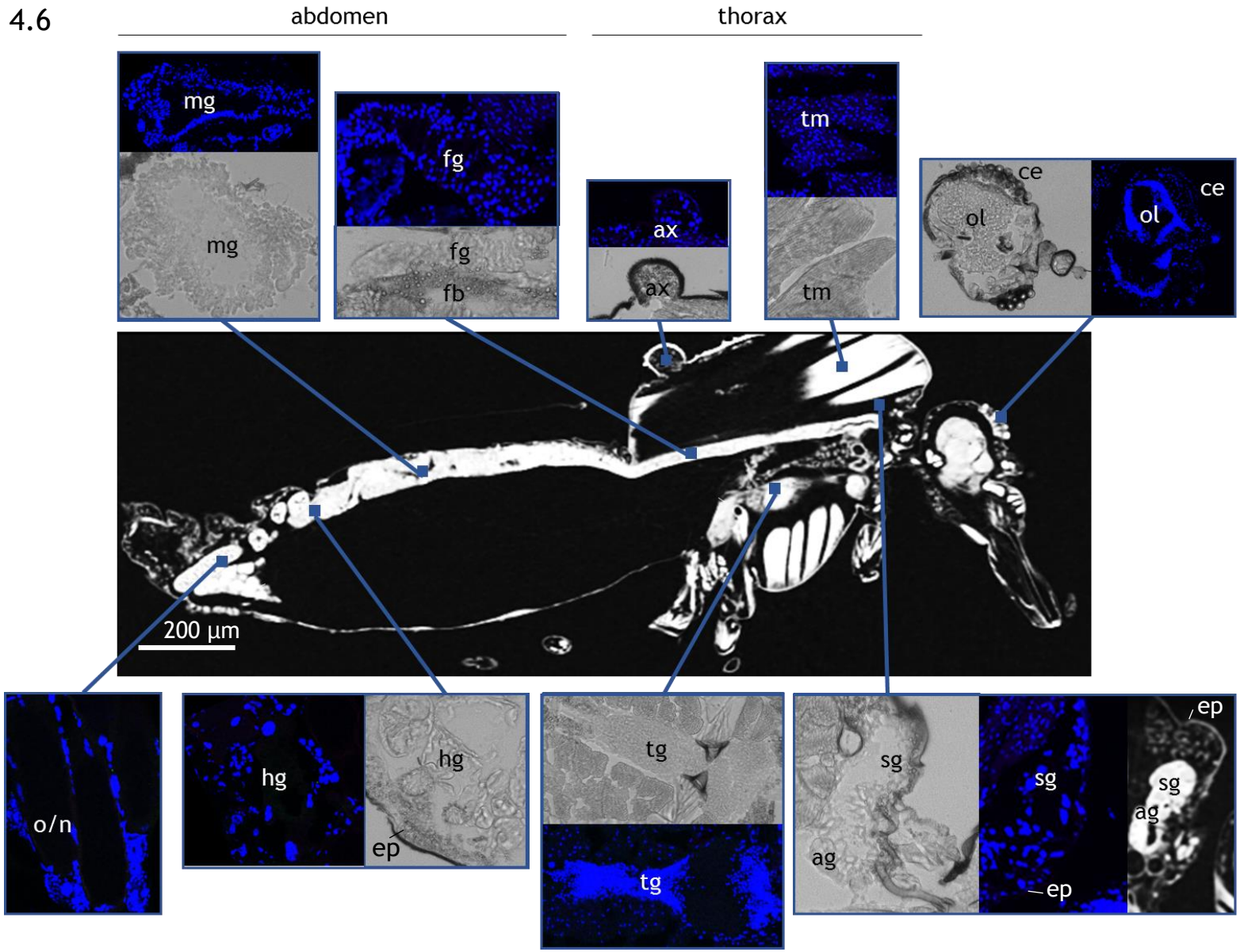

138

Figure 4.7

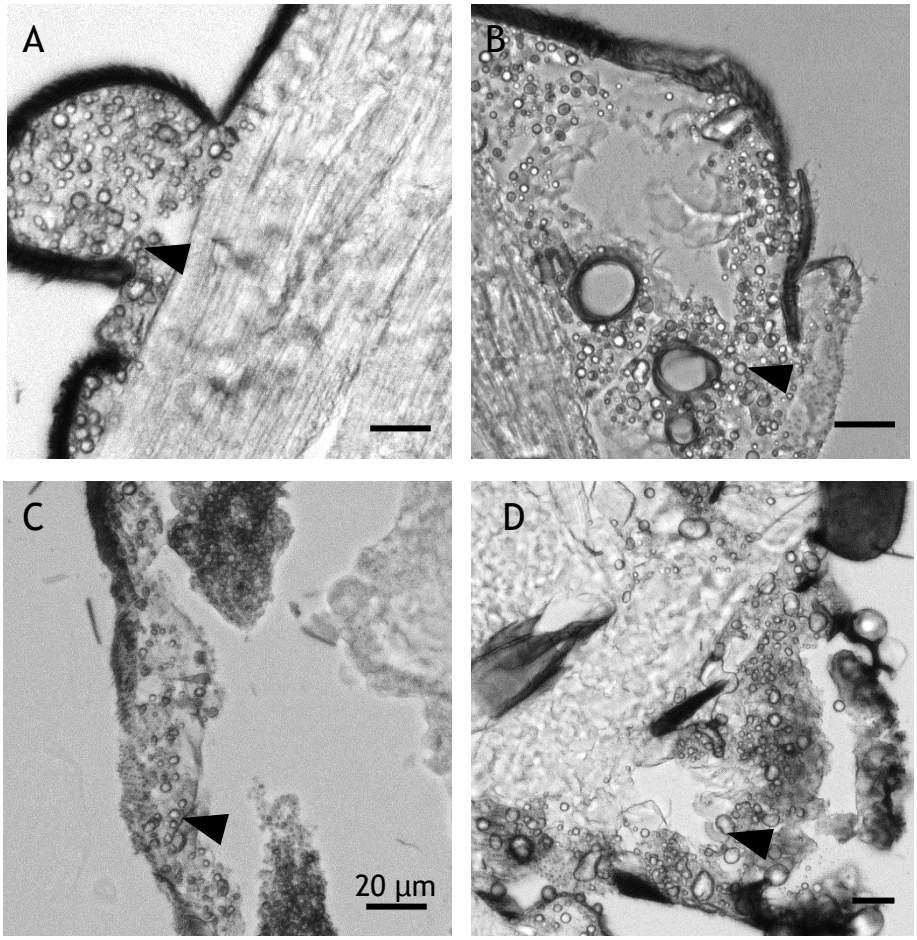

Figure 4.7: The morphology of the axillary apparatus, fat body, epithelium and compound eyes are comparable.

Showing sections of (**A**) the axillary apparatus, (**B**) the fat body, (**C**) the abdominal epithelium and (**D**) compound eye of *Culicoides,* stained with Fast Green cytoplasmic stain. Arrows denote the location of lipid droplets, with darker plasma membrane staining, which are comparable across different tissues (scale = 20µm).

Figure 4.8

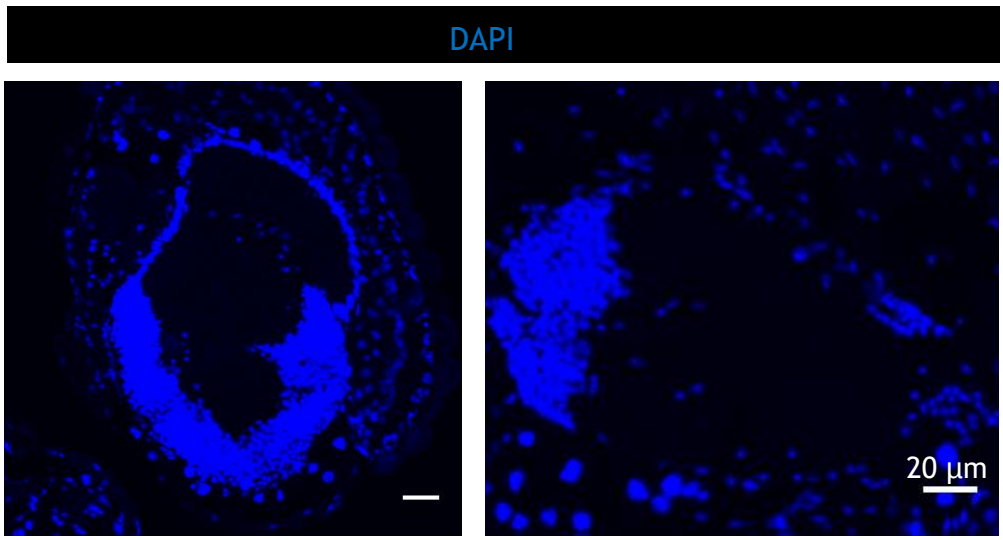

Figure 4.8: Nuclei are small and closely associated in the thoracic ganglia and optic lobe.

Representative image of counterstained cell nuclei in a section of (**A**) the thoracic ganglia and (**B**) the optic lobe, which includes the central brain, of *Culicoides* (scale = 20µm).

4.3.2 Validation of stage 1 counting: accuracy of cell nuclei counts

A automated image analysis procedure (the Automated Infected Cell Counter (AICC)), was used to assess the quantity of BTV in *Culicoides* tissues. The AICC ruleset was tested on images from 54 adult *C. sonorensis*. Single images of the midgut, foregut, hindgut, thoracic muscle, fat body, abdominal and thoracic epithelium, compound eyes and the axillary apparatus were analysed for every *Culicoides*, giving a total of 486 images. Computation time was approximately 8 to 12 seconds per an image, depending on the number of pixel clusters identified. The number of pixel clusters, corresponding to nuclei (figure 4.9), identified per image was variable and ranged from 2 to 583 clusters.

Nuclei counts obtained using the AICC were validated by comparing each image separately with manual nuclei count, which was considered to represent true nuclei numbers. The numbers of overestimated (OE) and underestimated nuclei (UE), were counted in each image by subtracting the manual count (MC) from automated nuclei count (AC) for a given image (table 4.1). Subtraction of overestimated nuclei from automated count gave the number of

correctly identified nuclei. The performance of the AICC was evaluated by calculating count precision and sensitivity using equation 4.4.

Equation 4.4

$$\text{Precision} = \frac{(\text{AC}-\text{OE})}{\text{AC}}$$

$$\text{Sensitivity} = \frac{(\text{AC}-\text{OE})}{(\text{AC}-\text{OE})+\text{UE}}$$

Figure 4.9

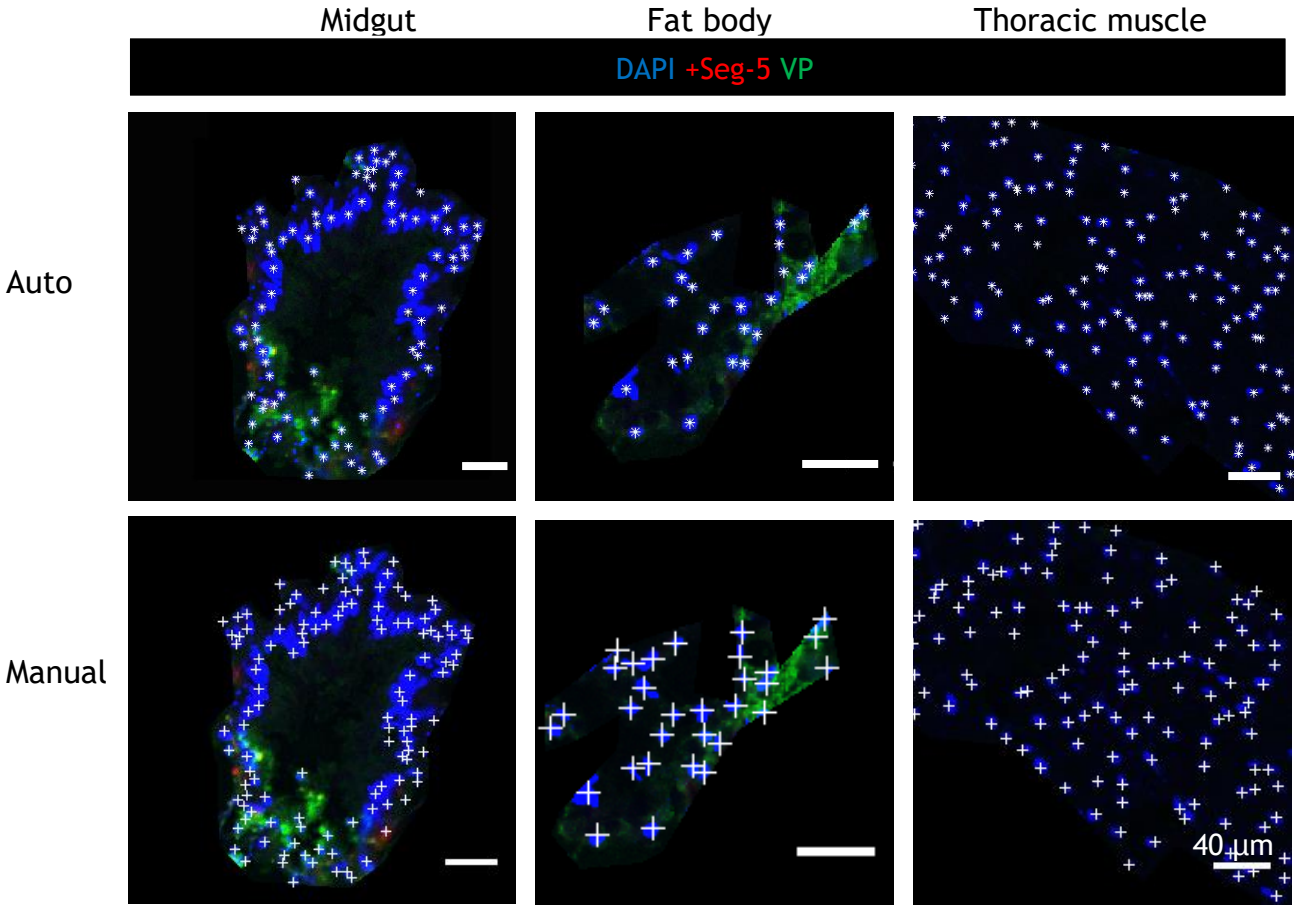

Figure 4.9: Manual and automatic detection of cell nuclei.

Cell nuclei were identified automatically (Auto) and manually (Manual) in images of the midgut, foregut, hindgut, thoracic muscle, fat body, abdominal and thoracic epithelium, compound eyes and the axillary apparatus of *Culicoides* sections. Representative images of the midgut, fat body and thoracic muscle are shown. Each white point shows an identified counterstained nucleus (blue). BTV protein (VP, green) and +Seg-5 RNA (red) are shown (scale = 40 µm).

Table 4.1: Number of nuclei counted in each tissue.

Tissue	Manual count	Auto count	Over-estimated nuclei (% Auto Count)	Under-estimated nuclei (% Auto Count)	Correctly identified nuclei	Sens	Prec
Thoracic muscle	14061	14638	1299 (8.87%)	722 (4.93%)	13339	0.95	0.91
Midgut	7113	6691	481 (7.19%)	903 (13.49%)	6210	0.87	0.93
Compound eyes	4745	3734	309 (8.27%)	1320 (35.35%)	3425	0.72	0.92
Abdominal epithelium	3778	3959	494 (12.48%)	313 (7.91%)	3465	0.92	0.88
Thoracic epithelium	2396	1821	110 (6.04%)	685 (37.62%)	1711	0.71	0.94
Axillary apparatus	1425	1190	61 (5.13%)	296 (24.87%)	1129	0.79	0.95
Fat body	2100	1822	33 (1.81%)	311 (17.07%)	1789	0.85	0.98
Foregut	5307	4210	133 (3.16%)	1230 (29.22%)	4077	0.77	0.97
Hindgut	1614	1442	65 (4.51%)	237 (16.43%)	1377	0.85	0.96
Total	42539	39507	2985 (7.56%)	6017 (15.23%)	30505	0.86	0.92

The number of nuclei counted varied with tissue type and was greatest in the thoracic muscle (table 4.1). Cell counts in the thoracic muscle were between 4.1 to 84.1% greater than other tissues analysed ($p<0.001$), except the thoracic epithelium ($p = 0.117$) (table 4.2). Overestimated nuclei ranged from 1.81% (33/1182) to 12.48% (494/3959) of automated count and were lowest in the fat body, where only 33 of 1822 nuclei were falsely identified. The percentage of overestimated nuclei increased with the number of automatically counted nuclei ($rho = 0.389$, $p<0.001$), indicating that imprecision in identifying cell nuclei increases with the number of nuclei counted.

Automated counting gave lower totals than manual counting in most tissues and the percentage of unidentified nuclei between images ranged from 4.93% (722/14638) to 37.62% (685/1821) of the total obtained by automated counting. The percentage of underestimated nuclei was greater when smaller numbers of nuclei were counted ($rho = -0.462$, $p<0.001$), indicating a reduction in precision of the AICC for counting fewer cell nuclei. The relatively high number of unidentified nuclei in tissues including the thoracic

epithelium, resulted in a reduction in count sensitivity. Despite this, sensitivity was high when considering nuclei numbers in all images analysed and ranged from 0.71 to 0.95. Nuclei counts obtained automatically were precise in the tissues analysed, particularly in the fat body where precision was 0.98 (table 4.1). The accuracy of the AICC was assessed by calculating the F1-score of the weighted average of precision (Prec) and sensitivity (Sens) (Mech et al., 2011, Powers, 2011) (equation 4.5), where an F1-score of 0.5 would denote a random classifier. The overall F1-score was 0.89, demonstrating a high performance for nuclei identification.

Equation 4.5

$$F_1 = 2\ \frac{\text{Prec.Sens}}{\text{Prec+Sens}}$$

The automated nuclei count was 0.6% lower (which corresponded to a difference of between 1 to 2 cells) than manual count ($p<0.001$). Nuclei counts obtained using both methods were linearly correlated (Manual count x Auto count). There was approximately 20% variation ($\beta = 0.199$) between individual *C. sonorensis* in the number of automatically counted nuclei (Table 4.2). This likely reflected variation in the size of image regions.

Table 4.2: Parameter estimates for the number of nuclei counted automatically with manual count.

Parameter x Auto count	Slope β (95% CI)	SE
Intercept	3.881 (3.807, 3.955)**	0.038
Manual count	0.006 (0.005, 0.006)**	0.000
Thoracic muscle	Baseline	
Midgut	0.096 (0.057, 0.134)**	0.020
Compound eye	-0.212 (-0.260, -0.163)**	0.025
Abdominal epithelium	-0.041 (-0.092, 0.010)**	0.026
Thoracic epithelium	-0.614 (-0.677, -0.550)^{ns}	0.032
Axillary apparatus	-0.841 (-0.915, -0.767)**	0.038
Fat body	-0.555(-0.619, -0.481)**	0.033
Foregut	-0.148 (-0.192, -0.103)**	0.023
Hindgut	-0.701 (-0.770, -0.632)**	0.035

** = $p<0.001$

ns = non-significant

4.3.3 Validation of stage 2: accuracy of assigning cell nuclei to infected cells

Nuclei counted as described in the previous section, were automatically assigned to one of four classes of cells, based on the detection of pixel intensities > *T*min within a polygonal area defined in sections 4.2.2:

- Cells expressing +Seg-5 RNA, were identified by red pixel intensities > *T*min.
- Cells expressing BTV protein (predominantly VP5), were characterised by green pixel intensities > *T*min.
- Cells co-expressing BTV protein and +Seg-5 RNA, were identified by red and green pixels > *T*min.
- Uninfected cells, were identified by red and green pixel intensities ≤ *T*min.

The number of nuclei assigned to cells expressing both +Seg-5 and VP were compared to manually classified nuclei and, represented only 24.23% (576/2377) of automatically classified nuclei (X^2_2 = 24.50, $p<0.001$) and 28.08% (886/3155) of manually classified nuclei (X^2_2 = 20.74, $p<0.001$). Whereas cells expressing VP represented 42.74% (1016/2377) and 44.60% (1407/3155) of automatically and manually classified nuclei,

respectively. Due to a low incidence of co-expression, the accuracy of assigning nuclei to cells expressing +Seg-5 or VP using the AICC ruleset were examined separately.

Numbers of correctly classified nuclei were estimated in each image by subtracting the number of nuclei classified by manual observation (Manual count) from numbers obtained by automatic classification (Auto count). Nuclei that were incorrectly classified into cells expressing either +Seg-5 or VP (false positive nuclei, FP) were calculated. False positive nuclei may have arisen, from detection of autofluorescence > T_{min}, which is distinguishable by manual observation as low intensity pixels over a large area. Other nuclei may have been incorrectly classified as uninfected (False negative nuclei) if, for example, the polygonal area was imprecisely defined. The numbers of false positive and false negative nuclei were expressed as a percentage of automated count. Precision (Prec) and sensitivity (Sens) were estimated as described before (equation 4.4), with substitution of UE for false negative (FN) and OE for false positive (FP) nuclei (tables 4.3, 4.4).

Table 4.3: Classification of nuclei into cells expressing BTV +Seg-5 RNA.

Tissue	Manual count	Auto count	False positive nuclei	False negative nuclei	Correctly classified nuclei	Sens	Prec
			(% Auto Count)				
Thoracic muscle	59	103	54 (52.43%)	10 (9.71%)	49	0.83	0.48
Midgut	353	390	74 (18.97%)	37 (9.49%)	316	0.90	0.81
Compound eyes	818	647	56 (8.66%)	227 (35.09%)	591	0.72	0.91
Abdominal epithelium	599	440	87 (19.77%)	246 (55.91%)	353	0.59	0.80
Thoracic epithelium	56	56	8 (14.29%)	8 (14.29%)	48	0.86	0.86
Axillary apparatus	222	225	61 (27.11%)	58 (25.78%)	164	0.74	0.73
Fat body	448	347	35 (2.79%)	136 (53.55%)	312	0.65	0.97
Foregut	55	85	36 (42.35%)	6 (7.06%)	49	0.89	0.58
Hindgut	92	196	105 (53.57%)	1 (0.51%)	91	0.99	0.46
Total	2702	2489	516 (20.73%)	729 (29.29%)	1973	0.73	0.79

Table 4.4: Classification of nuclei into cells expressing BTV structural protein.

Tissue	Manual count	Auto count	False positive nuclei (% Auto Count)	False negative nuclei (% Auto Count)	Correctly classified nuclei	Sens	Prec
Thoracic muscle	92	113	32 (28.32%)	11 (9.73%)	81	0.88	0.72
Midgut	391	298	21 (7.05%)	114 (38.26%)	277	0.71	0.93
Compound eyes	795	518	32 (6.95%)	313 (60.42%)	482	0.61	0.93
Abdominal epithelium	627	471	33 (7.01%)	189 (40.13%)	438	0.70	0.93
Thoracic epithelium	96	71	12 (16.90%)	37 (52.11%)	59	0.61	0.83
Axillary apparatus	452	296	19 (6.42%)	175 (59.12%)	277	0.61	0.94
Fat body	594	394	35 (10.09%)	136 (39.19%)	312	0.70	0.90
Foregut	147	103	9 (8.74%)	53 (51.46%)	94	0.64	0.91
Hindgut	89	71	9 (12.68%)	27 (38.03%)	62	0.70	0.87
Total	3283	2335	182 (7.79%)	1130 (48.39%)	2153	0.66	0.92

The number of nuclei classified varied between the different tissue types for both VP (Table 4.3) and +Seg-5 (Table 4.4), indicating that the number of infected cells varies between tissues. Indeed, nuclei numbers in the thoracic muscle differed significantly from all tissues analysed ($p<0.001$), except the foregut (+Seg-5 RNA, $p = 0.410$; VP, $p = 0.601$). The number of nuclei assigned to cells expressing +Seg-5 (Manual count: rho = 0.08, $p = 0.06$; Auto count: rho = 0.08, $p = 0.07$) and VP (Manual count: rho = 0.04, $p = 0.36$; Auto count: rho = 0.14, $r^2 = 4\%$, $p<0.05$) were uncorrelated or weakly correlated with the number of nuclei identified. Indicating that the number of infected cells within a tissue depends on factors other than the number of cells available. Indeed, only 49 and 81 nuclei, respectively, were correctly classified into cells expressing +Seg-5 and VP in the thoracic muscle (tables 4.3, 4.4), despite detection of 13339 nuclei (table 4.1).

The precision of grouping nuclei based on +Seg-5 expression in most tissues was lower than by detection of VP, while the sensitivity was greater. This was particularly notable in the foregut, where the precision of +Seg-5 classification was 0.58 and sensitivity was 0.89

(Table 4.3), compared with 0.91 and 0.64, respectively, for VP (Table 4.4). The F1-score, which was calculated as before (equation 4.5), was 0.78 for +Seg-5 and 0.76 for VP classification, demonstrating a good performance of classification based on *T*min and polygonal area, compared to a random classifier.

The number of nuclei assigned manually to uninfected cells (true negative nuclei, TN) was calculated. The quality of classification of nuclei into uninfected or infected cell groups was further assessed using Matthew's correlation coefficient (MCC), which includes an additional term for TN (equation 4.6). MCC gives the direction of correlation (Powers, 2011), denoted by a value between -1 and +1, where +1 indicates perfect classification, 0 a random classification and -1, disagreement in nuclei grouping between in manual and automated methods (Mech et al., 2011, Baldi et al., 2000, Matthews, 1975).

Equation 4.6

$$\mathrm{MCC}(cn) = \frac{(TPi\ TNi) - (FPi\ FNi)}{\sqrt{TPi+FPi}.\sqrt{TPi+FNi}.\sqrt{TNi+FPi}.\sqrt{TNi+FNi}}$$

MCC was 0.72 for nuclei classified into cells expressing +Seg-5 and 0.64 for classification based on VP expression, indicating that assigning nuclei to cells using the AICC was non-random and of acceptable quality relative to a random classifier of value 0.

Counts of classified nuclei obtained using both manual and automated methods were correlated (Auto count x Manual count), but differed significantly ($p<0.001$). 4.3% and 4.0% fewer nuclei were classified automatically into cells expressing +Seg-5 RNA and VP, respectively, than manually. The number of nuclei automatically assigned to cells expressing +Seg-5 and VP differed by 94.2% ($\beta = 0.942$) and 65.0% ($\beta = 0.650$), respectively, between individual *C. sonorensis*; indicating that +Seg-5 and VP were expressed in a greater number of cells in some *C. sonorensis* than in others (tables 4.5, 4.6). This difference in expression between individual *C. sonorensis*, could reflect differences in the level of infection.

Table 4.5: Parameter estimates for the number of nuclei classified into cells expressing BTV +Seg-5 RNA with manual classification.

Parameter x Auto count	Slope β (95% CI)	SE
Intercept	0.299 (-0.023, 0.622)^{ns}	0.164
Manual count	0.043 (0.042, 0.045)**	0.002
Thoracic muscle	Baseline	
Midgut	0.955 (0.734, 1.176)**	0.112
Compound eye	0.669 (0.442, 0.895)**	0.115
Abdominal epithelium	0.595 (0.366, 0.823)**	0.116
Thoracic epithelium	-0.578 (-0.905, -0.252)**	0.166
Axillary apparatus	0.650 (0.415, 0.886)**	0.120
Fat body	0.505 (0.273, 0.737)**	0.118
Foregut	-0.121 (-0.409, 0.167)^{ns}	0.147
Hindgut	0.657 (0.417, 0.897)**	0.122

** = $p<0.001$

ns = non-significant

Table 4.6: Parameter estimates for the number of nuclei classified into cells expressing BTV protein with manual classification.

Parameter x Auto count	Slope β (95% CI)	SE
Intercept	0.503 (0.247, 0.760)**	0.130
Manual count	0.040 (0.037, 0.043)**	0.001
Thoracic muscle	Baseline	
Midgut	0.635 (0.415, 0.855)**	0.112
Compound eye	0.527 (0.305, 0.748)**	0.113
Abdominal epithelium	0.415 (0.189, 0.641)**	0.115
Thoracic epithelium	-0.458 (-0.755, -0.159)*	0.152
Axillary apparatus	0.625 (0.405, 0.845)**	0.112
Fat body	0.604 (0.387, 0.821)**	0.110
Foregut	-0.072 (-0.340, 0.197)^{ns}	0.136
Hindgut	-0.349 (-0.647, -0.05)*	0.152

* = $p<0.05$

** = $p<0.001$

ns = non-significant

To assess whether the minimum pixel intensity threshold (*T*min) detected low intensity labelling and effectively removed autofluorescence, the intensity ranking of images of the optic lobe, thoracic ganglia and salivary glands was compared to the presence of pixel intensities > *T*min (positive image) or ≤ *T*min (negative image) for +Seg-5 and VP. A total of 151 images were analysed.

The number of positive images was significantly greater for higher staining intensities for +Seg-5 (X^2_3 = 109.32, p<0.001) and VP (X^2_3 = 112.15, p<0.001), than for lower staining intensities (data not shown in figure). The number of positive images categorised as 'unlabelled' (false positive images) (figure 4.10A) and 'negative images' ranked as 'weakly' to 'strongly' labelled (false negative images) were calculated (figure 4.10B). False positive images accounted for ≤2% of images analysed, indicating a good performance of Tmin for detecting unlabelled images. Between 0 to 9.80% (4/51) of images analysed were incorrectly classified as negative. The false negative rate was highest for images with weak VP labelling (figure 4.10A), indicating, that in a minority of cases, the AICC may fail to detect low level green pixel intensities.

The numbers of images correctly classified as negative (true negative images, TN) or positive (true positive images, TP) were used to calculate MCC as described before (see equation 4.6). MCC was 0.88 for images that were classified, based on +Seg-5 and 0.81 for classification based on VP expression, indicating that grouping of images by detecting pixels > *T*min or ≤ *T*min was of very high quality compared with a random classifier. This provided further justification for the selected *T*min values (see section 4.2.2).

Figure 4.10

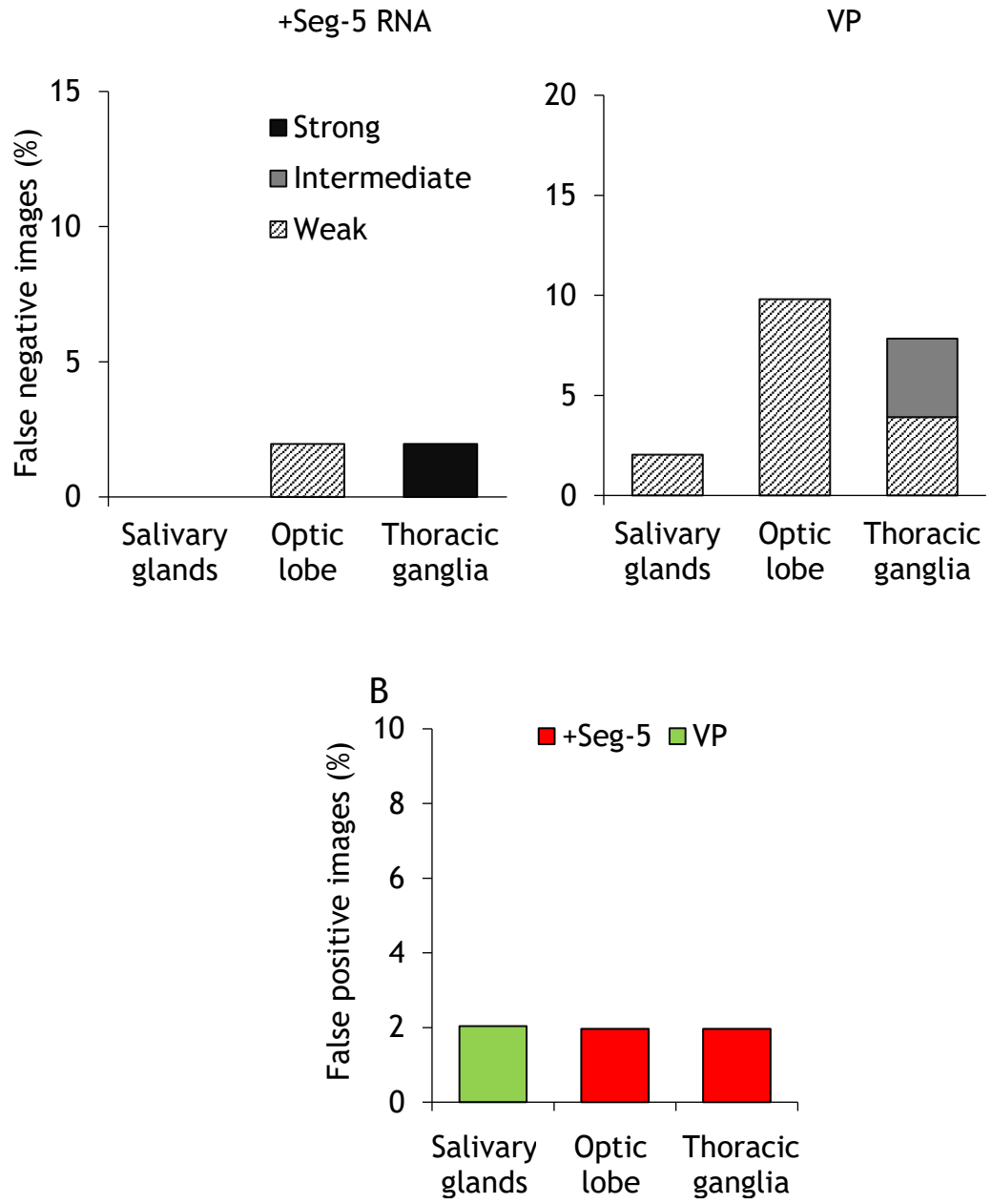

Figure 4.10: The percentage of false positive and false negative images.

Labelling intensity in images of the salivary glands (n = 49), optic lobe (n = 51) and thoracic ganglia (n = 51) was visually observed. Each image was categorised as exhibiting no labelling, weak, intermediate or strong labelling. (**A**) Images with red or green pixel intensities below the minimum threshold assigned by the AICC (≤*T*min) with weak to strong labelling (false negative images) were counted. (**B**) The number of images with no labelling, with red or green pixel intensities >*T*min (false positive images) were estimated. Red pixels represented BTV +Seg-5 RNA and green, structural protein (VP). The number of images were expressed as a percentage of the total images analysed for each tissue.

4.4 Discussion

A tissue-level understanding of insect morphology and a means of determining viral localisation and load, at precise cellular resolution, are needed to model viral replication within an individual arthropod vector. In Chapter 3, +Seg-5 RNA and protein (VP), of BTV-1 were localised in cells of sectioned *C. sonorensis*. The current Chapter describes the morphology of *C. sonorensis* tissues and presents an automated ruleset, enabling quantification of +Seg-5 and VP in confocal images of whole *Culicoides*. The developed ruleset, termed the AICC, accurately detects and identifies nuclei in a user-defined region, which can include as few as two cells. The AICC accurately identifies labelled pixels using a minimum intensity threshold and ultimately groups nuclei into individual polygonal areas. The number of polygons with pixel intensities above threshold identifies infected cells with high precision. The results obtained demonstrate that the AICC ruleset operates with comparable accuracy to manual observation in the tissues analysed and within a fraction of the time taken to manually count and classify nuclei. The data generated validate the use of the AICC to measure viral quantity and localisation within *Culicoides*, in Chapter 5. The AICC is also applicable to a wide range of invertebrate and mammalian systems.

A number of studies have applied automated algorithms to count infected cells (Zhang et al., 1998, Mech et al., 2011, Liempi et al., 2015), including macrophages infected with conidia of *Aspergillus fumigatus* (Mech et al., 2011, Kraibooj et al., 2015), CD4+ T-cells in sectioned HIV-1 infected lymphoid tissues (Zhang et al., 1998) and *Trypanosoma cruzi* in BeWo cells (Liempi et al., 2015). Such studies involved a degree of inaccuracy when assessed using an alternative cell count method, including FACs (Zhang et al., 1998) and manual observation (Mech et al., 2011), as used here.

The accuracy of counting using the AICC depended on tissue type and was lower when assigning nuclei to cells based on area and pixel intensity, than by identifying nuclei. Counting errors between images, given by the numbers of false positive or negative nuclei, was generally greater than levels in previous studies (Mech et al., 2011), although this varied (Theera-Umpon and Dhompongsa, 2007), possibly reflecting the complexity of tissue datasets, compared with those derived for cultured cells. Indeed, the number of CD4+ T cells/mg of lymphoid tissue counted by FACS and quantitative image analysis were within 50 to 75% (Zhang et al., 1998), which is comparable to or below ranges reported here of 88 to 98% and 46 to 97% precision for identifying and categorising nuclei, respectively.

The morphology of cell nuclei varied between and often within tissues, which imposed complications when manually identifying nuclei. Indeed, nuclei were frequently visually indistinguishable in the compound eyes. In such instances, automated counting may outperform manual observation, as the AICC empirically detected pixel clusters, without a shape parameter. Additional complexity arises due to the analysis of insect tissues, which exhibit autofluorescence (Koga et al., 2009, Thimm and Tebbe, 2003, Fukatsu et al., 1998) that can increase false positive detection rate. Although detection of unlabelled pixels only arose in up to 2% of images analysed, the use of clearing agents during labelling and alternative fixatives, such as Carnoy's solution (Koga et al., 2009), may be applied in future studies to quench autofluorescence, which was notably high in the hindgut (data not shown), to reduce incidence of false positive detection.

A reduced number of cells expressing +Seg-5 RNA, compared with those containing viral protein, in the tissues analysed could be due to suppression of translation of the viral mRNA by anti-viral immune pathways (reviewed in Chapter 1, section 1.3.2). Indeed, bunyamwera virus (BUNV) and la crosse virus (LACV) mRNA was severely reduced or undetectable 72 h after infection of C6/36 cells (Newton et al., 1981, Rossier et al., 1988) and positive strand S-RNA of Germiston bunyavirus remained at lower levels than genomic (negative strand) RNA during persistent infection of C6/36 cells (Delord et al., 1990). Translation is restricted during late-stage, persistent BUNV and LACV infection of C6/36 cells (Newton et al., 1981, Rossier et al., 1988).

A persistent state of infection is known to arise in *C. sonorensis* during BTV infection (Mellor, 1990, Fu et al., 1999), which may also be characterised by reduced replication. To avoid issues associated with detection of BTV during late-stage infection, as previously shown for DENV in *Ae. aegypti* (Salazar et al., 2007), antisera detecting BTV protein (see Chapter 3, section 3.2.5) was selected for use in studies in this thesis. A low incidence of viral protein and +Seg-5 RNA co-localisation was noted using both counting methods, that could reflect a difference in the timing of expression, or the sensitivity of immunofluorescent labelling, compared with FISH. Due to the absence of co-localisation, VP and +Seg-5 were analysed separately in studies presented in Chapter 5. Labelling with antibodies is subject to a varying degree of background signal, which could account for the increased accuracy of the AICC for counting cells expressing +Seg-5, than VP.

Overall, the accuracy of cell counts obtained using the AICC was substantially above levels expected of a random classifier and highly correlated with nuclei numbers obtained

manually. Additionally, the AICC was not subject to observer bias associated with manual counting, as applied objective, knowledge-based algorithms, which were consistent between tissues and individual insects. Identification of cell nuclei using the AICC was robust and reduced numerical variations caused by variation in staining intensity between images. Given these advantages, the AICC was applied to quantify BTV in studies presented in the subsequent chapter, Chapter 5.

Chapter 5

Tissue tropism of bluetongue virus in *Culicoides sonorensis*

5.1 Introduction

Vector competence describes the intrinsic ability of a vector to become infected and subsequently transmit a virus to a susceptible host (Gerry et al., 2001, Carpenter et al., 2015). An insect's vector competence is influenced by numerous environmental, ecological, genetic, and molecular factors (reviewed in Chapter 1, section 1.3); an aspect of vector competence which is relatively poorly described is the intrinsic process by which virus particles, present in ingested blood, infect, replicate in and disseminate between susceptible tissues and organs of the insect.

Despite variation in the tissues infected and the relative timing of their infection between studies of different arboviruses, which have included dengue virus (DENV) (Salazar et al., 2007, Sriurairatna and Bhamarapravati, 1977), St-Louis encephalitis virus (SLEV) (Whitfield et al., 1973) and West Nile virus (WNV)(Girard et al., 2004). Secretion of infectious virus particles in the saliva is usually considered essential for transmission of infectious virus to a vertebrate host. Transmissible virus particles are assumed to enter the saliva by replicating in the salivary glands; a process which is relatively well established for mosquito-borne arboviruses and has been demonstrated by a number of studies, including, eastern equine encephalitis virus (EEEV) in *Ae. triseriatus* (Whitfield et al., 1971), Venezulean equine encephalitis virus (VEEV), sindbis virus (SINV) (Gaidamovich et al., 1973) and DENV-2 (Salazar et al., 2007) in *Ae. aegypti*. Compared with mosquitoes, events during infection of other arthropod vector species, including *Culicoides*, are poorly understood.

The likelihood of BTV midgut infection, which can be an essential initial step towards vector competence of *Culicoides* (Fu et al., 1999), increases with the size of the infectious viral dose in the blood meal (Mertens et al., 1996a). As a result, *Culicoides* that ingest a higher dose of BTV are more likely to become infected. Correlation between the number of vectors infected and viral dose ingested is well established for a number of mosquito-borne arboviruses, including DENV-2 in *Ae. aegypti* (Pongsiri et al., 2014b, Bennett et al., 2002) and western equine encephalitis virus (WEEV) in *Cx. tarsalis* (Mahmood et al., 2006). However, the influence of the size of the infectious viral dose in the blood meal on disseminated infection rate varies between studies of different species of virus and mosquito (Bennett et al., 2002, Richards et al., 2007, Kramer et al., 1981), as MOI does not always reflect initial dose and changes at different stages of infection (Gutierrez et al., 2015) or in

different organs and varies between virus genotypes, shown for VEEV (Weaver et al., 1984, Smith et al., 2007).

A number of factors in addition to viral dose and genotype, influence vector competence of an insect. Laboratory reared and field caught *C. sonorensis* possess bacteria in their gut, belonging to genera that are known to inhibit viral infection, in other vector species (Ramirez and Dimopoulos, 2010, Campbell et al., 2004). Certain species of the bacterial symbiont, *Wolbachia,* can inhibit infection with a number of arboviruses in a density-dependent manner (Lu et al., 2012, Pan et al., 2012, van den Hurk et al., 2012) and were previously shown to inhibit replication of BTV-1/NS3-mCherry in *Drosophila* (Shaw et al., 2012). However, the overall influence of these commensal bacteria, on vector competence of *Culicoides* remain uncertain. If a high abundance of commensal bacteria is found to inhibit BTV infection and/or replication, employing strategies to manipulate midgut bacterial load, may provide a novel means of controlling transmission of BTV in the field.

This chapter aims to present a model of infection of an arbovirus in tissues of an insect vector, using BTV infection of laboratory colonised, North American *C. sonorensis* as a model system. A mammalian cell culture adapted BTV-1 from South Africa (BTV-1 SA, ICTVdb isolate accession number [RSArrrr/01]) was selected for these studies in order to enable a comparison of the data with previously published studies (Fu et al., 1999, Fu, 1995, Paweska et al., 2002a). Infection with BTV-1 SA was compared to a strain of BTV-11. The BTV-11 strain (BTV-11 USA, ICTVdb isolate accession number [USA2005/01]) was isolated from South Dakota where field populations of *C. sonorensis* occur (Schmidtmann et al., 2011) and had undergone few passages in cell culture. Hence, comparison of the selected BTV strains, could reveal key differences in the ability of viruses, isolated from different geographic regions, with different passage histories, to infect and replicate in *Culicoides*.

5.2 Results

5.2.1 Validation of a house-keeping gene for *Culicoides*

A 'house-keeping gene' for *Culicoides* was experimentally validated in order to facilitate the quantification of BTV RNA in the insect vector (see Chapter 2, section 2.14.2). A candidate house-keeping gene must maintain a constant level of expression under various experimental conditions (especially those used in this Chapter) in order to be used as a standard for normalising 'target' gene expression (Kozera and Rapacz, 2013). We focused on elongation factor 1 β (eF1β), which was previously used as a house-keeping gene for *C. sonorensis* (Mills et al., 2015). In order to determine whether the level of expression of eF1β varies under the experimental conditions described in this chapter, *Culicoides* were fed blood or sucrose and maintained for 7 days on sucrose, as described in Chapter 2 (section 2.3). RNA levels of eF1β were determined in eight *Culicoides* per group either immediately following or 7 days after treatment with blood or sucrose (see Chapter 2, section 2.14.1). Estimated copy numbers of eF1β ranged from 7.70 ± 0.23(SE) to 8.31 ± 0.12(SE) $\log_{10}$ per *Culicoides* (figure 5.1A). However, within a given insect they did not differ between blood and sucrose fed *Culicoides* at the time points tested (t-test: 0 days after treatment: $t_7 = 2.32$, $p = 0.05$; 7 days after treatment: $t_{10} = 1.13$, $p = 0.287$).

In a similar experiment, in order to determine whether the levels of expression of eF1β varied with the infection status, copies of BTV Seg-1 (as an indicator of BTV infection) and eF1β were determined 7 days after feeding on horse blood containing 7.0 $\log_{10}$ $TCID_{50}$/ml BTV-1 (P2 BSR) (for methods see Chapter 2, section 2.3). Infected *Culicoides* were identified as described before (Chapter 2, section 2.14.1) and eF1β copy numbers did not differ between BTV infected (n = 17) and uninfected (n = 17) individuals (t-test: $t_{22} = 0.32$, $p = 0.755$) (figure 5.1B), indicating that eF1β is suitable as a standard 'reference-gene' for these studies.

Figure 5.1

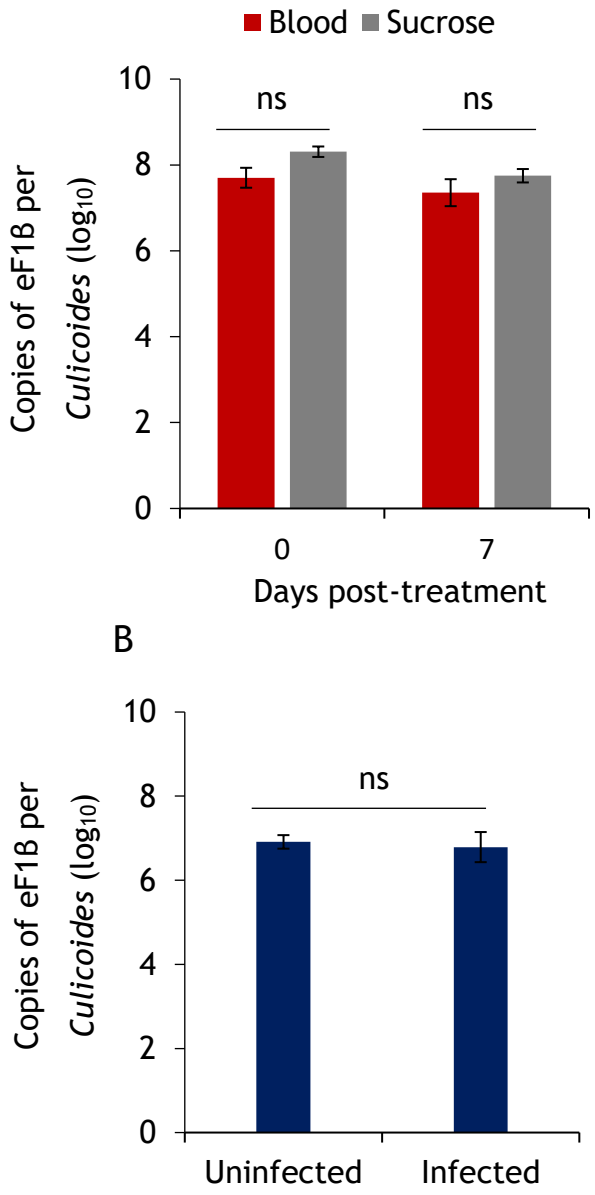

Figure 5.1: Copies of *Culicoides* gene ef1β do not alter with diet or BTV infection status. RNA levels of eF1β were determined in whole *Culicoides* carcasses by qPCR (**A**) after feeding on sucrose for 7 days or feeding on uninfected blood and maintained on sucrose for 7 days (Blood). Copies per an individual *Culicoides* carcase, tested within 4 h after blood or sugar feeding (0 days post-treatment) are shown. Eight individuals were tested for each group. Bars show the standard error of the mean. (**B**) Copies of eF1β in BTV infected (n = 17) and uninfected (n = 17) *Culicoides,* at 7 days after feeding on blood supplemented with 7.0 $\log_{10}$ $TCID_{50}$/ml of BTV-1 SA (P2 BSR). Bars show the standard error of the mean copies per an individual insect carcase ('ns' = non-significant difference using a Student's t-test).

5.2.2 The effect of removing midgut bacteria on BTV-1 infection rates

The effect of the midgut bacteria of *Culicoides* on the capacity of BTV-1 to establish infection in the vector was investigated by treating some vectors to remove their midgut bacteria as described before (Chapter 2, section 2.3.1). Briefly, antibiotics were administered *ad lib* in the sucrose solution. The mean bacterial load of homogenate from four groups of ten *Culicoides* midguts was measured by preparing a 10-fold dilution series of midgut homogenate, observing colony formation on culture plates, and calculating the colony-forming units (CFU/ml) (Chapter 2, equation 2.1).

The mean load of cultural bacteria was 6.99 $\log_{10}$ CFU/ml prior to antibiotic treatment (data not shown). The mean midgut bacterial load of untreated *Culicoides* maintained on sucrose for 7 days was 5.92 $\log_{10}$ CFU/ml, whereas those fed blood then maintained on sucrose for 7 days without antibiotic was 6.08 $\log_{10}$ CFU/ml (figure 5.2A). This unexpected reduction in CFU/ml in untreated individuals could reflect a decline in bacterial load with age, or differences in the sterility of the rearing environment of adults and pupae. No colonies were detected in *Culicoides* treated with antibiotics and in the control culture treated with Super Optimal broth with Catabolite repression (S.O.C) medium (data not shown).

The impact of bacteria upon the infection rate was tested by feeding *Culicoides* with blood containing 7.0 $\log_{10}$ $TCID_{50}$/ml of BTV-1. A control group was included, which was fed on blood containing DMEM (see methods Chapter 2, section 2.3). Antibiotic treated (n = 8) and untreated *Culicoides* (n = 8) ingested a mean of 9.96±0.05 and 9.88±0.05(SE) $\log_{10}$ copies of BTV Seg-1 per an insect, respectively, following blood feeding, which did not differ significantly (t-test: $t_{29} = 1.07$, $p = 0.30$) (data not shown). Removal of midgut bacteria through antibiotic treatment did not impact the RNA level of Seg-1 in carcasses of whole *Culicoides* (t-test: $t_{137} = 0.09$, $p = 0.92$) or the infection rate of *Culicoides* relative to the untreated control group (chi-square test: $X^2_1 = 0.10$, $p = 0.76$) when sampled by qPCR at 7 days after blood feeding (figure 5.2B). Because the removal of midgut bacteria appeared to have no effect on infection rate with BTV, no further studies were conducted in this area.

Figure 5.2: Antibiotic treatment eliminates bacterial load in the midguts of *Culicoides*, but does not alter infection with BTV-1.

(**A**) Bacterial colony formation (left panel) and bacterial loads (right panel) are shown, from homogenate of midguts (n = 10) from antibiotic treated or untreated *Culicoides* that were fed on sucrose or uninfected blood. Sucrose (with or without antibiotics) was provided *ad lib* for 7 days. Bars represent the standard error of the mean of four independent replicates. (**B**) *Culicoides* were fed blood containing 7.0 $\log_{10}$ $TCID_{50}$/ml of BTV-1. The number of BTV infected *Culicoides* that were treated with (n = 77) or without (n = 64) antibiotics were calculated 7 days post-blood meal and expressed as a percentage of *Culicoides* sampled (left panel). The level of Seg-1 RNA in each *Culicoides*, is shown (right panel), which was normalised to eF1β. Significance in Seg-1 RNA level was determined using a Student's t-test and percentage infection rates were tested using a Pearson's chi-squared test ('ns' = a non-significant difference). Each point represents copies in an individual *Culicoides.* Bars show the standard error of the mean (right panel) or the 95% confidence interval (left panel).

Figure 5.2

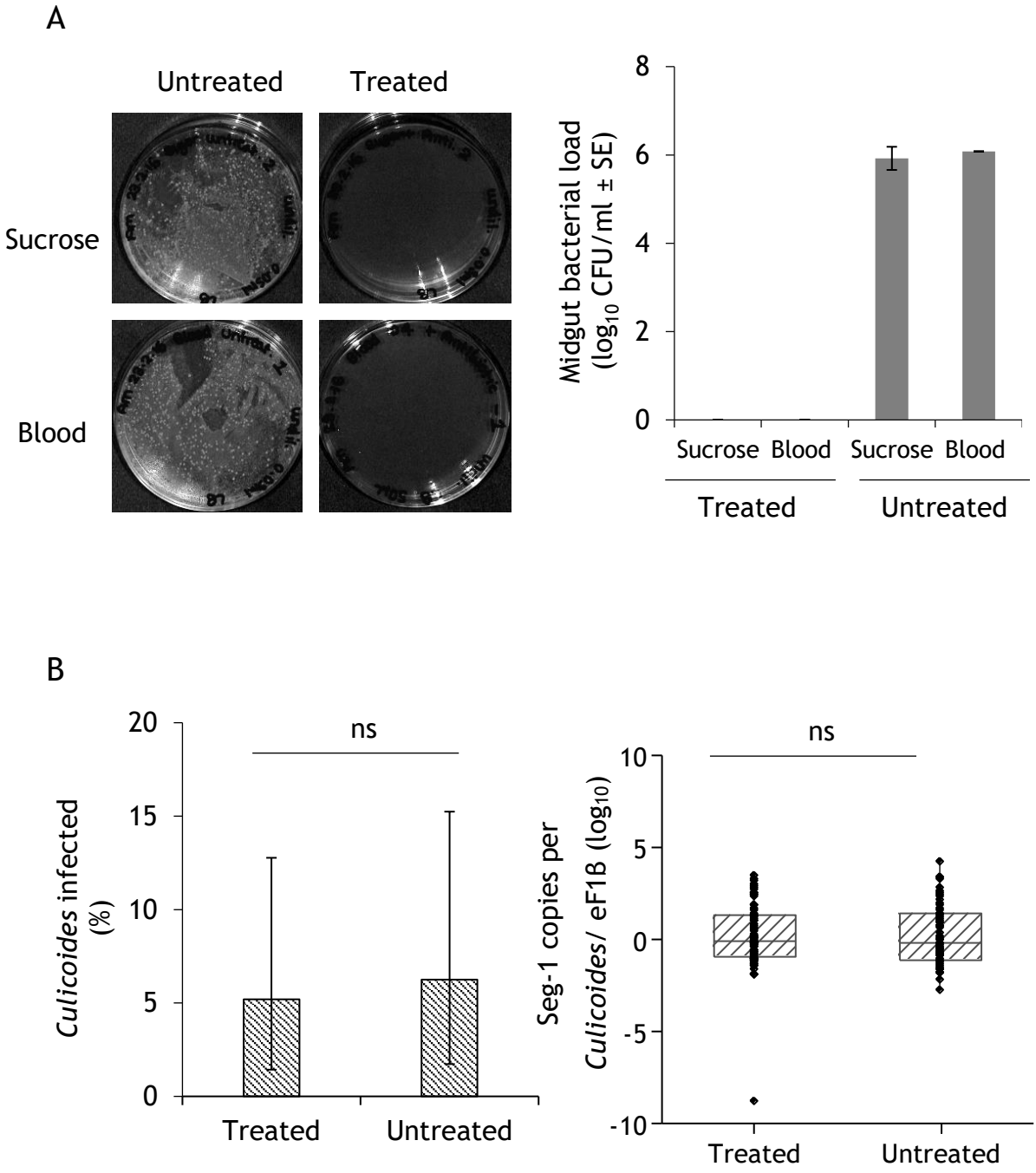
A
Untreated
Treated
Sucrose
Blood
Midgut bacterial load (log10 CFU/ml ± SE)
8
6
4
2
0
Sucrose Blood Sucrose Blood
Treated
Untreated
B
Culicoides infected (%)
20
15
10
5
0
ns
Treated
Untreated
Seg-1 copies per Culicoides/ eF1B (log10)
10
5
0
-5
-10
ns
Treated
Untreated

5.2.3 The infection rate of *Culicoides* with BTV-1 is directly proportional to viral dose

Culicoides were fed blood supplemented with a low dose (4.2 $\log_{10}$ $TCID_{50}$/ml), mid-dose (6.2 $\log_{10}$ $TCID_{50}$/ml) or high dose (7.0 $\log_{10}$ $TCID_{50}$/ml) of BTV-1 in order to determine which viral blood meal dose would maximise infection rate, without inducing changes in BTV localisation. The viral doses selected were within the range of BTV-1 titres observed during peak viraemia in experimentally infected Dorset Poll sheep (Baylis et al., 2008, Hamblin et al., 1998). Engorged *Culicoides* fed a high dose (n = 8) ingested 9.37±0.03 (SE) $\log_{10}$ copies of Seg-1 of BTV-1. Whereas, 8.37±0.06 and 5.17±0.34 $\log_{10}$ copies were ingested per an insect after feeding on mid (n = 8) or low dose blood meal (n = 8), respectively. As expected, these differences in ingested Seg-1 copy numbers were significant (ANOVA: $F_2 = 162.71$, $R^2 = 90.79\%$ =, $p<0.001$), which confirmed that *Culicoides* in the respective treatment groups ingested different BTV doses.

The infection rate was assayed by detecting BTV copies by qPCR in bodies and heads at 7 days post-blood meal (PBM), respectively, as described in Chapter 2 (sections 2.3 and 2.14.1). 15.48% of *Culicoides* became infected with BTV-1 after feeding on a high viral dose, compared with 12.41% fed on a mid-dose (chi-square: $X^2_1 = 0.338$, $p = 0.561$). No infected *Culicoides* were detected after feeding on the low dose of BTV-1 (figure 5.3A). *Culicoides* fed a high viral titre possessed 1.45 more normalised copies of Seg-1 in their bodies than *Culicoides* infected with a mid-titre of BTV-1, respectively, which differed significantly (Mann-Whitney *U*: $W = 19705$, $p<0.05$) (figure 5.3A). The low dose group was eliminated from further analysis as infection was not detected.

The disseminated infection rate was high. After 7 days post blood-meal, BTV was detected in the heads of 88.89% and 87.50% of those *Culicoides* that became infected after ingesting blood supplemented with a mid and high BTV-1 dose, respectively. These values were not statistically significant (chi-square: $X^2_1 = 0.01$, $p = 0.917$). The level of Seg-1 RNA in the heads of infected *Culicoides* did not differ with the ingested viral dose (Mann-Whitney *U*: $W = 399$, $p = 0.896$) (figure 5.3B), confirming that the size of viral dose ingested in the blood meal acts to increase overall infection rate, as shown previously for BTV-1 (Mertens et al., 1996a).

Figure 5.3: Infection rate increases with BTV-1 dose.

Groups of *Culicoides* were fed on a low dose (4.2 $\log_{10}$ $TCID_{50}$/ml; Low) (n = 59), mid dose (6.2 $\log_{10}$ $TCID_{50}$/ml; Mid) (n = 145) or a high dose (7.0 $\log_{10}$ $TCID_{50}$/ml; High) (n = 155) of BTV-1. (**A**) The percentage of infected *Culicoides* and (**B**) viral load, which was expressed as copies of Seg-1 in *Culicoides* bodies (normalised against eF1β copy number), were calculated. (**C**) The percentage of infected *Culicoides* with a disseminated infection (Seg-1 copies in the head) and (**D**) normalised copies of Seg-1 in *Culicoides* heads were calculated. Significance in percentage infection rates was determined using Pearson's chi-square test. Mann-Whitney *U* tests were applied to test significance in Seg-1 copies in heads and bodies ('ns' = non-significant; * = $p<0.05$). Each point in B and D represents copies in an individual *Culicoides* and bars show the standard error of the mean. Bars in A and C show the 95% confidence intervals.

Figure 5.3

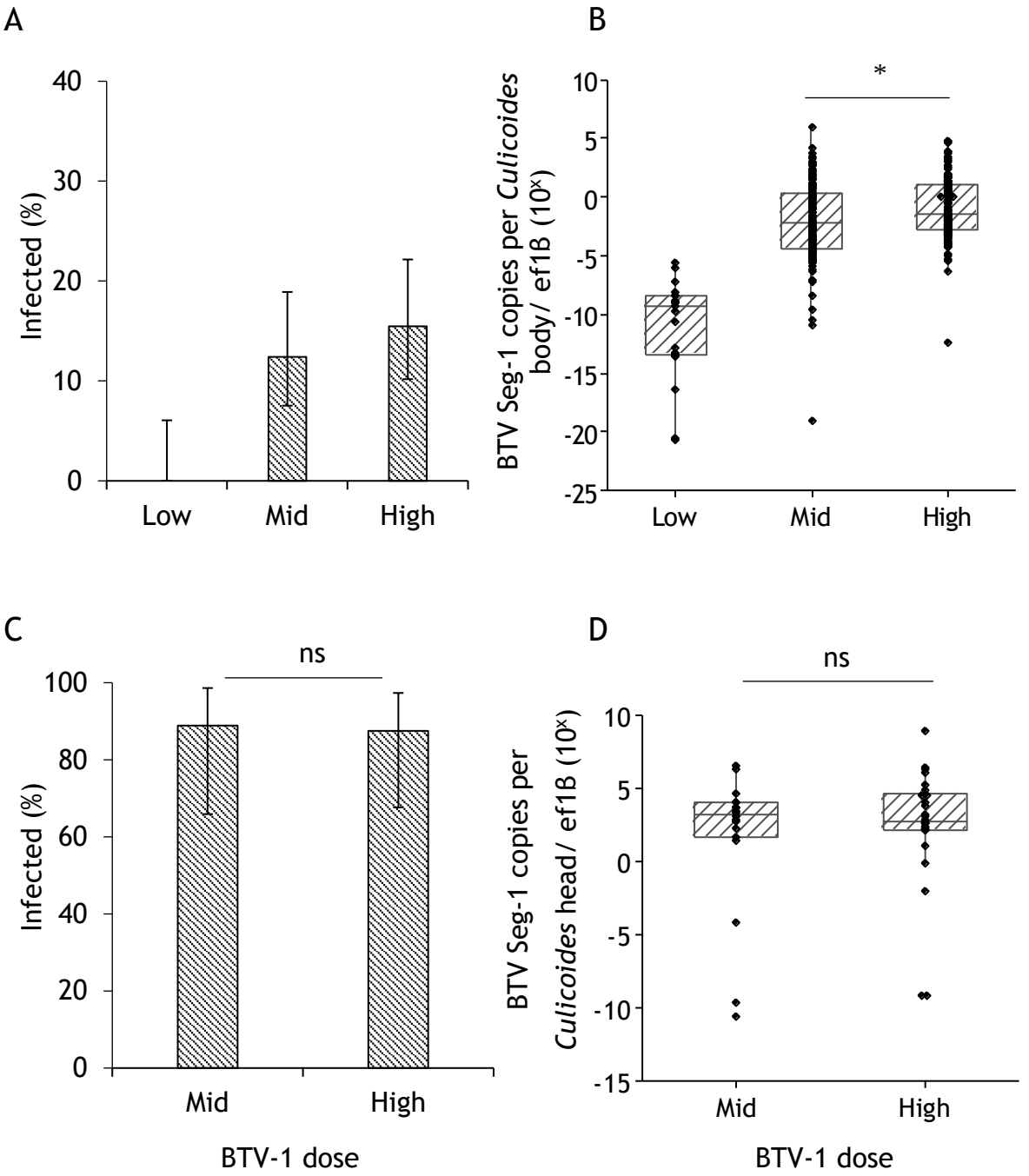
A
Infected (%)
40
30
20
10
0
Low
Mid
High
B
BTV Seg-1 copies per *Culicoides* body/ ef1B (10^x)
*
10
5
0
-5
-10
-15
-20
-25
Low
Mid
High
C
ns
Infected (%)
100
80
60
40
20
0
Mid
High
BTV-1 dose
D
ns
BTV Seg-1 copies per *Culicoides* head/ ef1B (10^x)
10
5
0
-5
-10
-15
Mid
High
BTV-1 dose

5.2.4 Ingestion of a higher viral dose does not alter the tissues infected by BTV-1

Next, we determined the levels of BTV RNA and protein in infected tissues. *Culicoides* were first fed blood containing a high dose (7.0 $\log_{10}$ $TCID_{50}$/ml) or a mid-dose (6.2 $\log_{10}$ $TCID_{50}$/ml) of BTV-1 (see Chapter 2, section 2.3). The BTV proteins (VP) and +Seg-5 RNA were dual-labelled in sections of *Culicoides* at 7 and 12 days PBM, as detailed in Chapter 2 (section 2.18.2).

Levels of Seg-1 RNA were tested in engorged *Culicoides* (n = 8) to confirm the viral dose administered in the blood-virus mixture. *Culicoides* fed with a high dose ingested a significantly higher level of Seg-1 RNA (9.76 ± 0.02(SE) $\log_{10}$ copies), than a mid-dose (8.87 ± 0.02 $\log_{10}$ copies) (t-test: $t_{15} = 20.51$, $p<0.001$). BTV-1 RNA was not detected in a control group of mock infected *C. sonorensis* after feeding on blood containing DMEM.

The number of *C. sonorensis* with a BTV infection localised to the midgut (a 'non-disseminated' infection) or a 'disseminated' infection (expression of VP and +Seg-5 in non-midgut tissues) are shown in table 5.1. Only 10.71% (6/56) of infected *Culicoides* remained with an infection localised to the midgut. The percentage of *Culicoides* becoming infected after ingesting a high-viral dose was almost double that of the group fed a mid-dose, consistent with previous findings (see section 5.2.3). The infection rate increased by 30.00% and 26.09% between 7 and 12 days PBM for *Culicoides* fed a mid or high viral dose, respectively.

Table 5.1: The number of BTV-1 infected *C. sonorensis* midges is directly correlated to the viral dose.

BTV dose ($log_{10}TCID_{50}$/ml)	Days post-blood meal	Number sampled	Number infected (%)	Number of infected with disseminated infection (%)	Number of infected with non-disseminated infection (%)
6.2	7	80	7 (9.0)	7 (100.0)	0 (0.0)
	12	73	10 (14.0)	7 (70.0)	3 (30.0)
7.0	7	126	21 (17.0)	18 (85.7)	3 (14.3)
	12	79	18 (23.0)	18 (100.0)	0 (0.0)

The percentage of cells expressing BTV-1 VP and +Seg-5 RNA were calculated from confocal images of *Culicoides* tissues using methods described previously (see Chapter 4, sections 4.2.1 and 4.2.2). The type of tissues infected with BTV-1 did not differ between the groups infected with high or medium viral doses, with the exception of the thoracic muscle. BTV +Seg-5 RNA and VP were detected in ≥1% of cells in the midgut, foregut, hindgut, compound eyes, thoracic ganglia, optic lobe, axillary apparatus, fat body, mouthparts, abdominal and thoracic epithelium. In addition, in <15% of individuals fed with a high viral dose, BTV-1 was also detected in the thoracic muscle at the latest time sampled. Importantly, +Seg-5 and VP were not detected at any stage in the salivary glands (figure 5.4).

In general, most tissues with the exception of the optic lobe, hindgut and thoracic epithelium, were infected more frequently after ingestion of a high viral dose. This was particularly noticeable in the foregut, where 83.33% (chi-square: $X^2_1 = 83.33$, $p<0.001$) more individuals showed infection in this tissue, after ingesting a high-viral dose than a mid-dose at 12 days PBM (figure 5.4). This could indicate an increased time required for viral dissemination during a BTV infection resulting from the lower dose. However, the percentage of cells expressing +Seg-5 in infected tissues did not differ significantly between doses tested (figure 5.7). Similar results were obtained for VP (data not shown). A comparable level of infection (figure 5.6), indicates that infection with the higher viral dose tested progresses at a similar rate within infected tissues, compared to individuals infected with the lower dose. As expected, VP and +Seg-5 were undetectable in uninfected control *Culicoides* (figure 5.5).

Figure 5.4

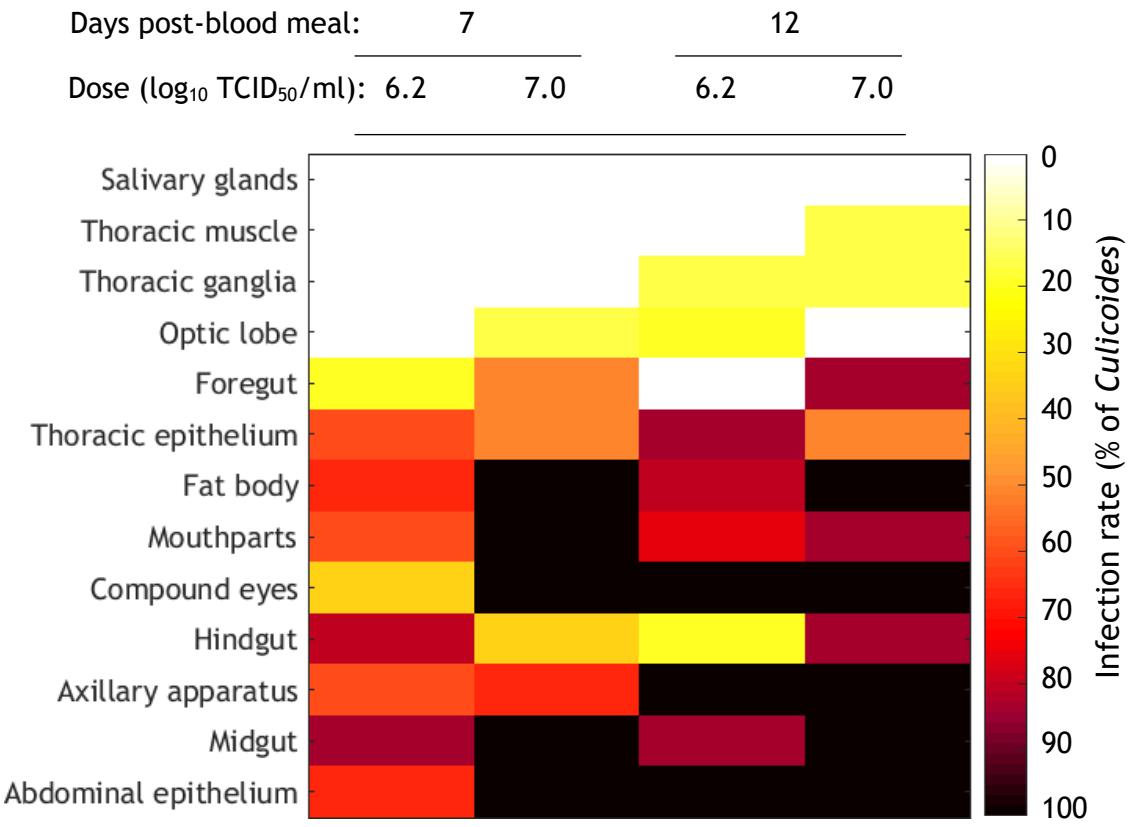

Figure 5.4: Infection rate of tissues of *Culicoides* midges after ingesting different BTV-1 doses.

The percentage of *Culicoides* expressing BTV +Seg-5 RNA and protein (VP) in ≥1% cells (or area for the salivary glands and neural tissues) were calculated for each tissue at 7 and 12 days after feeding on blood containing a mid-dose of 6.2 $\log_{10}$ $TCID_{50}$/ml or high dose of 7.0 $\log_{10}$ $TCID_{50}$/ml of BTV-1. To avoid biases associated with differences in sample size, six individuals were randomly sampled for each group of *Culicoides* confirmed as infected.

Figure 5.5

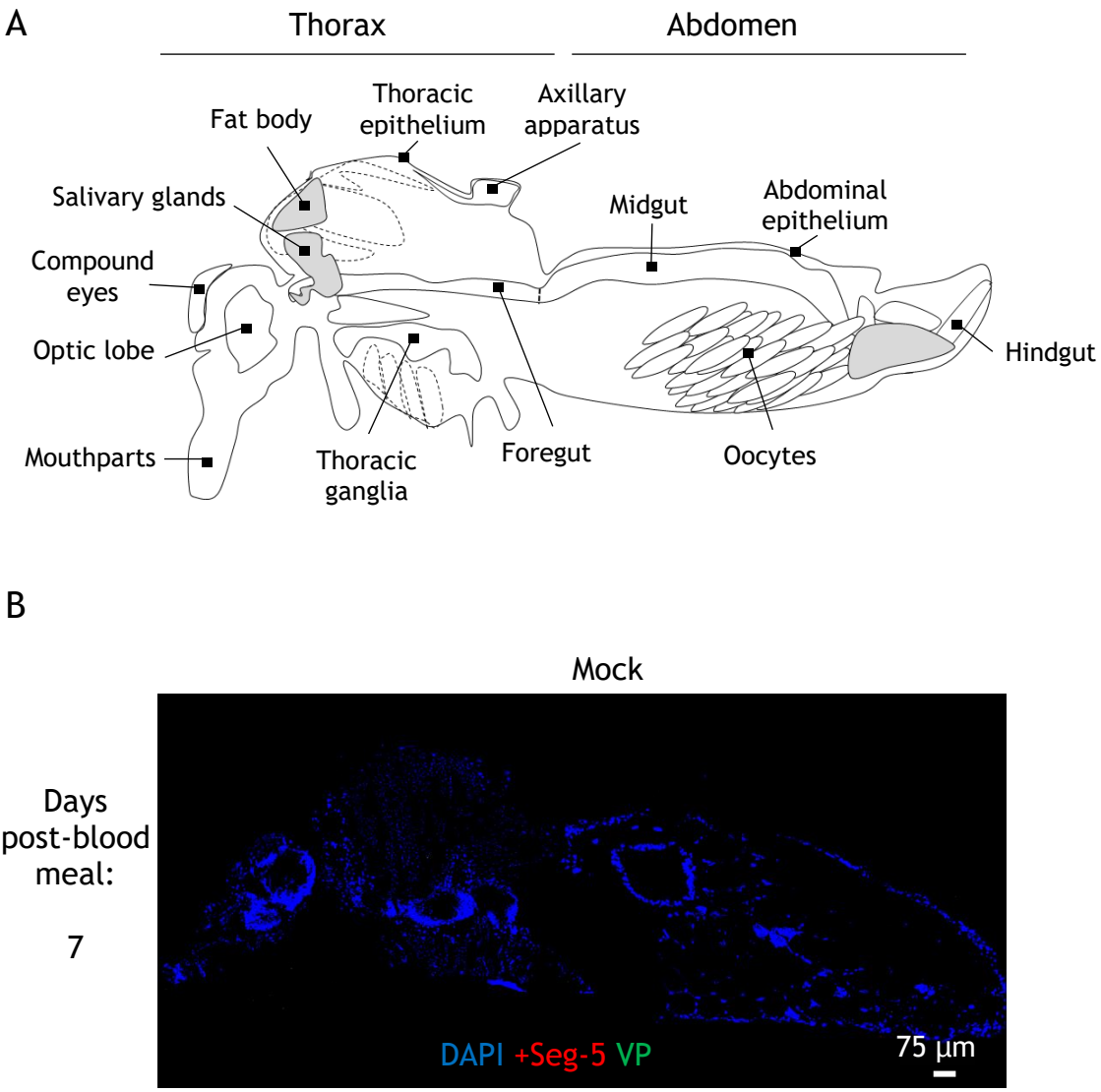

Figure 5.5: BTV is undetectable in mock infected *Culicoides*.

(**A**) Schematic diagram of a lateral section through *Culicoides* showing the location of tissues of interest. (**B**) Representative composite confocal image of a mock-infected *Culicoides* at 7 days after feeding on blood containing DMEM. BTV +Seg-5 RNA (red), protein (VP, green) and counterstained nuclei (blue) are shown (scale = 75 µm).

Figure 5.6: Progression of BTV infection in *Culicoides* fed with different BTV-1 doses.

Representative composite confocal images of infected *Culicoides* at 7 and 12 days after feeding on blood containing a mid-dose of 6.2 $\log_{10}$ $TCID_{50}$/ml or a high dose of 7.0 $\log_{10}$ $TCID_{50}$/ml of BTV-1. BTV +Seg-5 RNA (red), viral protein (VP, green) and nuclei (blue) are shown (scale = 75 µm).

Figure 5.6

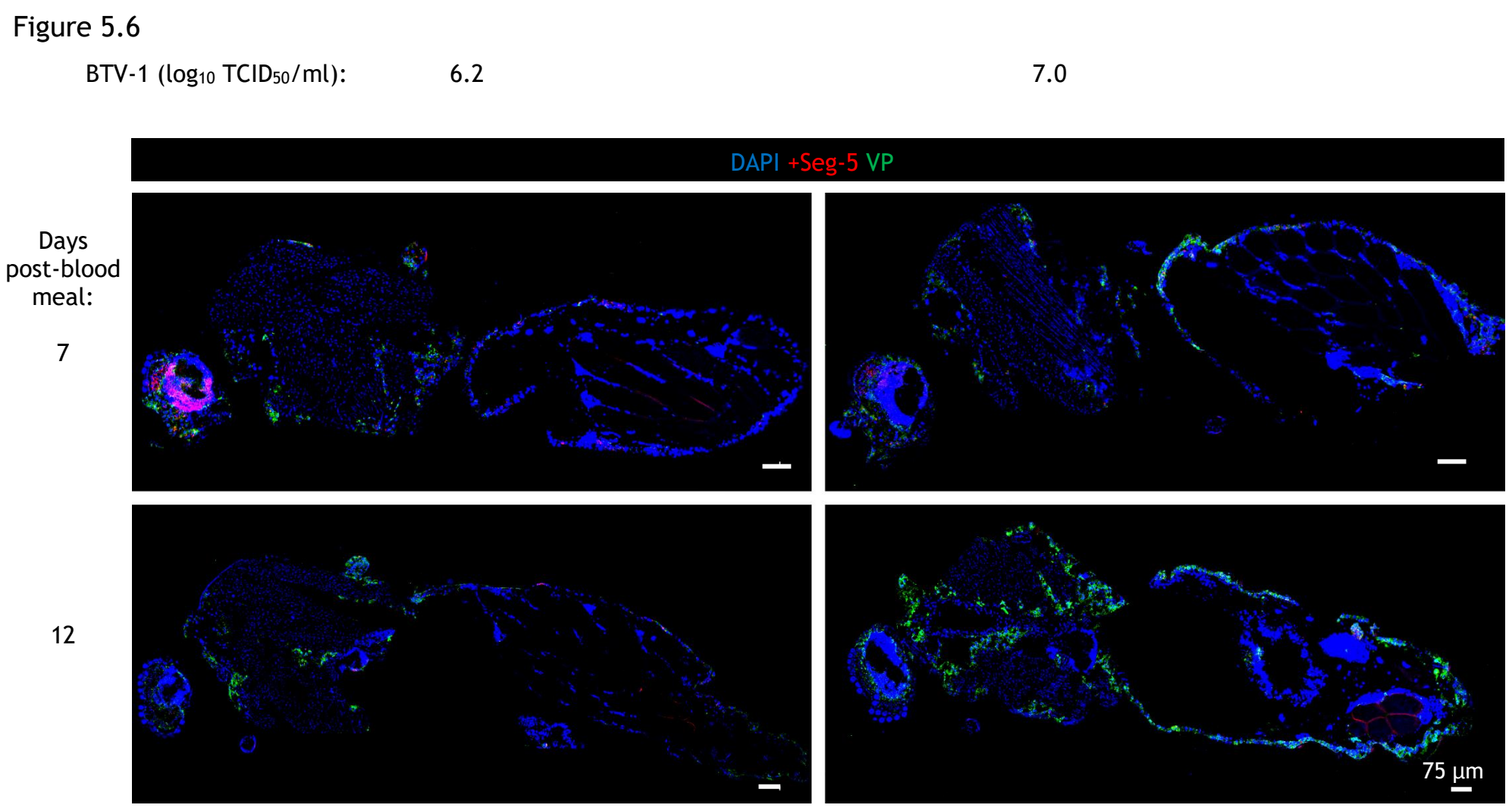
BTV-1 (log10 TCID50/ml):
6.2
7.0
DAPI +Seg-5 VP
Days post-blood meal:
7
12
75 µm

Figure 5.7: The percentage of cells expressing +Seg-5 RNA in tissues of *Culicoides* fed different BTV-1 doses.

Culicoides were fed blood containing a high dose of 7.0 $\log_{10}$ $TCID_{50}$/ml or mid-dose of 6.2 $\log_{10}$ $TCID_{50}$/ml of BTV-1. At (**A**) 7 days (7.0: n = 20; 6.2: n = 6) and (**B**) 12 days post-blood meal (7.0: n = 18; 6.2: n = 10), the percentage of cells (or area for the salivary glands, optic lobe and thoracic ganglion) expressing +Seg-5 RNA were determined in infected tissues (which expressed viral protein and +Seg-5 RNA in ≥1% of cells). Bars show the standard error of the mean.

Figure 5.7

A

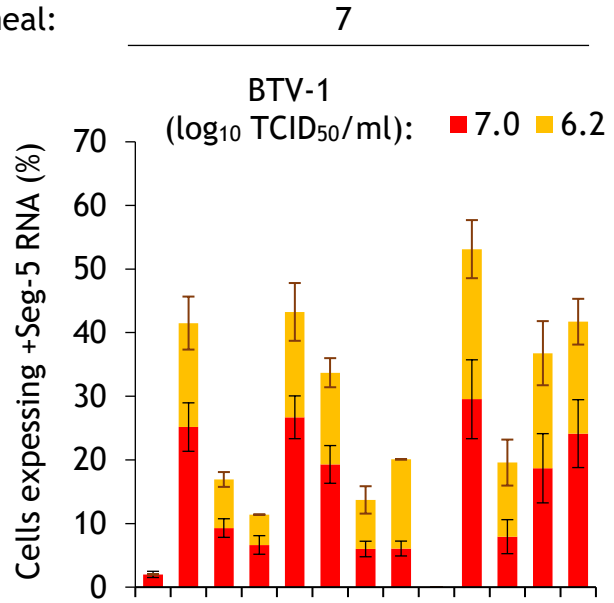
Days post-blood meal: 7
BTV-1
(log10 TCID50/ml): 7.0 6.2
Cells expessing +Seg-5 RNA (%)
70
60
50
40
30
20
10
0

B

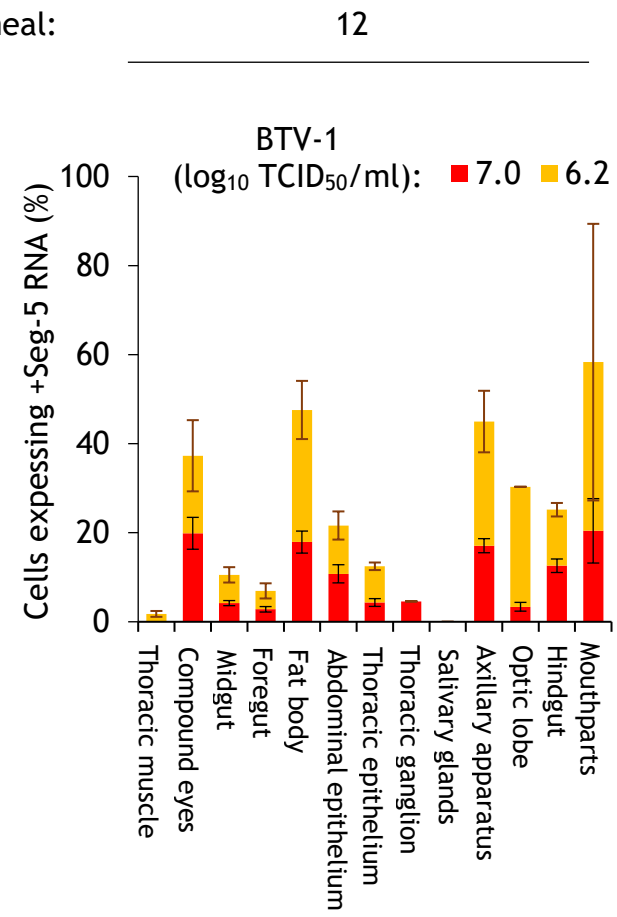
Days post-blood meal: 12
BTV-1
(log10 TCID50/ml): 7.0 6.2
Cells expessing +Seg-5 RNA (%)
100
80
60
40
20
0
Thoracic muscle
Compound eyes
Midgut
Foregut
Fat body
Abdominal epithelium
Thoracic epithelium
Thoracic ganglion
Salivary glands
Axillary apparatus
Optic lobe
Hindgut
Mouthparts

5.2.5 A greater number of midgut cells are infected after ingestion of a higher BTV-1 dose

Next, the effect of viral doses on the ability of BTV-1 to infect the midgut was determined. The number of infected midgut cells in *Culicoides* with a recently disseminated infection were calculated. A recently disseminated infection was defined as VP and +Seg-5 expression in ≤15% of cells in every non-midgut tissue analysed in the previous section (figure 5.8). A significant difference (t-test: $t_8 = 2.81$, $p<0.05$) was observed in the extent of infection of the midgut as indicated by a single focus of viral protein labelling in 3.39 ± 0.79 (SE)% and 1.01 ± 0.28% of midgut cells following ingestion of a high or mid-viral dose respectively (table 5.2). Similar results were obtained for +Seg-5 RNA (data not shown), indicating that BTV-1 infects a greater number of midgut cells following ingestion of a higher viral dose.

Table 5.2: Initial midgut infection of BTV-1 under varying blood meal viral doses.

BTV-1 ($log_{10}TCID_{50}$/ml)	Number of midguts sampled	Number of midguts infected (%)	Number of cells sampled (mean)	Number of cells expressing VP5 (%)	Mean cells expressing VP5 (%)
6.2	3	3 (100)	868 - 1355 (1052)	4 - 19 (0.46 – 1.40)	11 (1.01)*
7.0	8	8 (100)	925 - 5395 (2603)	23 – 196 (0.80 – 6.92)	81 (3.39)*

* = $p<0.05$, student's t-test

Figure 5.8

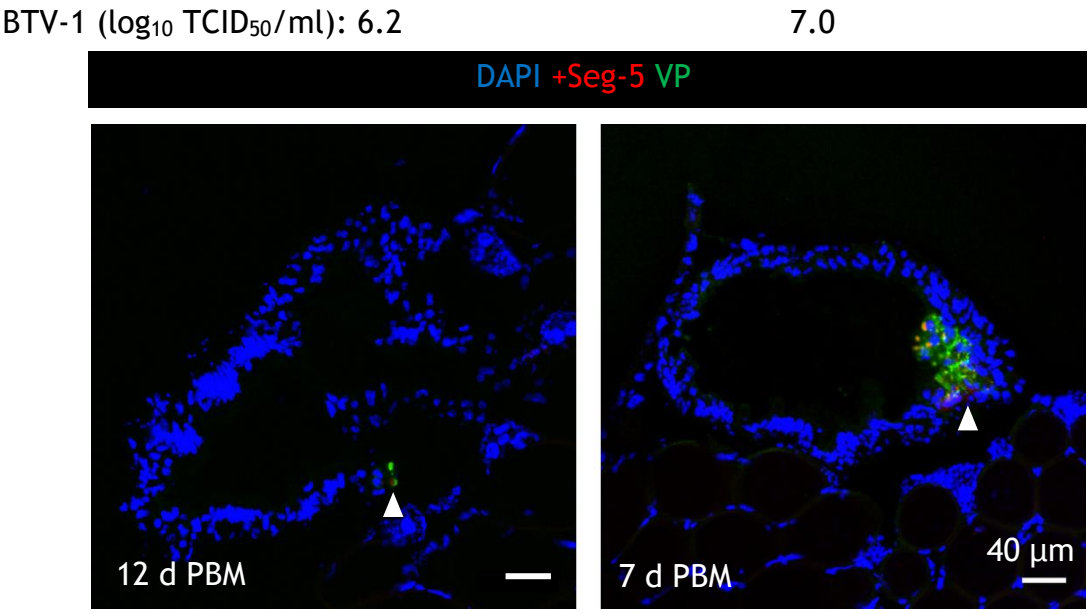

Figure 5.8: BTV-1 infects a greater number of midgut cells in *Culicoides* fed a blood meal containing a higher viral dose.

Representative images of sections of the midgut of *Culicoides* with a recently disseminated BTV infection (defined as ≤ 15% of cells of non-midgut tissues) at 7 and 12 days post-ingestion of a blood meal (d PBM) containing either a mid-dose of 6.2 log_{10} $TCID_{50}$/ml (Mid titre), or a high dose of 7.0 log_{10} $TCID_{50}$/ml (High titre) of BTV-1. Arrows indicate the location of cells expressing BTV protein (VP, green) and +Seg-5 RNA (red). Nuclei are shown in blue (scale = 40 µm).

5.2.6 Infection rate of BTV-11 in *Culicoides* is higher than BTV-1

The previous section indicates that ingestion of a higher BTV dose did not alter the tissues infected within individual insects, compared with a lower viral dose. Studies in the following sections were therefore conducted using the high viral dose of 7.0 $\log_{10}$ $TCID_{50}$/ml.

Culicoides were fed blood containing an equal viral load (7.0 $\log_{10}$ $TCID_{50}$/ml) of BTV-1 or BTV-11 in order to compare the relative abilities a South African and North American BTV strain to infect *Culicoides*. *Culicoides* (n per group = 8) ingested a mean of 9.92±0.06(SE) $\log_{10}$ copies of BTV-1 and 9.77±0.03 $\log_{10}$ copies of BTV-11 Seg-1 RNA (t-test: $t_9 = 2.32$, $p = 0.05$). Despite a low level of significance in ingested viral RNA level, levels of Seg-1 RNA in the blood meal did not differ between viruses and were for 11.86±0.09 $\log_{10}$ for BTV-1, and 11.90±0.01 $\log_{10}$ RNA copies per ml of blood-virus mixture for BTV-11 (t-test: $t_1 = 0.48$, $p = 0.72$).

Infection rate was assayed 7 days PBM using qPCR to detect Seg-1 RNA levels in whole insects as described in Chapter 2 (section 2.14.1). The primers and probe set used in the qPCR were complimentary to Seg-1 of both BTV stains tested (Shaw et al., 2007a) (for sequences see Chapter 2, table 2.5). BTV-11 infected 23.53% of *Culicoides*, whereas only 11.81% of *Culicoides* developed a BTV-1 infection (chi-square: $X^2_1 = 3.88$, $p<0.05$) (figure 5.9). This difference in infection rate was reflected by an increase in the level of Seg-1 RNA when *Culicoides* were fed on BTV-11 compared to BTV-1 (t-test: $t_{259} = 7.28$, $p <0.001$) (figure 5.9).

Figure 5.9

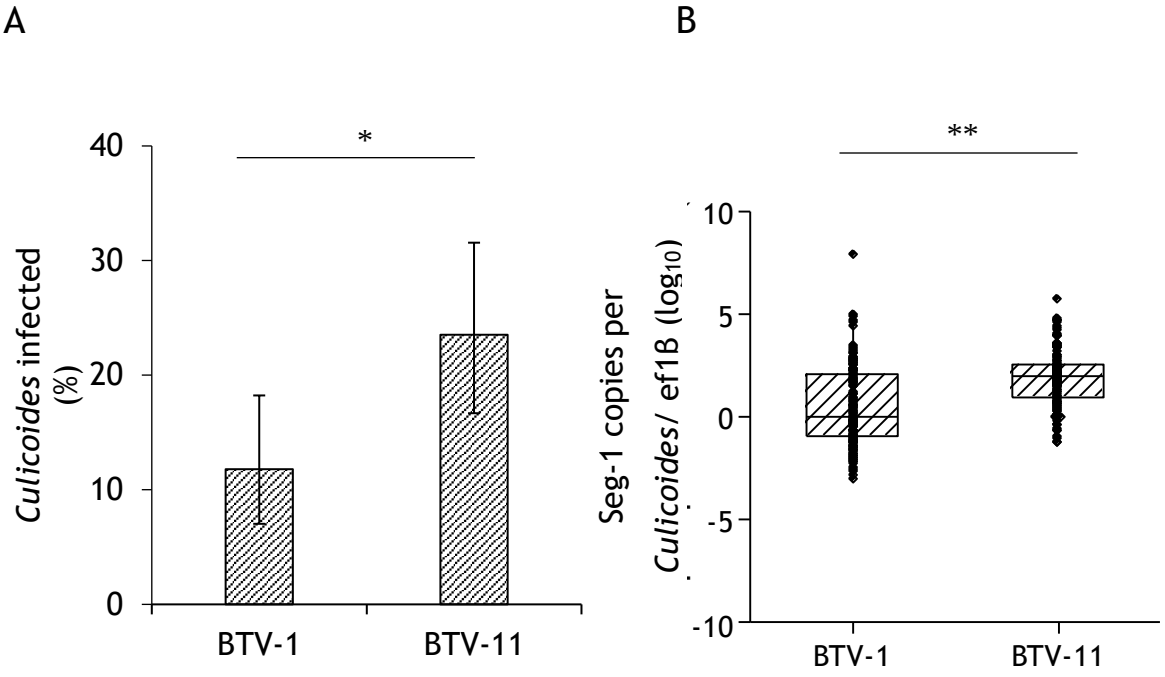

Figure 5.9: Higher infection rate of BTV-11 in *Culicoides* compared to BTV-1.

Culicoides were fed on blood supplemented with 7.0 $\log_{10}$ $TCID_{50}$/ml of BTV-1 (n = 144) or BTV-11 (n = 136). (**A**) The percentage of infected *Culicoides* was determined by the detection of BTV Seg-1 RNA and (**B**) the levels of Seg-1 in each *Culicoides* are shown 7 days after blood feeding. The significance of percentage infection rates was determined using a Pearson's chi-squared test and BTV Seg-1 RNA levels, using a Student's t-test (* = $p<0.05$ and ** = $p<0.001$). Each point in panel B represents BTV copies in an individual *Culicoides*. Bars in panel B represent the standard error of the mean and, in panel A, the 95% confidence interval.

5.2.7 BTV-11 disseminates in a greater number of *Culicoides* than BTV-1

We next assessed the differences in the dissemination rate of BTV-1 and BTV-11 in infected *Culicoides*. In a series of four (BTV-11) or five (BTV-1) independent experiments, *Culicoides* were fed on blood containing 7.0 $\log_{10}$ $TCID_{50}$/ml of BTV-1 or BTV-11. BTV dissemination was monitored by confocal microscopy in sections of *Culicoides* sacrificed at 4, 6, 7 and 12 days PBM, as detailed in Chapter 2 (section 2.18.2). Sections were co-labelled for both viral protein (VP) and +Seg-5 RNA. The engorged *Culicoides* had ingested mean Seg-1 RNA levels of 9.36 ± 0.05(SE) $\log_{10}$ of BTV-1 and 9.55 ± 0.04 $\log_{10}$ of BTV-11 (t-test: $t_{56} = 2.43$, $p<0.05$). Despite the low significance of ingested RNA level, the blood-virus mixture contained 11.98±0.10 $\log_{10}$ copies of BTV-1 or 11.99±0.03 $\log_{10}$ copies of BTV-11 Seg-1 RNA, which did not differ significantly (t-test: $t_{13} = 0.18$, $p = 0.857$). A control group of uninfected *Culicoides* were fed blood supplemented with DMEM and did not ingest any BTV copies (data not shown).

Survival plots are shown in figure 5.10 (see Chapter 2, section 2.3 for methods). The number of *Culicoides* surviving, relative to day 0, generally decreased over the time course. However, mortality did not differ between the mock-infected or groups of *Culicoides* fed blood supplemented with BTV-1 or BTV-11 at 4 (chi-square test: $X^2_2 = 5.14$, $p = 0.77$), 6 ($X^2_2 = 2.59$, $p = 0.273$) and 7 days PBM ($X^2_2 = 4.87$, $p = 0.09$). The survival rate of *Culicoides* 12 days PBM containing BTV-11 was significantly lower than that of the uninfected *Culicoides* (chi-square test: $X^2_2 = 12.40$, $p<0.05$).

Figure 5.10

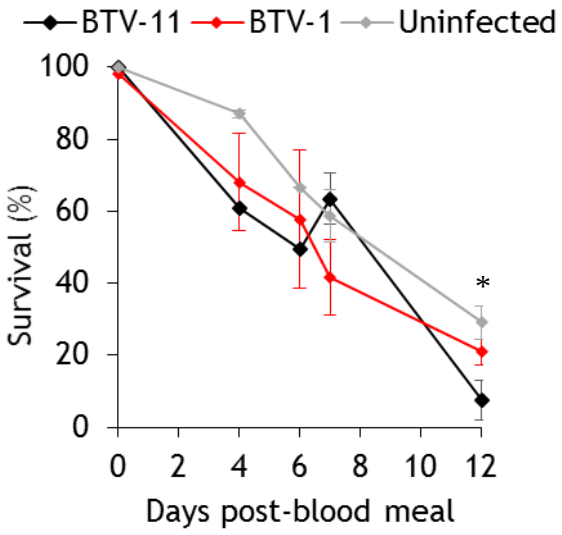

Figure 5.10: Survival of *Culicoides* fed BTV-1 or BTV-11 is comparable to mock infected *Culicoides*.

The percentage of *Culicoides* surviving after 4, 6, 7 and 12 days following feeding on blood supplemented with 7.0 $\log_{10}$ $TCID_{50}$/ml of BTV-11 or BTV-1 were calculated. A mock-infected control group was included, which were fed blood supplemented with DMEM. Bars show the standard error of the mean of four (BTV-11, Uninfected) or five (BTV-1) independent replicates. Each value used to calculate the mean represents the survival rate of a separate pot of *Culicoides* at time of sacrifice. Significance was determined using a Pearson's chi-squared test (* = $p<0.05$).

The number of *Culicoides* with an infection restricted to the midgut (a 'non-disseminated' infection) and disseminated infection (expression of VP and +Seg-5 in non-midgut tissues) are shown in table 5.3. At 4 days PBM, 66.7% and 12.5% of infected *Culicoides* had a non-disseminated BTV-1 or BTV-11 infection, respectively. The number of *Culicoides* with an infection restricted to the midgut, subsequently decreased to undetectable levels by 12 and 7 days PBM for BTV-1 and BTV-11, respectively. Conversely, the number of *Culicoides* with a disseminated infection increased with time PBM, reaching 23% for BTV-1 and 64% for BTV-11 by 12 days PBM (chi-square test: $X^2_1 = 19.32$, $p<0.001$). At this time point, BTV had disseminated in all infected *Culicoides*. The observed overall infection rate increased by 3.2 fold for BTV-1 (7 to 23%) and 1.6 fold (40 to 64%) for BTV-11 over the time course (table 5.3).

Table 5.3: Infection rates and dissemination of BTV-1 and BTV-11 in *Culicoides*.

	Days after blood meal	Number sampled	Number infected (%)	Number with disseminated infection (%)	Number with non-disseminated infection (%)
BTV-1	4	44	3 (7.0)	1 (33.3)	2 (66.7)
	6	50	6 (12.0)	3 (50.0)	3 (50.0)
	7	126	21 (17.0)	18 (85.7)	3 (14.3)
	12	79	18 (23.0)	18 (100.0)	0 (0.0)
BTV-11	4	40	16 (40.0)	14 (87.5)	2 (12.5)
	6	45	24 (53.0)	23 (95.8)	1 (4.2)
	7	48	27 (56.0)	27 (100.0)	0 (0.0)
	12	14	9 (64.0)	9 (100.0)	0 (0.0)

5.2.8 BTV-1 infection of the midgut in *Culicoides*

Previous studies have indicated that arboviruses, including BTV, replicate in midgut cells to a threshold titre prior to disseminating into the haemolymph (Hardy et al., 1983, Kramer et al., 1981). To test this in more detail, the number of midgut cells expressing VP were determined in *Culicoides* with a BTV-1 infection restricted to the midgut (n = 8) between 4 and 12 days PBM. BTV-11 was omitted from this analysis due to detection of only three infected *Culicoides* with an infection restricted to midgut cells (see table 5.3).

VP expression was compared between *Culicoides* with a recently disseminated BTV-1 infection (n = 8, characterised by expression of +Seg-5 RNA and VP in ≤15% of cells in all non-midgut tissues) (figure 5.11) and an infection restricted to the midgut (a non-disseminated infection). 2.79 ± 0.85(SE)% of midgut cells in infected but non-disseminated *Culicoides* and 3.14 ± 0.74% of midgut cells of *Culicoides* with a recently disseminated infection, expressed viral protein (t-test: $t_{12} = 0.31$, $p = 0.760$) (table 5.4). These data suggest that there is unlikely to be a threshold titre of BTV required for viral dissemination. Similar results were obtained for +Seg-5 (data not shown).

Table 5.4: Midgut infection of *Culicoides* with a non-disseminated or recently disseminated BTV-1 infection.

	Number of midguts sampled	Number of midguts infected (%)	Total cells sampled (mean)	Number of cells expressing VP5 (%)	Mean cells expressing VP5 (%)
Non-disseminated	8	8 (100)	749 - 2615 (1704)	25 - 114 (1.26 – 6.92)	45 (2.79)^{ns}
Disseminated	7	6 (86)	394 - 3518 (2169)	15 – 153 (0.80 – 6.12)	75 (3.14) ^{ns}

^{ns} = non-significant difference by Mann-Whitney *U* tests

Figure 5.11

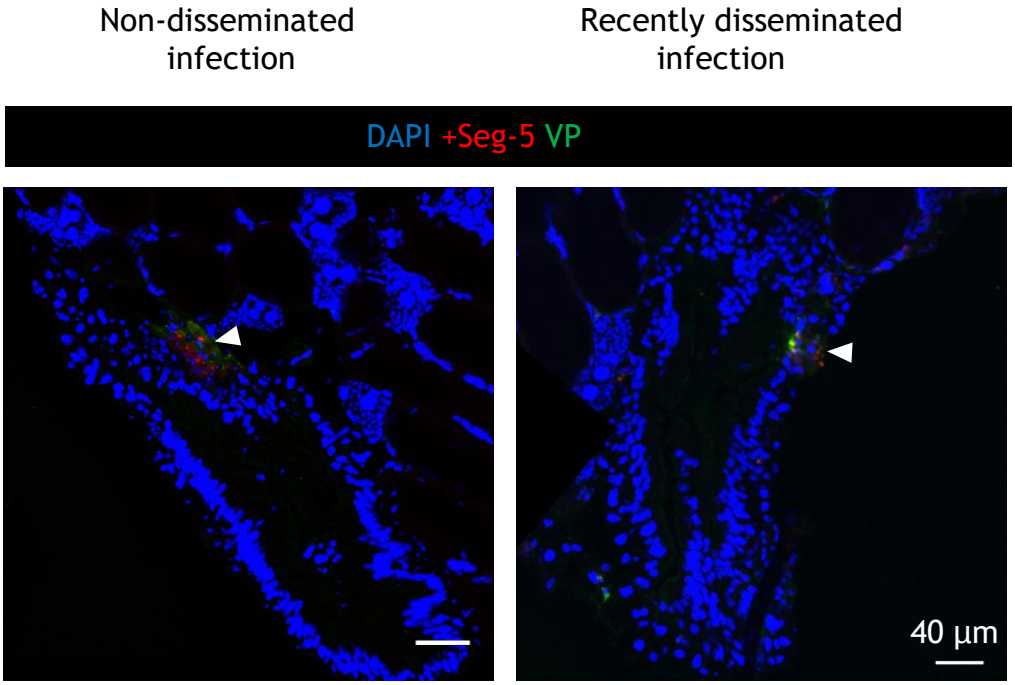

Figure 5.11: The number of infected midgut cells does not differ between *Culicoides* midges with a non-disseminated or a recently disseminated BTV-1 infection.

Representative sections of *Culicoides* midguts with either a non-disseminated or recently disseminated BTV infection at 6 and 4 days (respectively), after feeding on blood containing 7.0 $\log_{10}$ $TCID_{50}$/ml of BTV-1. A recently disseminated infection was characterised by detection of +Seg-5 RNA and VP in ≤15% of cells in all non-midgut tissues. Arrows indicate cells expressing BTV +Seg-5 (red) and protein, VP (green). Nuclei are shown in blue (scale = 40 µm).

5.2.10 BTV-11 infects a greater number of midgut cells than BTV-1

BTV-11 was previously shown to infect almost double the number of *Culicoides* compared with BTV-1 at the time points studied (see section 5.5.6). In order to understand the bases of these differences, VP expression was examined in midgut sections of *Culicoides* with a disseminated BTV-1 or BTV-11 infection (see table 5.3 for sample sizes). A single region of the posterior midgut cells of most infected *Culicoides* expressed VP and +Seg-5 RNA of BTV-1. As few as 0.88% (12/2267) of the midgut cells expressed VP in the *Culicoides* with a disseminated BTV-1 infection at 4 days PBM, indicating that dissemination can arise following infection of relatively few midgut cells.

The percentage of midgut cells that were detected expressing VP of BTV-1 and BTV-11 increased with time PBM. +Seg-5 and VP were expressed in a greater number of midgut cells in *Culicoides* infected with BTV-11 compared to BTV-1 (figure 5.12A). Between 15.46 to 47.78% more midgut cells (of the percentage of infected cells shown in figure 5.12B) expressed VP of BTV-11 than BTV-1 at the time points analysed. This difference in BTV VP expression was especially notable 7 days PBM, where VP of BTV-11 was expressed in 11.34 ± 2.30(SE)% of midgut cells, compared with 4.01 ± 0.57% of midgut cells for BTV-1 (Mann-Whitney *U*: W = 298.0, $p<0.05$).

Figure 5.12: BTV-11 infects a greater percentage of midgut cells than BTV-1.

(**A**) Representative images of a section of the midgut of an individual *Culicoides* between 4 and 12 days after feeding on blood (d PBM) supplemented with 7.0 $\log_{10}$ $TCID_{50}$/ml of BTV-11 or BTV-1. BTV protein (VP, green), +Seg-5 RNA (red) and nuclei (blue) are shown (scale = 40 µm).

(**B**) The percentage of midgut cells expressing viral protein (VP) were calculated at 4 days (BTV-1: n = 12, BTV-11: n = 14), 6 days (BTV-1: n = 7, BTV-11: n = 17), 7 days (BTV-1: n = 20, BTV-11: n = 16) and 12 days post-blood meal (BTV-1: n = 18, BTV-11: n =6) for each *Culicoides*. Bars represent the standard error of the mean. (* = $p<0.05$ by a Mann-Whitney *U* test).

Figure 5.12

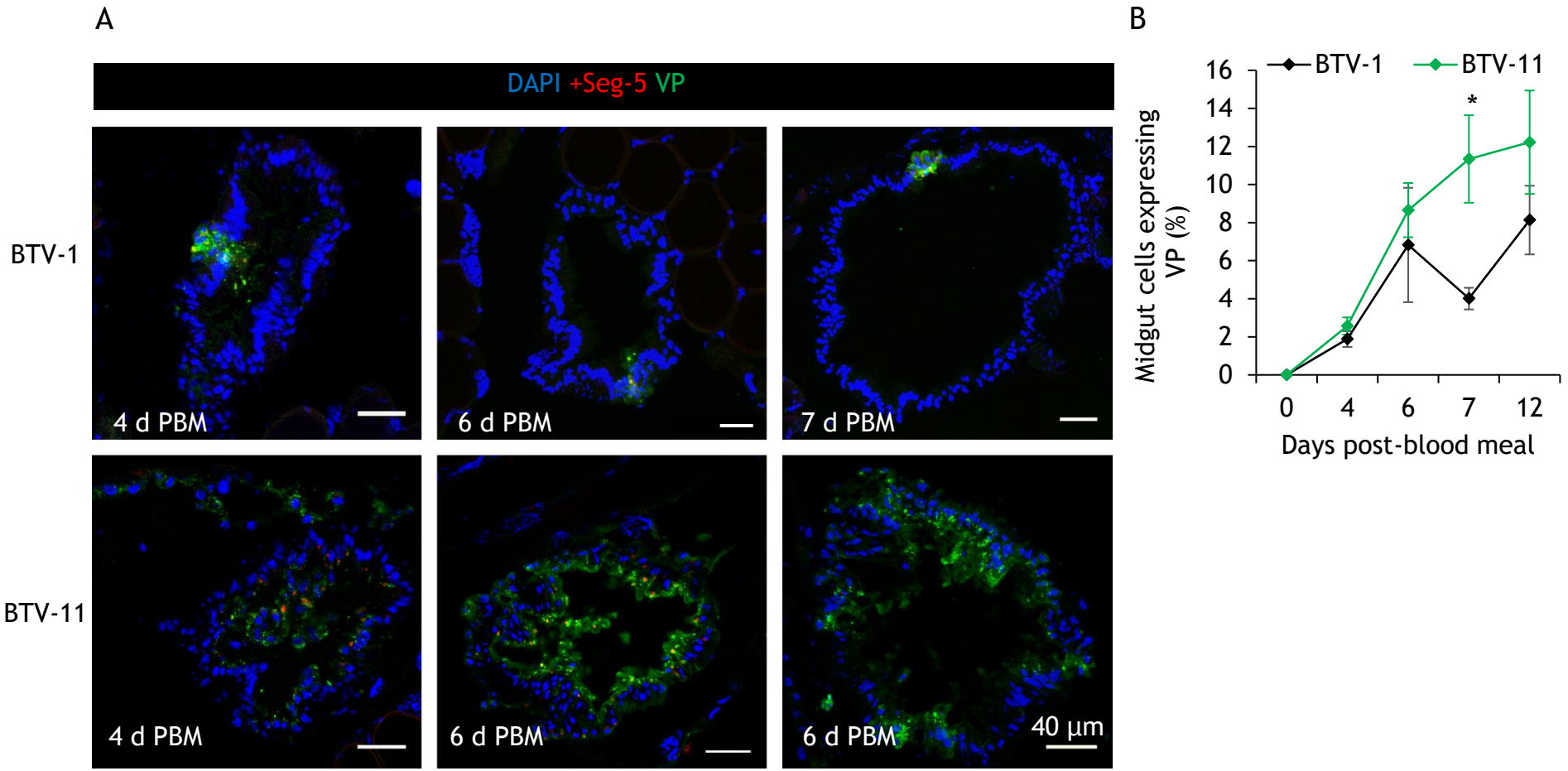
A
DAPI +Seg-5 VP
BTV-1
BTV-11
4 d PBM
6 d PBM
7 d PBM
4 d PBM
6 d PBM
6 d PBM
40 µm
B
BTV-1
BTV-11
Midgut cells expressing VP (%)
Days post-blood meal
0
2
4
6
8
10
12
14
16
0
4
6
7
12
*

5.2.11 Tissue tropism of BTV-1 in *Culicoides*

Next, the percentage of cells expressing BTV +Seg-5 RNA were calculated in tissues of *Culicoides* that had been successfully infected with BTV-1 at 4, 6, 7 and 12 days PBM (see table 5.3). Results are presented in figure 5.13, which shows the percentage of cells expressing +Seg-5 RNA in each tissue, and figure 5.14, which displays representative images of *Culicoides* from each time point. Comparable results were obtained for VP detection.

Since +Seg-5 RNAs are only expressed in detectable, single-stranded form (see section 3.2.5 of Chapter 3) following viral mRNA synthesis, detection may indicate cells in which BTV is actively replicating. +Seg-5 was detected in cells of the axillary apparatus, abdominal epithelium, fat body, thoracic epithelium, compound eyes and at low levels in midgut cells of 91.7% (11/12) of infected *Culicoides* tested at 4 days PBM. Only 41.7% (5/12) of infected *Culicoides* expressed +Seg-5 in cells of the thoracic epithelium and 55.6% (5/9) in the hindgut at this time point (figure 5.13). +Seg-5 was expressed in <1% of foregut cells (including cells of the proventriculus) until 6 days PBM (figures 5.13 and 5.14E), at which time +Seg-5 was expressed in ≥1% of foregut cells of 25.0% of *Culicoides*. The low prevalence of foregut infection indicates that the initial site of BTV-1 entry likely occurs in the midgut, consistent with previous observations (see section 5.2.5) (Fu, 1995, Fu et al., 1999).

The identity of the tissues infected by BTV-1 varied over time and between individuals (figures 5.13 and 5.14A). However, the abdominal epithelium, fat body, mouthparts, midgut, axillary apparatus and compound eyes were infected in the majority of *Culicoides* analysed (figures 5.13, 5.14B and 5.14F). The percentage of cells expressing +Seg-5 in infected tissues generally increased with time PBM (figures 5.13 and 15.14). BTV-1 replicated to its highest levels in the axillary apparatus over the time course of the experiment, infecting 27.69 ± 6.09(SE)% of cells by 12 days PBM (figure 5.13). Infection of the thoracic muscle was relatively rare. In this tissue, +Seg-5 was expressed in up to 3.07% (10/326) of thoracic muscle cells in 9.26% (5/54) of *C. sonorensis* sampled (figures 5.13 and 5.14D).

Neural tissues were infected as early as 7 days PBM, with the exception of a single individual at 6 days PBM (figures 5.11 and 5.14B to C), following viral replication in infected non-midgut tissues. Indeed, +Seg-5 was expressed in the optic lobe (including the central brain) of 16.67% (1/6) of *C. sonorensis* at 6 days PBM, increasing to 50.00% (9/18) by 12 days

PBM. Infection of the thoracic ganglia arose in 5.26% (1/19) of *C. sonorensis* at 7 days and 38.89% (7/18) by 12 days PBM (figures 5.13 and 5.14G). The area of the salivary glands expressing +Seg-5 remained below 0.2% in all *Culicoides* (figure 5.13).

Figure 5.13

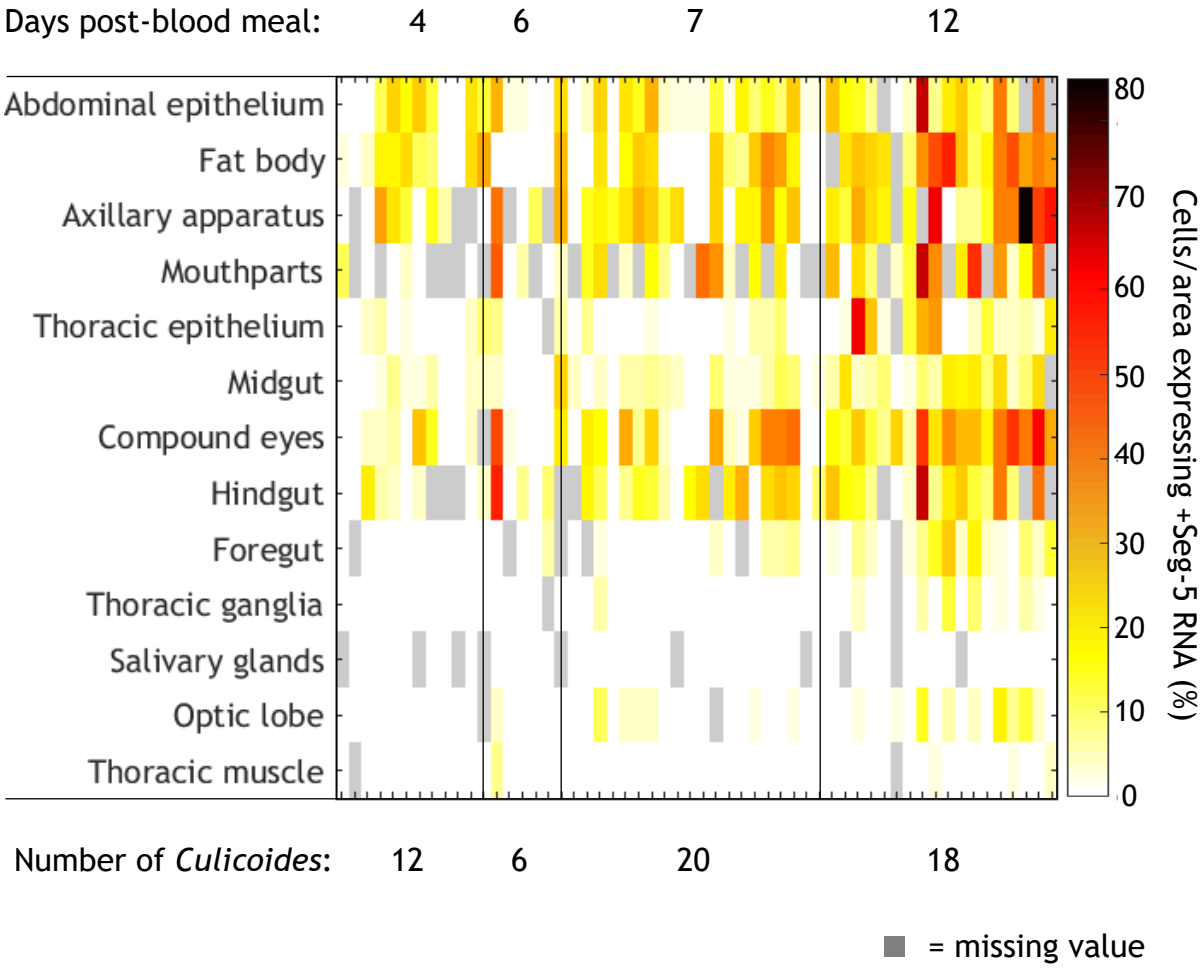

Figure 5.13: Progression of BTV-1 infection in *Culicoides*.

Heatmap representing cells expressing BTV + Seg-5 RNA, which were calculated as a percentage of the number of cells sampled for each tissue in individual *Culicoides* at 4 days (n = 12), 6 days (n = 6), 7 days (n = 20) and 12 days (n = 18) after feeding on blood supplemented with 7.0 $\log_{10}$ $TCID_{50}$/ml of BTV-1. Values are stated as a percentage area for the salivary glands, optic lobe and thoracic ganglia. Each column represents an individual *Culicoides*. Missing values are shown by the grey shaded areas.

Figure 5.14: BTV-1 replication in tissues of *Culicoides*.

(**A**) Reconstructed composite images of *Culicoides* are shown to cover the whole body. Representative images were captured at 4, 7 and 12 days post-blood meal (PBM) containing 7.0 $\log_{10}$ $TCID_{50}$/ml BTV-1 or 7 days after feeding on mock infected blood, which was supplemented with DMEM (Mock). BTV +Seg-5 RNA (red), BTV protein (VP, green) and nuclei (blue) are shown (scale = 75 µm).

Figure 5.14

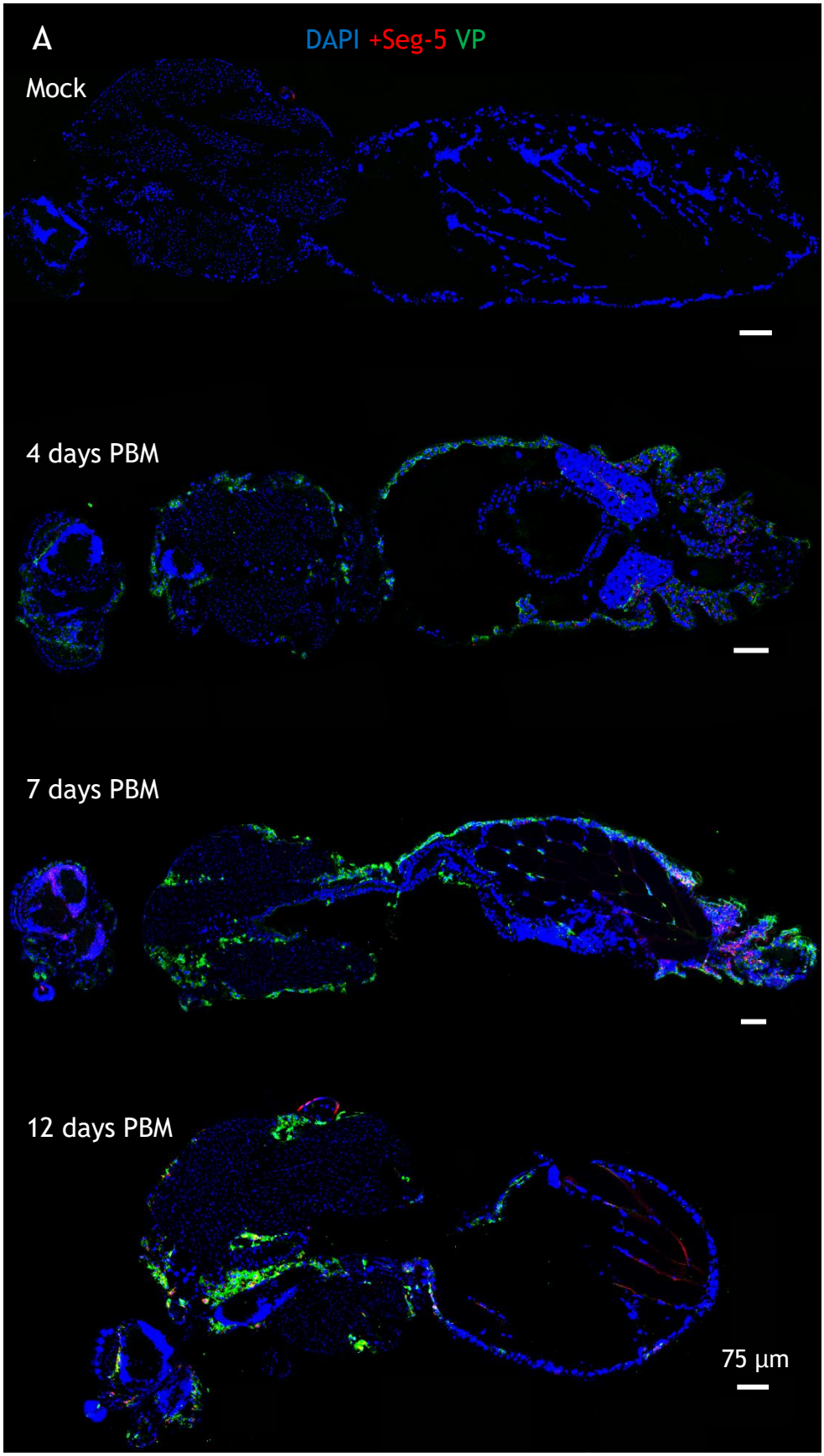

Figure 5.14: BTV-1 replication in tissues of *Culicoides*.

Representative images of confocal microscopy of *Culicoides*, showing BTV-1 +Seg-5 RNA (red) and protein (VP, green) at 7 and 12 days post-blood meal (d PBM), supplemented as described in figure 5.14A. (**B**) The optic lobe (white arrow), compound eyes (orange arrow), fat body (purple arrow), (**C**) thoracic ganglia (arrow), (**D**) thoracic muscle and epithelium (arrow), (**E**) foregut (arrow), (**F**) midgut, abdominal epithelium (arrow), (**G**) hindgut (white arrow) and oocytes (square). Nuclei are shown (blue) (scale = 40 µm).

Figure 5.14

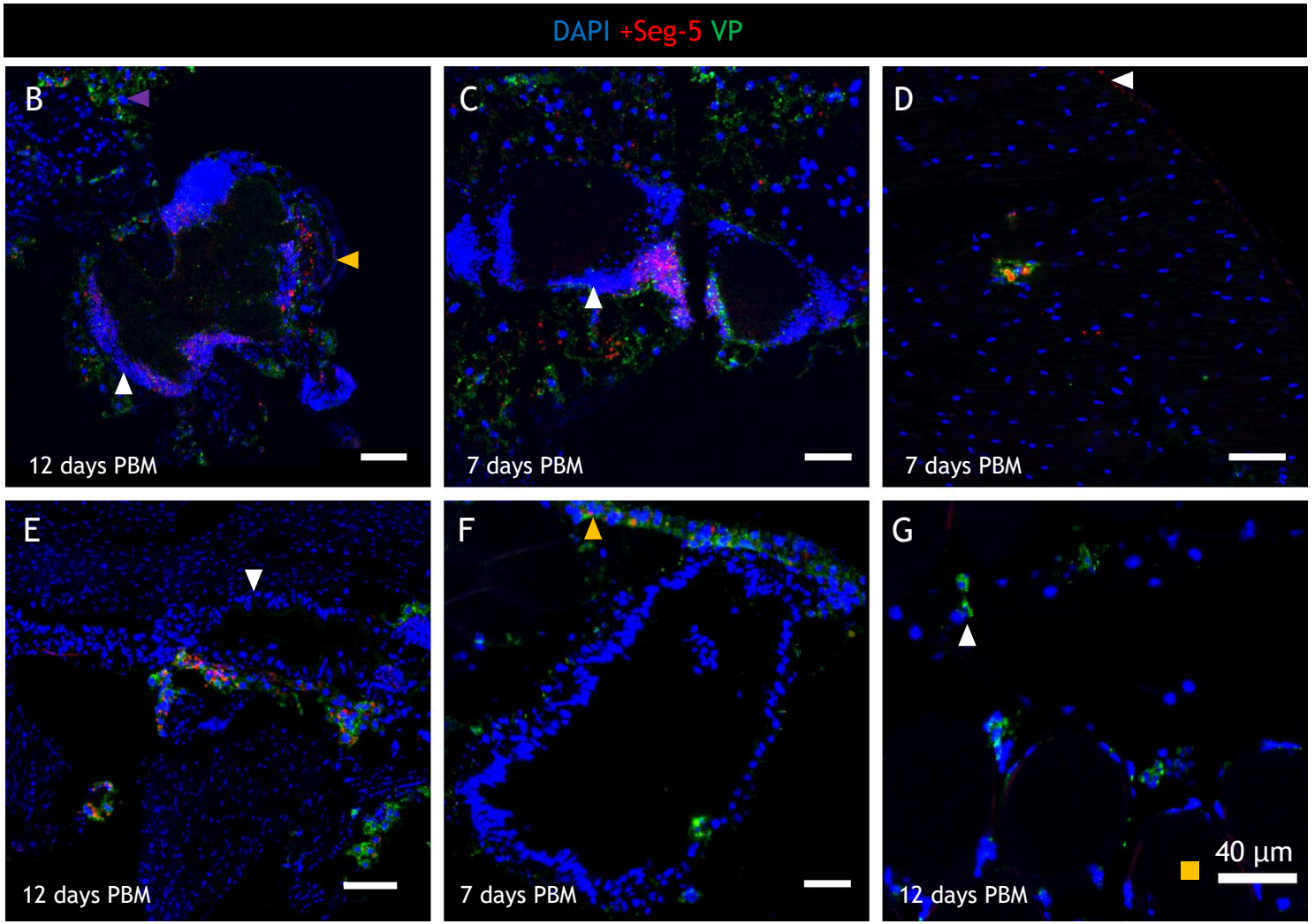
DAPI +Seg-5 VP
B
12 days PBM
C
7 days PBM
D
7 days PBM
E
12 days PBM
F
7 days PBM
G
12 days PBM
40 µm

5.2.12 BTV-1 and BTV-11 are undetectable in the salivary glands and oocytes of infected *Culicoides*

Many arboviruses replicate in the reproductive organs (ovaries and egg chambers) (Wang et al., 2010, Chandler et al., 1998) and salivary glands of a transmissible insect vector prior to vertical transmission to progeny or direct transmission to a host, respectively (Drolet et al., 2005, Salazar et al., 2007, Romoser et al., 1992). Previous studies described the detection of BTV-1 (Fu, 1995) and BTV-8 in the salivary glands of IT inoculated *Culicoides* by TEM (Bowne and Jones, 1966). The previous section (see sections 5.2.4 and 5.2.11) failed to detect +Seg-5 RNA, indicating lack of Seg-5 RNA in the salivary glands of *Culicoides* infected with BTV-1.

To further assess whether BTV-1 and BTV-11 can infect the salivary glands of *Culicoides*, +Seg-5 RNA and VP were examined in the salivary gland sections of *Culicoides* with a disseminated BTV infection (BTV-1: n = 46, BTV-11: n = 36) (figure 5.15A to C). Both viral strains failed to replicate to detectable levels of either VP or +Seg-5 in the salivary glands of *Culicoides* (values not shown). Similarly, VP and +Seg-5 of BTV-1 and BTV-11 were undetectable in the nurse cells and oocytes of all *Culicoides* at the time points sampled (figure 5.16) (values not shown) (see table 5.3 for sample sizes).

Figure 5.15: BTV-1 and BTV-11 are undetectable in the salivary glands of *Culicoides*.

(**A**) Representative images of a section of the anterior thorax and head of *Culicoides* with a disseminated infection at 6 or 7 days (d PBM) after feeding on blood supplemented with 7.0 $\log_{10}$ $TCID_{50}$/ml of BTV-11 or BTV-1. Arrows indicate the location of the salivary glands (sg). BTV protein (VP) (green), +Seg-5 RNA (red) and nuclei (blue) are shown (scale = 40 µm). (**B**) Light micrographs of a section of anterior thorax and head (upper panel) and whole salivary glands (lower panel) of an uninfected *Culicoides*. The salivary glands are outlined in red in the upper panel (scale = 40 µm).

Figure 5.15

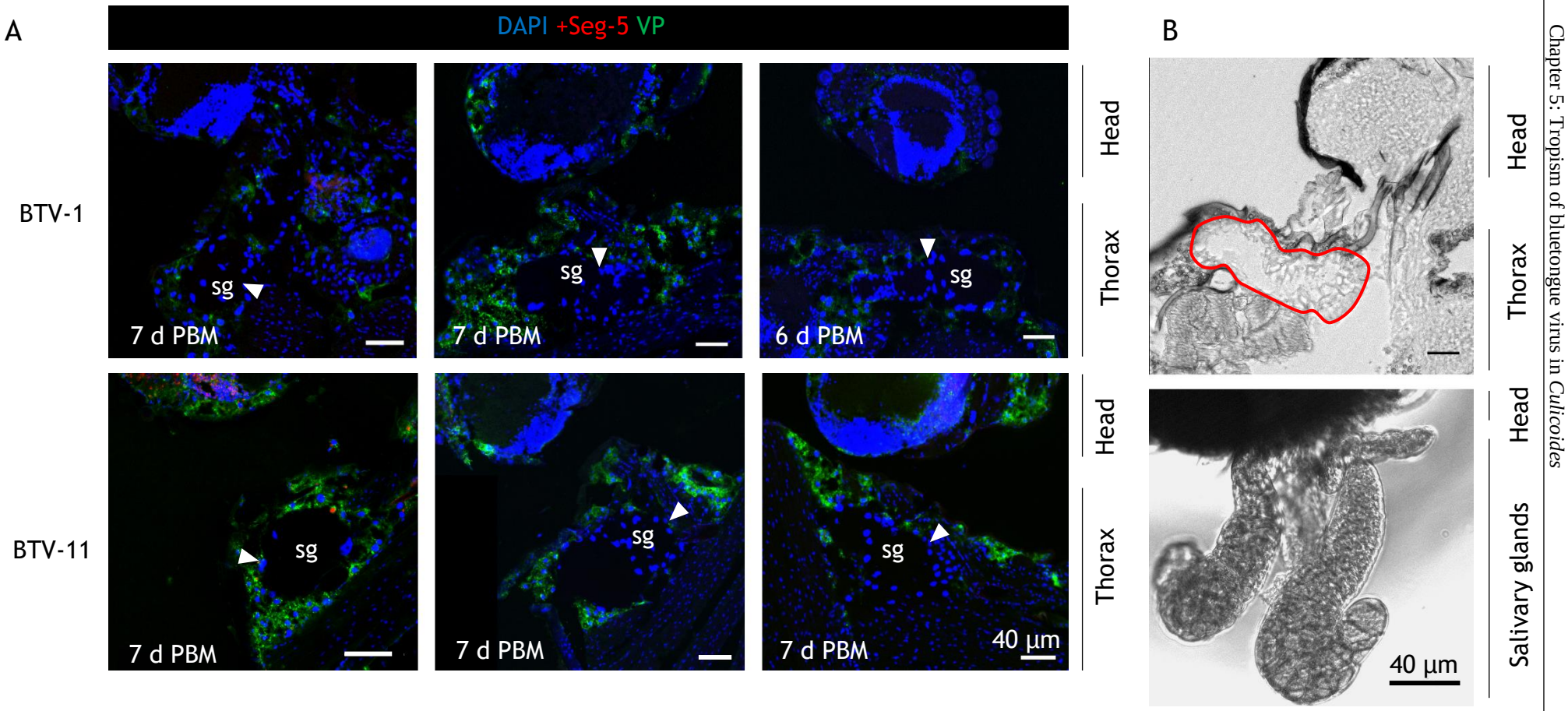
A
DAPI +Seg-5 VP
BTV-1
BTV-11
sg
7 d PBM
6 d PBM
40 µm
Head
Thorax
B
Head
Thorax
Head
Salivary glands
40 µm

Figure 5.16

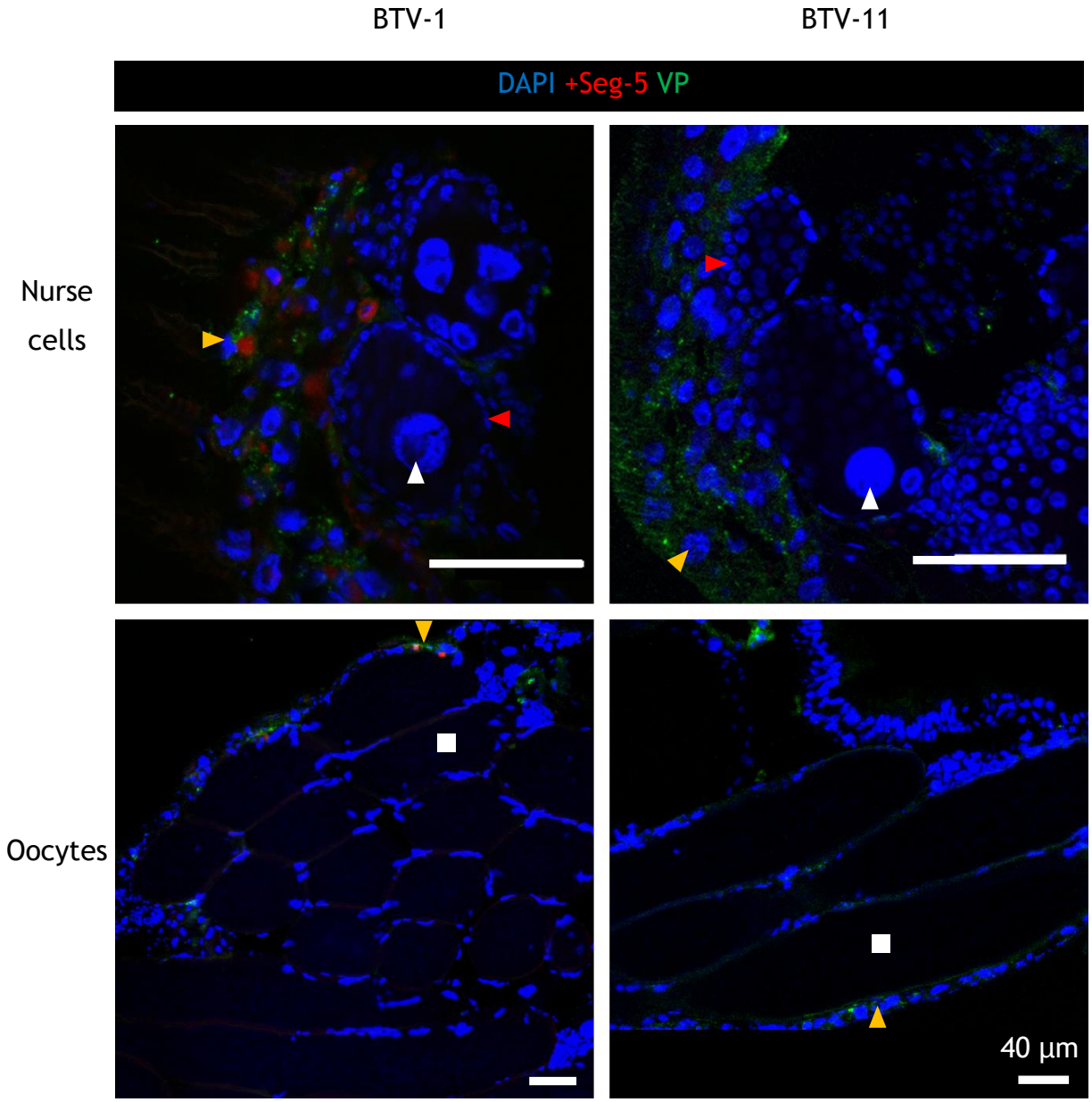

Figure 5.16: BTV-1 and BTV-11 are undetectable in the egg chambers of *Culicoides*. Representative images of abdominal sections of *Culicoides* with a disseminated infection showing the nurse cells (upper panel) and oocytes (lower panel) at 12 and 6 days after feeding on blood supplemented with 7.0 $\log_{10}$ $TCID_{50}$/ml of BTV-11 or BTV-1, respectively. The location of nurse cell nuclei (white arrows), follicular cells (red arrows), oocytes (squares) and the abdominal epithelium (orange arrow) are indicated. BTV protein (VP, green), +Seg-5 RNA (red) and nuclei (blue) are shown (scale = 40 µm).

Whilst no BTV was detected in the salivary glands, labelling was evident in the mouthparts. BTV protein (VP) and +Seg-5 RNA were observed in cells of the labium (the inner mouthparts) and mandibles (involved in mastication of host tissue) (figure 5.17A) between 4 and 12 days PBM.

Between 71.42% to 100% of *Culicoides* with a disseminated BTV-1 infection expressed VP or +Seg-5 in ≥1% of cells of the mouthparts. These individuals were considered to have infected mouthparts. BTV-11 infected the mouthparts of 66.67% to 100% of infected *Culicoides* at time points examined (figure 5.17B). There was no difference in the percentage of cells infected by BTV-1 or BTV-11 in the mouthparts (figure 5.17B; 4 days PBM: $W = 68.0$, $p = 0.325$; 6 days PBM: $t_7 = 0.70$, $p = 0.506$; 7 days PBM: $t_{14} = 2.05$, $p = 0.06$; 12 days PBM: $t_3 = 1.47$, $p = 0.238$).

Infection levels in the mouthparts of infected insects were high, and increased with time. Indeed, up to 38.50±4.99(SE)% (BTV-1) and 28.34±5.98% (BTV-11) of cells expressed VP in the mouthparts at 12 days PBM, which was the latest time point analysed (figure 5.17C).

Figure 5.17: BTV-1 and BTV-11 replicate in the mouthparts of *Culicoides*.

(**A**) Representative images of a section of the head and anterior thorax of *Culicoides* 7 and 6 days after feeding on blood containing 7.0 $\log_{10}$ $TCID_{50}$/ml of BTV-1 or BTV-11, respectively. The proboscis is outlined and shown also in the right inset of each image. White arrows indicate infection of the labium. The 'food channel' is shown by the purple arrow and labrum by the red arrow. BTV protein (VP, green), +Seg-5 RNA (red) and nuclei (blue) are shown (scale = 40 μm).

(**B**) The percentage of *Culicoides* with infected mouthparts (expressing VP or +Seg-5 in ≥1% of cells) were calculated 4 days (BTV-1: n = 6, BTV-11: n = 12), 6 days (BTV-1: n = 5, BTV-11: n = 11), 7 days (BTV-1: n = 12, BTV-11: n = 6) and 12 days (BTV-1: n = 14, BTV-11: n = 4) post-feeding on blood supplemented with BTV-1 or BTV-11 as described in figure 5.16A. Only individuals with a disseminated BTV infection were analysed. Bars show the 95% confidence interval.

(**C**) The percentage of mouthpart cells expressing viral protein (VP) was calculated at times analysed for each infected *Culicoides* (shown in figure 5.16B). Bars show the standard error of the mean.

Figure 5.17

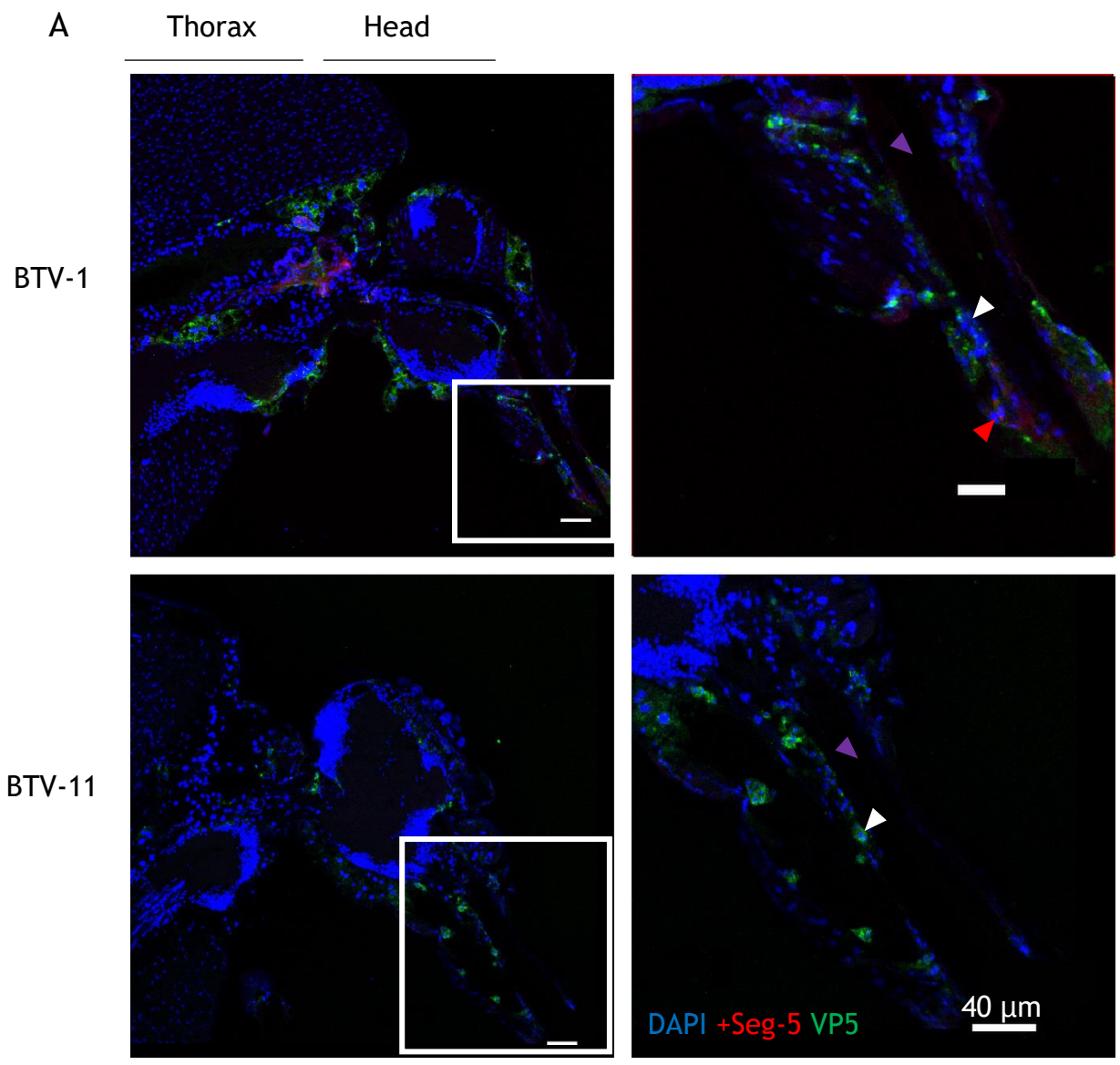
A
Thorax
Head
BTV-1
BTV-11
DAPI +Seg-5 VP5
40 µm
B
BTV-1
BTV-11
Culicoides with infected mouthparts (%)
100
80
60
40
20
0
0
4
6
7
12
Days post-blood meal
C
BTV-1
BTV-11
Mouthpart cells expressing VP (%)
50
40
30
20
10
0
0
4
6
7
12

5.3 Discussion

A tissue-level understanding of the processes arising during replication of an arbovirus within an arthropod vector is required to better understand vector competence and inform models that help predict the transmission and incidence of vector-borne viral diseases. Studies in this Chapter used powerful imaging techniques in BTV-infected *Culicoides* in order to demonstrate temporal changes in the infection and replication of two distinct BTV strains in tissues of an arthropod vector. The overall course of viral infection and spread within the insect vector was similar to previously observed, including similar target tissues (Fu, 1995, Fu et al., 1999), following viral dose and strain-dependent infection of midgut cells (as previously demonstrated in mosquitoes) (Smith et al., 2008, Kenney et al., 2012, Veronesi et al., 2008). However, a key difference in the tropism of BTV in *C. sonorensis*, compared with mosquito-borne arboviruses, was that virus could not be detected in the salivary glands. Data in this chapter present convincing evidence for the existence of an alternative mechanism of BTV transmission by means of the mouthparts. This is a new paradigm for arbovirus transmission by an insect vector.

A localised infection of the midgut in *Culicoides* inevitably progresses to dissemination in various tissues, contrary to previous suggestions (Jennings and Mellor, 1987). Indeed, 66.7% and 12.5% of *Culicoides* sampled showed a localised BTV-1 or BTV-11 midgut infection respectively at 4 days PBM, but this number declined to negligible levels by the latest time point analysed. The theory that arboviruses replicate to a threshold titre in midgut cells prior to disseminating (Girard et al., 2004) appears unlikely to be true of BTV-1 in *C. sonorensis*, as the number of infected midgut cells increased with time and did not reflect the dissemination status of infection.

BTV infected the foregut (which included the proventriculus), compound eyes, thoracic ganglia, optic lobe, fat body and epithelial cells following dissemination, also consistent with previous studies (Fu, 1995, Fu et al., 1999). BTV was also detected in the hindgut, as shown previously for Venezuelan equine encephalitis (Smith et al., 2008) and DENV-2 viruses (Salazar et al., 2007). The variation in BTV-1 titre in individual *C. sonorensis* shown before (Jennings and Mellor, 1987, Fu et al., 1999) could reflect differences in the timing of infection of tissues, as demonstrated here. BTV replicated in the axillary apparatus, abdominal epithelium, fat body, thoracic epithelium and compound eyes at 4 days PBM, the earliest time point examined, consistent with previous studies (Fu, 1995, Fu et al., 1999).

Infection of the majority of the fat body indicates, that adipocytes, which are rounded cells present in the fat body (Cohen, 2009) are susceptible to BTV replication, consistent with observations described in this thesis (see Chapter 4, section 4.3.1). Further studies are needed to confirm exactly which cell types are most susceptible to BTV infection in different tissues.

The number of cells expressing BTV ssRNA increased over time in susceptible tissues, consistent with previous studies showing an increase in infectious virus (Foster and Jones, 1979) and viral antigen (Mullens et al., 1995) with time in whole *C. sonorensis*. The fat body was infected in most *Culicoides* tested, which may reflect its direct contact with the haemolymph (Cohen, 2009). RVFV (Romoser et al., 1992) and SINV (Bowers et al., 2003) infect skeletal muscles, however only ≤3.07% of thoracic muscle cells were infected with BTV in 9.26% of the infected *Culicoides* analysed. This result is compatible with previous studies of *C. sonorensis*, which failed to detect BTV-1 in the thoracic muscle by IHC (Fu, 1995, Fu et al., 1999). Moreover, limited infection of the thoracic muscle is consistent with studies of EEEV in *Culiseta melanura* (Weaver et al., 1990) and DENV-2 in *Ae. aegypti* (Salazar et al., 2007). The thoracic muscles are involved in flight, which imposes a high metabolic cost (Davis and Fraenkel, 1940). Viral replication in flight muscle cells may inhibit flight activity (and consequently reduce transmission efficiency), as shown during EEEV infection of *Cx. tarsalis* (Lee et al., 2000), perhaps by inducing energetically costly antiviral immune pathways (Schmid-Hempel, 2005) or apoptosis (Vaidyanathan and Scott, 2006, Girard et al., 2007, Girard et al., 2005). Such mechanisms may account for increased mortality 12 days after ingestion of BTV-11, as suggested previously (Romoser et al., 1992). Low level BTV replication in flight muscle cells could represent a fitness trade-off, however further empirical evidence, beyond studies in this thesis, is needed to support this hypothesis.

BTV-11 infected a greater number of *C. sonorensis* than BTV-1, but maintained a similar disseminated infection rate as a percentage of those individuals infected. The increase in infection rate over time, noted for both viruses, could reflect limitations of the methods used for detecting low levels of infection. In line with experiments using different viral doses, the ability of BTV to infect the posterior midgut could underlie the different infection rates noted between BTV isolates. Indeed, rates of replication in *Culicoides* are comparable between multiple orbiviruses (Carpenter et al., 2011) and no differences in the identity of the tissues infected were noted between BTV strains or doses tested here. Midgut infection, involved as few as four cells, depending on BTV dose and strain. Similarly low numbers of initially infected midgut cells were shown for VEEV replicons in *Cx. taeniopus* (Forrester et al., 2010, Kenney et al., 2012). A disseminated BTV infection in the field could arise from

infection of a comparable number of midgut cells as estimated here, as the viral doses tested reflected titres detected during peak viraemia in sheep (Hamblin et al., 1998). Given the small number of susceptible cells, midgut infection may impose a substantial, dose and strain-dependent bottleneck on BTV, similarly to VEEV (Forrester et al., 2010). Further examination of midgut infection with a wider range of BTV doses and strains is needed to determine the minimum viral dose required for infection.

Contrary to studies showing DENV-2 and RVFV infection in multiple, irregularly distributed *Ae. aegypti* (Salazar et al., 2007) and *Cx. pipiens* (Romoser et al., 1992) midgut cells, BTV infected cells were clustered in a single region of the posterior midgut. This infected region was larger for BTV-11, which is transmitted by *C. sonorensis* in the field (Schmidtmann et al., 2011), than the highly cell culture adapted, South African strain of BTV-1. Different strains of BTV circulate in regions inhabited by different populations of *Culicoides*. Hence, inherent differences could exist in the susceptibility of midgut cells of specific vector species, to infection with different BTV strains, and may have an important effect on transmission of different BTV strains/serotypes in different geographic regions. Proving such strain-dependent differences in midgut infection, would involve testing multiple BTV strains with comparable passage histories and, if possible, field caught insects.

The insect midgut is composed of several heterologous cell types (Filimonova, 2005, Billingsley and Lehane, 1996b, Zieler et al., 2000). A small/restricted population of cells may be susceptible to BTV-1 infection, whereas the BTV-11 tested may be able to infect additional cell types. However, a temporal increase in the number of infected midgut cells was demonstrated here and may negate this hypothesis. It is perhaps more likely that the mechanisms and/or cell types used by different BTVs for entry into midgut cells may differ. Indeed, both clathrin-mediated endocytosis (CME) (Forzan et al., 2007) and macropinocytosis pathways (Gold et al., 2010, Stevens, 2016) have been implicated in BTV entry. Further studies are needed to investigate the entry mechanisms of multiple BTV strains.

Immune pathways, including the Toll pathway (reviewed in Chapter 1, section 1.3.3) are elicited by commensal gut bacteria and have been shown to inhibit species of *Plasmodium* in *A. gambiae* (Dong et al., 2006, Dong et al., 2009) and DENV replication in *Ae. aegypti* (Xi et al., 2008, Ramirez and Dimopoulos, 2010). Bacteria may also act directly, for instance by generating ROS (Cirimotich et al., 2011a), promoting viral infectivity (Carissimo et al., 2015), or inhibiting virion binding to midgut cells (Cirimotich et al., 2011b). Antibiotic

treatment eliminated LB cultural bacteria from *Culicoides* midguts, relative to controls which were maintained on sucrose in the absence of antibiotic. This removal of endogenous midgut bacteria did not alter infection rate with BTV-1, contrary to findings of DENV-2 in *Ae. aegypti* (Xi et al., 2008), indicating that the presence of commensal midgut bacteria (which are eliminated by antibiotic treatment) are not associated with an increased or reduced susceptibility of *Culicoides* to BTV infection. Although KC cells were shown to possess an antiviral RNAi response (Schnettler et al., 2013), the Toll and IMD pathways have yet to be identified in *Culicoides* and studies of the antiviral responses in *Culicoides* are still in their infancy, partly due to lack of a published genome. An improved understanding of the anti-BTV immune response in this species is needed in order to fully understand vector competence and the role of gut bacteria.

The neural optic lobe (which included the central brain) and thoracic ganglia became infected following dissemination, at 6 to 7 days PBM, which was later than previously estimated by IHC (Fu et al., 1999). The *Culicoides* nervous system is therefore unlikely to provide the route of BTV dissemination from the midgut to the other tissues, as was previously shown for WNV in *Cx. quinquefasciatus* (Girard et al., 2004) and Whataroa virus in *Ae. australis* (Miles et al., 1973). Infection of the neural tissues at 6 to 7 days PBM corresponded to the time of expected BTV transmission (Fu et al., 1999). Behavioural changes in mosquitoes, that promote virus transmission, are associated with arbovirus infection of neural tissues (Grimstad et al., 1980, Platt et al., 1997a, Lima-Camara et al., 2011b). Although BTV infection of the compound eyes of field-caught *C. sonorensis* was suggested to induce light adversity (McDermott et al., 2015), a direct association between BTV infection and behavioural traits has yet to be proven.

Certain arboviruses can persist in the vector population by a transovarial transmission route (Rosen et al., 1983, Watts et al., 1973, Rosen et al., 1978) (reviewed in Chapter 1, section 1.3.1). However, an absence of viral RNA or protein in the oocytes and nurse cells compliments previous studies indicating that transovarial transmission of BTV is unlikely (Fu et al., 1999, Nunamaker et al., 1990, Jones and Foster, 1971), despite previous detection of BTV RNA in field-caught larvae (White et al., 2005). It was previously speculated that transmission of BTV virions in the saliva is the sole means of BTV passage to a new host (Mellor, 2000, Muller, 1987). To access the saliva, mosquito-borne arboviruses replicate in the insect salivary glands (Salazar et al., 2007, Drolet et al., 2005, Romoser et al., 1992). However, an absence of viral ssRNA or protein in the salivary glands of *Culicoides*, indicated that this may not be true for the BTV strains tested, despite previous observation

of BTV-1 SA (which was used in studies in this thesis) and BTV-8 particles in the salivary glands by early IHC and TEM studies (Bowne and Jones, 1966, Fu, 1995). Such differences could reflect limitations associated with previous methodologies, which tested IT inoculated *Culicoides* (Bowne and Jones, 1966, Fu, 1995) and only presented a single image, which failed to correctly identify the salivary glands (Fu, 1995). Further evidence for the role of the salivary glands in transmission of BTV by *Culicoides* is needed.

Viruses can be mechanically transmitted by the cuticular lining of the insect mouthparts (Buxton et al., 1985), indicating that transfer of virus particles from the mouthparts is possible. BTV-1 and BTV-11 strains tested were detected in the mouthparts of *Culicoides* at 4 days PBM, which is the expected time of BTV-1 transmission at 25ºC by *C. sonorensis* (Carpenter et al., 2011). Both BTV strains infected approximately 30% to 40% of cells in the mouthparts by 12 days PBM, including cells lining the labium, which indents into the skin of a host during blood feeding (Sutcliffe and Deepan, 1988). Other infected areas included the mandibles, which are involved in mastication of host tissue (Sutcliffe and Deepan, 1988). A high prevalence of mouthpart infection in *Culicoides* noted here with a disseminated infection, is consistent with the very high efficiency of BTV transmission by these (full disseminated) insects, and an absence of post-dissemination mechanisms inhibiting BTV oral transmission (Fu et al., 1999). Since the salivary duct is separated from the labium (Sutcliffe and Deepan, 1988), virus particles may be directly transferred directly, without contacting the saliva. Further studies are needed in order to determine how virions enter the host during blood feeding. It is not known how widespread transmission of virus particles from the mouthparts is, or whether the process is characteristic in the transmission of other *Culicoides*-borne viruses (including non-orbiviruses) or specific to the transmission of BTV by *Culicoides* species. Despite these caveats, the studies described in this chapter have revealed a new paradigm and a novel route of transmission for arboviruses. By quantifying the extent of viral infection in different tissues, we have unveiled a mechanism whereby an arbovirus can be transmitted via an insect bite without needing to first replicate within the salivary glands.

Chapter 6

Conclusions and future work

Arboviruses are taxonomically diverse (Theiler and Downes, 1973) and many arboviruses are of international socioeconomic importance. It is imperative to understand the biology of these viruses in order to develop novel and effective strategies for controlling the spread of epizootic vector-borne diseases, such as bluetongue. An aspect of their lifecycle that distinguishes arboviruses from other viral groups is the requirement for replication in an arthropod vector, specifically, a mosquito, tick, sandfly, blackfly or midge. Most studies of the ability of an insect to become infected and transmit an arbovirus, which is described as an insect's 'vector competence' (Gerry et al., 2001, Carpenter et al., 2015), consider only population level infection rates (Bennett et al., 2002, Venter et al., 1998, Paweska et al., 2002b). Such approaches do not fully explain what causes the observed variations in the transmission potential of individual insects.

Infection with an arbovirus and dissemination of infecting viral particles through susceptible arthropod tissues is complex and, at present, is poorly understood at the level of the individual insect for most vector groups. Much of our current understanding of the processes involved is based on studies of mosquitoes under constant laboratory conditions (Salazar et al., 2007, Miller et al., 1989, Faran et al., 1988) and overlook realistic changes in environmental conditions and variation between viral strains that can have an impact on vector-virus interactions. The work described in this thesis is intended to explore the replication of an arbovirus in its arthropod vector. To achieve this, the interaction of BTV with the North American vector, *C. sonorensis,* was studied as a model virus-vector system. Figure 6.1 illustrates the proposed model, based on data generated in this thesis, by which BTV infects *Culicoides*.

Figure 6.1

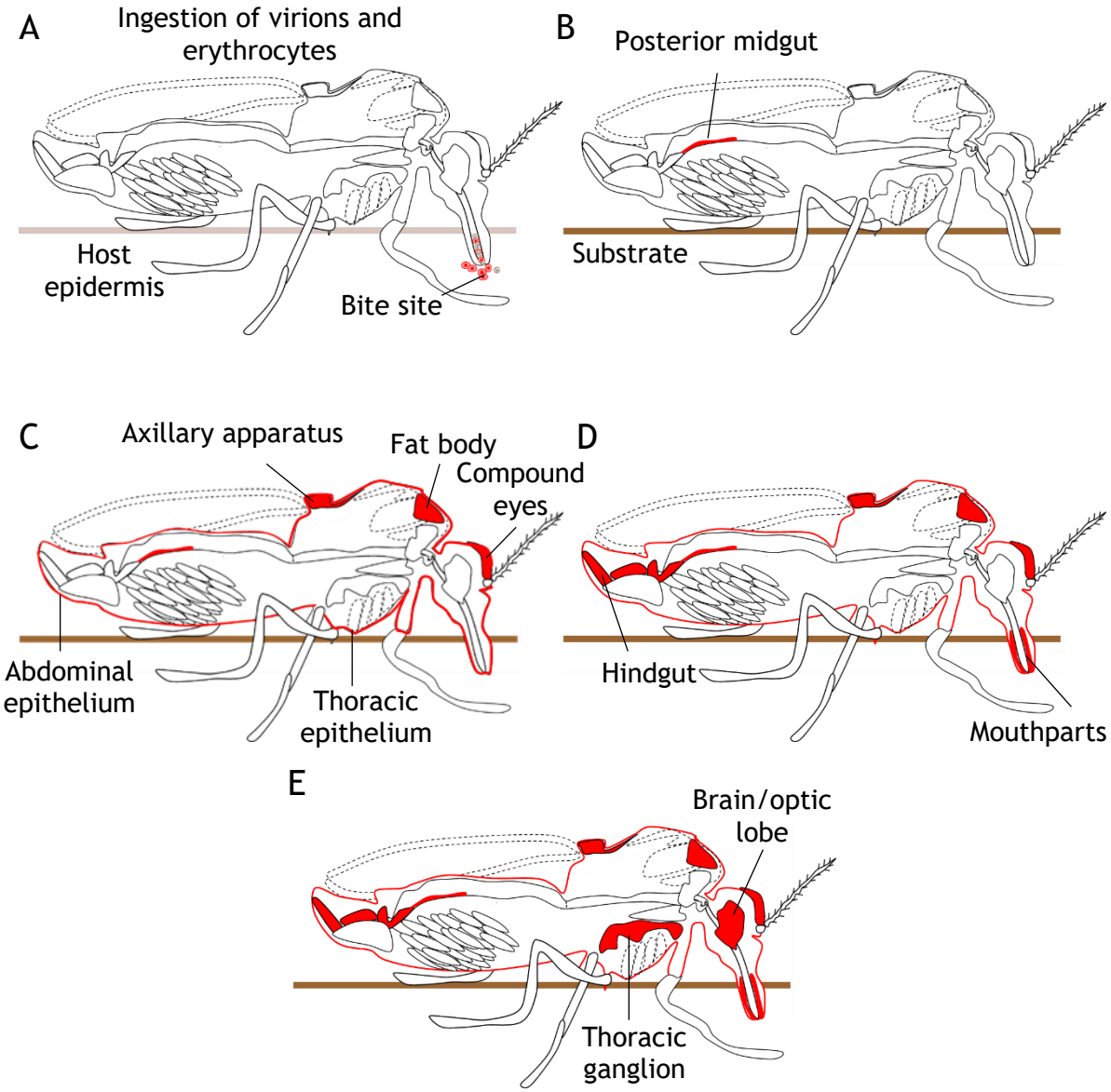

Figure 6.1: Schematic model of BTV infection of *Culicoides*.

(**A**) Virus particles are ingested during blood feeding on a viraemic host. (**B**) BTV particles infect and replicate in a region of posterior midgut cells of a susceptible vector. The number of cells infected is viral strain and dose-dependent. (**C**) Virus particles randomly infect cells of the abdominal and thoracic epithelium, fat body, axillary apparatus and compound eyes. (**D**) The foregut and limited thoracic muscle cells become infected in a few individuals (not shown on diagram). BTV replicates in the hindgut and mouthparts, at which stage, virions can be transmitted directly from the mouthparts to a host during biting. (**E**) BTV infects the neural tissues, including the brain. The salivary glands and oocytes remain uninfected. Infected tissues are highlighted (red).

Reporter viruses can provide a direct means of observing viral localisation and replication in insect tissues, reducing both time and costs, as previously shown (Shaw et al., 2012). Given these advantages, a genetically engineered, recombinant BTV-1, which expressed eGFP as a fusion with the *C*-terminus of NS1, was designed and rescued in the studies described in Chapter 3. Although this 'reporter' BTV enabled observation of NS1-eGFP protein in KC cells, growth was reduced compared with the parental BTV-1. Furthermore, non-fluorescent variants were isolated even after a small number of passages in KC cells, which were subsequently found to contain deletions in the eGFP coding sequence. Optimising a reporter BTV to enhance the stability of the reporter gene would involve identifying an insertion strategy or site in a genome segment that would maintain 'wild-type' protein function and expression, whilst being tolerated during the virus lifecycle. The development of an alternative and stable reporter virus was considered to be beyond the scope of this project.

As an alternative for the detection of BTV replication, BTV Seg-5 +RNA and viral proteins were fluorescently co-labelled in sections of whole-*Culicoides*. The application of immunolabelling and FISH (to detect viral protein and nucleic acid, respectively) supports the use of 'unmodified' field strains of BTV. The use of whole-insect sections minimises the issue of cross-contamination, associated with qPCR analysis of excised tissues, as well as providing a direct comparison of different tissues within the same insect, thereby eliminating any subjectivity as to which tissues could potentially be infected by BTV.

The localisation of a mammalian cell adapted BTV-1 isolate (ICTVdb isolate accession number [RSArrrr/01]), which forms the basis of much of our understanding of BTV biology, was compared to that of a field strain of BTV-11 (ICTVdb isolate accession number [USA2005/01]) that was isolated from an area known to support populations of *C. sonorensis* (Schmidtmann et al., 2011).

In the published literature, virus localisation in insects is often detected by confocal imaging, and traditionally quantitative approaches, such as qPCR (Salazar et al., 2007) or virus titration (Dong et al., 2016), are used to measure viral load. However, these methods do not allow viral quantity to be directly correlated with localisation, as separate samples are processed for the different methodologies.

Image-based quantification has revolutionised studies of pathogen invasion and replication within a single host organism (Amino et al., 2006, Palha et al., 2013). Current image analysis software is costly, optimised for evaluation of cultured cells, or low-throughput tasks. High-throughput, objective algorithms were therefore developed in Chapter 4 for counting cells in confocal image datasets from tissue samples and are 'termed' the 'Automated Infected Cell Counter' (AICC). The AICC can be used to rapidly quantify cells expressing an intracellular fluorescence label in a variety of host organisms, and could have applications in various fields of histopathology, including diagnostics (Han et al., 2012). In this thesis, BTV infected cells were counted using the AICC, giving an accuracy comparable to manual counting in the selected *Culicoides* tissues.

The BTV-1 infection rate in adult *Culicoides* (which depends on the dose of virus ingested (Mertens et al., 1996b)) was lower than that of BTV-11. It was therefore hypothesised in Chapter 5 that the characteristics of midgut infection by BTV-11 would be inherently different from those of BTV-1. Indeed previous studies of cell entry suggest that different BTV strains / serotypes, with different passage histories, can use different cell attachment and entry mechanisms (Stevens, 2016, Forzan et al., 2007, Gold et al., 2010). Chapter 5 demonstrated that BTV-1 and BTV-11 both infect the posterior midgut, which has previously been identified as a site of BTV-1 entry (Fu et al., 1999). The studies described in this thesis show that BTV-1 infected fewer posterior midgut cells than BTV-11, suggesting that variation could exist in the ability of different viral strains, or viruses with different passage histories, to infect the midgut. The genetic determinants for the enhanced growth phenotype of BTV-11 could be identified by generating chimeric viruses from the BTV-1 and BTV-11 strains, co-infecting *Culicoides*, then recovering viral populations from the peripheral tissues, enabling abundant viral genotypes to be identified.

An obvious increase in the number of infected midgut cells was observed at higher BTV-1 doses and may be attributed to a dose-dependent entry mechanism. A greater abundance of infectious BTV particles at higher doses would increase the probability of a BTV particle binding to and entering a midgut cell at higher doses. However, further studies would be needed to test a wider range of BTV doses and confirm the existence of such a mechanism. The finding that BTV dose and strain can alter infection efficiency of midgut cells and infection rates in *C. sonorensis*, illustrates that multiple factors, associated with the initial virus attachment and entry steps, are fundamentally important in determining the susceptibility of *Culicoides* to BTV infection in the field.

Prior to the studies conducted in this thesis, two permanent states of BTV infection were thought to occur in *Culicoides*, a non-disseminated infection, where virus remains restricted to the midgut cells (Jennings and Mellor, 1987, Fu et al., 1999), or a disseminated infection, where virus particles replicate to a threshold titre in the midgut (Hardy et al., 1983, Kramer et al., 1981), then infect and replicate in non-midgut tissues. Studies in Chapter 5 indicate that, contrary to this theory, a non-disseminated infection represents an early, temporary phase during infection, as BTV-1 and 11 were both observed in non-midgut tissues in every infected *C. sonorensis* by the latest sampling point. Additionally, data showed that BTV-1 infected a comparable number of midgut cells of *C. sonorensis* prior to and shortly after dissemination and the number of infected cells increased with time. These data indicate that dissemination eventually occurs in all infected *C. sonorensis*, but at variable times after midgut infection. Given this finding, any factors that can inhibit or enhance virus attachment and entry in the midgut cells can impose important limitations, or can enhance BTV transmission by *Culicoides*.

In light of the fact that BTV replication proceeded at different rates in different individuals, it is conceivable that mortality could limit transmission by individuals with a slower replication rate. Such differences in the rates of replication likely accounted for the variation between individual *Culicoides* in BTV copy number in Chapter 5 and viral titre, noted in previous studies (Fu et al., 1999). The cause of these differences in replication rate is not known, but could reflect differences in the efficiency of the antiviral immune responses between individuals. Further work is needed to identify the genes and characterise the pathways, such as RNAi (Schnettler et al., 2013), involved in the antiviral response of *Culicoides*. Publication of the *Culicoides* genome would greatly facilitate such studies.

BTV was unable to replicate in the oocytes, or to high levels in thoracic muscle cells, indicating that different cell types exhibit differential permissibility for BTV infection and replication. The reasons for this cell or tissue type restriction upon BTV replication are not known, but could reflect the degree of contact of the tissue with the haemolymph, limitations associated with the requirements for BTV entry and replication, or the availability of different cell surface receptors, which have mostly been studied in mammalian cell culture.

A common feature of all arboviruses, including BTV (Fu, 1995, Bowne and Jones, 1966), is thought to be their ability to infect and replicate in the salivary glands of an arthropod vector (Gaidamovich et al., 1973, Mellor, 2000, Nuttall et al., 1994). However, the confocal microscopy studies described in Chapter 5 of this thesis failed to detect BTV-1 or BTV-11

RNA or protein in the salivary glands of infected *C. sonorensis*. These data provide strong evidence to indicate that BTV does not infect or replicate to detectable levels in the salivary glands of *Culicoides*. This is the first time that an arbovirus has not been shown to infect the salivary glands of a vector, and has considerable implications for our current understanding of vector-borne transmission of a pathogen by these insects. Given the significance of this finding, it is important to examine the salivary glands of infected insects using another method, such as immunolabelling of whole salivary glands.

Absence of viral replication in the salivary glands could provide numerous fitness advantages for the virus and the vector by avoiding apoptosis (Kelly et al., 2012, Girard et al., 2007, Dong et al., 2016), and thus disruption to salivary gland function (Girard et al., 2005, Kaufman et al., 2001), which have been demonstrated in mosquitoes. Since salivary molecules are known to suppress the host's immune response and promote arboviral infection of a host (Schneider and Higgs, 2008, Schneider et al., 2004, Styer et al., 2011), the lack of disruption to salivary protease production could promote viral transmission.

The finding that BTV strains tested in this thesis may not infect the salivary glands of *Culicoides*, raises the fundamentally important question of how BTV particles are transmitted to the mammalian host. This thesis proposes an alternative mechanism of transmission by which BTV particles can directly enter the host from the infected cells of an insect's mandibles or labium during probing and blood feeding. However, further proof of concept studies are needed to provide a model of this process.

It is not known how widespread transmission of arbovirus particles from the mouthparts is, or whether this process is characteristic in the transmission of other orbiviruses or specific to the transmission of BTV by *Culicoides* midges. Studies of the infection of mosquito-borne orbiviruses, such as Peruvian horse sickness virus or Yunnan virus (Attoui et al., 2009), and *Culicoides*-borne viruses, such as Schmallenberg virus (SBV), African horse sickness virus (AHSV) and Epizootic hemorrhagic disease virus (EHDV), would be useful in answering this question. Despite these cravats, based on studies presented in Chapter 5 of this thesis, the widely accepted view that transmission of an arbovirus invariably occurs by replication in the salivary glands is untrue and diversity between virus-vector systems in the means of transmission exists.

In summary, the findings described here, suggest that arbovirologists and entomologists may need to reassess the existing models of infection of arthropod vectors and subsequent virus transmission.

Appendix

A1. Conditions for real-time PCR

55°C for 30 minutes.		: Reverse transcription.
95°C for 10 minutes.		: Reverse transcriptase inactivation and *Taq* activation.
95°C for 15 seconds. 60°C for 1 minute.	40 cycles	: PCR amplification.

A2. RNA standards

Figure A.1

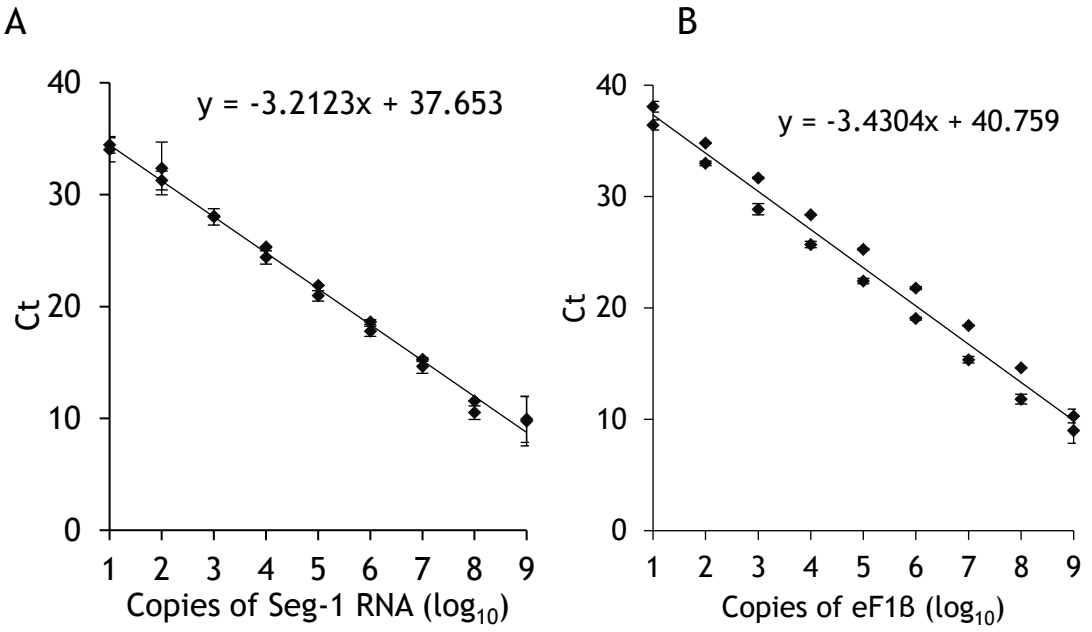

Figure A.1: RNA standards for calculating copies of Seg-1 and eF1β.

In vitro transcribed (**A**) BTV Seg-1 RNA and (**B**) *C. sonorensis* eF1β RNA were diluted from 9 $\log_{10}$ copies to 1 copy and amplified using primers listed in Chapter 2 (table 2.5, section 2.13). Amplification was performed in two independent experiments to determine the cycle threshold (Ct) of each dilution. Efficiency of amplification, given by R^2 was 99% for Seg-1 and 98% for eF1β. Bars represent the standard error of the mean of three independent replicate dilutions.

A3. MATLAB script for the 'Automated Infected Cell Counter'

The 'Automated Infected Cell Counter' scripts are detailed in the following section. Processes described in sections A.3.3 to A.3.5 are grouped into two distinct stages. Stage 1 involves the calculation of total cells in an image and stage 2, grouping of nuclei (identified in stage 1) into infected or uninfected cells (see section 4.2 of Chapter 4 for further details).

A3.1 Generation of image regions of interest (ROIs)

```
% change directory
startdr = cd;
cd('N:\\Integrative Entomology\\private\\Staff folders\\Alice\\02_Analyses\\01_Matlab\\02_Data\\2016-12-29 Time course experiment results\\BTV11 D4PF\\Stacks');
tifflist = dir('*.tif'); % load all TIFF files in directory

if isempty(tifflist),
   error('No tiffs in folder');
end; % give error if no files in directory

for tiff_id = 1: length(tifflist); % for all TIFF files
   disp(['working with file: ', char(tifflist(tiff_id).name),'.']); % display file name
   layers_struct = imfinfo(tifflist(tiff_id).name); % layer information for specified image

   for layer_id = 1: length(layers_struct); % for all layers in image tiff_id
      disp(['layer: ' num2str(layer_id)]); % display layer id
      layer = imread(tifflist(tiff_id).name, layer_id); % load in layer 'layer_id' of image 'tiff_id'
      figure, imshow(layer); % display loaded image
      pause(1) % pause for 1 second
      decision = input('Make ROI? (y/n/x)(case-sensitive)', 's'); % choose to create a ROI
      if decision == 'y'
         mask = roipoly(layer); % manually define ROI for layer 'layer_id' of image 'tiff_id'
         pause(1)  % pause for 1 second.
```

```
        roi = bsxfun(@times, layer, cast(mask, class(layer)));% apply ROI mask to image layer
        masktissue = input('what tissue is this?', 's'); % manually define tissue in ROI

        if sum(strcmp(masktissue, {'sg', 'ep(a)', 'ep(t)', 'mg', 'b', 'oo', 'fg', 'hg', 'ax', 'tg', 'ce', 'fb', 'tm', 'mp', 'crop'}) == 1);
            pause(); % pause script
            tiffname = sprintf('%02d', tiff_id); % define full name of TIFF
            fname = [('Midge_') num2str(tiffname) ('layer_') num2str(layer_id) ('tissue_') num2str(masktissue)];

            fname % debug check file name is correct
            path = sprintf(['N:\\Integrative Entomology\\private\\Staff folders\\Alice\\02_Analyses\\01_Matlab\\02_Data\\2016-12-29 Time course experiment results\\BTV11 D4PF\\ROIs\\',fname,'.tif']); % specify path for saving ROIs
            imwrite(roi, path) % save ROI to unique file name

        else display('this is not a valid selection. Valid = mg sg oo hg fg b ce ep(a) tm mp ep(t) fb tm crop ax') % display an error if incorrect tissue name defined
        end
    elseif decision == 'n' % return to beginning of loop
        continue
    else %decision == 'x' % exit loop
        break
    end
  end
end
```

A3.2 Load ROI and create variables for saving data

```
% ---------- user-modified section ----------
TIFFpath = 'N:\\Integrative Entomology\\private\\Staff folders\\Alice\\02_Analyses\\01_Matlab\\02_Data\\2016-12-29 Time course experiment results\\BTV11 D4PF\\ROIs\\b'; % specify file location

n_midges = 15; % define the number of midges in the folder
% -------------------------------------------------------------
startdr = cd; % save previous directory
cd(TIFFpath); % change directory to user specified path

tifflist = dir('*tif'); % give error if directory contains no TIFF files
if isempty(tifflist),
   error('No tiffs in folder');
end;

% Create list of sheets already in the output Excel file (cell array called 'sheets')
sheets = {};
if length(dir('pos_cells.xls')) == 1
   [status,sheets] = xlsfinfo('pos_cells.xls');
elseif length(dir('pos_cells.xls')) > 1
   error('more than one file containing string POS_CELLS.XLS');
end
row = 0; % variable for saving data
for m = 1:length(n_midges) % for each midge...
   rownum = 0; % variables for saving data
   totarea_uM = 0;
   NND_centroids = []; % create empty cells
   NND = [];
   centroid_diameters = [];

   % Initialise variables that store nuclei counts for each midge
   totnuc_allROI = 0;
   Tot_nuc = zeros(length(tifflist),1);
```

```
midgeTIFFs = dir(['Midge_*tif']);
R_areaum = [];
G_areaum = [];
pos_Rcells = [];
pos_Gcells = [];

for TIFFnum = 1:length(midgeTIFFs) % for each TIFF
  disp(['working with file: ', char(midgeTIFFs(TIFFnum).name),'.']); % display the file name
  InfRtotal = 0; % assign 0 create variable for accumulating values
  InfGtotal = 0; % need to 0 for each tiff

  tissue_roi = imread(midgeTIFFs(TIFFnum).name); % load in image
  midgeID = ['Midge_', num2str(m)]; % define an identifier for each midge
  if length(strmatch(midgeID, sheets)) > 0 % if an excel sheet already exisits…
    choice = input('Data already exist for this midge. Press a to append or any other key
to abort. Case sensitive','s'); % choose to append data to file or not
    switch choice
      case 'a'
        [num,txt,raw] = xlsread('pos_cells.xls',midgeID);
        if size(num,1) ~= size(txt,1) % give error if missing data
          error('numerical and text data lengths do not match - missing data detected');
        else
          rownum = size(num,1); % start writing in row after the last entry
        end
      otherwise
        return % terminate script if you do not wish to append data
    end
  end
```

A3.3 Stage 1. Calculate the total number of nuclei (cells)

```
B = tissue_roi(:, :, 3); % select blue colour channel of greyscale image and remove 0 pixel
values

  Blue = B; test = sum(Blue); Blue(:,test==0)=[]; test = sum(Blue,2); Blue(test==0,:)=[];
```

```
total = numel(Blue); % gives number of pixels
B4 = im2bw(Blue, graythresh(Blue(total*0.1:end))); % convert greyscale to binary image
B5 = imfill(B4,'holes'); % fill image from boarders
B6 = bwareaopen(B5, 1); %
clear B4; % clear variables that are no longer needed
clear B5;
D = bwdist(~B6); % apply inverse distance transform
D = -D;
D(~B6) = -Inf;
L = watershed(D); % apply watershed transform to segment nuclei from image
rgb_nuclei = label2rgb(L, 'jet', [.5 .5 .5]);

% obtain centre points of clustered blue pixels (nuclei) in the binarised image
centroidxy = regionprops('Table', L, 'Centroid', 'MajorAxisLength', 'MinorAxisLength');
centroidxy(1,:)=[]; % delete row with centre point of image
centroids = centroidxy.Centroid; % assign centre points to a variable
Tot_nuc = size(centroidxy,1); % create empty cell vector to store the number of nuclei
x = centroids(:,1);
y = centroids(:,2);
if ((size(x,1)) > 2)
   x_seg = centroids(:,1); % determine the coordinates of centroids for ROI
   y_seg = centroids(:,2);
   [v,c] = voronoin([x_seg(:) y_seg(:)]); % apply voronoi diagram
   xx1 = v(:,1); % determine x y from voronoi points
   yy1 = v(:,2);
   MaskV1 = voronoi2mask(x_seg(:), y_seg(:),size(Blue)); % create a voronoi diagram
```

A3.4 Stage 2. Apply a minimum pixel intensity threshold (*T*min) to the red and green channels and calculate fluorescent area

```
   Red = tissue_roi(:, :, 1); % define channels and remove 0 pixel intensity values
   R = Red; test = sum(R); R(:,test==0)=[]; test = sum(R,2); R(test==0,:)=[];
   Green = tissue_roi(:, :, 2);
  G = Green; test = sum(G); G(:,test==0)=[]; test = sum(G,2); G(test==0,:)=[];
```

```
% specify values for Tmin
R(R<60) = 0; % remove lowest 23.53% of pixel intensities from red channel.
G(G<100) = 0; % Remove lowest 39.22% of pixel intensities from green channel.

rt = table2array(regionprops('Table',R,'Area'));% obtain number of red pixels
R_areaum = sum(rt);R_areaum = R_areaum.*(1/1.76^2); % convert to µm^2
gt = table2array(regionprops('Table',G,'Area')); % obtain number of green pixels
G_areaum = sum(gt);G_areaum = G_areaum.*(1/1.76^2); % convert to µm^2
bt = table2array(regionprops('Table',B,'Area')); % obtain number of blue pixels
B_areaum = sum(bt);B_areaum = B_areaum.*(1/1.76^2); % convert to µm^2
[xG yG] = find(G); % find pixels over threshold and list coordinates
[xR yR] = find(R);

GpixN = size(xG); % determine number G pixels with intensities greater than Tmin
RpixN = size(xR); % determine number R pixels with intensities greater than Tmin.
```

A3.5 Stage 2. Assign nuclei to cells expressing red or green pixel intensities above *T*min (infected cells)

```
if ((size(x,1)) > 2)
  for i = 1:length(c) % for each polygon fill with colour
    if all(c{i}~=1) % if all values 1
      patch(v(c{i},1),v(c{i},2),i); % fill polygons
      ind = c{i}';
      %v(1,:)=[]; % remove infinity
      poly_area(i,1) = polyarea(v(ind,1),v(ind,2)); % determine area of polygons
    end
    if RpixN == 0
      InR =0;
      disp('No seg-5 positive cells');
    else
      InR = inpolygon(xR,yR,xx1(c{i}),yy1(c{i}));
      InR = sum(InR);
      if InR>0
```

```
                InR = 1; % assign value 1 to n pixels that are in polygon
            end
            InfRtotal = InfRtotal + InR; % total polygons containing pixels
        end
        InfRtotal % debug display nuclei grouped into cells with red pixel intensities >Tmin

        if GpixN == 0
            InG = 0; % no cells
            disp('No VP5/7 positive cells');
        else
            InG = inpolygon(xG,yG,xx1(c{i}),yy1(c{i}));
            InG = sum(InG);
            if InG>0
                InG = 1; % assign value 1 to n pixels that are in polygon
            end
        end
        InfGtotal = InfGtotal + InG; % total polygons containing pixels
        InfGtotal % debug display nuclei grouped into cells with green pixel intensities >Tmin
      end
    end
    % save data to excel files
    xlswrite('pos_cells.xls',[m, {tifflist(TIFFnum).name}, {size(centroidxy,1)}, {InfRtotal},
{InfGtotal},{R_areaum},{G_areaum},{B_areaum}],
[sprintf('A%d',rownum+1),':',sprintf('H%d',rownum+1)]);
    rownum = rownum+1;
    end
  end
  end
  save('ROI_debug'); % debug
```

A4. MATLAB script for generalised linear mixed effects models (GLMMs) of automated and manual cell counts

```
% select directory containing data file.
d = cd('\\IAHP-FAS1A\\common\\Integrative Entomology\\private\\Staff folders\\Alice\\02_Analyses\\01_Matlab\\02_Data\\01_Cell_Count Model validation');

filename = '2016-11-01 Automatic vs manual cell count.xls';
sheet = 3;
range = '(A3:A455):(L3:L455)';
count = xlsread(filename, sheet,range); % load in data from excel file excluding headers

a = count(:,1); % define variable for auto total cell count
b = count(:,2); % define variable for manual total cell count
x = count(:,3); % define variable for manual red cell count
y = count(:,4); % define variable for auto red cell count
d = count(:,5) % define variable for manual green cell count
e = count(:,6); % define variable for auto green cell count
z = count(:,7); % define variable for midge identity
c = count(:,8); % define variable for tissue identity

% convert variables into table for generalised linear mixed effects model (GLMM) analysis
tabcount = array2table(count,'VariableNames',{'tota','totm','Rm','Ra','Gm','Ga','midgeid','tissueid','expid','var1','var2','var3'});

tabcount.midgeid = categorical(tabcount.midgeid); % specify categorical variables.
tabcount.tissueid = categorical(tabcount.tissueid);
```

A4.1 Total nuclei cell counts

```
histogram(a,20); % plot a histogram to determine which distribution best describes the data
kstest(a)% test for normality of the dependent variable

tot_glmm =
fitglme(tabcount,'tota~1+totm+tissueid+(1|midgeid)','Distribution','poisson','link','log','DummyVarCoding','reference'); % fit GLMM with automated cell count as a response.
ciR = coefCI(tot_glmm); % determine the confidence intervals

plotResiduals(tot_glmm,'fitted'); % test homoscedasticity by plotting residuals against fitted values
plotResiduals(tot_glmm,'probability') % test residuals for normality
res = table2array(tot_glmm.Residuals);
res_White = TestHet(res(:,1),[y,z,c],'-W') % perform White's test for homoscedasticity
devtest = devianceTest(tot_glmm); % perform deviance test to determine whether the model differs from a constant model

% analysis of outlying values
N = length(a); % define the sample size
plotDiagnostics(tot_glmm,'cookd') % determine change in vector coefficients due to deletion of given value using Cook's distance
outliers = find((tot_glmm.Diagnostics.CooksDistance)>(4/N)) % identify outlying values
```

A4.2 Infected cell numbers

```
histogram(y,20); % plot histograms to determine which distribution best describes data
histogram(e,20);
kstest(y)% test for normality of dependent variable
kstest(e);
% fit GLMM to counts of cells expressing BTV +Seg-5 RNA (red channel).
R_glmm =
fitglme(tabcount,'Ra~1+Rm+tissueid+(1|midgeid)','Distribution','poisson','link','log','DummyVarCoding','reference'); % fit GLMM using automatic cell count as a response
```

```
% fit GLMM to counts of cells expressing BTV capsid protein (VP5, green channel).
G_glmm =
fitglme(tabcount,'Ga~1+Gm+tissueid+(1|midgeid)','Distribution','poisson','link','log','Dummy
VarCoding','reference');

% test homoscedasticity by plotting residuals against fitted values
plotResiduals(R_glmm,'fitted');
plotResiduals(G_glmm,'fitted');

resR = table2array(R_glmm.Residuals); % assign residuals to a variable
resG = table2array(G_glmm.Residuals);
res_White = TestHet(resR(:,1),[y,z,c],'-W') % White's test for homoscedasticity.
resG_White = TestHet(resG(:,1),[yG,z,c],'-W')

plotResiduals(R_glmm,'probability') % test normality of residuals.
plotResiduals(G_glmm,'probability')

ciR = coefCI(R_glmm); % determine confidence intervals
ciG = coefCI(G_glmm);

devtest = devianceTest(R_glmm); % perform deviance tests.
devtest = devianceTest(G_glmm);

plotDiagnostics(R_glmm,'cookd') % identify outlying values.
plotDiagnostics(G_glmm,'cookd')
outliers = find((R_glmm.Diagnostics.CooksDistance)>(4/N))
outliers = find((G_glmm.Diagnostics.CooksDistance)>(4/N))
```

A5. Comparison of the number of co-infected and singly infected cells

The script detailed in the following section continues from scripts listed in Appendix sections A3.2 to A3.3.

A5.1 Calculation of the number of infected cells.

```
if ((size(x_seg,1)) > 2) % if more than 2 centroids (nuclei) in image
   [v,c] = voronoin([x_seg(:) y_seg(:)]); % apply voronoi diagram
   xx1 = v(:,1); % coordinates of polygons
   yy1 = v(:,2);
   R = tissue_roi(:, :, 1); % define red channel
   G = tissue_roi(:, :, 2); % define green channel
   R(R<60) = 0; % remove lowest 23.53% pixels
   G(G<100) = 0; % Remove lowest 39.22% pixels
   [xG yG] = find(G); % find pixels over threshold and list coordinates
   [xR yR] = find(R);
   for i = 1:length(c) % for each polygon fill with colour
      if all(c{i}~=1) % if all values 1
         patch(v(c{i},1),v(c{i},2),i); % fill polygons
         ind = c{i}';
         InG = inpolygon(xG,yG,xx1(c{i}),yy1(c{i})); %  polygon green pixels
         InG = sum(InG);
         InR = inpolygon(xR,yR,xx1(c{i}),yy1(c{i})); %  polygon red pixels
         InR = sum(InR);
      end

      if InR+InG == 0 % no R or G pixels
         InR =0;
         InG =0;
         InRG = 0; % 0 value for polygon
```

```
        disp('No seg-5 or VP5 positive cells in polygon');

    elseif InR == 0
        InG = 1; % assign value 1 to n pixels that are in polygon
        InR = 0;
        InRG = 0;

    elseif InG == 0
        InG = 0; % assign value 1 to n pixels that are in polygon
        InR = 1;
        InRG = 0;

    else InRG = 1;
        InG = 0;
        InR = 0;
    end
    InfRtotal = InfRtotal + InR; % total polygons containing pixels
    InfGtotal = InfGtotal + InG;
    InfRGtotal = InfRGtotal + InRG;
  end
end
xlswrite('pos_cells.xls',[m, {tifflist(TIFFnum).name}, {size(centroidxy,1)}, {InfRtotal}, {InfGtotal},{InfRGtotal}], [sprintf('A%d',rownum+1),':',sprintf('F%d',rownum+1)]);
rownum = rownum+1; % save number of R, G or R and G cells.
end
end
```

A5.2 Test for differences in the number of co-infected and singly infected cells

```
% specify file location and load data
path = 'N:\\Integrative Entomology\\private\\Staff folders\\Alice\\02_Analyses\\01_Matlab\\02_Data\\2016-07-12 Dose experiment results\\Analyses\\02_NND analysis';
cd(path);
filename = '2017-02-05 Validation of colabeled cells V1-0.xls';
sheet = 3;
range = '(A2:A282):(J2:J282)';
count = xlsread(filename, sheet,range); % load data excluding headers

Ra = count(:,5); % define variables for red and green automated cell count
Ga = count(:,6);
RGa = count(:,7); % define variable for co-infected automated cell count

countRG = [Ra,Ga,RGa] % create array containing all values

[p,t, stats] = friedman(countRG,1) % apply friedman's test to differences between groups
sum(countRG)
[c,m,h,nms] = multcompare(stats) % use a multiple comparison test to determine where the differences lie

Rm = count(:,8); % define variables for red and green manual cell count
Gm = count(:,9);
RGm = count(:,10); % define variable for co-infected manual cell count

countRGm = [Rm,Gm,RGm] % create array containing all values
[p,t, stats] = friedman(countRGm,1) % apply friedman's test
[c,m,h,nms] = multcompare(stats) % apply a multiple comparison test
```

References

AL-KHAZRAJI, B. K., MEDEIROS, P. J., NOVIELLI, N. M. & JACKSON, D. N. 2011. An automated cell-counting algorithm for fluorescently-stained cells in migration assays. *Biological Procedures Online,* 13.

ALEXANDER, K. A., MACLACHLAN, N. J., KAT, P. W., HOUSE, C., OBRIEN, S. J., LERCHE, N. W., SAWYER, M., FRANK, L. G., HOLEKAMP, K., SMALE, L., MCNUTT, J. W., LAURENSON, M. K., MILLS, M. G. L. & OSBURN, B. I. 1994. Evidence of Natural Bluetongue Virus-Infection among African Carnivores. *American Journal of Tropical Medicine and Hygiene,* 51**,** 568-576.

ALTO, B. W., LOUNIBOS, L. P., MORES, C. N. & REISKIND, M. H. 2008. Larval competition alters susceptibility of adult Aedes mosquitoes to dengue infection. *Proc Biol Sci,* 275.

AMINO, R., THIBERGE, S., MARTIN, B., CELLI, S., SHORTE, S., FRISCHKNECHT, F. & MENARD, R. 2006. Quantitative imaging of Plasmodium transmission from mosquito to mammal. *Nat Med,* 12**,** 220-4.

ANDERSON, S. L., RICHARDS, S. L., TABACHNICK, W. J. & SMARTT, C. T. 2010. Effects of West Nile Virus Dose and Extrinsic Incubation Temperature on Temporal Progression of Vector Competence in Culex Pipiens Quinquefasciatus. *Journal of the American Mosquito Control Association,* 26**,** 103-107.

ANTHONY, S. J., DARPEL, K. E., BELAGANAHALLI, M. N., MAAN, N., NOMIKOU, K., SUTTON, G., ATTOUI, H., MAAN, S. & MERTENS, P. P. 2011. RNA segment 9 exists as a duplex concatemer in an Australian strain of epizootic haemorrhagic disease virus (EHDV): Genetic analysis and evidence for the presence of concatemers as a normal feature of orbivirus replication. *Virology,* 420**,** 164-71.

ARNAUD, N., DABO, S., MAILLARD, P., BUDKOWSKA, A., KALLIAMPAKOU, K. I., MAVROMARA, P., GARCIN, D., HUGON, J., GATIGNOL, A., AKAZAWA, D., WAKITA, T. & MEURS, E. F. 2010. Hepatitis C Virus Controls Interferon Production through PKR Activation. *Plos One,* 5.

ARNOT, C. J., GAY, N. J. & GANGLOFF, M. 2010. Molecular mechanism that induces activation of Spatzle, the ligand for the Drosophila Toll receptor. *J Biol Chem,* 285**,** 19502-9.

ATASHEVA, S., GORCHAKOV, R., ENGLISH, R., FROLOV, I. & FROLOVA, E. 2007. Development of Sindbis viruses encoding nsP2/GFP chimeric proteins and their application for studying nsP2 functioning. *J Virol,* 81**,** 5046-57.

ATKINSON, C. T. 1988. Epizootiology of Haemoproteus-Meleagridis (Protozoa, Haemosporina) in Florida - Potential Vectors and Prevalence in Naturally Infected Culicoides (Diptera, Ceratopogonidae). *Journal of Medical Entomology,* 25**,** 39-44.

ATTARZADEH-YAZDI, G., FRAGKOUDIS, R., CHI, Y., SIU, R. W. C., ULPER, L., BARRY, G., RODRIGUEZ-ANDRES, J., NASH, A. A., BOULOY, M., MERITS, A., FAZAKERLEY, J. K. & KOHL, A. 2009. Cell-to-Cell Spread of the RNA Interference Response Suppresses Semliki Forest Virus (SFV) Infection of Mosquito Cell Cultures and Cannot Be Antagonized by SFV. *Journal of Virology,* 83**,** 5735-5748.

ATTOUI, H., MENDEZ-LOPEZ, M. R., RAO, S. J., HURTADO-ALENDES, A., LIZARASO-CAPARO, F., JAAFAR, F. M., SAMUEL, A. R., BELHOUCHET, M., PRITCHARD, L. I., MELVILLE, L., WEIR, R. P., HYATT, A. D., DAVIS, S. S., LUNT, R., CALISHER, C. H., TESH, R. B., FUJITA, R. & MERTENS, P. P. C. 2009. Peruvian horse sickness virus and Yunnan orbivirus, isolated from vertebrates and mosquitoes in Peru and Australia. *Virology,* 394**,** 298-310.

AVADHANULA, V., WEASNER, B. P., HARDY, G. G., KUMAR, J. P. & HARDY, R. W. 2009. A Novel System for the Launch of Alphavirus RNA Synthesis Reveals a Role for the Imd Pathway in Arthropod Antiviral Response. *Plos Pathogens,* 5.

BAILLIE, V. L. & BOUWER, G. 2013. The effect of inoculum dose on the genetic diversity detected within Helicoverpa armigera nucleopolyhedrovirus populations. *Journal of General Virology,* 94**,** 2524-2529.

BALASURIYA, U. B., NADLER, S. A., WILSON, W. C., PRITCHARD, L. I., SMYTHE, A. B., SAVINI, G., MONACO, F., DE SANTIS, P., ZHANG, N., TABACHNICK, W. J. & MACLACHLAN, N. J. 2008. The NS3 proteins of global strains of bluetongue virus evolve into regional topotypes through negative (purifying) selection. *Vet Microbiol,* 126**,** 91-100.

BALDI, P., BRUNAK, S., CHAUVIN, Y., ANDERSEN, C. A. & NIELSEN, H. 2000. Assessing the accuracy of prediction algorithms for classification: an overview. *Bioinformatics,* 16**,** 412-24.

BANSAL, O. B., STOKES, A., BISAL, A., BISHOP, D. & ROY, P. 1998. Membrane organization of bluetongue virus nonstructural glycoprotein NS3. *Journal of Virology,* 72**,** 3362-3369.

BAQAR, S., HAYES, C. G. & AHMED, T. 1980. The Effect of Larval Rearing Conditions and Adult Age on the Susceptibility of Culex-Tritaeniorhynchus to Infection with West Nile Virus. *Mosquito News,* 40**,** 165-171.

BARA, J., RAPTI, Z., CACERES, C. E. & MUTURI, E. J. 2015. Effect of Larval Competition on Extrinsic Incubation Period and Vectorial Capacity of Aedes albopictus for Dengue Virus. *PLoS One,* 10**,** e0126703.

BARNARD, A. C., NIJHOF, A. M., FICK, W., STUTZER, C. & MARITZ-OLIVIER, C. 2012. RNAi in Arthropods: Insight into the Machinery and Applications for Understanding the Pathogen-Vector Interface. *Genes (Basel),* 3**,** 702-41.

BARNARD, D. R. & JONES, R. H. 1980. Culicoides-Variipennis (Diptera, Ceratopogonidae) - Seasonal Abundance, Overwintering, and Voltinism in Northeastern Colorado. *Environmental Entomology,* 9**,** 709-712.

BATTEN, C. A., HENSTOCK, M. R., STEEDMAN, H. M., WADDINGTON, S., EDWARDS, L. & OURA, C. A. L. 2013. Bluetongue virus serotype 26: Infection kinetics, pathogenesis and possible contact transmission in goats. *Veterinary Microbiology,* 162**,** 62-67.

BATTEN, C. A., MAAN, S., SHAW, A. E., MAAN, N. S. & MERTENS, P. P. C. 2008. A European field strain of bluetongue virus derived from two parental vaccine strains by genome segment reassortment. *Virus Research,* 137**,** 56-63.

BAYLIS, M., O'CONNELL, L. & MELLOR, P. S. 2008. Rates of bluetongue virus transmission between Culicoides sonorensis and sheep. *Med Vet Entomol,* 22**,** 228-37.

BEATON, A. R., RODRIGUEZ, J., REDDY, Y. K. & ROY, P. 2002. The membrane trafficking protein calpactin forms a complex with bluetongue virus protein NS3 and mediates virus release. *Proc Natl Acad Sci U S A,* 99**,** 13154-9.

BEKKER, J., DE KOCK, G. & QUINLAN, J. 1934. The occurrence and identification of bluetongue in cattle-the so-called pseudo-foot and mouth disease in South Africa. . *Onderstepoort Journal of Veterinary Science and Animal Industry,* 2.

BELHOUCHET, M., MOHD JAAFAR, F., FIRTH, A. E., GRIMES, J. M., MERTENS, P. P. & ATTOUI, H. 2011. Detection of a fourth orbivirus non-structural protein. *PLoS One,* 6**,** e25697.

BENNETT, K. E., FLICK, D., FLEMING, K. H., JOCHIM, R., BEATY, B. J. & BLACK, W. C. 2005. Quantitative trait loci that control dengue-2 virus dissemination in the mosquito Aedes aegypti. *Genetics,* 170**,** 185-194.

BENNETT, K. E., OLSON, K. E., MUNOZ MDE, L., FERNANDEZ-SALAS, I., FARFAN-ALE, J. A., HIGGS, S., BLACK, W. C. T. & BEATY, B. J. 2002. Variation in vector competence for dengue 2 virus among 24 collections of Aedes aegypti from Mexico and the United States. *Am J Trop Med Hyg,* 67**,** 85-92.

BERGOLD, G. H., SUAREZ, O. M. & MUNZ, K. 1968. Multiplication in and transmission by Aedes aegypti of vesicular stomatitis virus. *J Invertebr Pathol,* 11**,** 406-28.

BEUTLER, B. 2004. Innate immunity: an overview. *Mol Immunol,* 40**,** 845-59.

BHATTACHARYA, B. & ROY, P. 2008. Bluetongue virus outer capsid protein VP5 interacts with membrane lipid rafts via a SNARE domain. *J Virol,* 82**,** 10600-12.

BIAN, G., XU, Y., LU, P., XIE, Y. & XI, Z. 2010. The endosymbiotic bacterium Wolbachia induces resistance to dengue virus in Aedes aegypti. *PLoS Pathog,* 6**,** e1000833.

BILLINGSLEY, P. & LEHANE, M. J. 1996a. *Biology of the insect midgut.,* London, Chapman & Hall.

BILLINGSLEY, P. F. 1990. Blood Digestion in the Mosquito, Anopheles-Stephensi Liston (Diptera, Culicidae) - Partial Characterization and Post-Feeding Activity of Midgut Aminopeptidases. *Archives of Insect Biochemistry and Physiology,* 15**,** 149-163.

BILLINGSLEY, P. F. & HECKER, H. 1991. Blood Digestion in the Mosquito, Anopheles-Stephensi Liston (Diptera, Culicidae), Activity and Distribution of Trypsin, Aminopeptidase, and Alpha-Glucosidase in the Midgut. *Journal of Medical Entomology,* 28**,** 865-871.

BILLINGSLEY, P. F. & LEHANE, M. J. 1996b. *Structure and ultrastructure of the insect midgut,* London, Chapman & Hall.

BISHOP, J. V., MEJIA, J. S., DE LEON, A. A. P., TABACHNICK, W. J. & TITUS, R. G. 2006. Salivary gland extracts of Culicoides sonorensis inhibit murine lymphocyte proliferation and no production by macrophages. *American Journal of Tropical Medicine and Hygiene,* 75**,** 532-536.

BLACKWELL, A. 1997. Diel flight periodicity of the biting midge Culicoides impunctatus and the effects of meteorological conditions. *Medical and Veterinary Entomology,* 11**,** 361-367.

BLACKWELL, A. 2004. A morphological investigation of Culicoides spp. biting midges (Diptera : Ceratopogonidae) from the Caribbean. *Journal of Vector Ecology,* 29**,** 51-61.

BOLLEN, K. A. 1990. Outlier Screening and a Distribution-Free Test for Vanishing Tetrads. *Sociological Methods & Research,* 19**,** 80-92.

BONNEAU, K. R., DEMAULA, C. D., MULLENS, B. A. & MACLACHLAN, N. J. 2002. Duration of viraemia infectious to *Culicoides sonorensis* in bluetongue virus-infected cattle and sheep. *Veterinary Microbiology,* 88**,** 115-125.

BONNEAU, K. R. & MACLACHLAN, N. J. 2004. Genetic diversification of field strains of bluetongue virus. *Vet Ital,* 40**,** 446-7.

BOORMAN, J. 1960. Observations on the amount of virus present in the haemolymph of Aedes aegypti infected with Uganda S, yellow fever and Semliki Forest viruses. *Trans R Soc Trop Med Hyg,* 54**,** 362-5.

BORKENT, A. 2000. Biting midges (Diptera: Ceratopogonidae) from lower cretaceous Lebanese amber with a discussion of the diversity and patterns found in other ambers. . *In:* GRIMALDI, D. (ed.) *Studies on Fossils in Amber, with Particular Reference to the Cretaceous of New Jersey.* Leiden, The Netherlands: Backhuys Publishers.

BORKENT, A. 2014. The Pupae of the Biting Midges of the World (Diptera: Ceratopogonidae), With a Generic Key and Analysis of the Phylogenetic Relationships Between Genera. *Zootaxa,* 3879**,** 1-+.

BORKENT, A. 2016. *World species of biting midges (Diptera: Ceratopogonidae).* [Online]. http://wwx.inhs.illinois.edu/files/4514/6410/0252/CeratopogonidaeCatalog.pdf. . [Accessed 06/02/2016 2016].

BOSIO, C. F., BEATY, B. J. & BLACK, W. C. T. 1998. Quantitative genetics of vector competence for dengue-2 virus in Aedes aegypti. *Am J Trop Med Hyg,* 59**,** 965-70.

BOSIO, C. F., FULTON, R. E., SALASEK, M. L., BEATY, B. J. & BLACK, W. C. 2000. Quantitative trait loci that control vector competence for dengue-2 virus in the mosquito Aedes aegypti. *Genetics,* 156**,** 687-698.

BOWERS, D. F., ABELL, B. A. & BROWN, D. T. 1995. Replication and Tissue Tropism of the Alphavirus Sindbis in the Mosquito Aedes-Albopictus. *Virology,* 212**,** 1-12.

BOWERS, D. F., COLEMAN, C. G. & BROWN, D. T. 2003. Sindbis virus-associated pathology in Aedes albopictus (Diptera : Culicidae). *Journal of Medical Entomology,* 40**,** 698-705.

BOWNE, J. G. & JONES, R. H. 1966. Observations on bluetongue virus in the salivary glands of an insect vector, Culicoides variipennis. *Virology,* 30**,** 127-33.

BOYCE, M., CELMA, C. C. & ROY, P. 2012a. Bluetongue virus non-structural protein 1 is a positive regulator of viral protein synthesis. *Virol J,* 9**,** 178.

BOYCE, M., CELMA, C. C. P. & ROY, P. 2008. Development of reverse genetics systems for bluetongue virus: Recovery of infectious virus from synthetic RNA transcripts. *Journal of Virology,* 82**,** 8339-8348.

BOYCE, M., CELMA, C. C. P. & ROY, P. 2012b. Bluetongue virus non-structural protein 1 is a positive regulator of viral protein synthesis. *Virology Journal,* 9.

BOYCE, M., MCCRAE, M. A., BOYCE, P. & KIM, J. T. 2016. Inter-segment complementarity in orbiviruses: a driver for co-ordinated genome packaging in the Reoviridae? *J Gen Virol,* 97**,** 1145-57.

BOYCE, M. & ROY, P. 2007. Recovery of infectious bluetongue virus from RNA. *J Virol,* 81**,** 2179-86.

BOYCE, M., WEHRFRITZ, J., NOAD, R. & ROY, P. 2004. Purified recombinant bluetongue virus VP1 exhibits RNA replicase activity. *Journal of Virology,* 78**,** 3994-4002.

BRAC, T. 1983. Charged Sieving by the Basal Lamina and the Distribution of Anionic Sites on the External Surfaces of Fat-Body Cells. *Tissue & Cell,* 15**,** 489-498.

BRACKNEY, D. E., FOY, B. D. & OLSON, K. E. 2008. The effects of midgut serine proteases on dengue virus type 2 infectivity of Aedes aegypti. *American Journal of Tropical Medicine and Hygiene,* 79**,** 267-274.

BRAULT, A. C., FOY, B. D., MYLES, K. M., KELLY, C. L. H., HIGGS, S., WEAVER, S. C., OLSON, K. E., MILLER, B. R. & POWERS, A. M. 2004a. Infection patterns of o'nyong nyong virus in the malaria-transmitting mosquito, Anopheles gambiae. *Insect Molecular Biology,* 13**,** 625-635.

BRAULT, A. C., POWERS, A. M., ORTIZ, D., ESTRADA-FRANCO, J. G., NAVARRO-LOPEZ, R. & WEAVER, S. C. 2004b. Venezuelan equine encephalitis emergence: enhanced vector infection from a single amino acid substitution in the envelope glycoprotein. *Proc Natl Acad Sci U S A,* 101**,** 11344-9.

BREWER, A. W. & MACLACHLAN, N. J. 1992. Ultrastructural Characterization of the Interaction of Bluetongue Virus with Bovine Erythrocytes Invitro. *Veterinary Pathology,* 29**,** 356-359.

BREWER, A. W. & MACLACHLAN, N. J. 1994. The Pathogenesis of Bluetongue Virus-Infection of Bovine Blood-Cells in-Vitro - Ultrastructural Characterization. *Archives of Virology,* 136**,** 287-298.

BRIEGEL, H. & LEA, A. O. 1975. Relationship between Protein and Proteolytic Activity in Midgut of Mosquitos. *Journal of Insect Physiology,* 21**,** 1597-1604.

BROOKES, S. M., HYATT, A. D. & EATON, B. T. 1993. Characterization of virus inclusion bodies in bluetongue virus-infected cells. *J Gen Virol,* 74 (Pt 3)**,** 525-30.

BUKAUSKAITE, D., ZIEGYTE, R., PALINAUSKAS, V., IEZHOVA, T. A., DIMITROV, D., ILGUNAS, M., BERNOTIENE, R., MARKOVETS, M. Y. & VALKIUNAS, G. 2015. Biting midges (Culicoides, Diptera) transmit Haemoproteus parasites of owls: evidence from sporogony and molecular phylogeny. *Parasites & Vectors,* 8.

BURKHARDT, C., SUNG, P. Y., CELMA, C. C. & ROY, P. 2014. Structural constraints in the packaging of bluetongue virus genomic segments. *Journal of General Virology,* 95**,** 2240-2250.

BUXTON, B. A., HINKLE, N. C. & SCHULTZ, R. D. 1985. Role of Insects in the Transmission of Bovine Leukosis Virus - Potential for Transmission by Stable Flies, Horn Flies, and Tabanids. *American Journal of Veterinary Research,* 46**,** 123-126.

CAMPBELL, C. L., MUMMEY, D. L., SCHMIDTMANN, E. T. & WILSON, W. C. 2004. Culture-independent analysis of midgut microbiota in the arbovirus vector Culicoides sonorensis (Diptera: Ceratopogonidae). *J Med Entomol,* 41**,** 340-8.

CAMPBELL, K. M., GETIS, A., ALDSTADT, J., KUZERA, K., UNGCHUSAK, K., LEVINE, R. A. & SCOTT, T. W. 2008. A Unifying Framework for the Complex Regional Dynamics of Multi-Serotype Dengue Virus Transmission. *American Journal of Tropical Medicine and Hygiene,* 79**,** 15-16.

CAMPBELL, M. M. & KETTLE, D. S. 1975. Oogenesis in Culicoides-Brevitarsis Kieffer (Diptera-Ceratopogonidae) and Development of a Plastron-Like Layer on Egg. *Australian Journal of Zoology,* 23**,** 203-218.

CAO-LORMEAU, V. M. 2009. Dengue viruses binding proteins from Aedes aegypti and Aedes polynesiensis salivary glands. *Virol J,* 6**,** 35.

CARISSIMO, G., PONDEVILLE, E., MCFARLANE, M., DIETRICH, I., MITRI, C., BISCHOFF, E., ANTONIEWSKI, C., BOURGOUIN, C., FAILLOUX, A. B., KOHL, A. & VERNICK, K. D. 2015. Antiviral immunity of Anopheles gambiae is highly compartmentalized, with distinct roles for RNA interference and gut microbiota. *Proc Natl Acad Sci U S A,* 112**,** E176-85.

CARPENTER, A. E., KAMENTSKY, L. & ELICEIRI, K. W. 2012. A call for bioimaging software usability. *Nature Methods,* 9**,** 666-670.

CARPENTER, S., LUNT, H. L., ARAV, D., VENTER, G. J. & MELLOR, P. S. 2006. Oral susceptibility to bluetongue virus of Culicoides (Diptera : Ceratopogonidae) from the United Kingdom. *Journal of Medical Entomology,* 43**,** 73-78.

CARPENTER, S., MERTENS, P., MELLOR, D. J., GIBBENS, N., MIDDLEMISS, C., STEPHAN, L., PAPADOPOULOU, C., BURGIN, L., BAYLISS, M., SPRAY, M., GUBBINS, S. & CRITCHLEY, P. 2016. Qualitative risk assessment: bluetongue virus (BTV-8) entry into the UK. . *In:* ROBERTS, H., MOIR, R., MATT, C., SPRAY, M., BODEN, L. & BESSELL, P. (eds.). Department for Environment and Rural Affairs. .

CARPENTER, S., SZMARAGD, C., BARBER, J., LABUSCHAGNE, K., GUBBINS, S. & MELLOR, P. 2008. An assessment of Culicoides surveillance techniques in northern Europe: have we underestimated a potential bluetongue virus vector? *Journal of Applied Ecology,* 45**,** 1237-1245.

CARPENTER, S., VERONESI, E., MULLENS, B. & VENTER, G. 2015. Vector competence of Culicoides for arboviruses: three major periods of research, their influence on current studies and future directions. *Rev Sci Tech,* 34**,** 97-112.

CARPENTER, S., WILSON, A., BARBER, J., VERONESI, E., MELLOR, P., VENTER, G. & GUBBINS, S. 2011. Temperature Dependence of the Extrinsic Incubation Period of Orbiviruses in Culicoides Biting Midges. *PLoS ONE,* 6.

CARPENTER, S., WILSON, A. & MELLOR, P. S. 2009. *Culicoides* and the emergence of bluetongue virus in northern Europe. *Trends in Microbiology,* 17**,** 172-178.

CARRINGTON, L. B., SEIFERT, S. N., ARMIJOS, M. V., LAMBRECHTS, L. & SCOTT, T. W. 2013. Reduction of Aedes aegypti vector competence for dengue virus under large temperature fluctuations. *Am J Trop Med Hyg,* 88**,** 689-97.

CASALS, J. 1973. Arbovirus infections. . *Serological epidemiology.* . New York: Academic Press.

CASTILLO, J. C., ROBERTSON, A. E. & STRAND, M. R. 2006. Characterization of hemocytes from the mosquitoes Anopheles gambiae and Aedes aegypti. *Insect Biochemistry and Molecular Biology,* 36**,** 891-903.

CELMA, C. C. & ROY, P. 2009. A viral nonstructural protein regulates bluetongue virus trafficking and release. *J Virol,* 83**,** 6806-16.

CHAMBERLAIN, R. W. & SUDIA, W. D. 1961. Mechanism of transmission of viruses by mosquitoes. *Annu Rev Entomol,* 6**,** 371-90.

CHANDLER, L. J., BLAIR, C. D. & BEATY, B. J. 1998. La Crosse virus infection of Aedes triseriatus (Diptera: Culicidae) ovaries before dissemination of virus from the midgut. *J Med Entomol,* 35**,** 567-72.

CHAUVEAU, E., DOCEUL, V., LARA, E., BREARD, E., SAILLEAU, C., VIDALAIN, P. O., MEURS, E. F., DABO, S., SCHWARTZ-CORNIL, I., ZIENTARA, S. & VITOUR, D. 2013. NS3 of bluetongue virus interferes with the induction of type I interferon. *J Virol,* 87**,** 8241-6.

CHAWLA-SARKAR, M., LINDNER, D. J., LIU, Y. F., WILLIAMS, B., SEN, G. C., SILVERMAN, R. H. & BORDEN, E. C. 2003. Apoptosis and interferons: Role of interferon-stimulated genes as mediators of apoptosis. *Apoptosis,* 8**,** 237-249.

CHEE, H. Y. & ABUBAKAR, S. 2004. Identification of a 48 kDa tubulin or tubulin-like C6/36 mosquito cells protein that binds dengue virus 2 using mass spectrometry. *Biochemical and Biophysical Research Communications,* 320**,** 11-17.

CHEN, Q., GONG, B., MAHMOUD-AHMED, A. S., ZHOU, A., HSI, E. D., HUSSEIN, M. & ALMASAN, A. 2001. Apo2L/TRAIL and Bcl-2-related proteins regulate type I interferon-induced apoptosis in multiple myeloma. *Blood,* 98**,** 2183-92.

CHEN, Y. C., WANG, S. Y. & KING, C. C. 1999. Bacterial lipopolysaccharide inhibits dengue virus infection of primary human monocytes/macrophages by blockade of virus entry via a CD14-dependent mechanism. *Journal of Virology,* 73**,** 2650-2657.

CHEN, Y. P., MAGUIRE, T., HILEMAN, R. E., FROMM, J. R., ESKO, J. D., LINHARDT, R. J. & MARKS, R. M. 1997. Dengue virus infectivity depends on envelope protein binding to target cell heparan sulfate. *Nature Medicine,* 3**,** 866-871.

CHU, J. J. H., LEONG, P. W. H. & NG, M. L. 2006. Analysis of the endocytic pathway mediating the infectious entry of mosquito-borne flavivirus West Nile into Aedes albopictus mosquito (C6/36) cells. *Virology,* 349**,** 463-475.

CINELLI, R. A., FERRARI, A., PELLEGRINI, V., TYAGI, M., GIACCA, M. & BELTRAM, F. 2000. The enhanced green fluorescent protein as a tool for the analysis of protein dynamics and localization: local fluorescence study at the single-molecule level. *Photochem Photobiol,* 71**,** 771-6.

CIRIMOTICH, C. M., DONG, Y. M., CLAYTON, A. M., SANDIFORD, S. L., SOUZA-NETO, J. A., MULENGA, M. & DIMOPOULOS, G. 2011a. Natural Microbe-Mediated Refractoriness to Plasmodium Infection in Anopheles gambiae. *Science,* 332**,** 855-858.

CIRIMOTICH, C. M., RAMIREZ, J. L. & DIMOPOULOS, G. 2011b. Native Microbiota Shape Insect Vector Competence for Human Pathogens. *Cell Host & Microbe,* 10**,** 307-310.

CLARKE, D. K., DUARTE, E. A., MOYA, A., ELENA, S. F., DOMINGO, E. & HOLLAND, J. 1993. Genetic bottlenecks and population passages cause profound fitness differences in RNA viruses. *J Virol,* 67**,** 222-8.

COHEN, E. 2009. Fat body. *In:* RESH, V. H. & CARDE, R. T. (eds.) *Encylopedia of insects.* 2 ed. London: Elsevier Inc.

COOMBES, J. L. & ROBEY, E. A. 2010. Dynamic imaging of host-pathogen interactions in vivo. *Nat Rev Immunol,* 10**,** 353-64.

COOPER, L. A. & SCOTT, T. W. 2001. Differential evolution of eastern equine encephalitis virus populations in response to host cell type. *Genetics,* 157**,** 1403-12.

CORREA, T. G., FERREIRA, J. M., RIET-CORREA, G., RUAS, J. L., SCHILD, A. L., RIET-CORREA, F., GUIMARAES, A. & FELIPPE-BAUER, M. L. 2007. Seasonal allergic dermatitis in sheep in southern Brazil caused by Culicoides insignis (Diptera : Ceratopogonidae). *Veterinary Parasitology,* 145**,** 181-185.

COWLEY, J. A. & GORMAN, B. M. 1987. Genetic reassortants for identification of the genome segment coding for the bluetongue virus hemagglutinin. *J Virol,* 61**,** 2304-6.

COX, J., BROWN, H. E. & RICO-HESSE, R. 2011. Variation in vector competence for dengue viruses does not depend on mosquito midgut binding affinity. *PLoS Negl Trop Dis,* 5**,** e1172.

CRIBB, B. W. & CHITRA, E. 1998. Ultrastructure of the eggs of Culicoides molestus (Diptera: Ceratopogonidae). *J Am Mosq Control Assoc,* 14**,** 363-8.

DARPEL, K. E., BATTEN, C. A., VERONESI, E., SHAW, A. E., ANTHONY, S., BACHANEK-BANKOWSKA, K., KGOSANA, L., BIN-TARIF, A., CARPENTER, S., MÜLLER-DOBLIES, U., TAKAMATSU, H., MELLOR, P. S., MERTENS, P. P. C. & OURA, C. A. L. 2007. Clinical signs and pathology shown by British sheep and cattle infected with bluetongue virus serotype 8 derived from the 2006 outbreak in northern Europe. *Veterinary Record,* 161**,** 253-261.

DARPEL, K. E., LANGNER, K. F. A., NIMTZ, M., ANTHONY, S. J., BROWNLIE, J., TAKAMATSU, H.-H., MELLOR, P. S. & MERTENS, P. P. C. 2011. Saliva proteins of vector Culicoides modify structure and infectivity of bluetongue virus particles. *PLoS ONE,* 6**,** e17545.

DAVIS, R. A. & FRAENKEL, G. 1940. The oxygen consumption of flies during flight. *Journal of Experimental Biology,* 17**,** 402-407.

DEDDOUCHE, S., MATT, N., BUDD, A., MUELLER, S., KEMP, C., GALIANA-ARNOUX, D., DOSTERT, C., ANTONIEWSKI, C., HOFFMANN, J. A. & IMLER, J. L. 2008. The DExD/H-box helicase Dicer-2 mediates the induction of antiviral activity in drosophila. *Nature Immunology,* 9**,** 1425-1432.

DELEON, A. A. P. & TABACHNICK, W. J. 1996. Apyrase activity and adenosine diphosphate induced platelet aggregation inhibition by the salivary gland proteins of Culicoides variipennis, the North American vector of bluetongue viruses. *Veterinary Parasitology,* 61**,** 327-338.

DELORD, B., POVEDA, J. D., ASTIERGIN, T., GERBAUD, S., WATTIAUX, J. P. & FLEURY, H. J. A. 1990. Quantitative Insitu Hybridization Using Strand Specific Rna Probes - Expression of the Bunyavirus Germiston S-Segment in Mosquito Cells. *Molecular and Cellular Probes,* 4**,** 247-259.

DERKSEN, A. C. & GRANADOS, R. R. 1988. Alteration of a lepidopteran peritrophic membrane by baculoviruses and enhancement of viral infectivity. *Virology,* 167**,** 242-50.

DESSELBERGER, U. 2017. Reverse genetics of rotavirus. *Proc Natl Acad Sci U S A,* 114**,** 2106-2108.

DIPROSE, J. M., BURROUGHS, J. N., SUTTON, G. C., GOLDSMITH, A., GOUET, P., MALBY, R., OVERTON, I., ZIENTARA, S., MERTENS, P. P., STUART, D. I. & GRIMES, J. M. 2001. Translocation portals for the substrates and products of a viral transcription complex: the bluetongue virus core. *EMBO J,* 20**,** 7229-39.

DODSON, B. L., KRAMER, L. D. & RASGON, J. L. 2011. Larval Nutritional Stress Does Not Affect Vector Competence for West Nile Virus (WNV) in Culex tarsalis. *Vector-Borne and Zoonotic Diseases,* 11**,** 1493-1497.

DODSON, B. L., KRAMER, L. D. & RASGON, J. L. 2012. Effects of larval rearing temperature on immature development and West Nile virus vector competence of Culex tarsalis. *Parasit Vectors,* 5**,** 199.

DOMINGO, E. & HOLLAND, J. J. 1997. RNA virus mutations and fitness for survival. *Annual Review of Microbiology,* 51**,** 151-178.

DONG, S. Z., KANTOR, A. M., LIN, J. Y., PASSARELLI, A. L., CLEM, R. J. & FRANZ, A. W. E. 2016. Infection pattern and transmission potential of chikungunya virus in two New World laboratory-adapted Aedes aegypti strains. *Scientific Reports,* 6.

DONG, Y., AGUILAR, R., XI, Z., WARR, E., MONGIN, E. & DIMOPOULOS, G. 2006. Anopheles gambiae immune responses to human and rodent Plasmodium parasite species. *PLoS Pathog,* 2**,** e52.

DONG, Y., MANFREDINI, F. & DIMOPOULOS, G. 2009. Implication of the mosquito midgut microbiota in the defense against malaria parasites. *PLoS Pathog,* 5**,** e1000423.

DOSTERT, C., JOUANGUY, E., IRVING, P., TROXLER, L., GALIANA-ARNOUX, D., HETRU, C., HOFFMANN, J. A. & IMLER, J. L. 2005. The Jak-STAT signaling pathway is required but not sufficient for the antiviral response of drosophila. *Nat Immunol,* 6**,** 946-53.

DOWNES, J. A. 1955. Observations on the swarming flight and mating of Culicoides (Diptera: Ceratopogonidae). *Ecological Entomology,* 106**,** 213-236.

DOWNES, J. A. & WIRTH, W. W. 1981. Ceratopogonidae. *Manual of Nearctic Diptera. ,* 674**,** 393-421.

DROLET, B. S., CAMPBELL, C. L., STUART, M. A. & WILSON, W. C. 2005. Vector competence of Culicoides sonorensis (Diptera: Ceratopogonidae) for vesicular stomatitis virus. *J Med Entomol,* 42**,** 409-18.

DRUETT, H. A. 1952. Bacterial invasion. *Nature,* 170**,** 288.

DU, J., BHATTACHARYA, B., WARD, T. H. & ROY, P. 2014. Trafficking of bluetongue virus visualized by recovery of tetracysteine-tagged virion particles. *J Virol,* 88**,** 12656-68.

DU TOIT, R. M. 1944. The transmission of bluetongue and horse sickness by *Culicoides*. *Onderstepoort Journal of Veterinary Science and Animal Industry,* 19**,** 7-16.

DUBRULLE, M., MOUSSON, L., MOUTAILLER, S., VAZEILLE, M. & FAILLOUX, A. B. 2009. Chikungunya virus and Aedes mosquitoes: saliva is infectious as soon as two days after oral infection. *PLoS One,* 4**,** e5895.

DYCE, A. L. & MARSHALL, B. D. 1989. An Early Record of Culicoides Species (Diptera, Ceratopogonidae) Developing in the Dung of Game Animals in Southern-Africa. *Onderstepoort Journal of Veterinary Research,* 56**,** 85-86.

EATON, B. T. & CRAMERI, G. S. 1989. The site of bluetongue virus attachment to glycophorins from a number of animal erythrocytes. *J Gen Virol,* 70 (Pt 12)**,** 3347-53.

EATON, B. T. & GOULD, A. R. 1987. Isolation and Characterization of Orbivirus Genotypic Variants. *Virus Research,* 6**,** 363-382.

EBERT, D. & WEISSER, W. W. 1997. Optimal killing for obligate killers: The evolution of life histories and virulence of semelparous parasites. *Proceedings of the Royal Society B-Biological Sciences,* 264**,** 985-991.

EL HUSSEIN, A., RAMIG, R. F., HOLBROOK, F. R. & BEATY, B. J. 1989. Asynchronous mixed infection of Culicoides variipennis with bluetongue virus serotypes 10 and 17. *J Gen Virol,* 70 (Pt 12)**,** 3355-62.

ERASMUS, B. J. 1975. Bluetongue in sheep and goats. *Australian Veterinary Journal,* 51**,** 165-169.

FARAN, M. E., ROMOSER, W. S., ROUTIER, R. G. & BAILEY, C. L. 1988. The Distribution of Rift Valley Fever Virus in the Mosquito Culex Pipiens as Revealed by Viral Titration of Dissected Organs and Tissues. *The American Journal of Tropical Medicine and Hygiene,* 39**,** 206-213.

FELIX, C. R., BETSCHART, B., BILLINGSLEY, P. F. & FREYVOGEL, T. A. 1991. Post-Feeding Induction of Trypsin in the Midgut of Aedes-Aegypti L (Diptera, Culicidae) Is Separable into 2 Cellular-Phases. *Insect Biochemistry,* 21**,** 197-203.

FILIMONOVA, G. F. 2004. Formation of the peritrophic membrane in the gut of Culicoides punctatus (Diptera: Ceratopogonidae). . *Parazitologiia,* 38**,** 12-19.

FILIMONOVA, S. A. 2005. Morphological Study of Digestive Cycle in Bloodsucking Biting Midges of Genus Culicoides. . *Journal of Evolutionary Biochemistry and Physiology,* 41**,** 221-232.

FLYNT, A., LIU, N., MARTIN, R. & LAI, E. C. 2009. Dicing of viral replication intermediates during silencing of latent Drosophila viruses. *Proceedings of the National Academy of Sciences of the United States of America,* 106**,** 5270-5275.

FORRESTER, L., GUERBOIS, M., SEYMOUR, R. L., SPRATT, H. & WEAVER, S. C. 2010. Vector-borne transmission imposes a severe bottleneck on an RNA virus population. *Plos Pathogens,* 8**,** e1002897.

FORRESTER, N. L., COFFEY, L. L. & WEAVER, S. C. 2014. Arboviral Bottlenecks and Challenges to Maintaining Diversity and Fitness during Mosquito Transmission (vol 6, pg 3991, 2014). *Viruses-Basel,* 6**,** 4422-4423.

FORZAN, M., MARSH, M. & ROY, P. 2007. Bluetongue virus entry into cells. *Journal of Virology,* 81**,** 4819-4827.

FORZAN, M., WIRBLICH, C. & ROY, P. 2004. A capsid protein of nonenveloped Bluetongue virus exhibits membrane fusion activity. *Proceedings of the National Academy of Sciences of the United States of America,* 101**,** 2100-2105.

FOSTER, N. M. & JONES, R. H. 1973. Bluetongue virus transmission with Culicoides variipennis via embryonating chicken eggs. *J Med Entomol,* 10**,** 529-32.

FOSTER, N. M. & JONES, R. H. 1979. Multiplication rate of bluetongue virus in the vector *Culicoides variipennis* (Diptera, Ceratopogonidae) infected orally. *Journal of Medical Entomology,* 15**,** 302-303.

FOSTER, N. M., JONES, R. H. & LUEDKE, A. J. 1968. Transmission of Attenuated and Virulent Bluetongue Virus with Culicoides Variipennis Infected Orally Via Sheep. *American Journal of Veterinary Research,* 29**,** 275-&.

FOSTER, N. M., JONES, R. H. & MCCRORY, B. R. 1963. Preliminary Investigations on Insect Transmission of Bluetongue Virus in Sheep. *Am J Vet Res,* 24**,** 1195-200.

FOXI, C. & DELRIO, G. 2010. Larval habitats and seasonal abundance of Culicoides biting midges found in association with sheep in northern Sardinia, Italy. *Medical and Veterinary Entomology,* 24**,** 199-209.

FREYVOGEL, T. A. & STAEUBLI, W. 1965. The Formation of the Peritrophic Membrane in Culicidae. *Acta Trop,* 22**,** 118-47.

FRIEDMAN, M. 1937. The use of ranks to avoid the assumption of normality implicit in the analysis of variance. *Journal of the American Statistical Association,* 32**,** 675-701.

FRISCHKNECHT, F., BALDACCI, P., MARTIN, B., ZIMMER, C., THIBERGE, S., OLIVO-MARIN, J. C., SHORTE, S. L. & MENARD, R. 2004. Imaging movement of malaria parasites during transmission by Anopheles mosquitoes. *Cell Microbiol,* 6**,** 687-94.

FROLOVA, E., GORCHAKOV, R., GARMASHOVA, N., ATASHEVA, S., VERGARA, L. A. & FROLOV, I. 2006. Formation of nsP3-specific protein complexes during Sindbis virus replication. *J Virol,* 80**,** 4122-34.

FU, H. 1995. *Mechanisms controlling the infection of Culicoides biting midges with bluetongue virus.* PhD, University of Hertfordshire.

FU, H., LEAKE, C. J., MERTENS, P. P. C. & MELLOR, P. S. 1999. The barriers to bluetongue virus infection, dissemination and transmission in the vector, *Culicoides variipennis* (Diptera : Ceratopogonidae). *Archives of Virology,* 144**,** 747-761.

FUKATSU, T., WATANABE, K. & SEKIGUCHI, Y. 1998. Specific detection of intracellular symbiotic bacteria of aphids by oligonucleotide-probed in situ hybridization. *Applied Entomology and Zoology,* 33**,** 461-472.

FUKUSHO, A., YU, Y., YAMAGUCHI, S. & ROY, P. 1989. Completion of the sequence of bluetongue virus serotype 10 by the characterization of a structural protein, VP6, and a non-structural protein, NS2. *J Gen Virol,* 70 (Pt 7)**,** 1677-89.

FUKUYAMA, S., KATSURA, H., ZHAO, D. M., OZAWA, M., ANDO, T., SHOEMAKER, J. E., ISHIKAWA, I., YAMADA, S., NEUMANN, G., WATANABE, S., KITANO, H. & KAWAOKA, Y. 2015. Multi-spectral fluorescent reporter influenza viruses (Color-flu) as powerful tools for in vivo studies. *Nature Communications,* 6.

FURUMOTO, W. A. & MICKEY, R. 1967. A Mathematical Model for Infectivity-Dilution Curve of Tobacco Mosaic Virus - Theoretical Considerations. *Virology,* 32**,** 216-&.

GAIDAMOVICH, S. Y., KHUTORETSKAYA, N. V., LVOVA, A. I. & SVESHNIKOVA, N. A. 1973. Immunofluorescent staining study of the salivary glands of mosquitoes infected with group A arboviruses. *Intervirology,* 1**,** 193-200.

GAIO, A. D., GUSMAO, D. S., SANTOS, A. V., BERBERT-MOLINA, M. A., PIMENTA, P. F. P. & LEMOS, F. J. A. 2011. Contribution of midgut bacteria to blood digestion and egg production in aedes aegypti (diptera: culicidae) (L.). *Parasites & Vectors,* 4.

GARRETT-JONES, C. 1964. Prognosis for Interruption of Malaria Transmission through Assessment of the Mosquito's Vectorial Capacity. *Nature,* 204**,** 1173-5.

GERRY, A. C. & MULLENS, B. A. 1998. Response of male Culicoides variipennis sonorensis (Diptera : Ceratopogonidae) to carbon dioxide and observations of mating behavior on and near cattle. *Journal of Medical Entomology,* 35**,** 239-244.

GERRY, A. C., MULLENS, B. A., MACLACHLAN, N. J. & MECHAM, J. O. 2001. Seasonal transmission of bluetongue virus by *Culicoides sonorensis* (Diptera: Ceratopogonidae) at a southern California dairy and evaluation of vectorial capacity as a predictor of bluetongue virus transmission. *Journal of Medical Entomology,* 38**,** 197-209.

GIRARD, Y. A., KLINGLER, K. A. & HIGGS, S. 2004. West Nile virus dissemination and tissue tropisms in orally infected Culex pipiens quinquefasciatus. *Vector-Borne and Zoonotic Diseases,* 4**,** 109-122.

GIRARD, Y. A., POPOV, V., WEN, J., HAN, V. & HIGGS, S. 2005. Ultrastructural study of West Nile virus pathogenesis in Culex pipiens quinquefasciatus (Diptera : Culicidae). *Journal of Medical Entomology,* 42**,** 429-444.

GIRARD, Y. A., SCHNEIDER, B. S., MCGEE, C. E., WEN, J., HAN, V. C., POPOV, V., MASON, P. W. & HIGGS, S. 2007. Salivary gland morphology and virus transmission during long-term cytopathologic West Nile virus infection in Culex mosquitoes. *American Journal of Tropical Medicine and Hygiene,* 76**,** 118-128.

GOIC, B., VODOVAR, N., MONDOTTE, J. A., MONOT, C., FRANGEUL, L., BLANC, H., GAUSSON, V., VERA-OTAROLA, J., CRISTOFARI, G. & SALEH, M. C. 2013. RNA-mediated interference and reverse transcription control the persistence of RNA viruses in the insect model Drosophila. *Nat Immunol,* 14**,** 396-403.

GOLD, S., MONAGHAN, P., MERTENS, P. & JACKSON, T. 2010. A Clathrin Independent Macropinocytosis-Like Entry Mechanism Used by Bluetongue Virus-1 during Infection of BHK Cells. *Plos One,* 5.

GOMEZ-MACHORRO, C., BENNETT, K. E., MUNOZ, M. D. & BLACK, W. C. 2004. Quantitative trait loci affecting dengue midgut infection barriers in an advanced intercross line of Aedes aegypti. *Insect Molecular Biology,* 13**,** 637-648.

GOUET, P., DIPROSE, J. M., GRIMES, J. M., MALBY, R., BURROUGHS, J. N., ZIENTARA, S., STUART, D. I. & MERTENS, P. P. 1999. The highly ordered double-stranded RNA genome of bluetongue virus revealed by crystallography. *Cell,* 97**,** 481-90.

GOULD, A. R. & HYATT, A. D. 1994. The Orbivirus Genus - Diversity, Structure, Replication and Phylogenetic-Relationships. *Comparative Immunology Microbiology and Infectious Diseases,* 17**,** 163-188.

GRAF, R. & BRIEGEL, H. 1989. The Synthetic Pathway of Trypsin in the Mosquito Aedes-Aegypti L (Diptera, Culicidae) and Invitro Stimulation in Isolated Midguts. *Insect Biochemistry,* 19**,** 129-137.

GREEN, S. B. 1991. How Many Subjects Does It Take to Do a Regression-Analysis. *Multivariate Behavioral Research,* 26**,** 499-510.

GRIMES, J., BASAK, A., ROY, P. & STUART, D. 1995. The crystal structure of bluetongue virus VP7. *Nature,* 373**,** 167-170.

GRIMES, J. M., BURROUGHS, J. N., GOUET, P., DIPROSE, J. M., MALBY, R., ZIENTARA, S., MERTENS, P. P. C. & STUART, D. I. 1998. The atomic structure of the bluetongue virus core. *Nature,* 395**,** 470-478.

GRIMSTAD, P. R. & HARAMIS, L. D. 1984. AEDES TRISERIATUS (DIPTERA: CULICIDAE) AND LA CROSSE VIRUS III. Enhanced oral transmission by nutrition-deprived mosquitoes. *Journal of Medical Entomology,* 21**,** 249-256.

GRIMSTAD, P. R., PAULSON, S. L. & CRAIG, G. B. 1985. Vector Competence of Aedes-Hendersoni (Diptera, Culicidae) for La Crosse Virus and Evidence of a Salivary-Gland Escape Barrier. *Journal of Medical Entomology,* 22**,** 447-453.

GRIMSTAD, P. R., ROSS, Q. E. & CRAIG, G. B. 1980. Aedes-Triseriatus (Diptera, Culicidae) and La Crosse Virus .2. Modification of Mosquito Feeding-Behavior by Virus-Infection. *Journal of Medical Entomology,* 17**,** 1-7.

GRIMSTAD, P. R. & WALKER, E. D. 1991. Aedes-Triseriatus (Diptera, Culicidae) and La-Crosse Virus .4. Nutritional Deprivation of Larvae Affects the Adult Barriers to Infection and Transmission. *Journal of Medical Entomology,* 28**,** 378-386.

GUDLA, P. R., NANDY, K., COLLINS, J., MEABURN, K. J., MISTELI, T. & LOCKETT, S. J. 2008. A high-throughput system for segmenting nuclei using multiscale techniques. *Cytometry A,* 73**,** 451-66.

GUIRAKHOO, F., CATALAN, J. A. & MONATH, T. P. 1995. Adaptation of bluetongue virus in mosquito cells results in overexpression of NS3 proteins and release of virus particles. *Arch Virol,* 140**,** 967-74.

GUTIERREZ, S., PIROLLES, E., YVON, M., BAECKER, V., MICHALAKIS, Y. & BLANC, S. 2015. The Multiplicity of Cellular Infection Changes Depending on the Route of Cell Infection in a Plant Virus. *J Virol,* 89**,** 9665-75.

HAMBLIN, C., SALT, J. S., GRAHAM, S. D., HOPWOOD, K. & WADE-EVANS, A. M. 1998. Bluetongue virus serotypes 1 and 3 infection in Poll Dorset sheep. *Aust Vet J,* 76**,** 622-9.

HAN, J. W., BRECKON, T. P., RANDELL, D. A. & LANDINI, G. 2012. The application of support vector machine classification to detect cell nuclei for automated microscopy. *Machine Vision and Applications,* 23**,** 15-24.

HARDY, J. L., HOUK, E. J., KRAMER, L. D. & REEVES, W. C. 1983. Intrinsic factors affecting vector competence of mosquitoes for arboviruses. *Annu Rev Entomol,* 28**,** 229-62.

HARRUP, L. E., PURSE, B. V., GOLDING, N., MELLOR, P. S. & CARPENTER, S. 2013. Larval development and emergence sites of farm-associated Culicoides in the United Kingdom. *Medical and Veterinary Entomology,* 27**,** 441-449.

HARVEY, J. M., CLARK, G. M., OSBORNE, C. K. & ALLRED, D. C. 1999. Estrogen receptor status by immunohistochemistry is superior to the ligand-binding assay for predicting response to adjuvant endocrine therapy in breast cancer. *Journal of Clinical Oncology,* 17**,** 1474-1481.

HASSAN, S. H., WIRBLICH, C., FORZAN, M. & ROY, P. 2001. Expression and functional characterization of bluetongue virus VP5 protein: Role in cellular permeabilization. *Journal of Virology,* 75**,** 8356-8367.

HATANAKA, Y., HASHIZUME, K., NITTA, K., KATO, T., ITOH, I. & TANI, Y. 2003. Cytometrical image analysis for immunohistochemical hormone receptor status in breast carcinomas. *Pathology International,* 53**,** 693-699.

HE, C. Q., DING, N. Z., HE, M., LI, S. N., WANG, X. M., HE, H. B., LIU, X. F. & GUO, H. S. 2010. Intragenic Recombination as a Mechanism of Genetic Diversity in Bluetongue Virus. *Journal of Virology,* 84**,** 11487-11495.

HERSHBERGER, R. V. 1946. Differential Stains of Insect Tissues. *Ohio Journal of Science,* 46**,** 152-162.

HIGGINS, D. G. & SHARP, P. M. 1988. Clustal - a Package for Performing Multiple Sequence Alignment on a Microcomputer. *Gene,* 73**,** 237-244.

HOCHBERG, Y. & TAMHANE, A. C. 1987. *Multiple Comparison Procedures.,* Hoboken, NJ, John Wiley & Sons.

HOFFMANN, J. A. 2003. The immune response of Drosophila. *Nature,* 426**,** 33-8.

HOFMANN, M. A., RENZULLO, S., MADER, M., CHAIGNAT, V., WORWA, G. & THUER, B. 2008. Genetic characterization of Toggenburg Orbivirus, a new bluetongue virus, from goats, Switzerland. *Emerging Infectious Diseases,* 14**,** 1855.

HOUK, E. J., ARCUS, Y. M., HARDY, J. L. & KRAMER, L. D. 1990. Binding of Western Equine Encephalomyelitis Virus to Brush-Border Fragments Isolated from Mesenteronal Epithelial-Cells of Mosquitos. *Virus Research,* 17**,** 105-118.

HOUK, E. J., HARDY, J. L. & CHILES, R. E. 1981. Permeability of the Midgut Basal Lamina in the Mosquito, Culex-Tarsalis Coquillett (Insecta, Diptera). *Acta Tropica,* 38**,** 163-171.

HOUK, E. J., OBIE, F. & HARDY, J. L. 1979. Peritrophic Membrane Formation and the Midgut Barrier to Arboviral Infection in the Mosquito, Culex-Tarsalis Coquillett (Insecta, Diptera). *Acta Tropica,* 36**,** 39-45.

HUANG, G., VERGNE, E. & GUBLER, D. J. 1992. Failure of dengue viruses to replicate in Culex quinquefasciatus (Diptera: Culicidae). *J Med Entomol,* 29**,** 911-4.

HUISMANS, H. 1979. Protein-Synthesis in Bluetongue Virus-Infected Cells. *Virology,* 92**,** 385-396.

HUISMANS, H. & ELS, H. 1979a. Characterisation of tubules associated with the replication of the different orbiviruses. *Virology,* 92**,** 397-406.

HUISMANS, H. & ELS, H. J. 1979b. Characterization of the tubules associated with the replication of three different orbiviruses. *Virology,* 92**,** 397-406.

HUNT, G. J., TABACHNICK, W. J. & MCKINNON, C. N. 1989. Environmental factors affecting mortality of adult *Culicoides variipennis* (Diptera: Ceratopogonidae) in the laboratory. *Journal of the American Mosquito Control Association,* 5**,** 387-391.

HUTCHEON, D. 1881. Fever of epizootic catarrh. . *Rep Coll Vet Surg,* 1880**,** 12-15.

HUTCHEON, D. 1902. Malarial catarrh fever of sheep. *Veterinary Record,* 14**,** 629-6.

ISAEV, V. A. 1974. Photoperiodic induction of the diapause in the egg phase of the blood-sucking midge, Culicoides pulicaris punctatus Mg. (Diptera,Ceratopogonidae). *Parazitologiia,* 9**,** 501-506.

IWANAGA, S. & LEE, B. L. 2005. Recent advances in the innate immunity of invertebrate animals. *J Biochem Mol Biol,* 38**,** 128-50.

JANZEN, H. G., RHODES, A. J. & DOANE, F. W. 1970. Chikungunya virus in salivary glands of Aedes aegypti (L.): an electron microscope study. *Can J Microbiol,* 16**,** 581-6.

JENCKEL, M., BREARD, E., SCHULZ, C., SAILLEAU, C., VIAROUGE, C., HOFFMANN, B., HOPER, D., BEER, M. & ZIENTARA, S. 2015. Complete coding genome sequence of putative novel bluetongue virus serotype 27. *Genome Announc,* 3.

JENNINGS, D. M. & MELLOR, P. S. 1987. Variation in the responses of Culicoides variipennis (Diptera, Ceratopogonidae) to oral infection with bluetongue virus. *Arch Virol,* 95**,** 177-82.

JIA, D. S., MAO, Q. Z., CHEN, H. Y., WANG, A. M., LIU, Y. Y., WANG, H. T., XIE, L. H. & WEI, T. Y. 2014. Virus-Induced Tubule: a Vehicle for Rapid Spread of Virions through Basal Lamina from Midgut Epithelium in the Insect Vector. *Journal of Virology,* 88**,** 10488-10500.

JOBLING, B. 1928. The structure of the head and mouth parts in Culicoides pulicaris, L.(Diptera Nematocera). *Bulletin of Entomological Research,* 18**,** 211-236.

JONES, R. H. 1967. An Overwintering Population of Culicoides in Colorado. *Journal of Medical Entomology,* 4**,** 461-&.

JONES, R. H. & FOSTER, N. M. 1971. Transovarian transmission of bluetongue virus unlikely for *Culicoides variipennis*. *Mosquito News,* 31**,** 434-437.

KAHN, C. & ANON, M. 2005. Bluetongue. *Merck Veterinary Manual.*

KATO, N., MUELLER, C. R., FUCHS, J. F., MCELROY, K., WESSELY, V., HIGGS, S. & CHRISTENSEN, B. M. 2008. Evaluation of the function of a type I peritrophic matrix as a physical barrier for midgut epithelium invasion by mosquito-borne pathogens in Aedes aegypti. *Vector Borne Zoonotic Dis,* 8**,** 701-12.

KAUFMAN, W. R., BOWMAN, A. S. & NUTTALL, P. A. 2001. Salivary fluid secretion in the ixodid tick Rhipicephalus appendiculatus is inhibited by Thogoto virus infection. *Experimental and Applied Acarology,* 25**,** 661-674.

KELLY, E. M., MOON, D. C. & BOWERS, D. F. 2012. Apoptosis in mosquito salivary glands: Sindbis virus-associated and tissue homeostasis. *Journal of General Virology,* 93**,** 2419-2424.

KEMP, C. & IMLER, J. L. 2009. Antiviral immunity in drosophila. *Curr Opin Immunol,* 21**,** 3-9.

KENNEY, J. L., ADAMS, A. P., GORCHAKOV, R., LEAL, G. & WEAVER, S. C. 2012. Genetic and Anatomic Determinants of Enzootic Venezuelan Equine Encephalitis Virus Infection of Culex (Melanoconion) taeniopus. *Plos Neglected Tropical Diseases,* 6.

KETTLE, D. S. 1977. Biology and Bionomics of Bloodsucking Ceratopogonids. *Annual Review of Entomology,* 22**,** 33-51.

KINGSOLVER, M. B., HUANG, Z. & HARDY, R. W. 2013. Insect antiviral innate immunity: pathways, effectors, and connections. *J Mol Biol,* 425**,** 4921-36.

KITTEL, C., SEREINIG, S., FERKO, B., STASAKOVA, J., ROMANOVA, J., WOLKERSTORFER, A., KATINGER, H. & EGOROV, A. 2004. Rescue of influenza virus expressing GFP from the NS1 reading frame. *Virology,* 324**,** 67-73.

KOGA, R., TSUCHIDA, T. & FUKATSU, T. 2009. Quenching autofluorescence of insect tissues for in situ detection of endosymbionts. *Applied Entomology and Zoology,* 44**,** 281-291.

KOZERA, B. & RAPACZ, M. 2013. Reference genes in real-time PCR. *Journal of Applied Genetics,* 54**,** 391-406.

KRAIBOOJ, K., SCHOELER, H., SVENSSON, C. M., BRAKHAGE, A. A. & FIGGE, M. T. 2015. Automated quantification of the phagocytosis of Aspergillus fumigatus conidia by a novel image analysis algorithm. *Front Microbiol,* 6**,** 549.

KRAMER, L. D., HARDY, J. L., PRESSER, S. B. & HOUK, E. J. 1981. Dissemination barriers for western equine encephalomyelitis virus in Culex tarsalis infected after ingestion of low viral doses. *Am J Trop Med Hyg,* 30**,** 190-7.

KUADKITKAN, A., WIKAN, N., FONGSARAN, C. & SMITH, D. R. 2010. Identification and characterization of prohibitin as a receptor protein mediating DENV-2 entry into insect cells. *Virology,* 406**,** 149-161.

KUBERSKI, T. 1979. Fluorescent-Antibody Studies on the Development of Dengue-2 Virus in Aedes-Albopictus (Diptera, Culicidae). *Journal of Medical Entomology,* 16**,** 343-349.

KUMBERGER, P., FREY, F., SCHWARZ, U. S. & GRAW, F. 2016. Multiscale modeling of virus replication and spread. *Febs Letters,* 590**,** 1972-1986.

KUMMERER, B. M., GRYWNA, K., GLASKER, S., WIESELER, J. & DROSTEN, C. 2012. Construction of an infectious Chikungunya virus cDNA clone and stable insertion of mCherry reporter genes at two different sites. *Journal of General Virology,* 93**,** 1991-1995.

KUSS, S. K., ETHEREDGE, C. A. & PFEIFFER, J. K. 2008. Multiple host barriers restrict poliovirus trafficking in mice. *PLoS Pathog,* 4**,** e1000082.

LAMBRECHTS, L. 2011. Quantitative genetics of Aedes aegypti vector competence for dengue viruses: towards a new paradigm? *Trends in Parasitology,* 27**,** 111-114.

LAMBRECHTS, L., PAAIJMANS, K. P., FANSIRI, T., CARRINGTON, L. B., KRAMER, L. D., THOMAS, M. B. & SCOTT, T. W. 2011. Impact of daily temperature fluctuations on dengue virus transmission by Aedes aegypti. *Proceedings of the National Academy of Sciences,* 108**,** 7460-7465.

LAMBRECHTS, L. & SCOTT, T. W. 2009. Mode of transmission and the evolution of arbovirus virulence in mosquito vectors. *Proceedings of the Royal Society of London B: Biological Sciences,* 276**,** 1369-1378.

LAN, H., WANG, H., CHEN, Q., CHEN, H., JIA, D., MAO, Q. & WEI, T. 2016. Small interfering RNA pathway modulates persistent infection of a plant virus in its insect vector. *Sci Rep,* 6**,** 20699.

LAVOIPIERRE, M. M. 1965. Feeding Mechanism of Blood-Sucking Arthropods. *Nature,* 208**,** 302-+.

LEE, J. H., ROWLEY, W. A. & PLATT, K. B. 2000. Longevity and spontaneous flight activity of Culex tarsalis (Diptera : Culicidae) infected with western equine encephalomyelitis virus. *Journal of Medical Entomology,* 37**,** 187-193.

LEE, J. W., CHU, J. J. & NG, M. L. 2006. Quantifying the specific binding between West Nile virus envelope domain III protein and the cellular receptor alphaVbeta3 integrin. *J Biol Chem,* 281**,** 1352-60.

LEE, R. C. H., HAPUARACHCHI, H. C., CHEN, K. C., HUSSAIN, K. M., CHEN, H. X., LOW, S. L., NG, L. C., LIN, R., NG, M. M. L. & CHU, J. J. H. 2013. Mosquito

Cellular Factors and Functions in Mediating the Infectious entry of Chikungunya Virus. *Plos Neglected Tropical Diseases,* 7.

LEMAITRE, B., KROMER-METZGER, E., MICHAUT, L., NICOLAS, E., MEISTER, M., GEORGEL, P., REICHHART, J. M. & HOFFMANN, J. A. 1995. A recessive mutation, immune deficiency (imd), defines two distinct control pathways in the Drosophila host defense. *Proc Natl Acad Sci U S A,* 92**,** 9465-9.

LERDTHUSNEE, K., ROMOSER, W. S., FARAN, M. E. & DOHM, D. J. 1995. Rift-Valley Fever Virus in the Cardia of Culex-Pipiens - an Immunocytochemical and Ultrastructural-Study. *American Journal of Tropical Medicine and Hygiene,* 53**,** 331-337.

LI, F., FENG, L., PAN, W., DONG, Z., LI, C., SUN, C. & CHEN, L. 2010. Generation of replication-competent recombinant influenza A viruses carrying a reporter gene harbored in the neuraminidase segment. *J Virol,* 84**,** 12075-81.

LIEMPI, A., CASTILLO, C., CERDA, M., DROGUETT, D., DUASO, J., BARAHONA, K., HERNANDEZ, A., DIAZ-LUJAN, C., FRETES, R., HARTEL, S. & KEMMERLING, U. 2015. Trypanosoma cruzi infectivity assessment in "in vitro" culture systems by automated cell counting. *Acta Trop,* 143**,** 47-50.

LIMA-CAMARA, T. N., BRUNO, R. V., LUZ, P. M., CASTRO, M. G., LOURENCO-DE-OLIVEIRA, R., SORGINE, M. H. & PEIXOTO, A. A. 2011a. Dengue infection increases the locomotor activity of Aedes aegypti females. *PLoS One,* 6**,** e17690.

LIMA-CAMARA, T. N., BRUNO, R. V., LUZ, P. M., CASTRO, M. G., LOURENCO-DE-OLIVEIRA, R., SORGINE, M. H. F. & PEIXOTO, A. A. 2011b. Dengue Infection Increases the Locomotor Activity of Aedes aegypti Females. *Plos One,* 6.

LINTHICUM, K. J., PLATT, K., MYINT, K. S., LERDTHUSNEE, K., INNI, B. L. & GHN, D. W. 1996. Dengue 3 virus distribution in the mosquito Aedes aegypti: an immunocytochemical study. . *Medical and Veterinary Entomology,* 10**,** 87-92.

LORD, C. C. & DAY, J. F. 2001. Simulation studies of St. Louis encephalitis virus in south Florida. *Vector Borne Zoonotic Dis,* 1**,** 299-315.

LORD, C. C., RUTLEDGE, C. R. & TABACHNICK, W. J. 2006. Relationships between host viremia and vector susceptibility for arboviruses. *Journal of Medical Entomology,* 43**,** 623-630.

LU, H. H., ALEXANDER, L. & WIMMER, E. 1995a. Construction and Genetic-Analysis of Dicistronic Polioviruses Containing Open Reading Frames for Epitopes of Human-Immunodeficiency-Virus Type-1 Gp120. *Journal of Virology,* 69**,** 4797-4806.

LU, H. H., LI, X. Y., CUCONATI, A. & WIMMER, E. 1995b. Analysis of Picornavirus 2a(Pro) Proteins - Separation of Proteinase from Translation and Replication Functions. *Journal of Virology,* 69**,** 7445-7452.

LU, P., BIAN, G., PAN, X. & XI, Z. 2012. Wolbachia induces density-dependent inhibition to dengue virus in mosquito cells. *PLoS Negl Trop Dis,* 6**,** e1754.

LUEDKE, A. J., JONES, R. H. & JOCHIM, M. M. 1967. Transmission of Bluetongue between Sheep and Cattle by Culicoides Variipennis. *American Journal of Veterinary Research,* 28**,** 457-&.

LUHKEN, R., STEINKE, S., HOPPE, N. & KIEL, E. 2015. Effects of temperature and photoperiod on the development of overwintering immature Culicoides chiopterus and C-dewulfi. *Veterinary Parasitology,* 214**,** 195-199.

LUPLERTLOP, N., SURASOMBATPATTANA, P., PATRAMOOL, S., DUMAS, E., WASINPIYAMONGKOL, L., SAUNE, L., HAMEL, R., BERNARD, E., SERENO, D., THOMAS, F., PIQUEMAL, D., YSSEL, H., BRIANT, L. & MISSE, D. 2011. Induction of a peptide with activity against a broad spectrum of pathogens in the Aedes aegypti salivary gland, following Infection with Dengue Virus. *PLoS Pathog,* 7**,** e1001252.

LYSYK, T. J. & DANYK, T. 2007. Effect of Temperature on Life History Parameters of Adult Culicoides sonorensis (Diptera: Ceratopogonidae) in Relation to Geographic Origin and Vectorial Capacity for Bluetongue Virus. *Journal of Medical Entomology,* 44**,** 741-751.

MAAN, N. S., MAAN, S., NOMIKOU, K., GUIMERA, M., PULLINGER, G., SINGH, K. P., BELAGANAHALLI, M. N. & MERTENS, P. P. C. 2012. The Genome Sequence of Bluetongue Virus Type 2 from India: Evidence for Reassortment between Eastern and Western Topotype Field Strains. *Journal of Virology,* 86**,** 5967-5968.

MAAN, S., MAAN, N. S., NOMIKOU, K., BATTEN, C., ANTONY, F., BELAGANAHALLI, M. N., SAMY, A. M., REDA, A. A., AL-RASHID, S. A., EL BATEL, M., OURA, C. A. & MERTENS, P. P. 2011. Novel bluetongue virus serotype from Kuwait. *Emerg Infect Dis,* 17**,** 886-9.

MAAN, S., MAAN, N. S., ROSS-SMITH, N., BATTEN, C. A., SHAW, A. E., ANTHONY, S. J., SAMUEL, A. R., DARPEL, K. E., VERONESI, E., OURA, C. A., SINGH, K. P., NOMIKOU, K., POTGIETER, A. C., ATTOUI, H., VAN ROOIJ, E., VAN RIJN, P., DE CLERCQ, K., VANDENBUSSCHE, F., ZIENTARA, S., BREARD, E., SAILLEAU, C., BEER, M., HOFFMAN, B., MELLOR, P. S. & MERTENS, P. P. 2008. Sequence analysis of bluetongue virus serotype 8 from the Netherlands 2006 and comparison to other European strains. *Virology,* 377**,** 308-18.

MACIEL-DE-FREITAS, R., SYLVESTRE, G., GANDINI, M. & KOELLA, J. C. 2013. The influence of dengue virus serotype-2 infection on Aedes aegypti (Diptera: Culicidae) motivation and avidity to blood feed. *PLoS One,* 8**,** e65252.

MACLACHLAN, N. J. 2004. Bluetongue: pathogenesis and duration of viraemia. *Vet Ital,* 40**,** 462-7.

MACLACHLAN, N. J. 2011. Bluetongue: History, global epidemiology, and pathogenesis. *Preventive Veterinary Medicine,* 102**,** 107-111.

MACLACHLAN, N. J. & OSBURN, B. I. 2006. Impact of bluetongue virus infection on the international movement and trade of ruminants. *J Am Vet Med Assoc,* 228**,** 1346-9.

MADDRELL, S. H. P. & GARDINER, B. O. C. 1980. The Permeability of the Cuticular Lining of the Insect Alimentary Canal. *Journal of Experimental Biology,* 85**,** 227-237.

MAGALHAES, T. 2014. What is the association of heme aggregates with the peritrophic matrix of adult female mosquitoes? *Parasites & Vectors,* 7.

MAHMOOD, F., CHILES, R. E., FANG, Y., GREEN, E. N. & REISEN, W. K. 2006. Effects of time after infection, mosquito genotype, and infectious viral dose on the dynamics of Culex tarsalis vector competence for western equine encephalomyelitis virus. *J Am Mosq Control Assoc,* 22**,** 272-81.

MALPICA, N., DE SOLORZANO, C. O., VAQUERO, J. J., SANTOS, A., VALLCORBA, I., GARCIA-SAGREDO, J. M. & DEL POZO, F. 1997. Applying watershed algorithms to the segmentation of clustered nuclei. *Cytometry,* 28**,** 289-97.

MANICASSAMY, B., MANICASSAMY, S., BELICHA-VILLANUEVA, A., PISANELLI, G., PULENDRAN, B. & GARCIA-SASTRE, A. 2010. Analysis of in vivo dynamics of influenza virus infection in mice using a GFP reporter virus. *Proceedings of the National Academy of Sciences of the United States of America,* 107**,** 11531-11536.

MARTINEZ-COSTAS, J., SUTTON, G., RAMADEVI, N. & ROY, P. 1998. Guanylyltransferase and RNA 5 '-triphosphatase activities of the purified expressed VP4 protein of bluetongue virus. *Journal of Molecular Biology,* 280**,** 859-866.

MATSUO, E. & ROY, P. 2013. Minimum Requirements for Bluetongue Virus Primary Replication In Vivo. *Journal of Virology,* 87**,** 882-889.

MATTHEWS, B. W. 1975. Comparison of the predicted and observed secondary structure of T4 phage lysozyme. *Biochim Biophys Acta,* 405**,** 442-51.

MATZ, M. V., LUKYANOV, K. A. & LUKYANOV, S. A. 2002. Family of the green fluorescent protein: journey to the end of the rainbow. *Bioessays,* 24**,** 953-959.

MCDERMOTT, E. G., MAYO, C. E., GERRY, A. C., LAUDIER, D., MACLACHLAN, J. & MULLENS, B. A. 2015. Bluetongue virus infection creates light averse Culicoides vectors and serious errors in transmission risk estimates. *Parasites & Vectors,* 8.

MCDERMOTT, E. G. & MULLENS, B. A. 2014. Desiccation Tolerance in the Eggs of the Primary North American Bluetongue Virus Vector, Culicoides sonorensis (Diptera: Ceratopogonidae), and Implications for Vector Persistence. *Journal of Medical Entomology,* 51**,** 1151-1158.

MCELROY, K. L., GIRARD, Y. A., MCGEE, C. E., TSETSARKIN, K. A., VANLANDINGHAM, D. L. & HIGGS, S. 2008. Characterization of the antigen distribution and tissue tropisms of three phenotypically distinct yellow fever virus variants in orally infected Aedes aegypti mosquitoes. *Vector Borne Zoonotic Dis,* 8**,** 675-87.

MCGEE, C. E., SHUSTOV, A. V., TSETSARKIN, K., FROLOV, I. V., MASON, P. W., VANLANDINGHAM, D. L. & HIGGS, S. 2010. Infection, dissemination, and transmission of a West Nile virus green fluorescent protein infectious clone by Culex pipiens quinquefasciatus mosquitoes. *Vector Borne Zoonotic Dis,* 10**,** 267-74.

MCKEEVER, S., HAGAN, D. V. & WANG, X. Y. 1994. Comparative-Study of Mouthparts of 4 Species of Culicoides from Tibet. *Medical and Veterinary Entomology,* 8**,** 255-264.

MCKEEVER, S., WRIGHT, M. D. & HAGAN, D. V. 1988. Mouthparts of Females of 4 Culicoides Species (Diptera, Ceratopogonidae). *Annals of the Entomological Society of America,* 81**,** 332-341.

MECH, F., THYWISSEN, A., GUTHKE, R., BRAKHAGE, A. A. & FIGGE, M. T. 2011. Automated image analysis of the host-pathogen interaction between phagocytes and Aspergillus fumigatus. *PLoS One,* 6**,** e19591.

MEGAHED, M. M. 1956. Anatomy and Histology of the Alimentary Tract of the Female of the Biting Midge Culicoides-Nubeculosus-Meigen (Diptera - Heleidae=Ceratopogonidae). *Parasitology,* 46**,** 22-47.

MEISWINKEL, R., GOMULSKI, L. M., DELECOLLE, J. C., GOFFREDO, M. & GASPERI, G. 2004. The taxonomy of Culicoides vector complexes - unfinished business. *Bluetongue, Pt 1, Proceedings,* 40**,** 151-159.

MEISWINKEL, R., NEVILL, E. & VENTER, G. 1994. Vectors: *Culicoides* spp. *In:* COETZER, J., THOMSON, G. & TUSTIN, R. (eds.) *Infectious Diseases of Livestock with Special Reference to Southern Africa.* Cape Town: Oxford University Press.

MELLOR, P. S. 1971. A membrane feeding technique for the infection of Culicoides tuberculosus Mg. and Culocoides variipennis sonorensis Cog. with Onchocerca cervicalis Rail. and Henry. *Trans R Soc Trop Med Hyg,* 65**,** 199-201.

MELLOR, P. S. 1990. The replication of bluetongue virus in *Culicoides* vectors. *Current Topics in Microbiology and Immunology,* 162**,** 143-161.

MELLOR, P. S. 2000. Replication of arboviruses in insect vectors. *Journal of Comparative Pathology,* 123**,** 231-247.

MELLOR, P. S., BOORMAN, J. & BAYLIS, M. 2000. *Culicoides* biting midges: their role as arbovirus vectors. *Annual Review of Entomology,* 45**,** 307-340.

MELLOR, P. S., RAWLINGS, P., BAYLIS, M. & WELLBY, M. P. 1998. Effect of temperature on African horse sickness virus infection in *Culicoides*. *Archives of Virology,* Suppl. 14 155-163.

MELZI, E., CAPORALE, M., ROCCHI, M., MARTIN, V., GAMINO, V., DI PROVVIDO, A., MARRUCHELLA, G., ENTRICAN, G., SEVILLA, N. & PALMARINI, M. 2016. Follicular dendritic cell disruption as a novel mechanism of virus-induced immunosuppression. *Proceedings of the National Academy of Sciences of the United States of America,* 113**,** E6238-E6247.

MENG, X., KHANUJA, B. S. & IP, Y. T. 1999. Toll receptor-mediated Drosophila immune response requires Dif, an NF-kappaB factor. *Genes Dev,* 13**,** 792-7.

MERCADO-CURIEL, R. F., BLACK, W. C. & MUNOZ, M. D. 2008. A dengue receptor as possible genetic marker of vector competence in Aedes aegypti. *Bmc Microbiology,* 8.

MERCADO-CURIEL, R. F., ESQUINCA-AVILES, H. A., TOVAR, R., DIAZ-BADILLO, A., CAMACHO-NUEZ, M. & MUNOZ, M. L. 2006. The four serotypes of dengue recognize the same putative receptors in Aedes aegypti midgut and Ae. albopictus cells. *Bmc Microbiology,* 6.

MERTENS, P., ATTOUI, H., DUNCAN, R. & DERMODY, T. S. 2005. Reoviridae. *In:* FAUQUET, C. M., MAYO, C. E., MANILOFF, J., DESSELBERGER, U. & BALL, L. A. (eds.) *Virus Taxonomy. Eighth Report of the International Committee on Taxonomy of Viruses.* . London: Elsevier Academic Press.

MERTENS, P. P., BURROUGHS, J. N., WALTON, A., WELLBY, M. P., FU, H., O'HARA, R. S., BROOKES, S. M. & MELLOR, P. S. 1996a. Enhanced infectivity of modified bluetongue virus particles for two insect cell lines and for two Culicoides vector species. *Virology,* 217**,** 582-93.

MERTENS, P. P. & DIPROSE, J. 2004. The bluetongue virus core: a nano-scale transcription machine. *Virus Res,* 101**,** 29-43.

MERTENS, P. P., DIPROSE, J., MAAN, S., SINGH, K. P., ATTOUI, H. & SAMUEL, A. R. 2004. Bluetongue virus replication, molecular and structural biology. *Vet Ital,* 40**,** 426-37.

MERTENS, P. P. C., BROWN, F. & SANGAR, D. V. 1984. Assignment of the Genome Segments of Bluetongue Virus Type-1 to the Proteins Which They Encode. *Virology,* 135**,** 207-217.

MERTENS, P. P. C., BURROUGHS, J. N., WALTON, A., WELLBY, M. P., FU, H., O'HARA, R. S., BROOKES, S. M. & MELLOR, P. S. 1996b. Enhanced infectivity of modified bluetongue virus particles for two insect cell lines and for two *Culicoides* vector species. *Virology,* 217**,** 582-593.

MERTENS, P. P. C., MAAN, N. S., PRASAD, G., SAMUEL, A. R., SHAW, A. E., POTGIETER, A. C., ANTHONY, S. J. & MAAN, S. 2007. Design of primers and use of RT-PCR assays for typing European bluetongue virus isolates: differentiation of field and vaccine strains. *Journal of General Virology,* 88**,** 2811-2823.

MERTENS, P. P. C., PEDLEY, S., COWLEY, J., BURROUGHS, J. N., CORTEYN, A. H., JEGGO, M. H., JENNINGS, D. M. & GORMAN, B. M. 1989. Analysis of the Roles of Bluetongue Virus Outer Capsid Protein-Vp2 and Protein-Vp5 in Determination of Virus Serotype. *Virology,* 170**,** 561-565.

MIKHAILOV, M., MONASTYRSKAYA, K., BAKKER, T. & ROY, P. 1996. A new form of particulate single and multiple immunogen delivery system based on recombinant bluetongue virus-derived tubules. *Virology,* 217**,** 323-331.

MILES, J. A. R., PILLAI, J. S. & MAGUIRE, T. 1973. Multiplication of Whataroa Virus in Mosquitos. *Journal of Medical Entomology,* 10**,** 176-185.

MILLER, B. R. & MITCHELL, C. J. 1991. Genetic selection of a flavivirus-refractory strain of the yellow fever mosquito Aedes aegypti. *Am J Trop Med Hyg,* 45**,** 399-407.

MILLER, B. R., MITCHELL, C. J. & BALLINGER, M. E. 1989. Replication, tissue tropisms and transmission of yellow fever virus in Aedes albopictus. *Trans R Soc Trop Med Hyg,* 83**,** 252-5.

MILLS, M. K., NAYDUCH, D. & MICHEL, K. 2015. Inducing RNA interference in the arbovirus vector, Culicoides sonorensis. *Insect Molecular Biology,* 24**,** 105-114.

MIYASHITA, S. & KISHINO, H. 2010. Estimation of the Size of Genetic Bottlenecks in Cell-to-Cell Movement of Soil-Borne Wheat Mosaic Virus and the Possible Role of the Bottlenecks in Speeding Up Selection of Variations in trans-Acting Genes or Elements. *Journal of Virology,* 84**,** 1828-1837.

MODROF, J., LYMPEROPOULOS, K. & ROY, P. 2005. Phosphorylation of bluetongue virus nonstructural protein 2 is essential for formation of viral inclusion bodies. *J Virol,* 79**,** 10023-31.

MONASTYRSKAYA, K., BOOTH, T., NEL, L. & ROY, P. 1994. Mutation of Either of 2 Cysteine Residues or Deletion of the Amino or Carboxy-Terminus of Nonstructural Protein Ns1 of Bluetongue Virus Abrogates Virus-Specified Tubule Formation in Insect Cells. *Journal of Virology,* 68**,** 2169-2178.

MONASTYRSKAYA, K., GOULD, E. A. & ROY, P. 1995. Characterization and Modification of the Carboxy-Terminal Sequences of Bluetongue Virus Type-10 Ns1 Protein in Relation to Tubule Formation and Location of an Antigenic Epitope in the Vicinity of the Carboxy-Terminus of the Protein. *Journal of Virology,* 69**,** 2831-2841.

MORADPOUR, D., EVANS, M. J., GOSERT, R., YUAN, Z. H., BLUM, H. E., GOFF, S. P., LINDENBACH, B. D. & RICE, C. M. 2004. Insertion of green fluorescent protein into nonstructural protein 5A allows direct visualization of functional hepatitis C virus replication complexes. *Journal of Virology,* 78**,** 7400-7409.

MOURY, B., FABRE, F. & SENOUSSI, R. 2007. Estimation of the number of virus particles transmitted by an insect vector. *Proceedings of the National Academy of Sciences of the United States of America,* 104**,** 17891-17896.

MOURYA, D. T., RANADIVE, S. N., GOKHALE, M. D., BARDE, P. V., PADBIDRI, V. S. & BANERJEE, K. 1998. Putative chikungunya virus specific receptor proteins on the midgut brush border membrane of Aedes aegypti mosquito. *Indian Journal of Medical Research,* 107**,** 10-14.

MUELLER, S. & WIMMER, E. 1998. Expression of foreign proteins by poliovirus polyprotein fusion: analysis of genetic stability reveals rapid deletions and formation of cardioviruslike open reading frames. *J Virol,* 72**,** 20-31.

MULLENS, B. A. 1987. Seasonal Size Variability in Culicoides-Variipennis (Diptera, Ceratopogonidae) in Southern-California. *Journal of the American Mosquito Control Association,* 3**,** 512-513.

MULLENS, B. A., GERRY, A. C., LYSYK, T. J. & SCHMIDTMANN, E. T. 2004. Environmental effects on vector competence and virogenesis of bluetongue virus in *Culicoides*: interpreting laboratory data in a field context. *Veterinaria Italia,* 40**,** 160-166.

MULLENS, B. A. & HOLBROOK, F. R. 1991. Temperature effects on the gonotrophic cycle of *Culicoides variipennis* (Diptera: Ceratopogonidae). *Journal of the American Mosquito Control Association,* 7**,** 588-591.

MULLENS, B. A. & RUTZ, D. A. 1983. Voltinism and Seasonal Abundance of Culicoides-Variipennis (Diptera, Ceratopogonidae) in Central New-York State. *Annals of the Entomological Society of America,* 76**,** 913-917.

MULLENS, B. A., TABACHNICK, W. J., HOLBROOK, F. R. & THOMPSON, L. H. 1995. Effects of temperature on virogenesis of bluetongue virus serotype 11 in *Culicoides variipennis sonorensis*. *Medical and Veterinary Entomology,* 9**,** 71-76.

MULLER, M. J. 1987. Transmission and in vitro excretion of bluetongue virus serotype 1 by inoculated Culicoides brevitarsis (Diptera: Ceratopogonidae). *J Med Entomol,* 24**,** 206-11.

MUNOZ-MUNOZ, F., TALAVERA, S. & PAGES, N. 2011. Geometric Morphometrics of the Wing in the Subgenus Culicoides (Diptera: Ceratopogonidae): From Practical Implications to Evolutionary Interpretations. *Journal of Medical Entomology,* 48**,** 129-139.

MUNOZ, M. D., CISNEROS, A., CRUZ, J., DAS, P., TOVAR, R. & ORTEGA, A. 1998. Putative dengue virus receptors from mosquito cells. *Fems Microbiology Letters,* 168**,** 251-258.

MYLES, K. M., PIERRO, D. J. & OLSON, K. E. 2003. Deletions in the putative cell receptor-binding domain of Sindbis virus strain MRE16 E2 glycoprotein reduce midgut infectivity in Aedes aegypti. *J Virol,* 77**,** 8872-81.

NAITZA, S., ROSSE, C., KAPPLER, C., GEORGEL, P., BELVIN, M., GUBB, D., CAMONIS, J., HOFFMANN, J. A. & REICHHART, J. M. 2002. The Drosophila immune defense against gram-negative infection requires the death protein dFADD. *Immunity,* 17**,** 575-81.

NAVARRO, A., TRASK, S. D. & PATTON, J. T. 2013. Generation of genetically stable recombinant rotaviruses containing novel genome rearrangements and heterologous sequences by reverse genetics. *J Virol,* 87**,** 6211-20.

NAYDUCH, D., ERRAM, D., LEE, M. B., ZUREK, L. & SASKI, C. A. 2015. Impact of the blood meal on humoral immunity and microbiota in the gut of female Culicoides sonorensis. *Veterinaria Italiana,* 51**,** 385-392.

NAYDUCH, D., LEE, M. B. & SASKI, C. A. 2014. The Reference Transcriptome of the Adult Female Biting Midge (Culicoides sonorensis) and Differential Gene Expression Profiling during Teneral, Blood, and Sucrose Feeding Conditions. *Plos One,* 9.

NELSON, R. L. & BELLAMY, R. E. 1971. Patterns of Flight Activity of Culicoides-Variipennis (Coquillett) (Diptera-Ceratopogonidae). *Journal of Medical Entomology,* 8**,** 283-&.

NEVILL, E. M. 1971. Cattle and Culicoides biting midges as possible overwintering hosts of bluetongue virus. *Onderstepoort Journal of Veterinary Research,* 38**,** 65-72.

NEWTON, S. E., SHORT, N. J. & DALGARNO, L. 1981. Bunyamwera Virus-Replication in Cultured Aedes-Albopictus (Mosquito) Cells - Establishment of a Persistent Viral-Infection. *Journal of Virology,* 38**,** 1015-1024.

NOMIKOU, K., HUGHES, J., WASH, R., KELLAM, P., BREARD, E., ZIENTARA, S., PALMARINI, M., BIEK, R. & MERTENS, P. 2015. Widespread Reassortment Shapes the Evolution and Epidemiology of Bluetongue Virus following European Invasion. *PLoS Pathog,* 11**,** e1005056.

NOVELLA, I. S., HERSHEY, C. L., ESCARMIS, C., DOMINGO, E. & HOLLAND, J. J. 1999. Lack of evolutionary stasis during alternating replication of an arbovirus in insect and mammalian cells. *J Mol Biol,* 287**,** 459-65.

NUCKOLS, J. T., ZIEGLER, S. A., HUANG, Y. J. S., MCAULEY, A. J., VANLANDINGHAM, D. L., KLOWDEN, M. J., SPRATT, H., DAVEY, R. A. & HIGGS, S. 2013. Infection of Aedes albopictus with Chikungunya Virus Rectally Administered by Enema. *Vector-Borne and Zoonotic Diseases,* 13**,** 103-110.

NUNAMAKER, R. A., SIEBURTH, P. J., DEAN, V. C., WIGINGTON, J. G., NUNAMAKER, C. E. & MECHAM, J. O. 1990. Absence of transovarial transmission of bluetongue virus in *Culicoides variipennis*: immunogold labelling of bluetongue virtus antigen in developing oocytes from *Culicoides variipennis* (Coquillett). *Comparative Biochemistry and Physiology A: Comparative Physiology,* 96**,** 19-31.

NUTTALL, P. A., JONES, L. D., LABUDA, M. & KAUFMAN, W. R. 1994. Adaptations of Arboviruses to Ticks. *Journal of Medical Entomology,* 31**,** 1-9.

O'NEILL, K., OLSON, B. J. S. C., HUANG, N., UNIS, D. & CLEM, R. J. 2015. Rapid selection against arbovirus-induced apoptosis during infection of a mosquito vector. *Proceedings of the National Academy of Sciences of the United States of America,* 112**,** E1152-E1161.

O'TOOLE, D., DE LEON, A. A. P., HEARNE, C., MCHOLLAND, L., YUN, L. & TABACHNICK, W. 2003. Papular dermatitis induced in guinea pigs by the biting midge Culicoides sonorensis (Diptera : Ceratopogonidae). *Journal of Veterinary Diagnostic Investigation,* 15**,** 67-71.

OIE 2006. Bluetongue in Germany, Bluetongue in The Netherlands, Office International des Epizooties (OIE) Disease Information.

OIE 2016. Updated Situation Assessment No.15. *In:* ROBERTS, H. (ed.) *Bluetongue virus (BTV-8) in France.* Department for Environment, Food and Rural Affairs.

ORIHEL, T. C. 1975. The peritrophic membrane: its role as a barrier to infection of the arthropod host. London: Academic Press Inc.

OSBORNE, C. J., MAYO, C. E., MULLENS, B. A., MCDERMOTT, E. G., GERRY, A. C., REISEN, W. K. & MACLACHLAN, N. J. 2015. Lack of Evidence for Laboratory and Natural Vertical Transmission of Bluetongue Virus in Culicoides sonorensis (Diptera: Ceratopogonidae). *J Med Entomol,* 52**,** 274-7.

OTSU, N. 1975. A threshold selection method from gray-level histograms. *Automatica,* 11**,** 23-27.

OVIEDO, M. V. N., ROMOSER, W. S., JAMES, C. B. L., MAHMOOD, F. & REISEN, W. K. 2011. Infection dynamics of western equine encephalomyelitis virus (Togaviridae: Alphavirus) in four strains of Culex tarsalis (Diptera: Culicidae): an immunocytochemical study. *Research and Reports in Tropical Medicine,* 2**,** 65-77.

OWENS, R. J., LIMN, C. & ROY, P. 2004. Role of an arbovirus nonstructural protein in cellular pathogenesis and virus release. *J Virol,* 78**,** 6649-56.

PAAIJMANS, K. P., BLANFORD, S., BELL, A. S., BLANFORD, J. I., READ, A. F. & THOMAS, M. B. 2010. Influence of climate on malaria transmission depends on daily temperature variation. *Proc Natl Acad Sci U S A,* 107.

PAAIJMANS, K. P., READ, A. F. & THOMAS, M. B. 2009. Understanding the link between malaria risk and climate. *Proc Natl Acad Sci U S A,* 106.

PALHA, N., GUIVEL-BENHASSINE, F., BRIOLAT, V., LUTFALLA, G., SOURISSEAU, M., ELLETT, F., WANG, C. H., LIESCHKE, G. J., HERBOMEL, P., SCHWARTZ, O. & LEVRAUD, J. P. 2013. Real-time whole-body visualization of Chikungunya Virus infection and host interferon response in zebrafish. *PLoS Pathog,* 9**,** e1003619.

PAN, X., ZHOU, G., WU, J., BIAN, G., LU, P., RAIKHEL, A. S. & XI, Z. 2012. Wolbachia induces reactive oxygen species (ROS)-dependent activation of the Toll pathway to control dengue virus in the mosquito Aedes aegypti. *Proc Natl Acad Sci U S A,* 109**,** E23-31.

PARADKAR, P. N., TRINIDAD, L., VOYSEY, R., DUCHEMIN, J. B. & WALKER, P. J. 2012. Secreted Vago restricts West Nile virus infection in Culex mosquito cells by activating the Jak-STAT pathway. *Proc Natl Acad Sci U S A,* 109**,** 18915-20.

PARIKH, G. R., OLIVER, J. D. & BARTHOLOMAY, L. C. 2009. A haemocyte tropism for an arbovirus. *Journal of General Virology,* 90**,** 292-296.

PARKER, M. D., AKEY, D. H. & LAUERMAN, L. H. 1978. Persistence of Enterobacteriaceae in Female Adults of Biting Gnat Culicoides-Variipennis (Diptera-Ceratopogonidae). *Journal of Medical Entomology,* 14**,** 597-598.

PASCOA, V., OLIVEIRA, P. L., DANSA-PETRETSKI, M., SILVA, J. R., ALVARENGA, P. H., JACOBS-LORENA, M. & LEMOS, F. J. 2002. Aedes aegypti peritrophic matrix and its interaction with heme during blood digestion. *Insect Biochem Mol Biol,* 32**,** 517-23.

PATEL, A., MOHL, B. P. & ROY, P. 2016. Entry of Bluetongue Virus Capsid Requires the Late Endosome-specific Lipid Lysobisphosphatidic Acid. *J Biol Chem,* 291**,** 12408-19.

PAULSON, S. L., GRIMSTAD, P. R. & CRAIG, G. B., JR. 1989. Midgut and salivary gland barriers to La Crosse virus dissemination in mosquitoes of the Aedes triseriatus group. *Med Vet Entomol,* 3**,** 113-23.

PAWESKA, J. T., VENTER, G. J. & MELLOR, P. S. 2002a. Vector competence of South African Culicoides species for bluetongue virus serotype 1 (BTV-1) with special reference to the effect of temperature on the rate of virus replication in C-imicola and C-bolitinos. *Medical and Veterinary Entomology,* 16**,** 10-21.

PAWESKA, J. T., VENTER, G. J. & MELLOR, P. S. 2002b. Vector competence of South African *Culicoides* species for bluetongue virus serotype 1 (BTV-1) with special reference to the effect of temperature on the rate of virus replication in *C. imicola* and *C. bolitinos*. *Medical and Veterinary Entomology,* 16**,** 10-21.

PEREZ, J. T., GARCIA-SASTRE, A. & MANICASSAMY, B. 2013. Insertion of a GFP reporter gene in influenza virus. *Curr Protoc Microbiol,* Chapter 15**,** Unit 15G 4.

PESKO, K. & MORES, C. N. 2009. Effect of Sequential Exposure on Infection and Dissemination Rates for West Nile and St. Louis Encephalitis Viruses in Culex quinquefasciatus. *Vector-Borne and Zoonotic Diseases,* 9**,** 281-286.

PESKO, K., WESTBROOK, C. J., MORES, C. N., LOUNIBOS, L. P. & REISKIND, M. H. 2009. Effects of infectious virus dose and bloodmeal delivery method on susceptibility of Aedes aegypti and Aedes albopictus to chikungunya virus. *J Med Entomol,* 46**,** 395-9.

PETERS, N. C., EGEN, J. G., SECUNDINO, N., DEBRABANT, A., KIMBLIN, N., KAMHAWI, S., LAWYER, P., FAY, M. P., GERMAIN, R. N. & SACKS, D. 2008. In vivo imaging reveals an essential role for neutrophils in leishmaniasis transmitted by sand flies. *Science,* 321**,** 970-4.

PIERSON, T. C., DIAMOND, M. S., AHMED, A. A., VALENTINE, L. E., DAVIS, C. W., SAMUEL, M. A., HANNA, S. L., PUFFER, B. A. & DOMS, R. W. 2005. An infectious West Nile virus that expresses a GFP reporter gene. *Virology,* 334**,** 28-40.

PLATT, K. B., LINTHICUM, K. J., MYINT, K. S. A., INNIS, B. L., LERDTHUSNEE, K. & VAUGHN, D. W. 1997a. Impact of dengue virus infection on feeding behavior of Aedes aegypti. *American Journal of Tropical Medicine and Hygiene,* 57**,** 119-125.

PLATT, K. B., LINTHICUM, K. J., MYINT, K. S. A., INNIS, B. L., LERDTHUSNEE, K. & VAUGHN, D. W. 1997b. Impact of dengue virus infection on feeding behaviour of Aedes aegypti. *American Journal of Tropical Medicine and Hygiene,* 57**,** 119-125.

PONGSIRI, A., PONLAWAT, A., THAISOMBOONSUK, B., JARMAN, R. G., SCOTT, T. W. & LAMBRECHTS, L. 2014a. Differential susceptibility of two field aedes aegypti populations to a low infectious dose of dengue virus. *PLoS One,* 9**,** e92971.

PONGSIRI, A., PONLAWAT, A., THAISOMBOONSUK, B., JARMAN, R. G., SCOTT, T. W. & LAMBRECHTS, L. 2014b. Differential Susceptibility of Two Field Aedes aegypti Populations to a Low Infectious Dose of Dengue Virus. *Plos One,* 9.

POWER, J., GREENFIELD, P. F., NIELSEN, L. & REID, S. 1992. Modeling the Growth and Protein-Production by Insect Cells Following Infection by a Recombinant Baculovirus in Suspension-Culture. *Cytotechnology,* 9**,** 149-155.

POWERS, M. W. 2011. Evaluation: from precision, recall and F-measure to ROC, informedness, markedness & correlation *Journal of Machine Learning Technologies,* 2**,** 37-63.

PRASAD, B. V. V., YAMAGUCHI, S. & ROY, P. 1992. 3-Dimensional Structure of Single-Shelled Bluetongue Virus. *Journal of Virology,* 66**,** 2135-2142.

PREIBISCH, S., SAALFELD, S. & TOMANCAK, P. 2009. Globally optimal stitching of tiled 3D microscopic image acquisitions. *Bioinformatics,* 25**,** 1463-1465.

PULLINGER, G. D., BUSQUETS, M. G., NOMIKOU, K., BOYCE, M., ATTOUI, H. & MERTENS, P. P. 2016. Identification of the Genome Segments of Bluetongue Virus Serotype 26 (Isolate KUW2010/02) that Restrict Replication in a Culicoides sonorensis Cell Line (KC Cells). *Plos One,* 11.

PURSE, B. V., MELLOR, P. S., ROGERS, D. J., SAMUEL, A. R., MERTENS, P. P. & BAYLIS, M. 2005. Climate change and the recent emergence of bluetongue in Europe. *Nat Rev Microbiol,* 3**,** 171-81.

RAMADEVI, N., BURROUGHS, N. J., MERTENS, P. P. C., JONES, I. M. & ROY, P. 1998. Capping and methylation of mRNA by purified recombinant VP4 protein of bluetongue virus. *Proceedings of the National Academy of Sciences of the United States of America,* 95**,** 13537-13542.

RAMADEVI, N. & ROY, P. 1998. Bluetongue virus core protein VP4 has nucleoside triphosphate phosphohydrolase activity. *Journal of General Virology,* 79**,** 2475-2480.

RAMIREZ, J. L. & DIMOPOULOS, G. 2010. The Toll immune signaling pathway control conserved anti-dengue defenses across diverse Ae. aegypti strains and against multiple dengue virus serotypes. *Dev Comp Immunol,* 34**,** 625-9.

RAMIREZ, J. L., SOUZA-NETO, J., COSME, R. T., ROVIRA, J., ORTIZ, A., PASCALE, J. M. & DIMOPOULOS, G. 2012. Reciprocal Tripartite Interactions between the Aedes aegypti Midgut Microbiota, Innate Immune System and Dengue Virus Influences Vector Competence. *Plos Neglected Tropical Diseases,* 6.

RAO, P. P., HEGDE, N. R., REDDY, Y. N., KRISHNAJYOTHI, Y., REDDY, Y. V., SUSMITHA, B., GOLLAPALLI, S. R., PUTTY, K. & REDDY, G. H. 2016. Epidemiology of Bluetongue in India. *Transboundary and Emerging Diseases,* 63**,** E151-E164.

RASBAND, W. 2002. NIH ImageJ. *Research Service Branch, National Institute of Mental Health, National Institute of Health, Bethesda, MD.*

RATINIER, M., CAPORALE, M., GOLDER, M., FRANZONI, G., ALLAN, K., NUNES, S. F., ARMEZZANI, A., BAYOUMY, A., RIXON, F., SHAW, A. & PALMARINI, M. 2011. Identification and Characterization of a Novel Non-Structural Protein of Bluetongue Virus. *Plos Pathogens,* 7.

REDDY, J. T. & LOCKE, M. 1990. The Size Limited Penetration of Gold Particles through Insect Basal Laminae. *Journal of Insect Physiology,* 36**,** 397-407.

REISEN, W. K., FANG, Y. & MARTINEZ, V. M. 2005. Avian host and mosquito (Diptera: Culicidae) vector competence determine the efficiency of West Nile and St. Louis encephalitis virus transmission. *J Med Entomol,* 42**,** 367-75.

REMM, H. 1988. Family Ceratopogonidae. *Catalogue of palaearctic Diptera,* 3**,** 11-110.

RICHARDS, A. G. & RICHARDS, P. A. 1971. Origin and Composition of Peritrophic Membrane of Mosquito, Aedes-Aegypti. *Journal of Insect Physiology,* 17**,** 2253-&.

RICHARDS, A. G. & RICHARDS, P. A. 1977. The peritrophic membranes of insects. *Annu Rev Entomol,* 22**,** 219-40.

RICHARDS, S. L., LORD, C. C., PESKO, K. & TABACHNICK, W. J. 2009. Environmental and biological factors influencing Culex pipiens quinquefasciatus Say (Diptera: Culicidae) vector competence for Saint Louis encephalitis virus. *Am J Trop Med Hyg,* 81**,** 264-72.

RICHARDS, S. L., MORES, C. N., LORD, C. C. & TABACHNICK, W. J. 2007. Impact of extrinsic incubation temperature and virus exposure on vector competence of Culex pipiens quinquefasciatus say (Diptera : Culicidae) for West Nile virus. *Vector-Borne and Zoonotic Diseases,* 7**,** 629-636.

ROERDINK, J. & MEIJSTER, A. 2001. The Watershed Transform: Definitions, Algorithms and Parallelization Strategies. *Fundamenta Informaticae,* 41**,** 187-228.

ROMOSER, S., TURELL, M. J., LERDTHUSNEE, K., NEIRA, A., DOHM, D., LUDWIG, G. & WASIELOSKI, L. 2005. Pathogenesis of Rift Valley fever virus in mosquitoes - tracheal conduits & the basal lamina as an extra-cellular barrier. *Archives of Virology***,** 89-100.

ROMOSER, W. S., FARAN, M. E. & BAILEY, C. L. 1987. Newly Recognized Route of Arbovirus Dissemination from the Mosquito (Diptera, Culicidae) Midgut. *Journal of Medical Entomology,* 24**,** 431-432.

ROMOSER, W. S., FARAN, M. E., BAILEY, C. L. & LERDTHUSNEE, K. 1992. An Immunocytochemical Study of the Distribution of Rift-Valley Fever Virus in the Mosquito Culex-Pipiens. *American Journal of Tropical Medicine and Hygiene,* 46**,** 489-501.

ROMOSER, W. S., WASIELOSKI, L. P., JR., PUSHKO, P., KONDIG, J. P., LERDTHUSNEE, K., NEIRA, M. & LUDWIG, G. V. 2004. Evidence for arbovirus dissemination conduits from the mosquito (Diptera: Culicidae) midgut. *J Med Entomol,* 41**,** 467-75.

ROSEN, L., SHROYER, D. A., TESH, R. B., FREIER, J. E. & LIEN, J. C. 1983. Transovarial transmission of dengue viruses by mosquitoes: Aedes albopictus and Aedes aegypti. *Am J Trop Med Hyg,* 32**,** 1108-19.

ROSEN, L., TESH, R. B., LIEN, J. C. & CROSS, J. H. 1978. Transovarial Transmission of Japanese Encephalitis-Virus by Mosquitos. *Science,* 199**,** 909-911.

ROSSIER, C., RAJU, R. & KOLAKOFSKY, D. 1988. Lacrosse Virus Gene-Expression in Mammalian and Mosquito Cells. *Virology,* 165**,** 539-548.

ROY, P. 1989. Bluetongue virus genetics and genome structure. *Virus Res,* 13**,** 179-206.

ROY, P. 2005. Bluetongue virus proteins and particles and their role in virus entry, assembly, and release. *Virus Structure and Assembly,* 64**,** 69-123.

ROY, P. 2008a. Bluetongue virus: dissection of the polymerase complex. *Journal of General Virology,* 89**,** 1789-1804.

ROY, P. 2008b. Functional mapping of bluetongue virus proteins and their interactions with host proteins during virus replication. *Cell Biochemistry and Biophysics,* 50**,** 143-157.

RUSSELL, R. C., OTRANTO, D. & WALL, R. 2013. *The encyclopedia of medical and veterinary entomology,* Wallingford, Oxfordshire, UK ; Boston, MA, CABI.

SABIN, L. R., ZHENG, Q., THEKKAT, P., YANG, J., HANNON, G. J., GREGORY, B. D., TUDOR, M. & CHERRY, S. 2013. Dicer-2 Processes Diverse Viral RNA Species. *Plos One,* 8.

SALAS-BENITO, J., VALLE, J. R. D., SALAS-BENITO, M., CEBALLOS-OLVERA, I., MOSSO, C. & DEL ANGEL, R. M. 2007. Evidence that the 45-kD glycoprotein, part of a putative dengue virus receptor complex in the mosquito cell line c6/36, is a heat-shock-related protein. *American Journal of Tropical Medicine and Hygiene,* 77**,** 283-290.

SALAZAR, M. I., RICHARDSON, J. H., SANCHEZ-VARGAS, I., OLSON, K. E. & BEATY, B. J. 2007. Dengue virus type 2: replication and tropisms in orally infected Aedes aegypti mosquitoes. *BMC Microbiol,* 7**,** 9.

SAMAL, S. K., ELHUSSEIN, A., HOLBROOK, F. R., BEATY, B. J. & RAMIG, R. F. 1987a. Mixed Infection of Culicoides-Variipennis with Bluetongue Virus Serotype-10 and Serotype 17 - Evidence for High-Frequency Reassortment in the Vector. *Journal of General Virology,* 68**,** 2319-2329.

SAMAL, S. K., LIVINGSTON, C. W., MCCONNELL, S. & RAMIG, R. F. 1987b. Analysis of Mixed Infection of Sheep with Bluetongue Virus Serotype-10 and Serotype-17 - Evidence for Genetic Reassortment in the Vertebrate Host. *Journal of Virology,* 61**,** 1086-1091.

SANCHEZ-VARGAS, I., SCOTT, J. C., POOLE-SMITH, B. K., FRANZ, A. W., BARBOSA-SOLOMIEU, V., WILUSZ, J., OLSON, K. E. & BLAIR, C. D. 2009. Dengue virus type 2 infections of Aedes aegypti are modulated by the mosquito's RNA interference pathway. *PLoS Pathog,* 5**,** e1000299.

SANDERS, H. R., FOY, B. D., EVANS, A. M., ROSS, L. S., BEATY, B. J., OLSON, K. E. & GILL, S. S. 2005. Sindbis virus induces transport processes and alters expression of innate immunity pathway genes in the midgut of the disease vector, Aedes aegypti. *Insect Biochemistry and Molecular Biology,* 35**,** 1293-1307.

SCHMID-HEMPEL, P. 2005. Evolutionary ecology of insect immune defenses. *Annual Review of Entomology,* 50**,** 529-551.

SCHMIDTMANN, E. T., HERRERO, M. V., GREEN, A. L., DARGATZ, D. A., RODRIQUEZ, J. M. & WALTON, T. E. 2011. Distribution of Culicoides sonorensis (Diptera: Ceratopogonidae) in Nebraska, South Dakota, and North Dakota: Clarifying the Epidemiology of Bluetongue Disease in the Northern Great Plains Region of the United States. *Journal of Medical Entomology,* 48**,** 634-643.

SCHNEIDER, B. S. & HIGGS, S. 2008. The enhancement of arbovirus transmission and disease by mosquito saliva is associated with modulation of the host immune

response. *Transactions of the Royal Society of Tropical Medicine and Hygiene,* 102**,** 400-408.

SCHNEIDER, B. S., SOONG, L., ZEIDNER, N. S. & HIGGS, S. 2004. Aedes aegypti salivary gland extracts modulate anti-viral and TH1/TH2 cytokine responses to sindbis virus infection. *Viral Immunol,* 17**,** 565-73.

SCHNEIDER, J. R., MORI, A., ROMERO-SEVERSON, J., CHADEE, D. D. & SEVERSON, D. W. 2007. Investigations of dengue-2 susceptibility and body size among Aedes aegypti populations. *Medical and Veterinary Entomology,* 21**,** 370-376.

SCHNETTLER, E., RATINIER, M., WATSON, M., SHAW, A. E., MCFARLANE, M., VARELA, M., ELLIOTT, R. M., PALMARINI, M. & KOHL, A. 2013. RNA interference targets arbovirus replication in Culicoides cells. *J Virol,* 87**,** 2441-54.

SCHOLLE, F., GIRARD, Y. A., ZHAO, Q. Z., HIGGS, S. & MASON, P. W. 2004. trans-packaged West Nile virus-like particles: Infectious properties in vitro and in infected mosquito vectors. *Journal of Virology,* 78**,** 11605-11614.

SCHULZ, C., BREARD, E., SAILLEAU, C., JENCKEL, M., VIAROUGE, C., VITOUR, D., PALMARINI, M., GALLOIS, M., HOPER, D., HOFFMANN, B., BEER, M. & ZIENTARA, S. 2016. Bluetongue virus serotype 27: detection and characterization of two novel variants in Corsica, France. *Journal of General Virology,* 97**,** 2073-2083.

SCOTT, T. W., HILDRETH, S. W. & BEATY, B. J. 1984. The distribution and development of eastern equine encephalitis virus in its enzootic mosquito vector, Culiseta melanura. *Am J Trop Med Hyg,* 33**,** 300-10.

SEAGO, J., JULEFF, N., MOFFAT, K., BERRYMAN, S., CHRISTIE, J. M., CHARLESTON, B. & JACKSON, T. 2013. An infectious recombinant foot-and-mouth disease virus expressing a fluorescent marker protein. *Journal of General Virology,* 94**,** 1517-1527.

SEBLOVA, V., SADLOVA, J., VOJTKOVA, B., VOTYPKA, J., CARPENTER, S., BATES, P. A. & VOLF, P. 2015. The Biting Midge Culicoides sonorensis (Diptera: Ceratopogonidae) Is Capable of Developing Late Stage Infections of Leishmania enriettii. *Plos Neglected Tropical Diseases,* 9.

SELLERS, R. F. & MELLOR, P. S. 1993. Temperature and the persistence of viruses in *Culicoides* spp. during adverse conditions. *Revue Scientifique et Technique de l'Office International des Epizooties,* 12**,** 733-755.

SHANER, N. C., STEINBACH, P. A. & TSIEN, R. Y. 2005. A guide to choosing fluorescent proteins. *Nature Methods,* 2**,** 905-909.

SHAW, A. E., MONAGHAN, P., ALPAR, H. O., ANTHONY, S., DARPEL, K. E., BATTEN, C. A., CARPENTER, S., JONES, H., OURA, C. A. L., KING, D. P., ELLIOT, H., MELLOR, P. S. & MERTENS, P. P. C. 2007a. Development and validation of a real-time RT-PCR assay to detect genome bluetongue virus segment 1. *Journal of Virological Methods,* 145**,** 115-126.

SHAW, A. E., MONAGHAN, P., ALPAR, H. O., ANTHONY, S., DARPEL, K. E., BATTEN, C. A., GUERCIO, A., ALIMENA, G., VITALE, M., BANKOWSKA, K., CARPENTER, S., JONES, H., OURA, C. A. L., KING, D. P., ELLIOTT, H., MELLOR, P. S. & MERTENS, P. P. C. 2007b. Development and initial evaluation of a real-time RT-PCR assay to detect bluetongue virus genome segment 1. *Journal of Virological Methods,* 145**,** 115-126.

SHAW, A. E., VERONESI, E., MAURIN, G., FTAICH, N., GUIGUEN, F., RIXON, F., RATINIER, M., MERTENS, P., CARPENTER, S., PALMARINI, M., TERZIAN, C. & ARNAUD, F. 2012. Drosophila melanogaster as a Model Organism for Bluetongue Virus Replication and Tropism. *Journal of Virology,* 86**,** 9015-9024.

SHIN, D., CIVANA, A., ACEVEDO, C. & SMARTT, C. T. 2014. Transcriptomics of differential vector competence: West Nile virus infection in two populations of Culex pipiens quinquefasciatus linked to ovary development. *Bmc Genomics,* 15.

SIEBURTH, P. J., NUNAMAKER, C. E., ELLIS, J. & NUNAMAKER, R. A. 1991. Infection of the Midgut of Culicoides-Variipennis (Diptera, Ceratopogonidae) with Bluetongue Virus. *Journal of Medical Entomology,* 28**,** 74-85.

SIM, S., JUPATANAKUL, N., RAMIREZ, J. L., KANG, S., ROMERO-VIVAS, C. M., MOHAMMED, H. & DIMOPOULOS, G. 2013. Transcriptomic Profiling of Diverse Aedes aegypti Strains Reveals Increased Basal-level Immune Activation in Dengue Virus-refractory Populations and Identifies Novel Virus-vector Molecular Interactions. *Plos Neglected Tropical Diseases,* 7.

SIM, S., RAMIREZ, J. L. & DIMOPOULOS, G. 2012. Dengue Virus Infection of the Aedes aegypti Salivary Gland and Chemosensory Apparatus Induces Genes that Modulate Infection and Blood-Feeding Behavior. *Plos Pathogens,* 8.

SMITH, D. R., ADAMS, A. P., KENNEY, J. L., WANG, E. & WEAVER, S. C. 2008. Venezuelan equine encephalitis virus in the mosquito vector Aedes taeniorhynchus: infection initiated by a small number of susceptible epithelial cells and a population bottleneck. *Virology,* 372**,** 176-86.

SMITH, D. R., ARRIGO, N. C., LEAL, G., MUEHLBERGER, L. E. & WEAVER, S. C. 2007. Infection and dissemination of Venezuelan equine encephalitis virus in the

epidemic mosquito vector, Aedes taeniorhynchus. *American Journal of Tropical Medicine and Hygiene,* 77**,** 176-187.

SMITH, E. C., SEXTON, N. R. & DENISON, M. R. 2014. Thinking Outside the Triangle: Replication Fidelity of the Largest RNA Viruses. *Annu Rev Virol,* 1**,** 111-32.

SOUZA-NETO, J. A., SIM, S. & DIMOPOULOS, G. 2009. An evolutionary conserved function of the JAK-STAT pathway in anti-dengue defense. *Proc Natl Acad Sci U S A,* 106**,** 17841-6.

SPEARMAN, C. 1908. The method of 'right and wrong cases' ('constant stimuli') without Gauss formulae. *Br. J.Phychol.,* 2**,** 227-242.

SPREULL, J. 1905. Malarial catarrhal fever (bluetongue) of sheep in South Africa. *Journal of Comparative Pathology,* 18**,** 321-337.

SRIURAIRATNA, S. & BHAMARAPRAVATI, N. 1977. Replication of Dengue-2 Virus in Aedes-Albopictus Mosquitos - Electron-Microscopic Study. *American Journal of Tropical Medicine and Hygiene,* 26**,** 1199-1205.

ST GEORGE, T. D., STANDFAST, H. A., CYBINSKI, D. H., DYCE, A. L., MULLER, M. J., DOHERTY, R. L., CARLEY, J. G., FILIPPICH, C. & FRAZIER, C. L. 1978. The isolation of a bluetongue virus from Culicoides collected in the Northern Territory of Australia. *Aust Vet J,* 54**,** 153-4.

STAUBER, N., MARTINEZ-COSTAS, J., SUTTON, G., MONASTYRSKAYA, K. & ROY, P. 1997. Bluetongue virus VP6 protein binds ATP and exhibits an RNA-dependent ATPase function and a helicase activity that catalyze the unwinding of double-stranded RNA substrates. *J Virol,* 71**,** 7220-6.

STEVENS, L. 2016. *Understanding the early events in Bluetongue virus cell entry.* . Doctor of Philosophy, University of Surrey.

STEWART, M., HARDY, A., BARRY, G., PINTO, R. M., CAPORALE, M., MELZI, E., HUGHES, J., TAGGART, A., JANOWICZ, A., VARELA, M., RATINIER, M. & PALMARINI, M. 2015. Characterization of a second open reading frame in genome segment 10 of bluetongue virus. *Journal of General Virology,* 96**,** 3280-3293.

STYER, L. M., LIM, P. Y., LOUIE, K. L., ALBRIGHT, R. G., KRAMER, L. D. & BERNARD, K. A. 2011. Mosquito Saliva Causes Enhancement of West Nile Virus Infection in Mice. *Journal of Virology,* 85**,** 1517-1527.

SUMANOCHITRAPON, W., STRICKMAN, D., SITHIPRASASNA, R., KITTAYAPONG, P. & INNIS, B. L. 1998. Effect of size and geographic origin of Aedes aegypti on oral infection with Dengue-2 virus. *American Journal of Tropical Medicine and Hygiene,* 58**,** 283-286.

SUTCLIFFE, J. F. & DEEPAN, P. D. 1988. Anatomy and Function of the Mouthparts of the Biting Midge, Culicoides-Sanguisuga (Diptera, Ceratopogonidae). *Journal of Morphology,* 198**,** 353-365.

SUWANMANEE, S., CHAISRI, U., WASINPIYAMONGKOL, L. & LUPLERTLOP, N. 2009. Peritrophic membrane structure of Aedes aegypti (Diptera: Culicidae) mosquitoes after infection with dengue virus type 2 (D2-16681). *Applied Entomology and Zoology,* 44**,** 257-265.

TABACHNICK, W. J. 1991. Genetic control of oral susceptibility to infection of *Culicoides variipennis* with bluetongue virus. *American Journal of Tropical Medicine and Hygiene,* 45**,** 666-671.

TABACHNICK, W. J. 1996. Culicoides variipennis and bluetongue-virus epidemiology in the United States. *Annu Rev Entomol,* 41**,** 23-43.

TABACHNICK, W. J. 2004. *Culicoides* and the global epidemiology of bluetongue virus infection. *Veterinaria Italia,* 40**,** 145-150.

TAMBERG, N., LULLA, V., FRAGKOUDIS, R., LULLA, A., FAZAKERLEY, J. K. & MERITS, A. 2007. Insertion of EGFP into the replicase gene of Semliki Forest virus results in a novel, genetically stable marker virus. *Journal of General Virology,* 88**,** 1225-1230.

TAN, B. H., NASON, E., STAEUBER, N., JIANG, W. R., MONASTRYRSKAYA, K. & ROY, P. 2001. RGD tripeptide of bluetongue virus VP7 protein is responsible for core attachment to Culicoides cells. *Journal of Virology,* 75**,** 3937-3947.

TCHANKOUO-NGUETCHEU, S., BOURGUET, E., LENORMAND, P., ROUSSELLE, J. C., NAMANE, A. & CHOUMET, V. 2012. Infection by chikungunya virus modulates the expression of several proteins in Aedes aegypti salivary glands. *Parasites & Vectors,* 5.

TCHANKOUO-NGUETCHEU, S., KHUN, H., PINCET, L., ROUX, P., BAHUT, M., HUERRE, M., GUETTE, C. & CHOUMET, V. 2010. Differential protein modulation in midguts of Aedes aegypti infected with chikungunya and dengue 2 viruses. *PLoS One,* 5.

TETERINA, N. L., LEVENSON, E. A. & EHRENFELD, E. 2010. Viable polioviruses that encode 2A proteins with fluorescent protein tags. *J Virol,* 84**,** 1477-88.

THEERA-UMPON, N. & DHOMPONGSA, S. 2007. Morphological granulometric features of nucleus in automatic bone marrow white blood cell classification. *Ieee Transactions on Information Technology in Biomedicine,* 11**,** 353-359.

THEILER, A. 1904. Bluetongue in sheep. *Annual report of the Director of Agriculture, Transvaal for 1905***,** 110-121.

THEILER, A. & DOWNES, B. 1973. *The Arthropod-Borne Viruses of Vertebrates,* New Haven, Yale University Press.

THIMM, T. & TEBBE, C. C. 2003. Protocol for rapid fluorescence in situ hybridization of bacteria in cryosections of microarthropods. *Applied and Environmental Microbiology,* 69**,** 2875-2878.

THOMAS, C. P., BOOTH, T. F. & ROY, P. 1990. Synthesis of bluetongue virus-encoded phosphoprotein and formation of inclusion bodies by recombinant baculovirus in insect cells: it binds the single-stranded RNA species. *J Gen Virol,* 71 (Pt 9)**,** 2073-83.

TRAN, V., MOSER, L. A., POOLE, D. S. & MEHLE, A. 2013. Highly sensitive real-time in vivo imaging of an influenza reporter virus reveals dynamics of replication and spread. *J Virol,* 87**,** 13321-9.

TROMAS, N., ZWART, M. P., LAFFORGUE, G. & ELENA, S. F. 2014. Within-Host Spatiotemporal Dynamics of Plant Virus Infection at the Cellular Level. *PLoS Genet,* 10**,** e1004186.

TSIEN, R. Y. 1998. The green fluorescent protein. *Annual Review of Biochemistry,* 67**,** 509-544.

TURELL, M., DOHM, D., SARDELIS, M., O GUINN, M., ANDREADIS, T. & BLOW, J. 2005. An update on the potential of North American mosquitoes (Diptera: Culicidae) to transmit West Nile virus. *Journal of Medical Entomology,* 42**,** 57-62.

TURELL, M. J. & LUNDSTROM, J. O. 1990. EFFECT OF ENVIRONMENTAL-TEMPERATURE ON THE VECTOR COMPETENCE OF AEDES-AEGYPTI AND AE-TAENIORHYNCHUS FOR OCKELBO VIRUS. *American Journal of Tropical Medicine and Hygiene,* 43**,** 543-550.

URAKAWA, T., RITTER, D. G. & ROY, P. 1989. Expression of Largest Rna Segment and Synthesis of Vp1 Protein of Bluetongue Virus in Insect Cells by Recombinant Baculovirus - Association of Vp1 Protein with Rna-Polymerase Activity. *Nucleic Acids Research,* 17**,** 7395-7401.

URAKAWA, T. & ROY, P. 1988a. Bluetongue Virus Tubules Made in Insect Cells by Recombinant Baculoviruses - Expression of the Ns1-Gene of Bluetongue Virus Serotype-10. *Journal of Virology,* 62**,** 3919-3927.

URAKAWA, T. & ROY, P. 1988b. Bluetongue virus tubules made in insect cells by recombinant baculoviruses: expression of the NS1 gene of bluetongue virus serotype 10. *J Virol,* 62**,** 3919-27.

VAIDYANATHAN, R. & SCOTT, T. W. 2006. Apoptosis in mosquito midgut epithelia associated with West Nile virus infection. *Apoptosis,* 11**,** 1643-1651.

VAN DEN HURK, A. F., HALL-MENDELIN, S., PYKE, A. T., FRENTIU, F. D., MCELROY, K., DAY, A., HIGGS, S. & O'NEILL, S. L. 2012. Impact of Wolbachia on Infection with Chikungunya and Yellow Fever Viruses in the Mosquito Vector Aedes aegypti. *Plos Neglected Tropical Diseases,* 6.

VAN DIJK, A. A. & HUISMANS, H. 1988. In vitro transcription and translation of bluetongue virus mRNA. *J Gen Virol,* 69 (Pt 3)**,** 573-81.

VAUGHAN, J. A. & TURNER, E. C. 1987. Development of Immature Culicoides-Variipennis (Diptera, Ceratopogonidae) from Saltville, Virginia, at Constant Laboratory Temperatures. *Journal of Medical Entomology,* 24**,** 390-395.

VAZEILLE, M., MOUTAILLER, S., COUDRIER, D., ROUSSEAUX, C., KHUN, H., HUERRE, M., THIRIA, J., DEHECQ, J. S., FONTENILLE, D., SCHUFFENECKER, I., DESPRES, P. & FAILLOUX, A. B. 2007. Two Chikungunya isolates from the outbreak of La Reunion (Indian Ocean) exhibit different patterns of infection in the mosquito, Aedes albopictus. *PLoS One,* 2**,** e1168.

VENTER, G. J., PAWESKA, J. T., VAN DIJK, A. A., MELLOR, P. S. & TABACHNICK, W. J. 1998. Vector competence of *Culicoides bolitinos* and *C. imicola* for South African bluetongue virus serotypes 1, 3, and 4. *Medical and Veterinary Entomology,* 12**,** 378-385.

VERONESI, E., ANTONY, F., GUBBINS, S., GOLDING, N., BLACKWELL, A., MERTENS, P. P., BROWNLIE, J., DARPEL, K. E., MELLOR, P. S. & CARPENTER, S. 2013. Measurement of the infection and dissemination of bluetongue virus in culicoides biting midges using a semi-quantitative rt-PCR assay and isolation of infectious virus. *PLoS One,* 8**,** e70800.

VERONESI, E., MERTENS, P. P. C., SHAW, A. E., BROWNLIE, J., MELLOR, P. S. & CARPENTER, S. T. 2008. Quantifying bluetongue virus in adult Culicoides biting midges (Diptera : Ceratopogonidae). *Journal of Medical Entomology,* 45**,** 129-132.

VERONESI, E., VENTER, G. J., LABUSCHAGNE, K., MELLOR, P. S. & CARPENTER, S. 2009. Life-history parameters of Culicoides (Avaritia) imicola Kieffer in the laboratory at different rearing temperatures. *Vet Parasitol,* 163**,** 370-3.

VIDAL, S., KHUSH, R. S., LEULIER, F., TZOU, P., NAKAMURA, M. & LEMAITRE, B. 2001. Mutations in the Drosophila dTAK1 gene reveal a conserved function for MAPKKKs in the control of rel/NF-kappaB-dependent innate immune responses. *Genes Dev,* 15**,** 1900-12.

VILLALON, J. M., GHOSH, A. & JACOBS-LORENA, M. 2003. The peritrophic matrix limits the rate of digestion in adult Anopheles stephensi and Aedes aegypti mosquitoes. *J Insect Physiol,* 49**,** 891-5.

VON STETTEN, D., NOIRCLERC-SAVOYE, M., GOEDHART, J., GADELLA, T. W. J. & ROYANT, A. 2012. Structure of a fluorescent protein from Aequorea victoria bearing the obligate-monomer mutation A206K. *Acta Crystallographica Section F-Structural Biology and Crystallization Communications,* 68**,** 878-882.

WAHLBY, C., SINTORN, I. M., ERLANDSSON, F., BORGEFORS, G. & BENGTSSON, E. 2004. Combining intensity, edge and shape information for 2D and 3D segmentation of cell nuclei in tissue sections. *Journal of Microscopy,* 215**,** 67-76.

WALKER, A. R. 2001. Age structure of a population of Ixodes ricinus (Acari : Ixodidae) in relation to its seasonal questing. *Bulletin of Entomological Research,* 91**,** 69-78.

WALTON, T. E. 2004. The history of bluetongue and a current global overview. *Bluetongue, Pt 1, Proceedings,* 40**,** 31-38.

WANG, H., GORT, T., BOYLE, D. L. & CLEM, R. J. 2012. Effects of Manipulating Apoptosis on Sindbis Virus Infection of Aedes aegypti Mosquitoes. *Journal of Virology,* 86**,** 6546-6554.

WANG, Z. M., ZHANG, X. L., LI, C. X., ZHANG, Y. M., XIN, D. & ZHAO, T. Y. 2010. Dissemination of western equine encephalomyelitis virus in the potential vector, Culex pipiens pallens. *Journal of Vector Ecology,* 35**,** 313-317.

WATTS, D. M., PANTUWATANA, S., DEFOLIART, G. R., YUILL, T. M. & THOMPSON, W. H. 1973. Transovarial transmission of LaCrosse virus (California encephalitis group) in the mosquito, Aedes triseriatus. *Science,* 182**,** 1140-1.

WEAVER, S. C. 1986. Electron-Microscopic Analysis of Infection Patterns for Venezuelan Equine Encephalomyelitis Virus in the Vector Mosquito, Culex (Melanoconion) Taeniopus. *American Journal of Tropical Medicine and Hygiene,* 35**,** 624-631.

WEAVER, S. C., SCHERER, W. F., CUPP, E. W. & CASTELLO, D. A. 1984. Barriers to Dissemination of Venezuelan Encephalitis Viruses in the Middle American Enzootic Vector Mosquito, Culex (Melanoconion) Taeniopus. *American Journal of Tropical Medicine and Hygiene,* 33**,** 953-960.

WEAVER, S. C., SCOTT, T. W. & LORENZ, L. H. 1990. Patterns of Eastern Equine Encephalomyelitis Virus-Infection in Culiseta-Melanura (Diptera, Culicidae). *Journal of Medical Entomology,* 27**,** 878-891.

WEAVER, S. C., SCOTT, T. W., LORENZ, L. H., LERDTHUSNEE, K. & ROMOSER, W. S. 1988. Togavirus-Associated Pathologic-Changes in the Midgut of a Natural Mosquito Vector. *Journal of Virology,* 62**,** 2083-2090.

WEAVER, S. C., SCOTT, T. W., LORENZ, L. H. & REPIK, P. M. 1991. Detection of eastern equine encephalomyelitis virus deposition in Culiseta melanura following ingestion of radiolabeled virus in blood meals. *Am J Trop Med Hyg,* 44**,** 250-9.

WECHSLER, S. J., MCHOLLAND, L. E. & TABACHNICK, W. J. 1989. Cell-Lines from Culicoides-Variipennis (Diptera, Ceratopogonidae) Support Replication of Bluetongue Virus. *Journal of Invertebrate Pathology,* 54**,** 385-393.

WEISS, B. L., SAVAGE, A. F., GRIFFITH, B. C., WU, Y. & AKSOY, S. 2014. The peritrophic matrix mediates differential infection outcomes in the tsetse fly gut following challenge with commensal, pathogenic, and parasitic microbes. *J Immunol,* 193**,** 773-82.

WERTZ, G. W., MOUDY, R. & BALL, L. A. 2002. Adding genes to the RNA genome of vesicular stomatitis virus: Positional effects on stability of expression. *Journal of Virology,* 76**,** 7642-7650.

WESTBROOK, C. J., REISKIND, M. H., PESKO, K. N., GREENE, K. E. & LOUNIBOS, L. P. 2010. Larval environmental temperature and the susceptibility of Aedes albopictus Skuse (Diptera: Culicidae) to Chikungunya virus. *Vector Borne Zoonotic Dis,* 10**,** 241-7.

WHITE, D. M., WILSON, W. C., BLAIR, C. D. & BEATY, B. J. 2005. Studies on overwintering of bluetongue viruses in insects. *Journal of General Virology,* 86**,** 453-462.

WHITE, H. 1980. A Heteroskedasticity-Consistent Covariance-Matrix Estimator and a Direct Test for Heteroskedasticity. *Econometrica,* 48**,** 817-838.

WHITE, S. M., BURDEN, J. P., MAINI, P. K. & HAILS, R. S. 2012. Modelling the within-host growth of viral infections in insects. *Journal of Theoretical Biology,* 312**,** 34-43.

WHITFIELD, S. G., MURPHY, F. A. & SUDIA, W. D. 1971. Eastern Equine Encephalomyelitis Virus - an Electron Microscopic Study of Aedes-Triseriatus (Say) Salivary Gland Infection. *Virology,* 43**,** 110-+.

WHITFIELD, S. G., MURPHY, F. A. & SUDIA, W. D. 1973. St-Louis Encephalitis-Virus - Ultrastructural Study of Infection in a Mosquito Vector. *Virology,* 56**,** 70-87.

WILSON, A. J. & MELLOR, P. S. 2009. Bluetongue in Europe: past, present and future. *Philosophical Transactions of the Royal Society B-Biological Sciences,* 364**,** 2669-2681.

WIRBLICH, C., BHATTACHARYA, B. & ROY, P. 2006. Nonstructural protein 3 of bluetongue virus assists virus release by recruiting ESCRT-I protein Tsg101. *J Virol,* 80**,** 460-73.

WIRTH, W. W. 1989. The Culicoides of Southeast Asia (Diptera: Ceratopogonidae). Walter Reed Army Institute of Research Washington DC.

WITTMAN, E. J., MELLOR, P. S. & BAYLIS, M. 2001. Using climate data to map the potential distribution of Culicoides imicola (Diptera : Ceratopogonidae) in Europe. *Revue Scientifique Et Technique De L Office International Des Epizooties,* 20**,** 731-740.

WITTMANN, E. J. & BAYLIS, M. 2000. Climate change: effects on *Culicoides*-transmitted viruses and implications for the UK. *The Veterinary Journal,* 160**,** 107-117.

WITTMANN, E. J., MELLOR, P. S. & BAYLIS, M. 2002. Effect of temperature on the transmission of orbiviruses by the biting midge, *Culicoides sonorensis*. *Medical and Veterinary Entomology,* 16**,** 147-156.

WORWA, G., HILBE, M., CHAIGNAT, V., HOFMANN, M. A., GRIOT, C., EHRENSPERGER, F., DOHERR, M. G. & THUR, B. 2010. Virological and pathological findings in Bluetongue virus serotype 8 infected sheep. *Veterinary Microbiology,* 144**,** 264-273.

XI, Z., RAMIREZ, J. L. & DIMOPOULOS, G. 2008. The Aedes aegypti toll pathway controls dengue virus infection. *PLoS Pathog,* 4**,** e1000098.

YAZI MENDOZA, M., SALAS-BENITO, J. S., LANZ-MENDOZA, H., HERNANDEZ-MARTINEZ, S. & DEL ANGEL, R. M. 2002. A putative receptor for dengue virus in mosquito tissues: localization of a 45-kDa glycoprotein. *Am J Trop Med Hyg,* 67**,** 76-84.

YERUHAM, I., PERL, S. & BRAVERMAN, Y. 2004. Seasonal allergic dermatitis in sheep associated with Ctenocephalides and Culicoides bites. *Veterinary Dermatology,* 15**,** 377-380.

YURCHENCO, P. D. & OREAR, J. J. 1994. Basal Lamina Assembly. *Current Opinion in Cell Biology,* 6**,** 674-681.

ZHANG, M., ZHENG, X., WU, Y., GAN, M., HE, A., LI, Z., LIU, J. & ZHAN, X. 2010a. Quantitative analysis of replication and tropisms of Dengue virus type 2 in Aedes albopictus. *Am J Trop Med Hyg,* 83**,** 700-7.

ZHANG, W., CHIPMAN, P. R., CORVER, J., JOHNSON, P. R., ZHANG, Y., MUKHOPADHYAY, S., BAKER, T. S., STRAUSS, J. H., ROSSMANN, M. G. & KUHN, R. J. 2003. Visualization of membrane protein domains by cryo-electron microscopy of dengue virus. *Nat Struct Biol,* 10**,** 907-12.

ZHANG, X., BOYCE, M., BHATTACHARYA, B., ZHANG, X. K., SCHEIN, S., ROY, P. & ZHOU, Z. H. 2010b. Bluetongue virus coat protein VP2 contains sialic acid-binding domains, and VP5 resembles enveloped virus fusion proteins. *Proceedings of the National Academy of Sciences of the United States of America,* 107**,** 6292-6297.

ZHANG, Z. Q., NOTERMANS, D. W., SEDGEWICK, G., CAVERT, W., WIETGREFE, S., ZUPANCIC, M., GEBHARD, K., HENRY, K., BOIES, L., CHEN, Z., JENKINS, M., MILLS, R., MCDADE, H., GOODWIN, C., SCHUWIRTH, C. M., DANNER, S. A. & HAASE, A. T. 1998. Kinetics of CD4+ T cell repopulation of lymphoid tissues after treatment of HIV-1 infection. *Proc Natl Acad Sci U S A,* 95**,** 1154-9.

ZHOU, X. B. & WONG, S. T. C. 2006. Informatics challenges of high-throughput microscopy. *Ieee Signal Processing Magazine,* 23**,** 63-72.

ZIEGLER, S. A., NUCKOLS, J., MCGEE, C. E., HUANG, Y. J. S., VANLANDINGHAM, D. L., TESH, R. B. & HIGGS, S. 2011. In Vivo Imaging of Chikungunya Virus in Mice and Aedes Mosquitoes Using a Renilla Luciferase Clone. *Vector-Borne and Zoonotic Diseases,* 11**,** 1471-1477.

ZIEGYTE, R., BERNOTIENE, R., PALINAUSKAS, V. & VALKIUNAS, G. 2016. Haemoproteus tartakovskyi (Haemoproteidae): Complete sporogony in Culicoides nubeculosus (Ceratopogonidae), with implications for avian haemoproteid experimental research. *Experimental Parasitology,* 160**,** 17-22.

ZIELER, H., GARON, C. F., FISCHER, E. R. & SHAHABUDDIN, M. 2000. A tubular network associated with the brush-border surface of the Aedes aegypti midgut: Implications for pathogen transmission by mosquitoes. *Journal of Experimental Biology,* 203**,** 1599-1611.

ZUKER, M. 2003. Mfold web server for nucleic acid folding and hybridization prediction. *Nucleic Acids Research,* 31**,** 3406-3415.

ZWART, M. P., DAROS, J. A. & ELENA, S. F. 2011. One Is Enough: In Vivo Effective Population Size Is Dose-Dependent for a Plant RNA Virus. *Plos Pathogens,* 7.

ZWART, M. P., HEMERIK, L., CORY, J. S., DE VISSER, J. A. G. M., BIANCHI, F. J. J. A., VAN OERS, M. M., VLAK, J. M., HOEKSTRA, R. F. & VAN DER WERF, W. 2009. An experimental test of the independent action hypothesis in virus-insect pathosystems. *Proceedings of the Royal Society B-Biological Sciences,* 276**,** 2233-2242.